8-2019

Design and predicting performance of carbon nanotube reinforced cementitious materials : mechanical properties and dipersion characteristics.

Mahyar Ramezani
University of Louisville

DESIGN AND PREDICTING PERFORMANCE OF CARBON NANOTUBE REINFORCED CEMENTITIOUS MATERIALS: MECHANICAL PROPERTIES AND DISPERSION CHARACTERISTICS

By
Mahyar Ramezani

A Dissertation
Submitted to the faculty of the
J.B. Speed School of Engineering at the University of Louisville
In Partial Fulfillment of the Requirements for the Degree of

Doctor of Philosophy
In Civil Engineering

Department of Civil and Environmental Engineering
University of Louisville
Louisville, Kentucky

August 2019

DESIGN AND PREDICTING PERFORMANCE OF CARBON NANOTUBE REINFORCED CEMENTITIOUS MATERIALS: MECHANICAL PROPERTIES AND DISPERSION CHARACTERISTICS

By
Mahyar Ramezani

A Dissertation Approved on
July 24, 2019

By the Following Dissertation Committee:

_____
Dr. Young Hoon Kim, Dissertation Director

_____
Dr. Zhihui Sun, Dissertation Co-Director

_____
Dr. William Mark McGinley

_____
Dr. Gamini Sumanasekera

To my beloved parents for their continuous love and endless support.

My gratitude extends beyond words.

ACKNOWLEDGEMENTS

This research would not have been completed without the help and support of so many great people in so many ways. I would like to express my sincere appreciation to my advisor, Dr. Young Hoon Kim, for his excellent guidance and the countless hours of time and effort that he has dedicated to my success. Without his support and encouragement, I could not have made it to this stage of my Ph.D. study.

I wish to express my gratitude to my co-advisor, Dr. Zhihui Sun, for her invaluable contributions, insightful comments, and great patience during my Ph.D. program at the University of Louisville. I would like to thank Dr. William Mark McGinley and Dr. Gamini Sumanasekera for serving on my dissertation committee. I also wish to acknowledge Dr. Omid Ghasemi-Fare for his willingness to help me in many situations.

I would like to extend my gratitude to other CEE faculty members and staffs for their help, especially Mr. Bernie Miles and Ms. Gail Graves.

Last but foremost, I would like to truly appreciate my family for their prayer and unconditional support. I would like to express my sincere gratitude to my parents, my brother, Maziar, and my sister, Maral, whom have encouraged, inspired, and supported me throughout my whole life.

ABSTRACT

DESIGN AND PREDICTING PERFORMANCE OF CARBON NANOTUBE REINFORCED CEMENTITIOUS MATERIALS: MECHANICAL PROPERTIES AND DISPERSION CHARACTERISTICS

Mahyar Ramezani

July 24, 2019

Recently, Carbon Nanotubes (CNTs) are drawing considerable attention of researchers for reinforcing cementitious materials due to their excellent mechanical properties and high aspect ratio (length-to-diameter ratio). However, CNTs might not disperse well within the cement matrix, resulting in little improvement or even degradation of concrete properties. The uncertainty in producing the consistent results in different studies might be attributed to multiple interactions between the experimental variables affecting the nanotube dispersion and the final properties of CNT-cement nanocomposites. Therefore, this research mainly focused on proposing equations that can reliably capture these interactions in order to correlate CNT dispersion with the mechanical properties. The main experimental variables studied included CNT concentration, aspect ratio, ultrasonication energy, ultrasonication amplitude, surfactant-to-CNTs ratio, water-to-cement ratio, sand-to-cement ratio, and hydration age of specimen. The study reported in this research was conducted in two parts: experimental program and modeling.

In the experimental part of this research, a total of 63 different mix proportions were used to evaluate the flowability, mechanical properties, and durability characteristics of cement pastes and mortars containing CNTs. Using experimental test results reported in this study and the literature, three critical relations were proposed to consider the CNT dispersion, cement matrix composition, and hydration age of cement. The proposed critical relations were then added to available theoretical models in the literature. The flexural strength and elastic modulus of CNT-cement nanocomposites were predicted through a state-of-the-art probabilistic model using a Bayesian methodology. Finally, the developed probabilistic models were used to identify the optimum ranges of the experimental variables to maximize the mechanical properties. This was done through computing the conditional probability of not meeting the specified design requirement.

The experimental results indicated that addition of CNTs could significantly improve different properties of cementitious materials, if the optimum range of each variable was used. Also, to achieve the desired mechanical properties, various combinations of the experimental variables might be used. The proposed prediction models were shown to capture the interactions between the experimental variables for predicting the mechanical properties within ±15% and ±18% of the experimental test results for flexural strength and elastic modulus, respectively. Based on the findings of this research, contour plots were developed to provide practical guidelines for future engineers to design CNT-cement nanocomposites.

TABLE OF CONTENTS

LIST OF TABLES

APPENDIX

LIST OF FIGURES

APPENDIX

CHAPTER 1. INTRODUCTION

1.1. General

Portland cement concrete is the most widely used material in the construction industry due to the widespread availability of its constituents, fairly low price, and desirable performance (e.g., compressive strength and stiffness). However, concrete exhibits low tensile strength and fracture toughness, resulting in cracking (i.e., quasi-brittle behavior). Cracks affect the mechanical and durability properties of concrete. In terms of durability, cracks allow gases and liquids to penetrate into the material, deteriorating its mechanical properties over time. Therefore, the mitigation of crack formation/propagation is important.

Since the 1870s, the steel reinforcing bars have been widely used to compensate for the low tensile properties of concrete. Over the past few decades, synthetic fibers (macro to micro fibers) have attracted considerable attention of researchers to control the propagation of cracks [1-7]. Depending on the fiber type, the contributions of fibers rely on the shape and size of the fibers, their surface textures, the interfacial bond strength between the fibers and the matrix, crack bridging ability, and energy dissipation during crack propagation [8, 9]. In this regard, smaller fibers are effective at arresting comparably sized cracks at an earlier stage of cracking [10].

1.2. Problem Statement

Theoretically, the concrete crack widths can be as small as the nanoscale ($10^{-9}-10^{-7}\ m$) [11]. Therefore, even microfibers cannot stop the initiation of these cracks

[12, 13]. However, they are still capable of mitigating the crack propagation after the crack width reaches the microscopic scale ($10^{-6}-10^{-4}\ m$) [14, 15]. Being different from microfibers, nanofibers and nanotubes were reported to prevent or delay the nucleation of cracks at the nanoscale (see Figure 1-1) [16, 17]. Such small cracks would neither be regarded as damage nor affect the permeability.

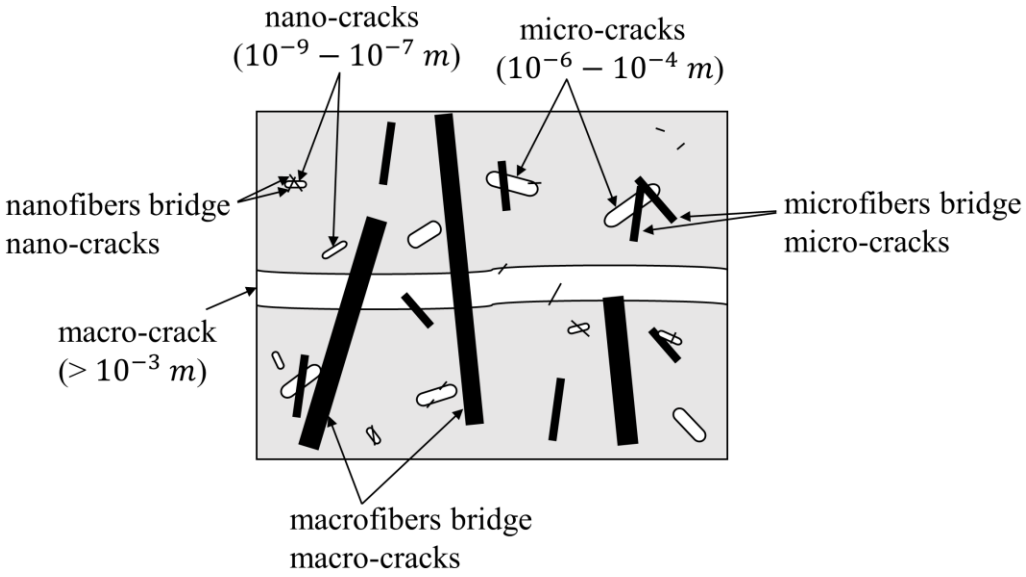

Figure 1-1. Bridging action of fibers across nano, micro, and macro cracks

Amongst various nanofibers, Carbon Nanotubes (CNTs) are considered as potential candidates for the next generation of high performance and multifunctional concrete structures because of their unique properties (physical, mechanical, thermal, and electrical) [18-22]. If CNTs are well dispersed, their high aspect ratio (length-to-diameter ratio) along with nanoscale size reduces the distance between adjacent nanotubes [23]. This results in a large number of CNTs at the crack plane, delaying the crack propagation. Besides, reduced permeability by using CNTs may also improve the durability of concrete (this study investigated the contribution of CNTs to mitigate the alkali-silica reaction; ASR).

There are two main issues concerning the incorporation of CNTs in cementitious materials: dispersion and the interfacial bond strength between CNTs and cement matrix.

The Van der Waals (VdW) forces resulting from the CNT nanoscale size and large surface area causes the CNTs to agglomerate (see Figure 1-2). The agglomeration of CNTs (i.e., poor dispersion) creates many matrix defect such as increased porosity and stress concentrations. This limits CNT ability to improve different characteristics of concrete such as its mechanical and durability properties [24-27]. To facilitate CNT dispersion, a surfactant-assisted ultrasonication procedure is the most common route [16].

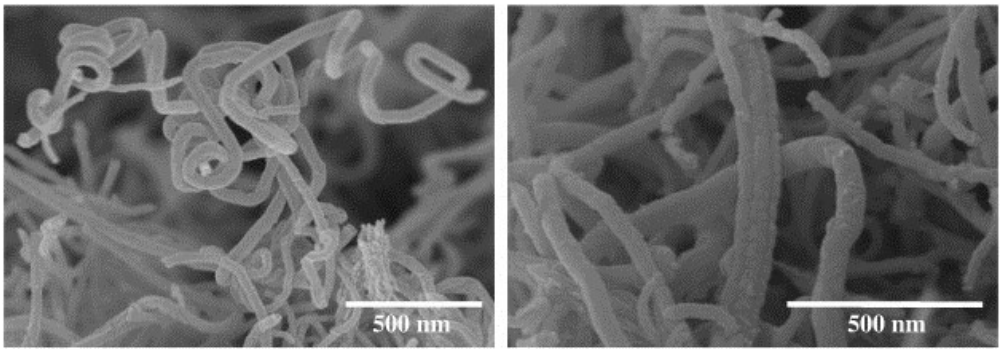

Figure 1-2. SEM images of CNT agglomerations in cement paste [16]

However, due to the complex dispersion procedure of CNTs, inconsistent experimental results of the influence of CNTs on different properties of cementitious materials have been reported [23, 27-33]. This inconsistency might be attributed to the interactions between the multiple variables affecting the dispersion quality and the final properties (e.g., mechanical properties). Therefore, there is yet no model available to predict the mechanical properties with reasonable accuracy. In addition, the high degree of uncertainty associated with incorporating CNTs (e.g., amount of structural defects on CNT surface, number of walls (layers), material properties, etc.) makes developing reliable models to establish their status in construction industry very challenging.

1.3. Research Objectives and Scope

The aim of this research is to develop analytical relations and prediction models to capture the interactions between the experimental variables in order to correlate between

CNT dispersion and the mechanical properties of concrete for practical applications. The specific objectives of this research are:

1) Propose critical relations (dispersion relation, hydration age relation, and matrix relation) that can capture the interactions between multiple influential variables affecting the mechanical properties of CNT-cement nanocomposites.
2) Quantify the degree of CNT dispersion to correlate between the dispersion quality and mechanical properties of cementitious materials.
3) Construct reliable and bias-free probabilistic models to predict the flexural strength and elastic modulus of CNT-cement nanocomposites (pastes and mortars) with respect to CNT properties, dispersion procedure, and matrix composition/hydration using a Bayesian approach.
4) Identify the optimum ranges of experimental variables to achieve superior mechanical properties of CNT-cement nanocomposites.
5) Propose practical guidelines for engineers to incorporate CNTs within Portland cement-based materials.
6) Investigate the influence of CNTs on mitigating ASR in cement mortars.

To achieve the objectives, this study was conducted in four phases. The overall procedure can be divided into three tracks that evaluate the influence of CNTs on mechanical properties (Track 1), flowability (Track 2), and durability characteristics (Track 3) of CNT-cement nanocomposites. Figure 1-3 shows the overall process used in this research program. In each phase, multiple tasks were performed, as described below.

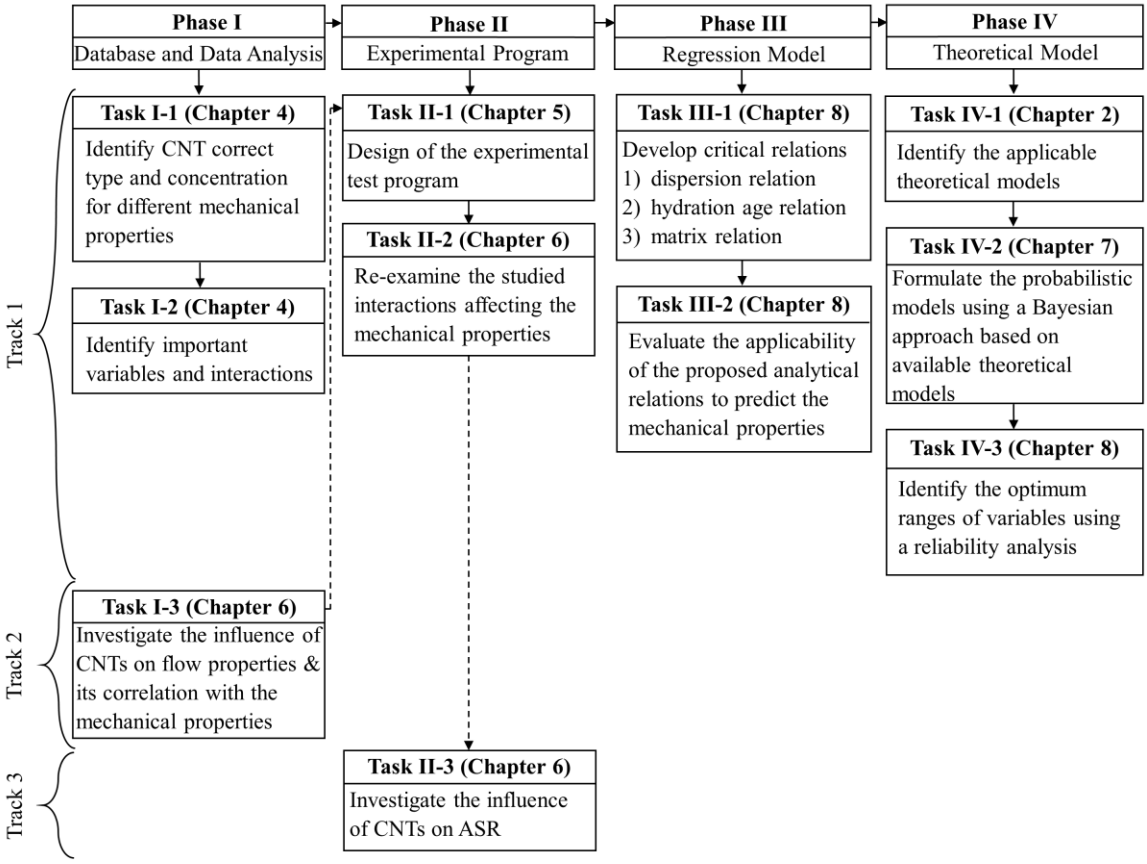

Figure 1-3. Overall procedure of this research program

In Phase I, three tasks were performed. In Task I-1, a database was established and analyzed to identify the correct type of CNTs and their optimum concentrations to tailor the mechanical properties for various structural applications, based on different strengthening mechanisms (see Chapter 4). In Task I-2, the database was thoroughly analyzed to identify the most important variables and their interactions that affected the mechanical properties of CNT-cement nanocomposites (see Section 4.10). At the same time as performing Task I-1 and Task I-2, an experimental study was conducted in Task I-3 (see Track 2 in Figure 1-3). The purpose of the experimental program was to find proper mix proportions by correlating between the flowability and mechanical properties of CNT-cement pastes and mortars (see Section 6.2).

Phase II consisted of three tasks. In Task II-1, an experimental program was designed to study the influences of important variables on mechanical and durability properties (see Chapter 5). Task II-2 re-examined the main interactions between the studied experimental variables affecting the mechanical properties (see Section 6.3). Task II-3 (see Track 3 in Figure 1-3) studied the contribution of CNTs to suppressing ASR in cement mortars, including mechanical (e.g., crack bridging) and chemical (e.g., CNT chemical functionalization) mechanisms (see Section 6.4).

In Phase III, two tasks were performed. In Task III-1, three critical relations were developed to capture the interactions between the variables that affect the mechanical properties of CNT-cement nanocomposites (see Section 8.2). In Task III-2, the ability of the proposed relations to predict the mechanical properties (herein, flexural strength and elastic modulus) was evaluated using a simple regression equation (see Section 8.3).

In Phase IV, the proposed critical relations were added to available theoretical models in the literature to predict the mechanical properties of CNT-cement nanocomposites. To achieve this goal, three tasks were performed. In Task IV-1, available theoretical models were identified (see Section 2.6.2). In Task IV-2, due to the high degree of uncertainty when incorporating CNTs, a Bayesian methodology was adopted to formulate the models in a probabilistic manner and to correct the effect of each variable on the mechanical properties (see Chapter 7). In Task IV-3, the probabilistic models were evaluated using extensive experimental test data, both from this research and from the literature. Finally, the developed probabilistic models were used to identify the most important variables and their optimum ranges using a reliability analysis (see Section 8.4).

To sum up, the scope of this research program was to investigate the influence of CNTs on the following properties of cementitious materials:

- flow properties
    - mini-cone slump diameter
    - plastic viscosity
    - yield stress
- mechanical properties
    - compressive strength
    - flexural strength
    - elastic modulus (static and dynamic)
- durability properties
    - ASR

1.4. Organization of this Dissertation

Chapter 2 provides a review on various mechanisms of CNTs that impact different properties of cementitious materials including microstructure, flow properties, mechanical properties, durability, and dimensional stability. Also, available theoretical models that have been used to predict the tensile/flexural strength and elastic modulus of composites containing CNTs are introduced. Chapter 3 presents the overview of the strategy for model development. In Chapter 4, a database was established and analyzed to identify optimum ranges of CNT intrinsic properties that produce superior mechanical properties of CNT-cement nanocomposites. Also, other potential variables and the interactions between them affecting the mechanical properties were identified. Chapter 5 describes the test matrix and test procedures for the experimental program. Chapter 6 presents the experimental test

results and analysis concerning the influence of CNTs on flowability, mechanical properties, and durability characteristics of CNT-cement pastes and mortars. Chapter 7 presents the background used to construct the probabilistic models. In Chapter 8, extensive experimental test data from this research and literature were used to develop analytical equations to reliably predict the flexural strength and elastic modulus of CNT-cement nanocomposites (pastes and mortars). Finally, Chapter 9 summarizes the key contributions of this research and gives recommendations for future work directions.

CHAPTER 2. LITERATURE REVIEW

2.1. General

This chapter first presents a concise review on CNT structure and its properties (Section 2.2). Then, various techniques used in the past research to overcome CNT dispersion issues for exploiting their exceptional properties within nanocomposites are summarized (Section 2.3). The influence of important variables on different properties of CNT-cement nanocomposites including microstructure (Section 2.4), flow properties (Section2.5), mechanical properties (Section 2.6), durability (Section 2.7), and dimensional stability (Section 2.8) are reviewed. Available theoretical models developed to predict the tensile/flexural strength (Section 2.6.2.1) and elastic modulus (Section 2.6.2.2) of nanocomposites containing CNTs are also discussed.

2.2. Fundamentals of CNTs

This section presents CNT structure (Section 2.2.1) and its properties (Section 2.2.2).

2.2.1. CNT Structure

CNTs are allotropes of carbon in a cylindrical form which can be categorized into two main groups of single-walled carbon nanotubes (SWCNTs; see Figure 2-1 (a)) and multi-walled carbon nanotubes (MWCNTs; see Figure 2-1 (b)), depending on the number of concentrically rolled up graphene sheets. The strong covalent bonds between adjacent carbon atoms in a plane are formed through sp^2 hybridization orbitals (σ bonds; see Figure 2-1 (c)) that gives CNTs their remarkable strength and stiffness [34, 35]. The remaining bonds are formed by 2p orbitals out of the plane in the *z* direction (π bonds; see Figure 2-1

(c)). The π orbitals are responsible for the VdW interactions [36, 37] that holds the neighboring layers of MWCNTs in their positions. The VdW forces are also the primary reason for the adherence of individual CNTs to one another, making them difficult to get dispersed in different media.

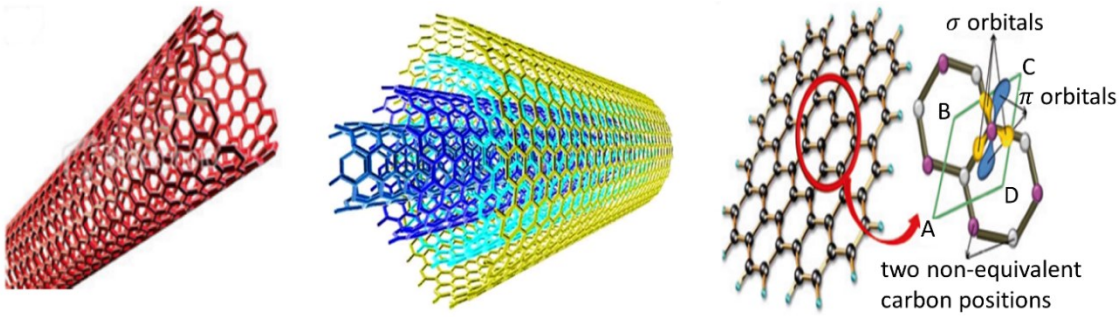

Figure 2-1. (a) SWCNT (b) MWCNT (c) orbital structure of CNT [35]

2.2.2. CNT Properties

The length of CNTs is not restricted and ranges from a few tens of micrometers up to even several centimeters [38, 39]. The diameter of CNTs depends on their number of walls. SWCNTs typically possess diameters smaller than 2 *nm*, while MWCNT diameter ranges from 5 to about 100 *nm* [40]. Therefore, CNTs can have extremely high aspect ratios (length-to-diameter ratio). Besides, CNT density varies greatly depending on their length, diameter, and the number of walls. Kim *et al*. [41] found that the density of two different types of MWCNTs having diameters of 15 and 22 *nm* was in the range of 1.74 ± 0.16 g/cm^3 (0.063 ± 0.006 $lb/in.^3$). Laurent *et al*. [42] theoretically calculated the density of CNTs with respect to their diameter and the number of walls. They reported that CNT density decreased as CNT diameter increased. Also, in case of a constant diameter, the more the number of walls, the higher the density was.

There are two methods to measure the mechanical properties of CNTs: the direct method and the indirect method. Note that direct measurement of the mechanical properties of individual CNTs is challenging due to their nanoscale sizes.

Indirect techniques had been developed to measure the mechanical properties using electrically [43] or thermally [44] induced vibrations of CNTs that were fixed at one end. Another indirect method of measuring the mechanical properties is stress-induced deformations of CNTs embedded in polymer matrices [45, 46].

Using a direct technique, Yu *et al*. [47] measured the tensile strength of individual MWCNTs that were attached to two opposing Atomic Force Microscopy (AFM) tips using carbonaceous deposits. They reported tensile strength and elastic modulus ranged from 11 to 63 *GPa* ($1.6 \times 10^3 - 9.1 \times 10^3$ *ksi*) and 270 to 950 *GPa* ($39.2 \times 10^3 - 138 \times 10^3$ *ksi*), respectively. Demczyc *et al*. [48] also fabricated a direct tensile testing apparatus to measure the mechanical properties of individual MWCNTs in the Transmission Electron Microscope (TEM). In their study, tensile strength and elastic modulus were reported to be 150 *GPa* (21.8×10^3 *ksi*) and 0.8 *TPa* (116×10^3 *ksi*), respectively. Therefore, CNTs possess tensile strength and elastic modulus of up to about 3000 and 20 times larger than those of concrete, respectively. In addition, researchers [48, 49] found that CNTs showed elastic behavior up to failure. CNT elastic strain capacity was found to be in the range of 10 to 15% [47, 50].

Besides the CNT superior mechanical properties and high aspect ratio, they also exhibit excellent electrical and thermal properties. For example, MWCNTs were reported to carry currents of up to $10^9 - 10^{10}$ *A/cm*^{2} [51]. Moreover, electrical properties of CNTs vary with changing in stress levels [21, 52]. Tombler *et al*. [53] observed the reduction of

the conductance by more than 100 times when SWCNTs deflected by 80 *nm*, corresponding to the strain value of about 3%. In addition, the thermal conductivity of approximately 3500 *W/m.K* and 3000 *W/m.K* was measured for SWCNTs [54] and MWCNTs [55], respectively. Furthermore, CNT thermal stability was found to be up to about 2800 ℃ (5072 ℉) and 750 ℃ (1382 ℉) in the vacuum and air, respectively. By comparison, metal wires that are used in microchips have a melting point between 600 and 1000 ℃ (1112-1832 ℉) [56].

Because of the remarkable multifunctional properties of CNTs, they are promising candidates for different applications in the construction industry [17, 33, 57-59]. However, the properties of cementitious materials containing CNTs are still not well understood and inconsistent experimental results have been reported [23, 27-33], due to difficulties in providing a uniform CNT dispersion. In cementitious materials, MWCNTs are predominantly used because of their lower prices as well as easier dispersibility compared with SWCNTs. Therefore, in this research MWCNTs were used. Hereafter, MWCNTs are simply referred to as CNTs.

2.3. CNT Dispersion Procedure

Previous studies reported that improper CNT dispersion created defects such as increased porosity and stress concentration between CNTs and matrix [20, 24, 25]. Furthermore, the existence of CNT clumps prevents the construction of an interconnected network of CNTs for mitigating crack propagation within the cement matrix [60]. Recognizing dispersion issues, many researchers tried to find effective techniques to properly disperse CNTs. This section briefly summarizes each method found in past research. Based on the literature, six representative dispersion techniques have been used:

1. dry mix of CNTs and cement (DM)
2. ball milling (BM)
3. dispersion of CNTs in cement via ultrasonication process (US+CC)
4. direct synthesis of CNTs onto the surface of cement or mineral admixtures (DS)
5. pre-dispersion of CNTs in water using an ultrasonication process without surfactants (US)
6. pre-dispersion of CNTs in water using a surfactant-assisted ultrasonication process (US+S)

The dry mixing procedure (DM) is not an efficient technique due to the high surface area of CNTs, resulting in a poor dispersion within the cement matrix [16, 61]. When using DM technique, fine particles such as silica fume [20, 62, 63], fly ash [64], or nanometakaolin [65] could be used to better disperse CNTs by physically separate them. In addition, utilizing fine particles such as silica fume can densify the cement matrix, resulting in higher interfacial bond strength between CNTs and cement hydration products [29, 66].

Ball milling process (BM) can be used to disperse CNTs through the collisions between the balls within the milling chamber that generates locally high pressure. However, ball milling process was found to decrease the high aspect ratio of CNTs by shortening their lengths [67], reducing their load carrying capacity [68]. Pierard *et al*. [69] observed the reduction in the average length of CNTs from 50 to 0.8 μm after lengthy ball milling. In addition, the ball-milled cement grains might create multiple problems such as high water consumption, thermal cracking, more chemical and autogenous shrinkage [70], and durability issues [71].

To produce cement grains fully covered with clusters of CNTs, Makar *et al*. [72] adopted a novel dispersion technique (US+CC). In their study, CNTs were dispersed using an ultrasonication process in isopropanol. The cement powder was then added to the beaker during ultrasonication process. The process was stopped after four hours and the isopropanol was let to evaporate in a vacuum system. Thereafter, the resulting CNT-cement cake was ground using a hand mortar and pestle. In another study, Hunashyal *et al*. [73] used ethanol for CNT dispersion in cement using US+CC technique.

Direct synthesis (DS) of CNTs on the surface of cement or mineral admixtures is an attractive method that can eliminate the tedious procedure of CNT dispersion [74]. Direct synthesis of CNTs on the surface of cement [75-84], silica fume [75, 80], fly ash [81, 85-87], and sand [81-83] using Chemical Vapor Deposition (CVD) or microwave irradiation have been reported. Note that multiple factors such as substrate material, inert gas, their flow speed rate, catalyst, and applied temperature affect the type and amount of carbon containing materials synthesized using the CVD method. Thus, optimization of these factors is crucial in obtaining the desired characteristics of CNT-cement nanocomposites. For example, if excessive CNTs is synthesized, they may interrupt the hydration process by completely covering the entire surface of cement grains, weakening the connection between the hydration products [76].

Amongst various dispersion techniques, pre-dispersion of CNTs in water using an ultrasonication process prior to mixing with cement is the most common route. In an ultrasonication process, the ultrasonicator (tip or bath machine) is used to form cavitation bubbles through shear stresses. The implosion of these microscopic cavitation bubbles results in the exfoliation of CNTs [88]. However, If no surfactant is used (US technique),

the exfoliated CNTs immediately begin to reagglomerate after stopping the ultrasonication process due to the VdW forces [89]. Therefore, an ultrasonication process is commonly used with the help of surfactants (US+S technique) to retain the quality of dispersion over time [37, 67, 90]. The effectiveness of the US+S technique depends on many factors including CNT concentration (or volume fraction) and aspect ratio, surfactant type and dosage, and the ultrasonication process (energy and amplitude). For example, when excessive surfactant dosage is used, multiple layers of surfactant molecules are formed around CNT surface, resulting in the re-agglomeration of CNTs due to the degraded electrostatic repulsion forces [60]. Meanwhile, the optimum dosage of surfactants depends on CNT and/or surfactant molecule size. To completely wet the CNT surface, four times higher dosage of sodium dodecyl sulfate (SDS) was needed compared with nonionic polyoxyethylene (Brij 35), which was attributed to the smaller size of SDS molecules compared with Brij 35 [60]. In addition, covalent attachments of functional groups such as carboxyl (COOH) or hydroxyl (OH) to the surface of CNTs might increase CNT dispersibility by improving their hydrophilicity [91]. However, some researchers reported the ineffectiveness of short COOH functional groups on CNT dispersion stability [92].

2.4. Microstructure of CNT-Cement Nanocomposites

Microstructure which is defined as the type, amount, and morphology of the existing phases in the hardened concrete can be appropriately changed to improve its macroscopic properties. Because of the nanoscale size along with the high aspect ratio of CNTs, they might improve the pore structure and hydration process of cementitious materials. However, to achieve a desired microstructure, CNT concentration, aspect ratio, their surface condition, as well as type and amount of surfactant must be carefully selected.

For example, utilizing sodiumdodecyl benzenesulfonate (SDBS) or natural Arabic gum as a surfactant was found to delay the cement hydration for a couple of days [92, 93]. Also, utilizing high dosage of Lignosulfonate substantially extended the setting time of cement [94]. Besides, utilizing poly-naphthalene sulfonate sodium salt inhibited the calcium silicate hydrate (C-S-H) nucleation on the surface of SWCNTs [95].

2.4.1. Hydration

CNTs have the potential to act as nucleation seeding sites for the formation of hydration products due to their nanoscale size and high surface energy. The acceleration in the hydration rate of CNT-cement nanocomposites was first noted by Makar *et al*. [72] through Vikers microhardness tests. Cement pastes incorporating SWCNTs showed a substantial increase in the hardness at early ages, followed by negligible differences after 14 days compared with the control specimens (without CNTs). This indicates the stimulation in the growth of hydration products in the presence of CNTs. In another study, Makar *et al*. [96] used Isothermal Conduction Calorimetry (ICC) to study the hydration process of cement with and without incorporation of SWCNTs. The results indicated that SWCNTs generated higher maximum heat flow, and also accelerated the hydration reaction. This was also confirmed by Scanning Electron Microscopy (SEM) images showing the preferential formation of C-S-H on the surface and along the length of SWCNTs.

Konsta-Gdotous *et al*. [11] performed nanoindentation test to study the effect of CNTs on the elastic modulus of cement pastes. They used a peak analyzing protocol and fitted the probability plot of the elastic modulus below 50 *GPa* (7252 *ksi*) to four different zones of porous phase, low and high density C-S-H, and calcium hydroxide (CH). The peak

value of the probability plots of cement pastes containing CNTs fell in the area corresponded to high density C-S-H, whereas plain cement paste had its peak value in low density C-S-H zone.

Fakhim *et al*. [97] studied the effect of various concentrations of CNTs ranging from 0.1 to 2% based on the weigh percent of cement powder (*c-wt*%) on cement hydration using Thermogravimetric Analysis (TGA). It was observed that CH and C-S-H weight losses in the presence of up to 0.3 *c-wt*% CNTs were more than those of the control specimen, indicating the acceleration in the hydration process of cement. Beyond CNT concentration of 0.3 *c-wt*%, the rate of the cement hydration was decreased. The reason behind the decrease in the rate of cement hydration beyond certain CNT concentrations is discussed in Section 4.10.5.

2.4.2. Porosity

Pores are important components of the microstructure, and their size distribution significantly influences the properties of a hardened material. If properly designed, CNTs might reduce the total porosity and refine the pore structure of cementitious materials. In this regard, CNT size and concentration, as well as surfactant type and dosage are critical parameters.

Incorporating excessive CNT concentrations may lead to CNT agglomeration (i.e., dispersion issues) which acts as pores and cracks between the hydration products. However, different threshold concentrations have been reported [24, 25, 97, 98]. Li *et al*. [98] observed that incorporation of 0.5 *c-wt*% CNTs decreased the total porosity and the macro-pores by about 64% and 82%, respectively, compared with the control specimen. Fakhim *et al*. [97] found the threshold CNT concentration of 0.3 *c-wt*%, beyond which the

porosity started to increase. Wang *et al*. [24] found the threshold concentration of 0.1 *c-wt*% CNTs which exhibited 32% lower porosity than the control specimen. The different threshold concentrations might be attributed to utilizing different types and dosages of surfactants and CNTs. For example, utilizing SDS as a surfactant entrained substantial air voids within the cement matrix [60, 99]. Besides, CNT properties (e.g., length, diameter, concentration) play important roles in determining the pore size distribution.

Figure 2-2 shows the schematic representation of the effect of CNT length, diameter, and concentration on the pore structure. Figure 2-2 (a) and (b) show the influence of low (L) and high (H) concentrations of the base CNTs; short length (SL) and small diameter (SD). Figure 2-2 (c) and (d) show the influence of the increase in CNT length (LL for long CNTs; see bolded letters in Figure 2-2 (c) and (d)) at low and high concentrations while using the same diameter as the base CNTs. Also, Figure 2-2 (e) and (f) represent the influence of the increase in the base CNT diameter at low and high concentrations (LD for large diameter CNTs; see bolded letters in Figure 2-2 (e) and (f)).

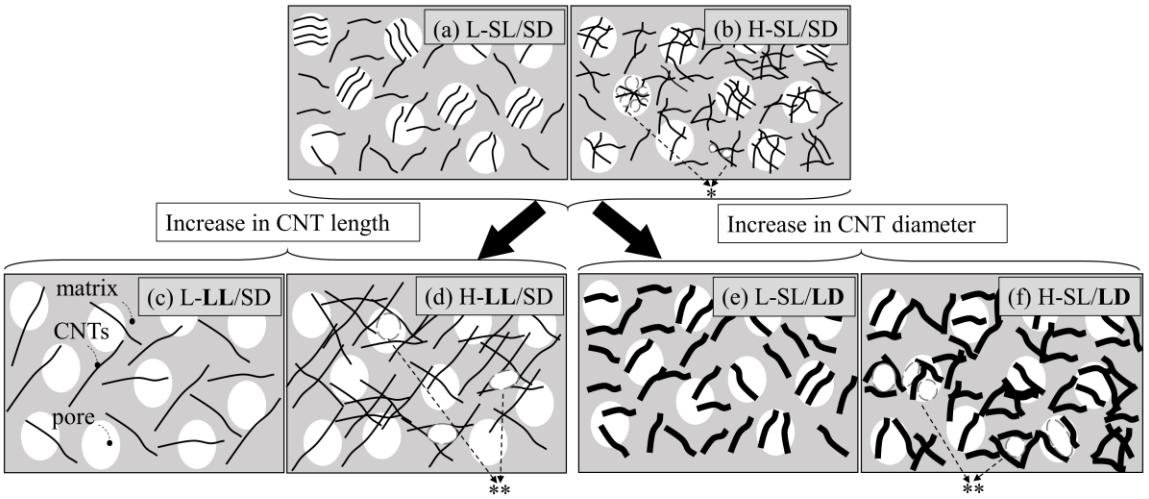

Figure 2-2. Effect of CNT length and diameter at different concentrations on the pore size distribution

Note: (L-: low concentration, H-: high concentration, SL: Short CNTs, LL: long CNTs, SD: small diameter CNTs, LD: large diameter CNTs). *short and small diameter CNTs, if clumped, divide the big pores into smaller pores, **long and large diameter CNTs, if clumped, produce bigger pore sizes.

When using a low concentration of various types of CNTs (see Figure 2-2 (a), (c), and (e)), the well-dispersed CNTs reduce the total porosity and refine the pore structure [25, 98]. However, utilizing excessive or high concentration of CNTs will contribute differently to the total porosity and pore size distribution. The agglomerated short and small diameter CNTs (see Figure 2-2 (b); H-SL/SD) might still be capable of filling the big pores into smaller pore sizes. Conversely, the agglomeration of either long (see Figure 2-2 (d); H-LL/SD) or large diameter (see Figure 2-2 (f); H-SL/LD) CNTs produces bigger pores due to their larger sizes. For example, Wang *et al*. [24] incorporated 0.15 *c-wt*% of CNTs having average length of 10 μm. They observed an increase in the total porosity by 1.5%, whereas the median volume pore diameter decreased by 26% compared with the control cement paste.

2.5. Flow Properties of CNT-Cement Nanocomposites

The flow properties are correlated with the constructability and early-age characteristics of concrete. Flowability is closely related to CNT concentration, their surface condition, as well as type and amount of surfactants. Addition of CNTs can reduce the flowability and increase the yield stress and plastic viscosity due to two main reasons: 1) filling the voids in cement composites due to their nanoscale sizes which increases the probability of collision, and 2) consumption of water to wet their large surface area which results in lower availability of water to act as lubricant in cement composites, leading to higher frictional forces between particles.

The early investigation indicated that the addition of CNTs to concrete could substantially reduce the flowability due to the increase in surface interaction as a result of the large surface area of CNTs [100]. Collins *et al*. [94] observed that employment of high

content of air entraining agent and lignosulfonate could help the flowability of CNT-cement mixture in exchange for high porosity and delayed setting, respectively. Therefore, using a surfactant that simultaneously helps both CNT dispersion and flowability of CNT-cement nanocomposites, without any adverse effect on the cement hydration, is an effective solution to combat flowability issues [12, 94]. Poly-carboxylate based superplasticizers (SP) were found to be the most suitable surfactants to assist CNT dispersion in cementitious materials due to the steric barrier and/or electrostatic repulsion [16, 23, 94]. Also, using SP allows adding greater concentrations of surfactants, resulting in better flowability [92]. Nevertheless, an excessive amount of SP can cause a drop in material integrity (e.g., segregation and bleeding). Thus, the optimization of SP dosage is important. To achieve enough flowability and effective dispersion of CNTs, Zou *et al*. [12] suggested a mass ratio of the adsorbed SP on the surface of nanotubes to CNTs equal to eight.

Collins *et al*. [94] observed that adding higher contents of CNTs further deteriorated the flowability of CNT-cement nanocomposites. They reported that flow diameter decreased by 15%, 33%, and 49% compared with the control mixture, at CNT concentrations of 0.5, 1, and 2 *c-wt*%, respectively. Other researchers have also reported the similar trend [12, 100, 101].

Furthermore, Kang *et al*. [63] ascertained that utilizing COOH-CNTs resulted in additional 5% reduction of mixture flowability compared with the usage of pristine CNTs. The reduced flowability in the case of COOH-CNTs was also reported by other researchers [92, 100]. This can be explained by two main mechanisms: 1) stronger bond between COOH-CNTs and surfactants which can possibly reduce their interaction with cement

particles [92], and 2) further adsorption of water by the hydrophilic COOH functional groups on the surface of CNTs.

2.6. Mechanical Properties of CNT-Cement Nanocomposites

This section first presents the mechanisms of CNTs affecting the mechanical properties (Section 2.6.1). Then, Section 2.6.2 discusses available theoretical models in the literature to predict the tensile/flexural strength (Section 2.6.2.1) and elastic modulus (Section 2.6.2.2) of nanocomposites containing CNTs.

2.6.1. Mechanisms of CNTs affecting the Mechanical Properties

Despite the potential benefits of CNTs to reinforce the cementitious materials, the mechanisms of CNTs affecting the mechanical properties are not fully understood. To date, most researchers have considered CNTs as just very fine fibers, meaning that they can be distributed on a much finer scale than other types of fibers in cementitious materials [23]. In other matrices (e.g., polymer, metal, and ceramic), however, researchers used CNT properties in different models (e.g., Kelly-Tyson model [102], Halpin-Tsai model [103], Pukanszky model [104], etc.) to predict the tensile/flexural strength, elastic modulus, and interfacial shear strength between CNTs and various matrices [105-109]. Therefore, this section discusses the different mechanisms of CNTs affecting the mechanical properties of CNT-cement nanocomposites.

The main mechanism that enhances the mechanical properties of CNT-cement nanocomposites is the bridging and better particle packing effects caused by the presence of CNTs. Despite the ongoing research efforts, there is yet no consensus on the contribution of CNTs to the mechanical properties of cementitious materials. Some researchers have reported significant improvement in mechanical properties [11, 63, 66, 75, 110-115], while

others have reported negligible improvement or even degradation in mechanical properties [20, 26, 29, 60, 64, 65, 99, 116-118]. The mechanical properties investigated include compressive strength, flexural (or tensile) strength, elastic modulus, and toughness. The inconsistent results are mainly attributed to CNT dispersion quality within the cement matrix [13, 29, 98]. The agglomeration of CNTs (i.e., poor dispersion) might produce defects in the form of pores, creating unreacted pockets, and degrading the load carrying capacity of CNTs, resulting in the reduction in mechanical properties [119, 120].

The interfacial bond strength between CNTs and matrix is an important parameter affecting the tensile/flexural strength. However, the interfacial bond strength has a negligible influence on the compressive strength. For example, Konsta-Gdoutos *et al*. [28] used two different types of CNTs to increase the mechanical properties of cement mortars. Both types of CNTs studied had similar lengths and diameters but different surface conditions: pristine CNTs (Type I) and mechanical functionalized CNTs (type II) designed to increase the interfacial bond strength between CNTs and cement matrix. When using type II CNTs, the 28-day flexural strength increased by 23% compared with type I CNTs. Nevertheless, the 28-day compressive strength did not show further improvement using either type I or type II CNTs. In another study, Dangolidis *et al*. [31] used CNTs with diameters ranging from 20 to 45 *nm* and length $\geq$ 10 μm to increase the mechanical properties of cement mortars. The results indicated that addition of 0.1 *c-wt*% CNTs resulted in 88% increase in the 28-day flexural strength, while the compressive strength only marginally increased (6%), compared with control specimens. This might be explained by different mechanisms of CNTs affecting the compressive and flexural strengths.

The compressive strength is closely related to the pore structure. Therefore, the compressive strength might be increased by filling the internal pores of concrete using CNTs. Consequently, smaller CNTs (i.e., shorter length and smaller diameter) can fill the bigger pores into the smaller pore sizes. This improves the pore structure of the cement matrix (i.e., lower porosity, refined pore structure, disconnected pores), resulting in significant improvement in the compressive strength. In this case, L-SL/SD outperforms with respect to the compressive strength (see Figure 2-2 (a)). In addition, H-SL/SD could still contribute to refining the pore structure due to their small sizes, which might be tolerable concerning the compressive strength (see Figure 2-2 (b)). The agglomeration of long and large diameter CNTs (see Figure 2-2 (d) and (f)) might adversely affect the compressive strength.

On the other side, if CNTs lack proper dispersion (see Figure 2-2 (b), (d) and (f)), the frictional forces become minimal within the agglomerated CNTs and they easily debond from the matrix [121, 122], degrading the flexural strength. Conversely, well dispersed CNTs can effectively link the hydration products and hinder the extension of cracks by absorbing part of the energy that is required for their propagation. This process demonstrates itself in three different ways of crack bridging, crack deflection, and CNT pullout. Figure 2-3 shows a typical SEM image of CNTs crossing the crack [72]. When CNTs are presented in the perpendicular direction to the crack plane, they are fully anchored on both sides of the crack. When CNTs are presented in a different direction of the crack plane, they are debonded from the matrix. In case of a good dispersion (L-SL/SD (see Figure 2-2 (a)), L-LL/SD (see Figure 2-2 (c)), and L-SL/LD (see Figure 2-2 (e)), higher aspect ratio CNTs (i.e., longer and smaller diameter CNTs; L-LL/SD) outperforms in the

flexural strength. Different contributions of CNT properties (e.g., length, diameter, aspect ratio, and concentration) to the mechanical properties are discussed in details in Chapter 4.

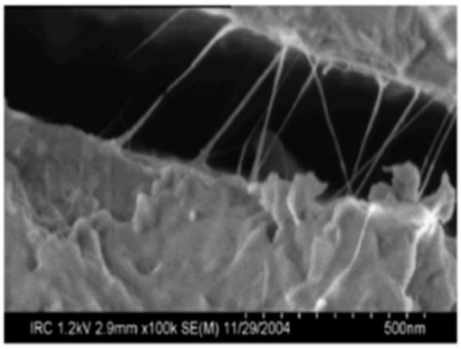

Figure 2-3. CNT crack bridging and pullout along the fracture surface within the cement matrix [72]

2.6.2. Existing Models

This section explains the theoretical background of the most widely used models to predict the tensile/flexural strength (Section 2.6.2.1) and elastic modulus (Section 2.6.2.2) of nanocomposites containing CNTs. Meanwhile, these models were previously used to predict the flexural strength and elastic modulus of concrete reinforced with short discrete fibers [123-125].

2.6.2.1. Flexural Strength

The tensile/flexural strength is characterized by the fracture mechanism which is determined by many important parameters such as interfacial shear strength, stress concentration, and defect size/spatial distributions [126]. Thus, there is yet no generally accepted theory in the literature [126].

Kelly-Tyson theory [102] which is the extension of the well-known rule of mixtures is extensively used to predict the tensile strength of brittle and ductile materials containing CNTs including polymers, metals, and ceramics [105, 106, 108, 109, 127-130]. In addition,

Kelly-Tyson theory was used to predict the flexural strength of concrete reinforced with short discrete fibers [123, 124]. Figure 2-4 shows the flowchart of the development of Kelly-Tyson model. There are 5 steps to develop Kelly-Tyson equation to predict the flexural strength of cementitious materials reinforced with CNTs. A brief description of each step is presented in this section.

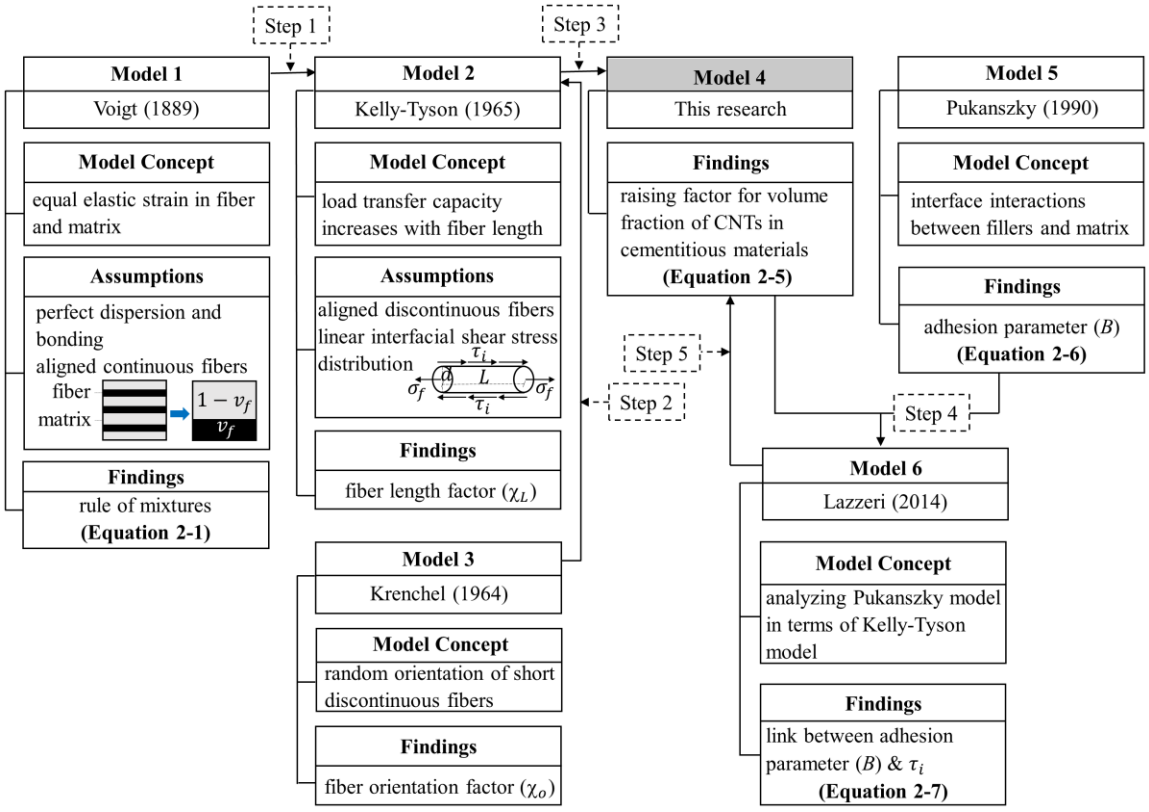

Figure 2-4. Development of Kelly-Tyson model

Note: The highlighted area (model 4) is selected for this research

For condition of equal elastic strain in fiber and matrix, the rule of mixtures (see Model 1 in Figure 2-4) is considered as the simplest way to model the tensile strength of composites reinforced with aligned continuous fibers [131]:

$$\sigma_c = \sigma_f v_f + \sigma_m (1 - v_f) \tag{2-1}$$

where σ_c is the ultimate tensile strength of the composite (*MPa* or *psi*), σ_f is the tensile strength of the fiber (*MPa* or *psi*), σ_m is the tensile strength of the matrix at ultimate strain

of the composite (*MPa* or *psi*), and v_f is the volume fraction of the fiber (unitless). To consider the contribution of randomly oriented short discrete fibers, Equation 2-1 can be modified as shown in step 2 of Figure 2-4 to include the fiber length (χ_L: Model 2 in Figure 2-4) and orientation (χ_o: Model 3 in Figure 2-4) factors:

$$\sigma_c = \chi_o \chi_L \sigma_f v_f + \sigma_m (1 - v_f) \tag{2-2}$$

In Model 2, Kelly and Tyson [102] extended the rule of mixture for aligned discontinuous fibers by assuming linear interfacial shear stress distribution along the fiber length. The applied load is transferred to fibers through shear stresses at the interface of the fiber and matrix. Then, shear stresses are developed from the ends of the fibers toward their midpoints. Kelly and Tyson [102] developed the length factor (χ_L) for fibers having lengths shorter (subcritical) or longer (supercritical) than the fiber critical length (L_c) to determine the mode of failure: fiber fracture or pullout. According to the Kelly-Tyson theory [102], there is a transfer length of half the critical length of fibers ($0.5L_c$) over which the interfacial shear stress (τ_i) in a fiber increases up to its maximum value (i.e., $\tau_{max} = \sigma_f$). Thus, the strength of composites significantly depends on L_c. Using the equilibrium conditions, L_c can be obtained:

$$L_c = \frac{\sigma_f d}{2\tau_i} \tag{2-3}$$

where d is the fiber diameter (*mm* or *in.*). If the fiber length (L) is smaller than L_c (*mm* or *in.*), fiber will pull out of the matrix (see Figure 2-5 (a)). If the fiber length is equal to or greater than L_c, fiber will break (see Figure 2-5 (b) and (c)). Therefore, the tensile strength of composites can be calculated as follows:

$$\sigma_c = \chi_o \left[\sum_{L=0}^{L<L_c} \tau_i \left(\frac{L}{d}\right) + \sum_{L=L_c}^{L} \left(1 - \frac{L_c}{2L}\right) \sigma_f \right] v_f + \sigma_m (1 - v_f) \quad (2\text{-}4)$$

where the first and second terms in the bracket are contributions from fibers with subcritical ($L < L_c$) and supercritical ($L \geq L_c$) length distributions. Assuming CNT tensile strength of 30 *GPa* (4351 *ksi*) [132], the diameter of 25 *nm*, and a very high τ_i = 10 *MPa* (1450 *psi*; see Table 2-1), L_c is estimated to be 37.5 μm (see Equation 2-3) which is generally greater than the length of CNTs within cementitious materials (i.e., $L < L_c$). Therefore, the contribution of CNTs with $L \geq L_c$ might be neglected.

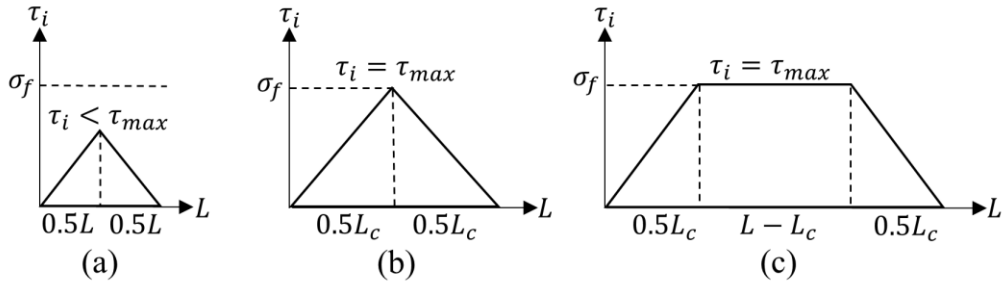

Figure 2-5. Distribution of the stress on a single fiber: (a) $L < L_c$ (b) $L = L_c$ (c) $L > L_c$

In Model 3, to account for the randomness in fiber orientations, the orientation factor (χ_o) can be calculated as $\chi_o = \sum_n a_n \cos^4 \Phi_n$ where a_n is the fraction of fibers having the orientation angle Φ_n with respect to the reference axis [133]. When using aligned fibers, the value of χ_o is one and it is equal to 3/8 and 1/6 for randomly orientated fibers in two and three dimensions, respectively [134]. Due to the nanoscale size of CNTs, they are assumed to be randomly arranged in three dimensions (i.e., $\chi_o = 1/6$) [135-137].

Based on the established database from the literature, the volume fraction of CNTs (v_f) used in cementitious materials ranges between 0.00004 and 0.00128. Therefore, when

using Equation 2-4, the predicted flexural strength of CNT-cement nanocomposites is almost the same as the flexural strength of the matrix. The preliminary study in this research showed that ${v_f}^{2/3}$ is appropriate to fit the data (see step 3 [Model 4] in Figure 2-4). Ahmed *et al*. [138] also found good correlations between $AR^{1/3}(v_f)^{2/3}$ and the improvement in the flexural strength of CNT-cement pastes. The modified form of the Kelly-Tyson equation to predict the flexural strength of CNT-cement nanocomposites can therefore be expressed as follows:

$$\sigma_c = {}^{1}/_{6}\,\tau_i(AR){v_f}^{2}/_{3} + \sigma_m\left(1 - {v_f}^{2}/_{3}\right) \tag{2-5}$$

To predict the flexural strength, τ_i must be quantified. The experimental investigation to measure τ_i is challenging or impractical due to the limitations associated with nanoscale size of CNTs. Therefore, theoretical approaches might be used to determine the interface properties (see step 4 in Figure 2-4).

In Model 5, Pukanszky [104] proposed a semi-empirical equation based on Nicolais-Narkis model [139] to correlate the tensile strength with the interface properties. Pukanszky model have been widely used to characterize the composites containing various nanomaterials including nanoclays, layered silica nanoparticles, and CNTs [105, 140, 141]:

$$\sigma_c = \sigma_m\left[\frac{1 - {v_f}^{2}/_{3}}{1 + 2.5\ {v_f}^{2}/_{3}}\right]e^{B{v_f}^{2/3}} \tag{2-6}$$

where B is the empirical adhesion parameter that reflects the capacity of stress transfer between fillers and matrix, which can be determined using the experimental test results. Using Equation 2-6, Pukanszky adhesion parameters (B) is calculated for the available database from the literature [11, 12, 16, 28, 29, 111-113, 142] and this research. The

minimum, maximum, mean, median, and standard deviation of *B* parameter is shown in Table 2-1.

Table 2-1. Statistics of Pukanszky Adhesion Parameter (*B*) and Interfacial Shear Stress (τ_i)

Parameter	Minimum	Maximum	Mean	Median	Standard deviation
B (unitless)	-7.827	255.9	54.92	44.19	43.85
τ_i (*MPa* [psi])	0.63 [91]	9.28 [1346]	2.98 [432]	1.97 [286]	2.27 [329]

In Model 6, Lazzeri *et al*. [143] stated that τ_i in Kelly-Tyson model [102] could be correlated with *B* in Pukanszky model [104]. Therefore, in this study, τ_i is attained using a relationship between Equations 2-5 and 2-6:

$$\tau_i = \frac{6\sigma_m(B - 2.5)}{AR} \tag{2-7}$$

where all variables were defined in previous equations. To calculate τ_i for each individual data, the average value of the adhesion parameter *B* ($B_{avg} = 54.92$; see Table 2-1) is used as a representative value for adhesion between CNTs and cement matrix. The statistics of τ_i between CNTs and cement matrix is presented in Table 2-1. In step 5 (see Figure 2-4), the estimated values of τ_i is used to predict the flexural strength using Equation 2-5.

2.6.2.2. Elastic Modulus

Different models have been developed to predict the elastic modulus of fiber reinforced composites such as Cox model [144], Mori-Tanaka model [145], and Halpin-Tsai model [103].

Cox [144] explained the reinforcing effect of short discrete fibers using the shear-lag theory. This model considers short aligned fibers fully embedded in a continuous matrix and assumes that no stress is transferred through the fiber ends. Considering the rule of mixtures, the longitudinal elastic modulus of composites can be derived. However, because

of the neglect of the stress transfer through the fiber ends, Cox model may result in inaccurate prediction of the elastic modulus [146, 147].

Mori-Tanaka model [145] is an effective field approximation based on the Eshelby theory. The main assumption of Mori-Tanaka model is that the average strains of inclusion and matrix are related to each other by a fourth order tensor. Also, the composite is subjected to uniform strain at infinity. Mori-Tanaka model calculates the average internal stress in composites containing different inclusions (e.g., fibers, particulates, etc.) with transformation strain. Also, the average elastic energy is considered allowing the interaction between the inclusions with the effect of the presence of the free boundary. To predict the elastic modulus using Mori-Tanaka model, three-dimensional elastic parameters of both matrix and inclusion are required.

Amongst various models, the Halpin-Tsai model is the most widely used method to predict the elastic modulus of composites because of its simplicity and relative high accuracy [148]. The Halpin-Tsai model has been extensively used to predict the elastic modulus of brittle and ductile materials containing CNTs such as polymers, metals and ceramics [128-130, 132, 149]. Also, the Halpin-Tsai model was used to evaluate the effective elastic moduli of steel-fiber reinforced concrete [125].

The Halpin-Tsai model [103] is a semi-empirical equation based on the work of Hill [150] that evaluates the elastic modulus of composites in terms of the equivalent fiber and matrix by taking into account the volume fraction of fibers and their geometry (i.e., shape and dimensions). The flowchart of the development of the Halpin-Tsai model is shown in Figure 2-6. There are four steps to develop the Halpin-Tsai model to predict the elastic modulus of composites reinforced with randomly oriented short discrete fibers.

Each step (model) has its own assumptions and findings to further simplify the previous researchers' findings. A brief description of each model is discussed below.

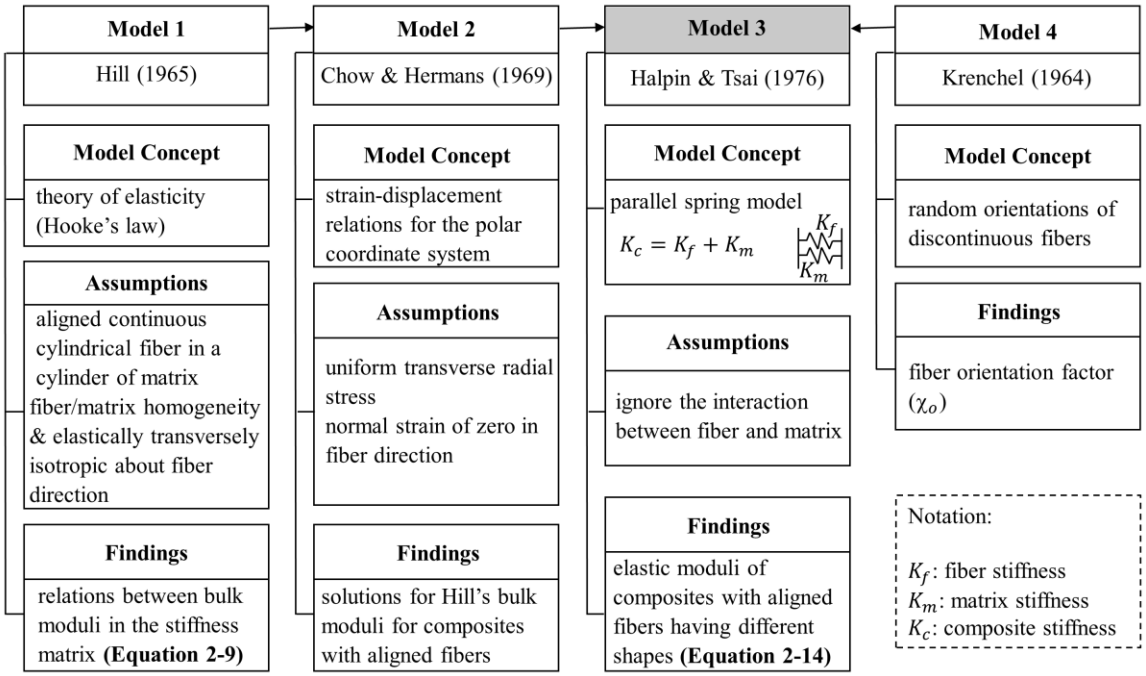

Figure 2-6. Development of Halpin-Tsai model

Note: The highlighted area (model 3) is selected for this research

In the first model, Hill [150] assumed a single cylindrical fiber was embedded in a cylinder of matrix and both of them were homogeneous and elastically transversely isotropic about the fiber direction (z direction). The stiffness matrix for elastically transversely isotropic materials has only five independent constants which can be correlated with Hill's notations of n, l, k, m, and μ [150]:

$$\begin{Bmatrix} \bar{\sigma}_z \\ \bar{\sigma}_x \\ \bar{\sigma}_y \\ \bar{\sigma}_{xy} \\ \bar{\sigma}_{yz} \\ \bar{\sigma}_{xz} \end{Bmatrix} = \begin{bmatrix} n & l & l & 0 & 0 & 0 \\ l & k+m & k-m & 0 & 0 & 0 \\ l & k-m & k+m & 0 & 0 & 0 \\ 0 & 0 & 0 & m & 0 & 0 \\ 0 & 0 & 0 & 0 & \mu & 0 \\ 0 & 0 & 0 & 0 & 0 & \mu \end{bmatrix} \begin{Bmatrix} \bar{\varepsilon}_z \\ \bar{\varepsilon}_x \\ \bar{\varepsilon}_y \\ 2\bar{\varepsilon}_{xy} \\ 2\bar{\varepsilon}_{yz} \\ 2\bar{\varepsilon}_{xz} \end{Bmatrix} \quad (2\text{-}8)$$

where n is the elastic modulus for longitudinal uniaxial straining, l is the associated cross modulus, k is the plain strain bulk modulus for lateral dilatation without longitudinal extension, m is the transverse shear modulus, μ is the longitudinal shear modulus, $\bar{\sigma}_{ij}$ is the average stress, and $\bar{\varepsilon}_{ij}$ is the average strain. Using the theory of elasticity (Hooke's law), Hill [150] showed that bulk moduli ($n, l,$ and k) are related to each other as expressed in Equation 2-9:

$$\frac{k_c - k_f}{l_c - l_f} = \frac{k_c - k_m}{l_c - l_m} = \frac{l - v_f l_f - (1 - v_f) l_m}{n - v_f n_f - (1 - v_f) n_m} = \frac{k_f - k_m}{l_f - l_m} \tag{2-9}$$

where the subscripts c, f, and m correspond to composite, fiber, and matrix, respectively.

In the second model, Chow and Hermans [151] proposed a solution in terms of Hill's bulk moduli for composites with aligned continuous cylindrical fibers with radius *a* embedded in a cylinder of matrix having radius *R* (see Figure 2-7).

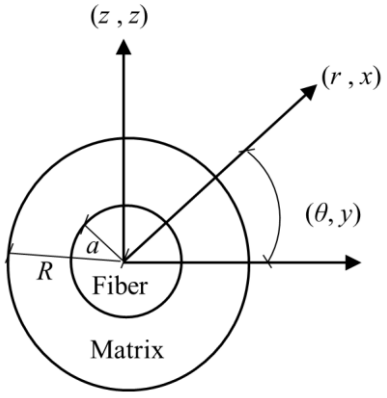

Figure 2-7. Relationship between Cartesian and Polar coordinate systems

Chow and Hermans [151] assumed that uniform transverse radial stress (*S*) is applied and the normal strain in the fiber direction ($\bar{\varepsilon}_z$) was kept equal to zero by applying the necessary normal stress ($\bar{\sigma}_z$) in the fiber direction (see Model 2 in Figure 2-6). Under these assumptions and because shear stresses and strains for axisymmetric response are

zero (there is symmetry about θ), the radial displacement for fiber and matrix might be expressed as follows:

$$\begin{cases} u_f = A_f r & ; \quad 0 < r < a \\ u_m = A_m r + \dfrac{B_m}{r} & ; \quad a < r < R \end{cases} \tag{2-10}$$

where u_f and u_m are radial displacements of fiber and matrix, respectively, r is radius, A and B are constants. Using $S = 2k_c A$ (at $r > R$) and radial strain of $\bar{\varepsilon}_r + \bar{\varepsilon}_\theta = 2A_f v_f + 2A_m(1 - v_f)$, Chow and Hermans [151] proposed the average stress of the unit volume of the composite as follows:

$$k_c = \frac{k_m(k_f m_m)(1 - v_f) + k_f(k_m + m_m)v_f}{(k_f + m_m)(1 - v_f) + (k_m + m_m)v_f} \tag{2-11}$$

$$m_c = m_m \frac{2v_f m_f(k_m m_m) + 2(1 - v_f)m_m m_m + (1 - v_f)k_m(m_f + m_m)}{2v_f m_m(k_m m_m) + 2(1 - v_f)m_f m_m + (1 - v_f)k_m(m_f + m_m)} \tag{2-12}$$

$$\mu_c = \frac{\mu_f + \mu_m[\mu_m(1 - v_f) + 2\mu_f \mu_m v_f]}{\mu_f + \mu_m(1 - v_f) + 2\mu_m v_f} \tag{2-13}$$

Later, Halpin and Tsai [103] further simplified Chow and Herman's solution [151] using engineering constants such as E and G with the extension of its applicability to various fiber geometries (see Model 3 in Figure 2-6). Halpin and Tsai used the parallel spring model (i.e., the stiffness of the composite is the summation of the fiber and matrix stiffness) and neglected the interaction between fiber and matrix due to the differences in their Poisson's ratio. The general form of the Halpin-Tsai model is as follows [103]:

$$E_c = \frac{1 + \xi E_{f'} v_f}{1 - E_{f'} v_f} E_m \tag{2-14}$$

where E_c is the elastic modulus of the composite (GPa or ksi), E_m is the elastic modulus of the matrix (GPa or ksi), ξ is the measure of fiber geometry (for cylindrical fibers, $\xi = 2\,{}^{L}/_{d}$), and $E_{f'}$ is the equivalent elastic modulus of fiber. The equivalent elastic modulus of randomly oriented short discontinuous fibers can be expressed as:

$$E_{f'} = \frac{\chi_o \frac{E_f}{E_m} - 1}{\chi_o \frac{E_f}{E_m} + \xi} \tag{2-15}$$

where χ_o is the fiber orientation factor (see Model 4 in Figure 2-6) and E_f is elastic modulus of the fiber (GPa or ksi). Note that the value of χ_o is one for aligned fibers (original Halpin-Tsai equation; see Model 3 in Figure 2-6).

Because both Kelly-Tyson and Halpin-Tsai models assume perfect dispersion and bonding (i.e., the models disregard improper CNT dispersion and inadequate adhesion between CNTs and matrix), mechanical properties increase as AR and/or v_f increases. Nevertheless, because of the inherent fabrication difficulties (e.g., dispersion and bonding issues), experimental studies exhibit nonlinear behavior: the mechanical properties increase as AR and/or v_f increases up to certain limits, beyond which mechanical properties degrade. To correct this bias and to capture the mechanisms of CNTs within cementitious materials (e.g., effect of CNT concentration on the rate of cement hydration), other important variables and their interactions must be considered (see Section 4.10).

2.7. Durability of CNT-Cement Nanocomposites

During their service life, concrete structures are exposed to physical and chemical attacks such as freeze and thaw action (Section 2.7.1), corrosion of steel reinforcement bars (Section 2.7.2), thermal resistivity (Section 2.7.3), and alkali-silica reaction (Section 2.7.4).

These attacks deteriorate the structural capacity of both concrete and reinforcement over time. CNTs were found to be effective in refining the pore structure of cementitious composites, if selected from the optimum size and concentration (see Section 2.4.2). A reduction in total porosity and pore sizes as well as disconnecting the capillary pores by adding CNTs improves the microstructure [11, 152]. Consequently, CNT-cement nanocomposites exhibit lower permeability which alleviates problems associated with durability.

2.7.1. Freeze and Thaw Action

Refined pore structures of cementitious composites by adding CNTs may result in improved freeze and thaw resistance. Li *et al*. [32] investigated the effect of 0.3 *c-wt*% of CNTs on the compressive strength of cement mortars subjected to 30, 60, and 90 cycles of frost action. They observed the lower rate of degradation in compressive strength of cement mortars containing CNTs. Addition of CNTs improved frost resistance by reducing the volume of pores bigger than 200 *nm*. Yakovlev *et al*. [153] also reported the increase in the frost resistance of concrete from 150 to 400 cycles using CNTs.

Wang *et al*. [154] studied the influence of CNTs to frost action resistance of concrete using three different surfactants: methylcellulose, silane, and sodium polyacrylate. They observed that CNT-concrete specimens using silane and sodium polyacrylate as surfactants exceeded 300 cycles due to their reduced permeability. Using methylcellulose, however, exhibited surface scaling and the failure of the specimens after 150 cycles. This might be attributed to the reduction in the coefficient of thermal expansion [155, 156]. Also, the increase in CNT concentration from 0.5 to 1 *c-wt*% did not improve frost resistance, which could be related to their poor dispersion within the cement matrix.

2.7.2. Corrosion of Steel Reinforcement Bars

The concentration of CNTs seems to be one of the most important factors to influence the corrosion of steel reinforcement bars. CNT concentration affects the permeability and electrical conductivity of CNT-cement nanocomposites. The high concentration of CNTs can increase the permeability and the galvanic coupling effect between steel reinforcement bars and nanotubes, expediting the corrosion rate. Lu *et al*. [26] studied the chloride permeability of ultrahigh strength concrete containing CNTs ranging from 0.03 to 0.15 *c-wt*%. The chloride diffusion coefficient decreased by 24% in concrete containing 0.05 *c-wt*% CNTs, compared with the plain concrete. However, the concentration of 0.15 *c-wt*% increased the diffusion coefficient by 14%.

Shah *et al*. [33] carried out half-cell potential tests to study the corrosion status of steel reinforcement bars for 65 days in cement mortars with 0.1 and 0.5 *c-wt*% of CNTs. The plain cement mortar entered the active corrosion zone at 25 days after casting. The addition of 0.5 *c-wt*% CNTs showed entering to the active corrosion zone at 46 days after casting. The cement mortars containing 0.1 *c-wt*% CNTs, however, did not enter the active corrosion area, indicating the prevention of the penetration of chloride ions.

Camacho *et al*. [27] also studied the influence of different contents of CNTs ranging from 0.05 to 0.5 *c-wt*% on the corrosion rate of steel bars in cement pastes. They observed that the initiation time of active corrosion was shorter for cement pastes containing various concentration of CNTs, resulting from the high level of porosity. Also, the corrosion rate increased at higher concentration of CNTs.

2.7.3. Thermal Resistivity

CNT are thermally stable up to certain temperatures depending on their level of lattice disorders. Pristine CNTs were found to start decomposition at 420 ℃ (788 °F) in the air [157], while COOH-CNTs started to decompose at the temperature of 180 ℃ (356 °F) [117]. Thus, presence of CNTs seems to increase the thermal resistivity of concrete. Besides, densification of cement matrix and nucleation effects due to the presence of CNTs might contribute to higher thermal resistivity.

Kim *et al*. [18] measured the compressive strength of both non-heated and cyclically self-heated (up to around 70 ℃ [158 °F]) cement pastes containing CNTs ranging from 0.3 to 2 *c-wt*%. They observed the increase in compressive strength of heated nanocomposites up to 1 *c-wt*% CNTs, compared with the control specimen. This might be attributed to the additional formation of hydration products that was confirmed by TGA. On the other hand, the compressive strength of heated cement paste containing 2 *c-wt*% CNTs was found to be lower than the non-heated specimen. This could be explained by the extension of internal cracks causing by the excessive amount of CNTs [20].

Amin *et al*. [158] also studied the effect of various concentrations of CNTs (0.02-0.2 *c-wt*%) on the thermal resistivity of cement pastes. The specimens were subjected to three high temperatures of 300 ℃ (572 °F), 600 ℃ (1112 °F), and 800 ℃ (1472 °F) for 3 hours. All CNT-cement pastes exposed to 300 ℃ (572 °F) showed the higher residual compressive strength (compressive strength at certain temperatures over compressive strength at room temperature. This was attributed to the internal autoclaving procedure of the pores filling by further hydration products when using CNTs. The maximum residual compressive strength at 300 ℃ (572 °F) was observed for cement paste incorporating 0.1

c-wt% CNTs, which also had the highest compressive strength at room temperature of 25 ℃ (77 °F). The residual compressive strength at 300 ℃ (572 °F) was 1.41 and 1.20 for CNT-cement pastes containing 0.1 *c-wt*% CNTs and control specimen, respectively. However, for both 600 ℃ (1112 °F) and 800 ℃ (1472 °F) exposure temperatures, the residual compressive strengths of CNT-cement pastes did not exhibit further improvement than the control specimen. This was attributed to the decomposition of CH and C-S-H at 450-500 ℃ (842-932 °F) [159, 160] and 800-900 ℃ (1472-1652 °F) [160], respectively, which increased the porosity and crack formation within the cement pastes.

2.7.4. Alkali-Silica Reaction

Alkali-silica reaction (ASR) is a detrimental chemical process between alkali hydroxides in the pore solution and a reactive form of silica in aggregates (e.g., amorphous silica, cryptocrystalline quartz, opal, etc.). This reaction creates alkali-lime-silica gel (referred to as ASR gel) [160] which absorbs moisture from the air. The ASR gel swells by taking up water, producing tensile stresses in the concrete, which eventually results in cracking. This leads to the loss in strength, stiffness, and other durability characteristics. The potential mechanisms of CNTs to control ASR can be classified into two main categories: mechanical and chemical mechanisms.

CNTs can reduce the permeability of cementitious materials through decreasing the porosity and refining the pore structure [25, 99]. This mitigates the easy transportation of the external alkali ions to the interior of concrete, reducing the rate of ASR [161]. Also, the increase in tensile strength of cementitious materials through controlling the crack propagation by adding CNTs [28, 31] might be considered as another mechanical contribution of CNTs to control ASR expansion.

The presence of CH was found to be essential for the formation of ASR gel [162, 163]. In terms of the chemical mechanism, previous research has shown that addition of CNTs in concrete lowered the amount of CH and pH value (alkalinity) of concrete pore solution [164]. As a result, aggregate dissolution rate might decrease. Also, reduced amount of CH changes the C-S-H gel structure and decreases its porosity, hindering the formation of ASR gel [165]. Besides, the presence of COOH or OH functional groups covalently bonded to the surface of CNTs (chemical functionalization) might engage with C-S-H [98], limiting their polymerization and branching [166]. This phenomenon may reduce the ion diffusion within the cement hydrates, suppressing the rate of ASR.

To the author's best knowledge, there is yet no study regarding the influence of CNTs on the properties of ASR-affected cement mortars. Therefore, this research evaluates the influence of CNTs on mitigating ASR-induced damages in cement mortars, presented in Section 6.4.

2.8. Dimensional Stability

Concrete structures undergo time-dependent deformations due to the ambient temperature/moisture. The early volumetric changes can cause the formation of cracks in the hardened concrete which are detrimental to both mechanical and durability properties. Voids smaller than 50 *nm* in diameter (referred to as micro-pores) play important roles in determining shrinkage and creep [99], due to their significant capillary forces [160]. Hu *et al*. [99] observed that CNTs could significantly reduce the number of micro-pores. Therefore, addition of CNTs might help to reduce the dimensional stability. This section discusses the influences of CNTs on shrinkage (Section 2.8.1) and creep (Section 2.8.2) of CNT-cement nanocomposites.

2.8.1. Shrinkage

This section discusses the influence of CNTs on the autogenous (Section 2.8.1.1) and drying (Section 2.8.1.2) shrinkage.

2.8.1.1. Autogenous Shrinkage

Autogenous shrinkage is the change in the volume of a young concrete as a result of the surface tension in capillaries due to the chemical shrinkage progress during cement hydration [160]. And, it was found to be directly proportional to the volume fraction of fine pores in cement matrix [167, 168]. Because CNTs were found to reduce the amount of micro-pores [99, 152], they can control the autogenous shrinkage with appropriate type and amount of CNTs. The efficient dispersion of CNTs reduces the amount of fine pores by filling the areas in between the C-S-H gel. This results in the reduction of autogenous shrinkage.

Konsta-Gdoutos *et al*. [11] carried out experimental tests on the autogenous shrinkage of cement pastes to assess the potential influence of CNTs on the early strain capacity of the samples. The addition of CNTs greatly decreased the autogenous shrinkage of cement pastes by up to about 40%. Blandine *et al*. [169] varied the concentrations of CNTs ranging from 0.005 to 0.1 *c-wt*% within cement pastes. They found that increasing in CNT concentration resulted in higher autogenous shrinkage. They also investigated the influences of both acid treated and untreated CNTs on the autogenous shrinkage and observed reduction in autogenous shrinkage by incorporation both acid treated and untreated CNTs, compared with the control specimen. Meanwhile, the reduction in the rate of the autogenous shrinkage was more pronounced when using untreated CNTs. However, Hawreen *et al*. [170] observed that incorporating either acid treated or untreated CNTs led

to autogenous shrinkage reduction and shrinkage dependency to the type of CNTs was negligible. They reported that incorporation of 0.05 to 0.1 *c-wt*% CNTs reduced the early shrinkage by 62%.

2.8.1.2. Drying Shrinkage

Hardened concrete undergoes contraction due to the removal of physically adsorbed water molecules from C-S-H when exposed to less than 100% relative humidity (RH). Addition of CNTs can decrease the amount of pores acting as evaporation paths for moisture migration to the environment, reducing the drying shrinkage.

Li *et al*. [32] examined the effect of 0.3 *c-wt*% of CNTs on drying shrinkage of cement mortars. The beam specimens were placed in a drying room with a temperature of 20 ℃ (68 ℉) and RH of 50%. After 6 days of curing, cement mortars containing CNTs were found to considerably decrease the evaporation of water from the specimens, reducing the drying shrinkage by 32%. Isfahani *et al*. [171] investigated the effect of pristine and COOH functionalized CNTs on drying shrinkage of cement pastes. They reported about 15% reduction of drying shrinkage when utilizing 0.1 *c-wt*% COOH functionalized or 0.3 *c-wt*% pristine CNTs.

2.8.2. Creep

Creep is regarded as the gradual increase in strain over time under a sustained stress [160]. Similar to the shrinkage, the source of creep is the hydrated cement paste, while aggregates restrict the dimensional variations. In addition, creep is inversely proportional to the strength and stiffness of concrete. Because CNTs can densify the cement paste microstructure through filling the micro-pores [99, 152], as well as controlling the micro-crack propagation through their bridging ability, they are expected to affect the source of

the creep. Therefore, CNTs might reduce the creep. However, the knowledge on the creep behavior of CNT-cement nanocomposites is very limited.

Ahmed *et al*. [172] measured the total creep (the summation of drying creep and basic creep) of concrete reinforced with different types (COOH-functionalized and pristine) and concentrations (0.05-0.1 *c-wt*%) of CNTs. The results indicated that incorporating CNTs, regardless of their type, decreased the total creep at one year by about 18%, compared with the control concrete specimen.

2.9. Summary

The improvements in flow, mechanical, and durability properties of CNT-cement nanocomposites can be explained by different mechanisms. CNT nucleation effect expedites hydration process and creates high-density hydration product regions. Also, CNTs refine the pore structures by filling them up and act as a bridge in the cement matrix to hamper crack propagation by absorbing part of the energy. To date, most researchers focused on CNT contribution to the mechanical properties and microstructure of CNT-cement nanocomposites. Recent studies showed improved mechanical properties, lower permeability, and reduced pore size distribution of cementitious materials after adding CNTs. This might improve the durability characteristics of CNTs such as freeze and thaw, alkali-silica reaction, and corrosion of steel reinforcement bars.

However, improvement of any property in CNT-cement nanocomposites depends on CNT dispersion quality. Various methods have been introduced in which pre-dispersion of CNTs in water using a surfactant-assisted ultrasonication process is the most common route. Meanwhile, compatibility of surfactants with cement hydration products must be considered. Poly-carboxylate based superplasticizers have been used in a broad range of

research due to their ability to disperse CNTs and compatibility with cement hydration process. Also, Poly-carboxylate based superplasticizers could help to overcome the low flowability of CNT-cement nanocomposites.

In addition to the dispersion procedure, CNT properties such as length, diameter, and its concentration play important roles in determining both the dispersion quality and the properties of concrete. Smaller CNTs, even if clumped, are still capable of filling the bigger pores into smaller pore sizes (smaller than 50 *nm*), benefiting the compressive strength and dimensional stability. Conversely, in case of a poor dispersion (i.e., CNT agglomerations), larger CNTs produce bigger pore sizes (larger than 50 *nm*), deteriorating the mechanical and durability properties. Therefore, optimization of CNT properties is of great importance. Besides, understanding the interactions between experimental variables is crucial to determine the mechanical properties. Due to the complex dispersion procedure and multiple interactions, there is yet no prediction model available in the literature that can be reliably used to evaluate the mechanical properties of CNT-cement nanocomposites.

CHAPTER 3. MODEL DEVELOPMENT STRATEGY: OVERVIEW

3.1. General

Many studies have been investigated the contribution of CNTs to the mechanical properties of cementitious materials [16, 23, 28, 30, 64, 138, 173]. A number of methodologies have been proposed to attain the superior improvement in mechanical properties using various combinations of the influential variables including CNT type [16, 23, 28, 174], its concentration (or volume fraction) [30, 138], dispersion procedure [12, 94], water-to-cement (*w/c*) ratio [170], sand-to-cement (*s/c*) ratio [16, 28], and age of specimen [31, 174]. Despite the ongoing research efforts, there is a major obstacle in efforts to utilize CNTs for practical applications [20, 175]. This might be attributed to the interactions between the experimental variables which makes it challenging to predict the mechanical properties.

Few researchers tried to include some of these interactions in prediction models. Hassan *et al*. [174] used response surface methodology to estimate the mechanical properties using different variables including dispersion procedure, testing age, and CNT concentration. The results revealed strong interactions between some variables. Ahmed *et al*. [138] proposed an equation to correlate the flexural strength of cement pastes containing CNTs with CNT aspect ratio (*AR*) and volume fraction (v_f). They found good correlations between $AR^{1/3}(v_f)^{2/3}$ and the improvement in the flexural strength. However, the existing models were developed using limited data, and they did not include the interactions between most important variables. Therefore, the main objective of this study is to propose

appropriate models to capture the interactions between important variables to predict the mechanical properties (flexural strength and elastic modulus).

3.2. Model Development

Figure 3-1 shows the flowchart of the overall procedure for developing the prediction models. The flowchart consists of four phases as discussed below.

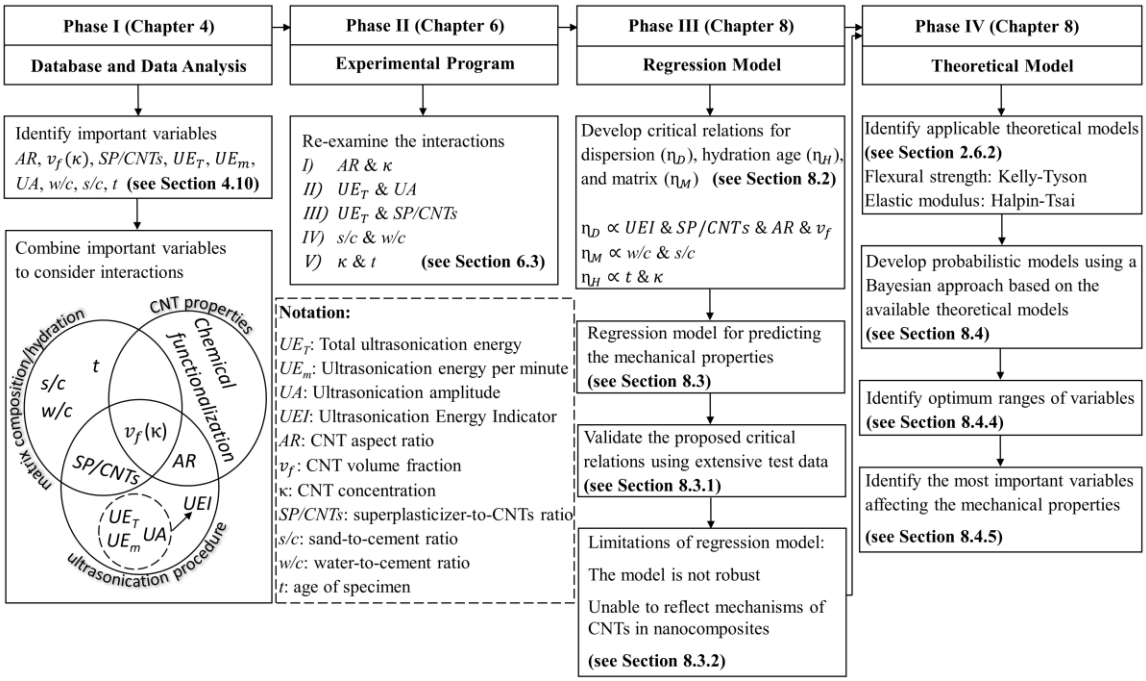

Figure 3-1. The overall procedure for predicting the mechanical properties

In Phase I (see Section 4.10), extensive literature data was analyzed to identify the most important variables and the interactions between them affecting the mechanical properties. The relationships between the most important variables are categorized into three groups of CNT properties, ultrasonication procedure, and matrix composition/hydration. These three groups can be visualized as circles in the Venn diagram. For example, the right circle in the Venn diagram represents the investigated variables related to CNT properties (AR, v_f (or CNT concentration; κ), and surface condition (herein, chemical functionalization)). In addition, since AR and v_f (κ) are also

important for ultrasonication procedure, they are placed in overlapping regions. Concerning CNT chemical functionalization, previous studies [28, 170] reported that the impact of chemical functionalization on the mechanical properties was minimal compared with other CNT properties (AR, v_f (or κ)). Therefore, in this research, CNT chemical functionalization was not considered as an important variable in the modeling process.

In Phase II (see Section 6.3), an experimental study is conducted to re-examine the main interactions between the studied variables affecting the mechanical properties.

In Phase III, using the findings of Phase I and Phase II, three analytical relations are developed to include the studied interactions (dispersion relation (η_D), matrix relation (η_M), and hydration age relation (η_H); see Section 8.2). Then, a simple regression model is used to predict the mechanical properties and validate the applicability of the proposed relations using extensive experimental test data from this research and the literature (see Section 8.3.1). Nevertheless, the regression model has limitations of the application (see Section 8.3.2): it does not reflect the mechanisms of CNTs affecting the mechanical properties (e.g., if CNTs are uniformly dispersed and there is perfect bonding, the mechanical properties increase as v_f and/or AR increases). In addition, the regression model is not robust to reliably predict the mechanical properties of new dataset.

In Phase IV, to overcome the limitations of the regression model, the proposed analytical relations will be added to available theoretical models in the literature (see Section 2.6.2) to predict the mechanical properties of CNT-cement nanocomposites. Also, due to the high degree of uncertainty while incorporating CNTs (e.g., amount of structural defects on CNT surface, number of walls, material properties, etc.), the models are formulated in a probabilistic manner to correct the effect of each variable on the mechanical

properties (see Section 8.4). The probabilistic models are then used to identify the optimum ranges of variables to maximize the mechanical properties (see Section 8.4.4). Finally, sensitivity and importance analyses are performed to determine the most important variables to affect the mechanical properties (see Section 8.4.5).

3.3. Summary

The logical procedure of developing the probabilistic models was presented in four phases. In Phase I, the primary variables and their interactions were identified for specific equations using previous researchers' findings. In Phase II, because the most possible relations between variables could not be captured using a single experimental test program of previous studies in the literature, a new experimental program was designed with selected variables for each specific equation and using fixed values of other potential variables. The test program can confirm the previous findings and addressed contradicting results. In Phase III, based on extensive experimental results from this research and the literature, analytical equations were proposed to find the relations between the experimental variables and their influence on the mechanical properties. Finally, in Phase IV, the proposed critical relations were added to available theoretical models in the literature to predict the studied mechanical properties (flexural strength and elastic modulus). The proposed models can provide valuable information for future researchers and engineers to incorporate CNTs within cementitious materials.

CHAPTER 4. ANALYZING THE MECHANICAL PROPERTIES OF CNT-CEMENT NANOCOMPOSITES: DATABASE AND STATISTICAL ANALYSIS*

4.1. General

This chapter provides a database from the available literature and identifies the optimum ranges of CNT properties (length, diameter, aspect ratio, and concentration) for improving compressive strength, flexural strength, elastic modulus, and toughness. To do this, Section 4.2 discusses the influence of various dispersion techniques on the strength. Section 4.3 identifies the important variables concerning CNT intrinsic properties affecting the mechanical properties and provides data distribution. Section 4.4 discusses the approach used for data analysis. Sections 4.5 and 4.6 present the influence of CNT properties on the strength and dispersion quality, respectively. Also, the detailed analysis of identifying different ranges for each CNT property in terms of compressive strength (Section 4.7.1) and flexural strength (Section 4.7.2) are presented. Then, the influences of CNT properties on the elastic modulus and toughness are discussed in Sections 4.8 and 4.9, respectively. Finally, Section 4.10 discusses the influences of other important variables and their interactions affecting the dispersion quality and the mechanical properties.

* The main part of this chapter is published in Magazine of Concrete Research
Ramezani, M., Kim, Y.H., and Sun, Z. "*Mechanical Properties of Carbon Nanotube Reinforced Cementitious Materials: Database and Statistical Analysis*." Magazine of Concrete Research (2019): 1-24

4.2. Effect of Dispersion Technique on the Strength

Through extensive literature review, six representative dispersion techniques have been identified to exploit the superior physical and mechanical properties of CNTs within cementitious materials (see Section 2.3). Figure 4-1 shows the boxplots of the percent change in compressive and flexural strengths of CNT-cement nanocomposites compared with the respective control specimens (i.e., without CNTs) for different dispersion techniques. The boxplots demonstrate median, first and third quartiles, minimum and maximum values, and the outliers (see Figure 4-1 (b)). A data is considered to be an outlier if it lies "1.5 × interquartile range" below the first quartile or above the third quartile.

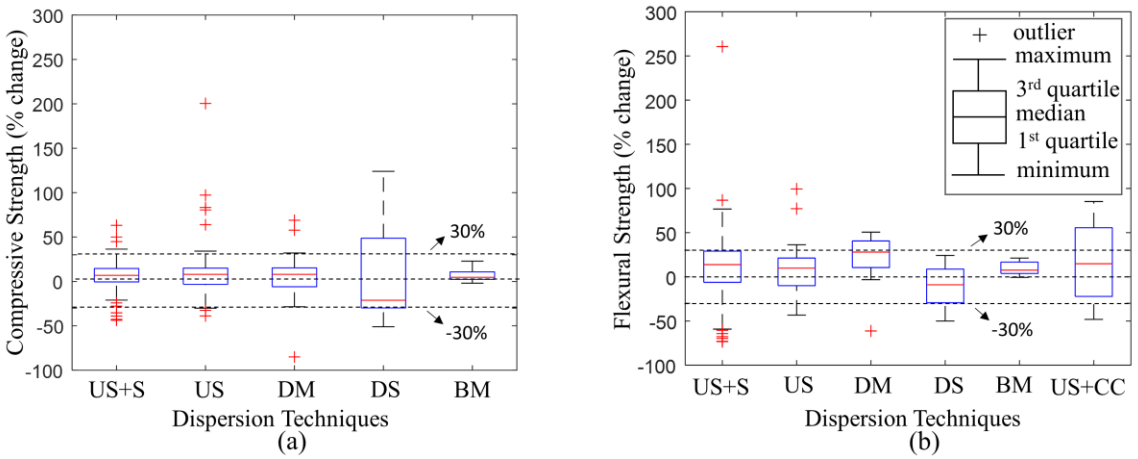

Figure 4-1. Influence of different dispersion techniques: (a) compressive strength (b) flexural strength

Note: US+S: pre-dispersion of CNTs in water using a surfactant assisted ultrasonication procedure, US: pre-dispersion of CNTs in water using an ultrasonication procedure without surfactant, DM: dry mix of CNTs and cement, DS: direct synthesis of CNTs onto the surface of cement or mineral admixtures, BM: ball milling, US+CC: dispersion of CNTs in cement via ultrasonication process

Also, Table 4-1 summarizes the influence of various dispersion techniques on the compressive and flexural strengths. The median values of the percent change in compressive and flexural strengths using various dispersion techniques are all positive, except for the DS method that exhibits the median values of -21% and -9% for compressive

strength and flexural strength, respectively.

Although the boxplots did not show a noticeable difference between various dispersion methods, the analysis of variance is used to statistically confirm the observed trends. The analysis of variance (ANOVA) which determines whether there are significant differences between the means of different groups is used to investigate the influence of various dispersion techniques on the compressive and flexural strengths. The probability value (p-value) is used to determine the significance of the analysis. If p-value ≤ 0.05, there is a significant difference between the groups. Table 4-2 compares the p-values of different dispersion techniques for compressive (f_{CS}) and flexural (f_{FS}) strengths. For example, for f_{CS}, the p-value of US+S compared with the US dispersion technique is 0.316, indicating no significant differences between these techniques in terms of increasing the compressive strength. When using the DS method, most of the p-values are close to 0.05 for f_{FS}. This might be explained by direct influences of several factors (e.g., substrate material, inert gas, their flow speed rate, catalyst, and applied temperature), resulting in high variations in CNT concentration from 0.3 [75] to 20 *c-wt%* [76, 78]. This is the primary reason for the high variations in compressive and flexural strengths using the DS dispersion method (see Figure 4-1).

Table 4-1. Effect of Dispersion Techniques on f_{CS} and f_{FS}

Dispersion technique	Number of studies	Compressive strength (f_{CS}; % change)						Flexural strength (f_{FS}; % change)					
		#>0	#<0	Min.	Max.	Avg.	Med.	#>0	#<0	Min.	Max.	Avg.	Med.
US+S	27	104	41	-44	63.2	5.9	6.8	108	44	-73.3	260.6	10.3	13.8
US	9	44	27	-39	200.4	9.4	7.9	22	13	-43.3	99.4	6.9	9.8
US+CC	1	-	-	-	-	-	-	3	1	-48.1	85.2	16.7	14.8
DM	7	26	12	-85	68.9	5.7	7.9	10	2	-61.3	50.6	20.9	28
BM	2	10	1	-2	22.9	7	4.6	6	1	-0.7	21.2	9.5	7.5
DS	4	12	15	-51	124	8.8	-21	3	7	-50	24.2	-12	-9

Note: #>0: number of observations greater than control specimen, #<0: number of observations lower than control specimen

Table 4-2. ANOVA Results: *p*-Values of Different Dispersion Techniques for f_{CS} and f_{FS}

Dispersion techniques	US+S		US		US+CC		DM		BM		DS	
	f_{CS}	f_{FS}	f_{CS}	f_{FS}	f_{CS}	f_{FS}	f_{CS}	f_{FS}	f_{CS}	f_{FS}	f_{CS}	f_{FS}
US+S	-	-	0.316	0.618	-*	0.744	0.944	0.348	0.834	0.956	0.596	0.068
US			-	-	-*	0.576	0.552	0.173	0.817	0.820	0.945	0.076
US+CC					-	-	-*	0.848	-*	0.735	-*	0.189
DM							-	-	0.860	0.355	0.750	0.012
BM									-	-	0.912	0.041
DS											-	-

Note: f_{CS}: compressive strength and f_{FS}: flexural strength "-" indicates that evaluation is not valid and "-*" indicates the data is not available to perform ANOVA analysis

The ANOVA results suggest that the influence of different dispersion techniques does not significantly contribute to the mechanical properties. However, to achieve a better dispersion, each particular method does have certain steps (or critical factors) that need to be followed. For example, when using the US+S method, the ultrasonication process (energy and amplitude), and surfactant and CNT types and dosages are important variables that would directly contribute to CNT dispersion [88, 176, 177]. Assuming the best efforts were given to achieving a good dispersion of CNTs in the reported studies, this chapter now focuses on the influences of CNT properties on the mechanical properties. More analyses are presented in the following sections.

4.3. Important Variables and Data Distribution

This section first identifies the possible important variables and their interactions affecting the mechanical properties (Section 4.3.1). Then, it provides data distribution used for data analysis (Section 4.3.2).

4.3.1. Important Variables

To identify the possible important variables, a thorough literature review was conducted. As shown by the dashed lines in Figure 4-1, the data of above 30% increase and below 30% decrease in f_{CS} and f_{FS} was further investigated. These ranges were close to the maximum and minimum strength level of most of the dispersion techniques. Therefore, other potential variables could be identified regardless of the dispersion method used. Through analyzing the experimental results, the observed trends demonstrated the need for discussion about the effects of CNT properties (length, diameter, aspect ratio, and concentration) on mechanical properties. Therefore, this study investigates the influences of four variables associated with CNTs: 1) average length ($\bar{L}$), 2) average diameter ($\bar{d}$), 3)

average aspect ratio ($\overline{AR}$), and 4) concentration ($\bar{\kappa}$). $\bar{L}$, $\bar{d}$, and $\overline{AR}$ of CNTs were determined according to the physical characteristics of CNTs reported in each study. For example, if the length and diameter of CNTs were reported to be between 10-30 μm and 20-40 nm, respectively, then $\bar{L}$, $\bar{d}$, and $\overline{AR}$ of 20 μm, 30 nm, and 667 (unitless) were used. It must be acknowledged that such data are provided by CNT manufactures. In the early stage of this study, a CNT manufacturer claimed that when CNT length was reported to be between 10 and 30 μm, 80 $wt\%$ of CNTs will be 20 μm long. Therefore, the average length and diameter of CNTs are assumed to be the representative characteristics of CNTs in data analysis.

Figure 4-3 shows the dominant ranges of the identified important variables with greater than 30% increase or lower than 30% decrease compared with the control, for f_{CS} and f_{FS}. The compressive strength increased by more than 30% using short ($\bar{L} < 15$ μm) or small diameter ($\bar{d} \leq 20$ nm) CNTs. Conversely, utilizing relatively long ($\bar{L} \geq 10$ μm) or large diameter ($\bar{d} \geq 20$ nm) CNTs resulted in more than 30% increase in the flexural strength. On the other side, when incorporating high concentrations of CNTs, longer CNTs were more detrimental to the compressive strength, resulted in more than 30% decrease compared with the control. This might be explained by different mechanisms of CNTs affecting the compressive and flexural strengths (see Section 2.6.1). Therefore, a better understanding of the effect of CNT properties is needed to provide practical guidelines for selecting the correct type of CNTs for improving the mechanical properties. In this chapter, the optimum ranges of CNT properties are identified to improve the mechanical properties with the minimal adverse effects of other variables.

Table 4-3. Dominant Ranges of Important Variables for f_{CS} and f_{FS}

Percent change (%)	Compressive strength (f_{CS})	Flexural strength (f_{FS})
>30	65% of data: $\bar{L} < 15$ μm	72% of data: $\bar{L} \geq 10$ μm
	60% of data: $\bar{d} \leq 20$ nm	67% of data: $\bar{d} \geq 20$ nm
	55% of data: $\bar{\kappa} \leq 0.15$ *c-wt%*	74% of data: $\bar{\kappa} \leq 0.15$ *c-wt%*
<-30	73% of data: $\bar{L} \geq 15$ μm	67% of data: $\bar{L} < 10$ μm
	82% of data: $\bar{d} < 10$ or $\bar{d} \geq 50$ nm	93% of data: $\bar{d} \leq 10$ or $\bar{d} \geq 50$ nm
	82% of data: $\bar{\kappa} > 0.2$ *c-wt%*	56% of data: $\bar{\kappa} > 0.15$ *c-wt%*

4.3.2. Data Distribution

A total of 42 studies (2363 data points) were collected from the literature for data analysis (see Table A-1 in the Appendix). Table 4-4 shows the number of available data points and the number of sources (independent studies) concerning different CNT properties ($\bar{L}$, $\bar{d}$, $\overline{AR}$, and $\bar{\kappa}$). Also, Table 4-5 shows the minimum, maximum, average, median, and standard deviation of the studied CNT properties obtained from the literature.

Table 4-4. Statistical Data Size used to Analyze Mechanical Properties

Mechanical properties	CNT properties			
	$\bar{L}$ # data / # studies	$\bar{d}$ # data / # studies	$\overline{AR}$ # data / # studies	$\bar{\kappa}$ # data / # studies
Compressive strength	216 / 20	255 / 26	216 / 20	266 / 29
Flexural strength	198 / 26	206 / 28	198 / 26	212 / 30
Elastic modulus	80 / 10	80 / 10	80 / 10	80 / 10
Toughness	69 / 10	69 / 10	69 / 10	69 / 10

Table 4-5. Ranges of CNT Properties used to Analyze Mechanical Properties

Mechanical properties	Statistics	$\bar{L}$ (μm)	$\bar{d}$ (nm)	$\overline{AR}$ (unitless)	$\bar{\kappa}$ (c-$wt\%$)
Compressive strength	minimum	3	1.5	125	0.01
	maximum	25.25	80	11666.67	1
	average	14.8	33.28	1222.32	0.33
	median	15	30	333.33	0.2
	standard deviation	5.82	23.86	2249.75	0.32
Flexural strength	minimum	1.5	1.5	75	0.01
	maximum	55	80	11666.67	2
	average	16.48	28.06	1310.05	0.24
	median	17.5	30	333.33	0.1
	standard deviation	13.74	23.23	2533.63	0.3
Elastic modulus	minimum	1.5	6.5 (OD < 8)*	157.89	0.03
	maximum	55	32.5	3000	0.2
	average	16.44	18.28	830.47	0.1
	median	15	9.5	487.18	0.09
	standard deviation	18.37	10.63	926.05	0.05
Toughness	minimum	1.5	1.5	157.89	0.02
	maximum	20	32.5	11666.67	0.2
	average	7.91	12.97	1388.03	0.11
	median	1.5	9.5	157.89	0.1
	standard deviation	7.67	9.23	2780.04	0.05

Note: *$\bar{d}$ of CNTs having outside diameter (OD) smaller than 8 *nm* was taken as 6.5 *nm* for data analysis

4.4. Approach

Using the collected data from the literature, the relationship between CNT properties and the mechanical properties (compressive strength, flexural strength, elastic modulus, and toughness) are evaluated to find the optimum ranges of CNT properties for superior mechanical properties.

Depending on the dispersion technique used, CNTs might undergo breakage. For example, for the effective dispersion using an ultrasonication process, ultrasonication energy must exceed the VdW forces but should be lower than the required energy to fracture CNTs [90]. Excessive ultrasonication energy was found to induce damages to CNTs by shortening their length [169, 178, 179]. Huang *et al*. [180] modeled the breakage

of CNTs due to the ultrasonication energy. They stated that there was a minimum length of CNTs beyond which CNTs did not undergo further breakage. The minimum length is a function of CNT diameter and strength [180]. Unfortunately, the length of CNTs after ultrasonication process was not reported in the literature. Therefore, the original length of CNTs was considered for data analysis. Similarly, the original length and diameter of CNTs reported by manufacturers without taking into consideration the breakage of CNTs due to the dispersion process were extensively used by other researchers to interpret the experimental test data or predict the mechanical properties of CNT nanocomposites (polymer, ceramic, metal, etc.) [16, 23, 136, 137, 181-183]. In this chapter, three coarse ranges are assigned to the studied CNT properties. This might minimize the effect of the breakage of CNTs due to the dispersion process. Besides, ANOVA was performed to statistically confirm the existence of different ranges in each investigated CNT property.

Also, due to a lack of the available data in the literature, this chapter investigates the influence of each investigated CNT property without taking into consideration the influence that other potential variables might have on mechanical properties (e.g., cement matrix composition, testing age, curing condition, type of CNTs, etc.). However, the Analysis of Covariance (ANCOVA) was used to evaluate the effect of other variables that were not the primary interest on the response (herein, f_{CS} and f_{FS}). The ANCOVA was performed to evaluate whether other potential variables (*w/c* ratio, *s/c* ratio, testing age) interacted with identified CNT properties ($\bar{L}$, $\bar{d}$, $\overline{AR}$, and $\bar{\kappa}$) on the response (see Table 4-6). When analyzing the influence of each CNT property on the compressive and flexural strengths, the ANCOVA confirmed that other potential variables had negligible influence (i.e., there is no interaction between the primary and potential variables). The *p*-values of

ANCOVA are greater than 0.05 between CNT properties and other investigated potential variables, except for the *p*-value between $\overline{AR}$ and *s/c* ratio for compressive strength (see Table 4-6; *p*-value = 0.04).

Table 4-6. ANCOVA Results: *p*-Values of Interaction between Potential and Primary Variables

Potential variable		Primary variable (CNT properties)						
	$\bar{L}$	$\bar{d}$	$\overline{AR}$	$\bar{\kappa}$	$\bar{L}$	$\bar{d}$	$\overline{AR}$	$\bar{\kappa}$
	Compressive strength (f_{CS})				Flexural strength (f_{FS})			
w/c	0.78	0.47	0.40	0.58	0.45	0.62	0.97	0.64
s/c	0.26	0.63	0.04	0.25	0.66	0.11	0.29	0.11
Age	0.66	0.57	0.58	0.33	0.52	0.45	0.49	0.89

4.5. Effect of CNT Properties on the Strength

Through analysis of extensive data in the literature, three different ranges were assigned to each CNT property. Table 4-7 lists different ranges of CNT properties for f_{CS} and f_{FS}. The detailed analysis of identifying these ranges would be presented in Sections 4.7.1 and 4.7.2 for f_{CS} and f_{FS}, respectively.

Table 4-7. Identified Ranges of CNT Properties for f_{CS} and f_{FS}

Important variable	Range 1		Range 2		Range 3	
	f_{CS}	f_{FS}	f_{CS}	f_{FS}	f_{CS}	f_{FS}
$\bar{L}$ (μm)	< 15	< 10	$15 \leq \bar{L} \leq 20$	$10 \leq \bar{L} \leq 20$	> 20	> 20
$\bar{d}$ (nm)	< 20	< 15	$20 \leq \bar{d} \leq 45$	$15 \leq \bar{d} \leq 32.5$	≥ 50	≥50
$\overline{AR}$ (unitless)	< 350	< 350	$350 \leq \overline{AR} \leq 1300$	$350 \leq \overline{AR} \leq 1800$	≥2500	≥2500
$\bar{\kappa}$ (*c-wt%*)	≤ 0.2	≤ 0.15	$0.2 < \bar{\kappa} \leq 0.5$	$0.15 < \bar{\kappa} \leq 0.5$	> 0.5	> 0.5

Note: $32.5 < \bar{d} < 50$ *nm* is not available for f_{FS}

4.5.1. Effect of CNT Length

Figure 4-2 shows the influence of three different CNT length ranges on the compressive and flexural strengths. Figure 4-2 (a) shows the boxplots for the change in compressive strength (f_{CS}) against the control with respect to three different ranges of CNT length. The *y*-axes represent the percent change of the compressive strength $\left(\Delta f_{CS}(\%)\right)$

that can be defined as $\Delta f_{CS}(\%) = \frac{f_{CS\,(CNTs)} - f_{CS\,(control)}}{f_{CS\,(control)}} \times 100\%$. Figure 4-2 (b) shows the effect of different ranges of $\bar{L}$ of CNTs on the flexural strength percent change ($\Delta f_{FS}(\%)$) that can be defined as $\Delta f_{FS}(\%) = \frac{f_{FS\,(CNTs)} - f_{FS\,(control)}}{f_{FS\,(control)}} \times 100\%$. Also, to statistically confirm the differences between various ranges of each CNT property (herein, $\bar{L}$), the ANOVA test results are included (see the *p*-values between different ranges in Figure 4-2).

Figure 4-2 (a) shows that as $\bar{L}$ increases from Range 1 to 3, the median, first quartile, and minimum values gradually decrease. In contrast, third quartile and maximum values indicate the limited contribution of CNT length to higher compressive strength. This can be statistically confirmed by the *p*-values smaller than 0.05 between Range 1 and other ranges. Therefore, Range 1 is identified as the optimum range to increase the compressive strength, as highlighted in Figure 4-2 (a).

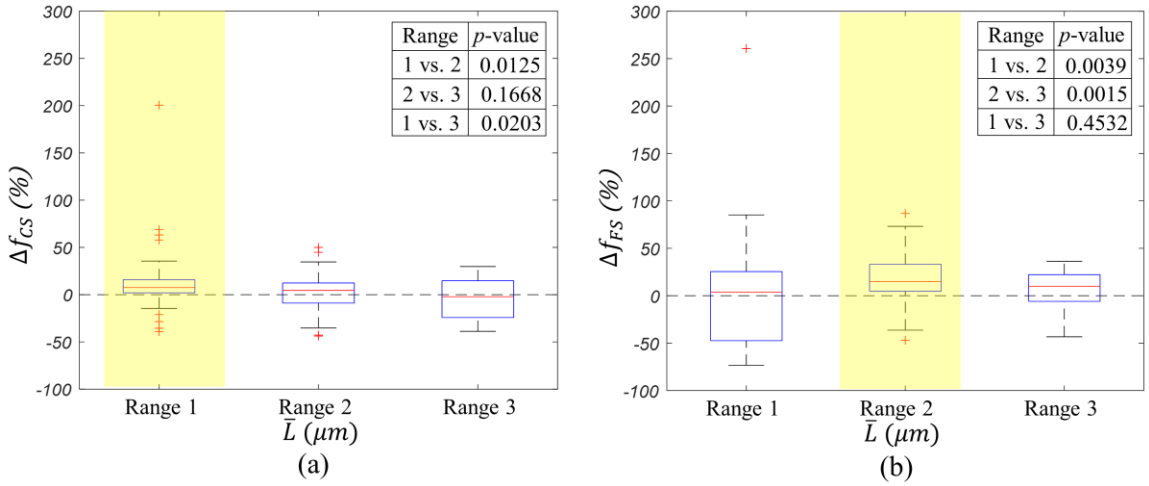

Figure 4-2. Effect of CNT length: (a) compressive strength (b) flexural strength

Figure 4-2 (b) shows that the minimum, first quartile, median, and third quartile values increase as $\bar{L}$ increases from Range 1 to Range 2. The $\Delta f_{FS}(\%)$ degraded beyond Range 2, most probably due to the dispersion issues. The *p*-value of Range 2 is lower than 0.05 when compared with length Ranges of 1 and 3, indicating that Range 2 exhibits a

higher mean of the flexural strength than other ranges. Therefore, Range 2 is selected as the optimum range for superior flexural strength, as highlighted in Figure 4-2 (b).

4.5.2. Effect of CNT Diameter

Figure 4-3 (a) and (b) show the boxplots of $\Delta f_{CS}(\%)$ and $\Delta f_{FS}(\%)$, respectively, with respect to various ranges of $\bar{d}$. Figure 4-3 (a) shows that as $\bar{d}$ increases from Range 1 to Range 2, the minimum and first quartile values increase. In contrast, the maximum value of $\Delta f_{CS}(\%)$ decreased from 50% to 35.5% and the third quartiles remained with minimal changes (15.9% ~17.1%). Therefore, CNTs within Range 2 exhibited more cases of positive $\Delta f_{CS}(\%)$. However, their contribution is limited. This trend suggests that CNT with smaller diameter are beneficial to increase the compressive strength. However, due to difficulties in getting proper dispersion of small diameter CNTs (Range 1), the likelihood of achieving $\Delta f_{CS}(\%) < 0$ is also high. This might be attributed to the larger surface area of smaller diameter CNTs which causes them to agglomerate, if not properly dispersed [184]. This can be statistically confirmed by the *p*-value smaller than 0.05 between Ranges 2 and 3 (*p*-value = 0.0033; see Figure 4-3 (a)), while there is no significant difference between the mean of $\Delta f_{CS}(\%)$ by showing the *p*-value of 0.3490 between Ranges 1 and 2. In Range 3, most cases exhibited the compressive strength lower than that of the control. Therefore, Range 2 is identified as the optimum range for superior compressive strength, as highlighted in Figure 4-3 (a).

Figure 4-3 (b) shows that despite the acceptable performance of CNTs with small $\bar{d}$ in the compressive strength (see Range 1 in Figure 4-3 (a)), CNTs with diameters within Range 1 did not show a clear positive impact on getting higher $\Delta f_{FS}(\%)$. This could be confirmed by a higher minimum, first quartile, median, and third quartile values of CNTs

with $\bar{d}$ within Range 2 compared with Range 1. In Range 3, the likelihood of obtaining positive $\Delta f_{FS}(\%)$ was significantly reduced compared with Range 2. Therefore, Range 2 might be considered as the optimum range for superior flexural strength, as highlighted in Figure 4-3 (b). This can also be statistically confirmed by the p-values smaller than 0.05 between Range 2 and other ranges.

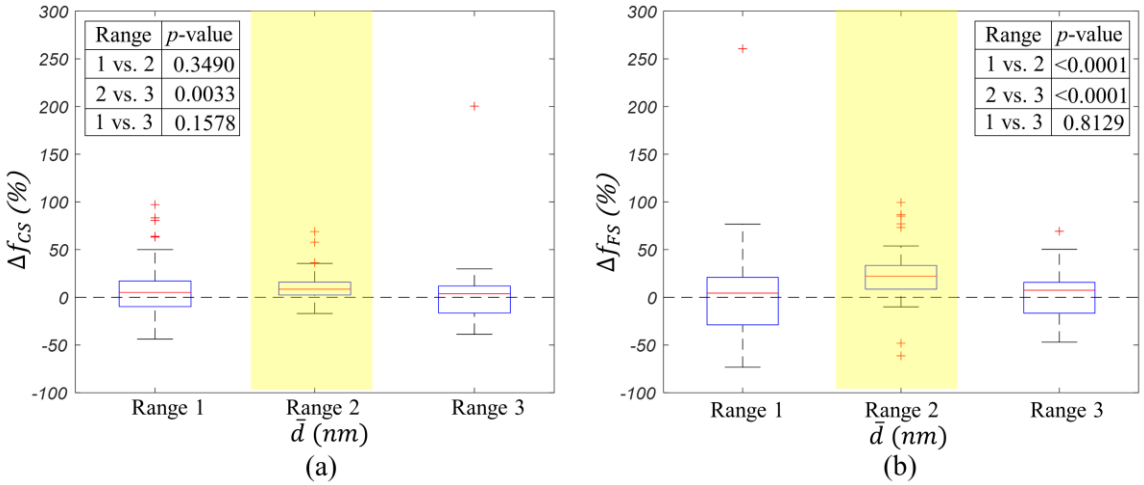

Figure 4-3. Effect of CNT diameter: (a) compressive strength (b) flexural strength

4.5.3. Effect of CNT Aspect Ratio

Figure 4-4 (a) and (b) show the boxplots of $\Delta f_{CS}(\%)$ and $\Delta f_{FS}(\%)$, respectively, with respect to various ranges of $\overline{AR}$. Figure 4-4 (a) shows that there is no noticeable impact of $\overline{AR}$ on $\Delta f_{CS}(\%)$. This can be confirmed by p-values > 0.05 between different ranges. However, CNTs within Range 2 exhibited lower variations in $\Delta f_{CS}(\%)$ compared with other ranges. Therefore, Range 2 is selected as the optimum range for improving the compressive strength, as highlighted in Figure 4-4 (a).

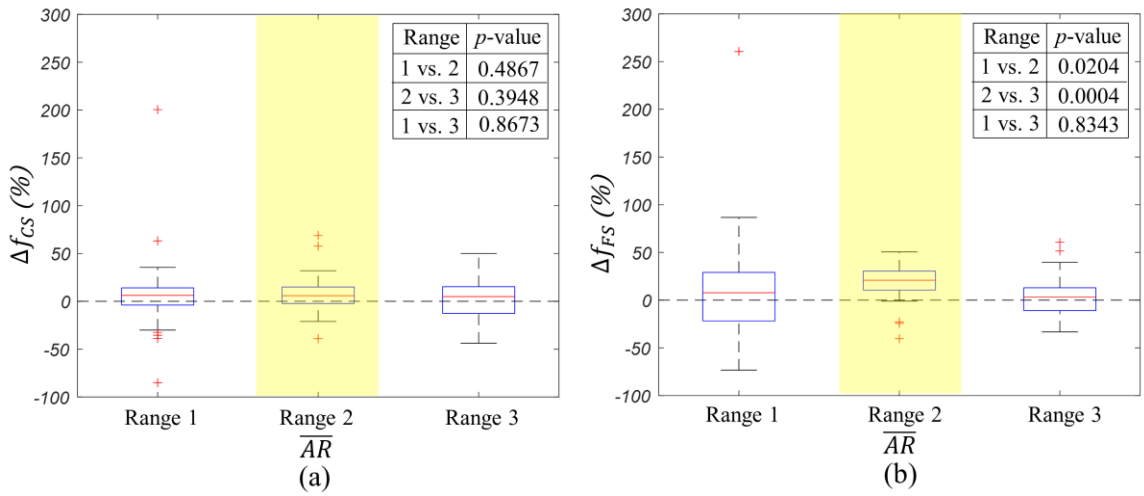

Figure 4-4. Effect of CNT aspect ratio: (a) compressive strength (b) flexural strength

Figure 4-4 (b) indicates that as $\overline{AR}$ increases from Range 1 to Range 2, the minimum, first quartile, median, and third quartile values increase. Beyond Range 2, $\Delta f_{FS}(\%)$ degrades and the likelihood of obtaining negative $\Delta f_{FS}(\%)$ increases. Therefore, Range 2 might be considered as the optimum range for superior flexural strength, as highlighted in Figure 4-4 (b). This can also be statistically confirmed by the *p*-values smaller than 0.05 between Range 2 and other ranges. Also, CNTs within Range 2 exhibit low level of variations in $\Delta f_{FS}(\%)$.

4.5.4. Effect of CNT Concentration

Figure 4-5 (a) and (b) show the effect of different ranges of $\bar{\kappa}$ on $\Delta f_{CS}(\%)$ and $\Delta f_{FS}(\%)$, respectively. Figure 4-5 (a) shows that the dominant data of $\Delta f_{CS}(\%)$ falls in the positive zone for CNT concentration within Range 1 (see the positive median and first quartile values of Range 1 in Figure 4-5 (a)). Although the *p*-value between Ranges 1 and 2 shows no significant difference (*p*-value = 0.2610 > 0.05), the compressive strength of Range 2 degrades compared with Range 1. The first quartile value of Range 2 is negative, while the median value is still positive. Therefore, Range 1 is considered as the optimum

range for superior compressive strength, as highlighted in Figure 4-5 (a). In Range 3, most of the data falls in the negative zone. Therefore, this range of CNT concentration is not recommended. The *p*-values smaller than 0.05 between Range 3 and other ranges can confirm this.

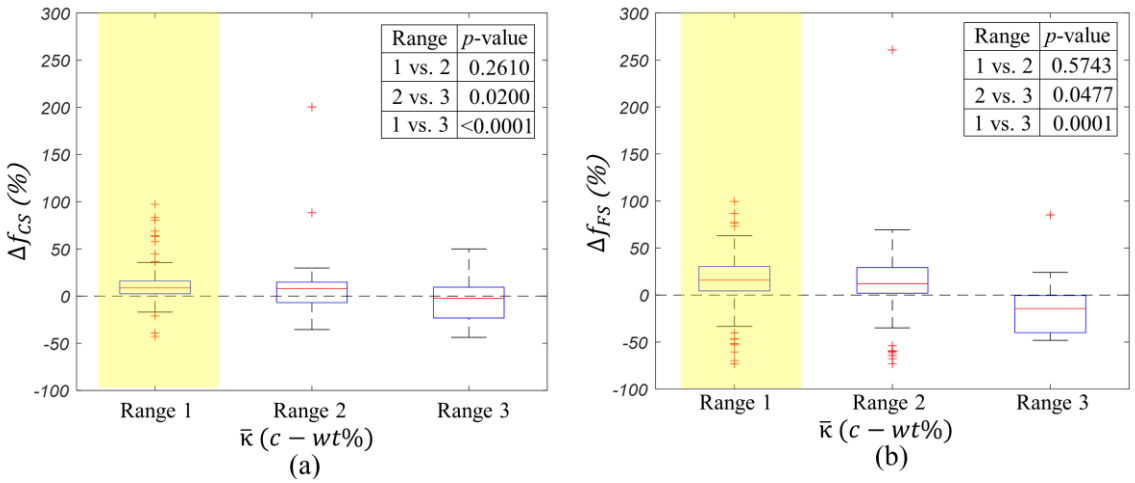

Figure 4-5. Effect of CNT concentration: (a) compressive strength (b) flexural strength

The similar trend could also be observed in Figure 4-5 (b) where first quartile, median, and third quartile values continuously decreased from Range 1 to Range 3. Therefore, Range 1 is considered as the optimum range for superior flexural strength, as highlighted in Figure 4-5 (b).

In addition, Figure 4-2 through Figure 4-5 demonstrate that within the identified optimum ranges; 1) lower variations in both $\Delta f_{CS}(\%)$ and $\Delta f_{FS}(\%)$ can be observed compared with other ranges, and 2) the majority of data is greater than zero (i.e., $\Delta f_{CS}(\%)$ and $\Delta f_{FS}(\%) > 0$). This further confirms the superior performance of CNTs if selected from the optimum ranges. However, these figures yield no information on CNT dispersion quality and its influence on the strength. This will be discussed in details in the following section.

4.6. Effect of CNT Dispersion Quality on the Strength

This section discusses how the quality of dispersion affects the strength concerning $\bar{L}$, $\bar{d}$, $\overline{AR}$, and $\bar{\kappa}$. The good quality of dispersion leads to increase the mechanical properties as CNT concentration increases. However, when the quality of dispersion is poor, the mechanical properties degrade by adding CNTs [16, 20, 114, 185]. Thus, in this section, the quality of CNT dispersion is indirectly evaluated using the relationship between the increment in CNT concentrations ($\Delta\bar{\kappa} = \bar{\kappa}_2 - \bar{\kappa}_1;\ \bar{\kappa}_2 > \bar{\kappa}_1$) and the difference between the measured strengths between two levels of CNT concentration (ΔS: compressive strength ($\Delta S_{CS} = f_{CS(\bar{\kappa}_2)} - f_{CS(\bar{\kappa}_1)}$) and flexural strength ($\Delta S_{FS} = f_{FS(\bar{\kappa}_2)} - f_{FS(\bar{\kappa}_1)}$)), in each individual study. Similarly, Konsta Gdoutos *et al*. [16] indirectly evaluated the dispersion quality using the measured fracture load of cement pastes containing CNTs. By comparing $\Delta S/\Delta\bar{\kappa}$ for both compressive and flexural strengths, it is possible to study how the degradation in dispersion quality differently affects the compressive and flexural strengths. For example, when CNTs are short many cases that showed poor dispersion quality still had higher compressive strength than the control. However, in case of the flexural strength, most cases that showed poor dispersion quality exhibited lower flexural strength than the control. This shows different contributions of CNT length to compressive and flexural strengths.

With this in mind, the data obtained from the literature was categorized into two groups of uniform and poor dispersion. The categorization was merely done by taking into account the ratio of the strength change ($\Delta S = S_{\bar{\kappa}_2} - S_{\bar{\kappa}_1}$) to the increment in CNT concentration ($\Delta\bar{\kappa}$), for each individual study. When the value of $\Delta S/\Delta\bar{\kappa}$ is positive, the strength is increased by adding additional CNTs. This indicates a possible uniform

dispersion. When the value of $\Delta S/\Delta\bar{\kappa}$ is negative or zero, the compressive or flexural strength degrades by adding a higher concentration of CNTs. This indicates a possible poor dispersion of CNTs within the cement matrix. Note that $\Delta\bar{\kappa}$ is always positive, however, ΔS can be either positive (i.e., increase in the strength while adding additional CNTs) or negative (i.e., reduction in the strength while adding additional CNTs). Also, the negative value of $\Delta S/\Delta\bar{\kappa}$ does not mean lower strength than the control.

Figure 4-2 through Figure 4-5 have no information on the number of observations (N_{obs}) for the quality of dispersion ($\Delta S/\Delta\bar{\kappa}$) and its impact on the strength changes within the proposed ranges against the control (Δf_{CS} or Δf_{FS}). When counting either positive or negative value of $\Delta S/\Delta\bar{\kappa}$ and Δf (Δf_{CS} or Δf_{FS}) with respect to different CNT properties, it can be useful to assess the condition of dispersion quality and strength level of each range, simultaneously.

4.6.1. Effect of CNT Length

Figure 4-6 shows the N_{obs} of either positive or negative value of $\Delta S/\Delta\bar{\kappa}$ and Δf at the given ranges of CNT length. Figure 4-6 (a) and (c) show the N_{obs} of positive and negative $\Delta S/\Delta\bar{\kappa}$ for compressive ($\frac{\Delta S_{CS}}{\Delta\bar{\kappa}}$) and flexural strengths ($\frac{\Delta S_{FS}}{\Delta\bar{\kappa}}$), respectively. Also, Figure 4-6 (b) and (d) show the N_{obs} of positive and negative Δf_{CS} and Δf_{FS}, respectively, with respect to different length ranges.

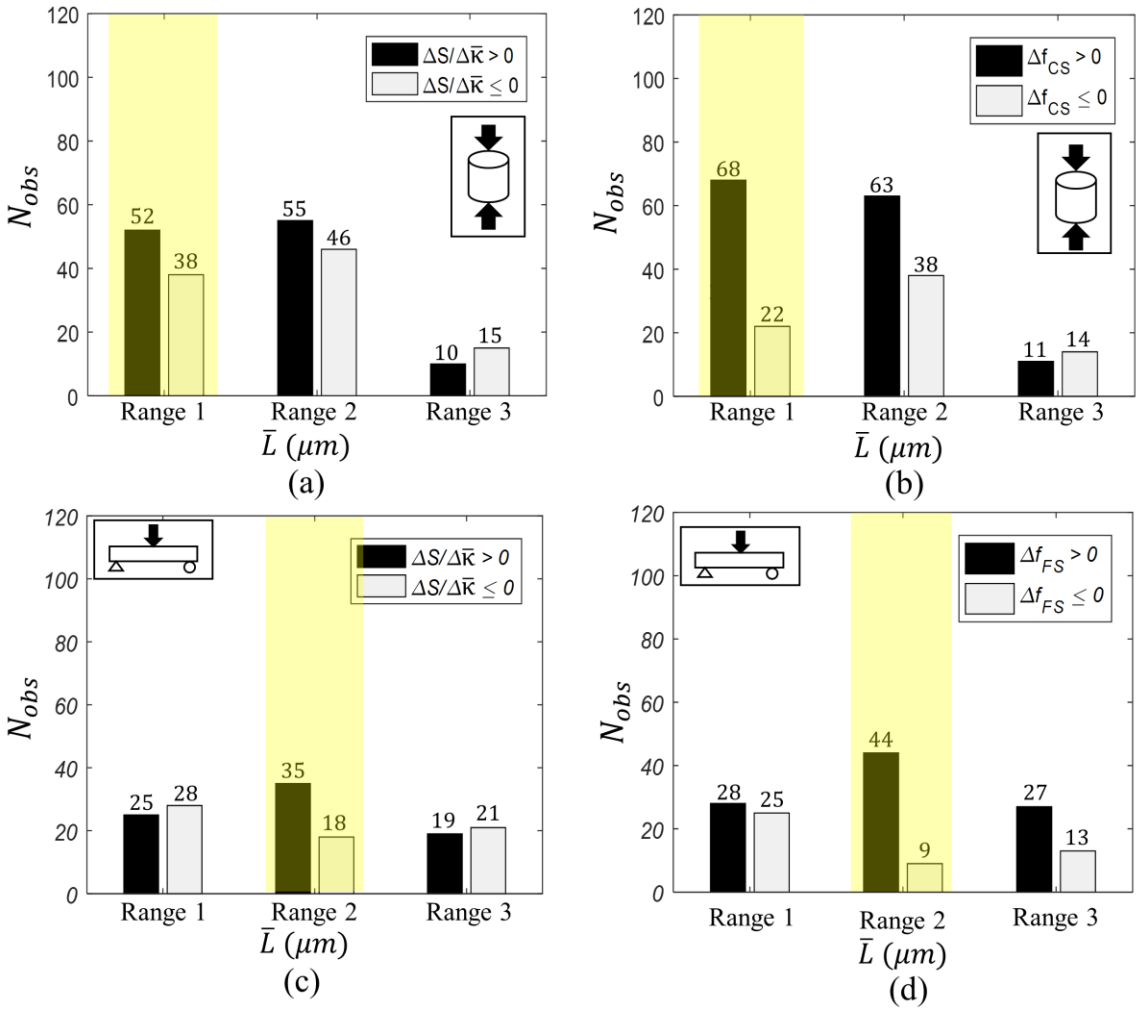

Figure 4-6. Effect of $\bar{L}$ of CNTs on quality of dispersion ($\frac{\Delta S}{\Delta \bar{\kappa}}$) and strength gain/loss (Δf) for compressive and flexural strengths

Figure 4-6 (a) shows the N_{obs} of positive and negative values of the difference in the compressive strength between $f_{CS(\bar{\kappa}_2)}$ and $f_{CS(\bar{\kappa}_1)}$ versus the increment in the CNT concentration ($\Delta\bar{\kappa} = \bar{\kappa}_2 - \bar{\kappa}_1$). In case of $\frac{\Delta S_{CS}}{\Delta \bar{\kappa}} \leq 0$ (i.e., poor dispersion), shorter CNTs exhibited higher N_{obs} of positive Δf_{CS} than longer CNTs, as seen in Figure 4-6 (a) and (b), simultaneously. For example, CNTs with $\bar{L}$ of Range 1 showed 38 N_{obs} of negative dispersion indication ($\frac{\Delta S_{CS}}{\Delta \bar{\kappa}} \leq 0$), while there were only 22 N_{obs} of negative Δf_{CS} (42% of poor dispersion still showed positive Δf_{CS}). Increasing CNT $\bar{L}$ to Range 2 and Range 3 led

to only 17% and 7% $\Delta f_{CS} > 0$ in case of $\frac{\Delta S_{CS}}{\Delta \bar{\kappa}} \leq 0$, respectively. This could be attributed to the effect of CNT length on the pore size distribution (see Figure 2-2 in Chapter 2). Kang *et al*. [63] also observed an increase in the compressive strength of cement pastes containing CNTs with $\bar{L}$ = 12.5 μm, resulted from the substantial decrease in the average pore diameter, even though the total porosity was increased.

Despite the compressive strength, Figure 4-6 (c) shows the higher N_{obs} of negative $\Delta S/\Delta \bar{\kappa}$ (herein, $\frac{\Delta S_{FS}}{\Delta \bar{\kappa}}$) than positive $\frac{\Delta S_{FS}}{\Delta \bar{\kappa}}$ for $\bar{L}$ of Range 1. Also, the N_{obs} of positive and negative Δf_{FS} were 28 and 25, respectively. This observation is in good agreement with the findings in Figure 4-2 (b) that showed short CNTs (Range 1) had limited contribution to increase $\Delta f_{FS}(\%)$. This might be explained by the ineffectiveness of short CNTs in bridging the cracks. With an increase in CNT length to Range 2, there were 35 N_{obs} of $\frac{\Delta S_{FS}}{\Delta \bar{\kappa}} > 0$ and 18 N_{obs} of $\frac{\Delta S_{FS}}{\Delta \bar{\kappa}} \leq 0$. Also, 83% of the total N_{obs} was correlated to $\Delta f_{FS} > 0$ (44 positive out of 53 total N_{obs}). This shows that longer CNTs outperforms in the flexural strength than compressive strength, as highlighted in Figure 4-6 (c) and (d). However, an increase in CNT length to Range 3 degraded the quality of dispersion, adversely affecting the flexural strength due to the creation of bigger pore sizes and premature debonding of CNTs from the cement matrix.

In summary, shorter CNTs exhibited better performance in terms of compressive strength. However, this trend was not observed for flexural strength. In general, CNTs with $\bar{L}$ between 10 and 20 μm showed higher strength gain compared to the control for both compressive and flexural strengths. This effect is more pronounced for flexural strength. This might be explained by the better anchorage of longer CNTs in hydration products that can bridge the ongoing cracks.

4.6.2. Effect of CNT Diameter

Figure 4-7 shows the N_{obs} of either positive or negative value of $\Delta S/\Delta\bar{\kappa}$ and Δf for both compressive (Figure 4-7 (a) and (b)) and flexural (Figure 4-7 (c) and (d)) strengths, respectively, at the given ranges of CNT diameter.

As shown in Figure 4-7 (a), the N_{obs} of $\frac{\Delta S_{CS}}{\Delta\bar{\kappa}}$ for CNTs with $\bar{d}$ of Range 1 was almost identical for poor (i.e., $\frac{\Delta S_{CS}}{\Delta\bar{\kappa}} \leq 0$) and uniform (i.e., $\frac{\Delta S_{CS}}{\Delta\bar{\kappa}} > 0$) dispersions. Nevertheless, 22% of $\frac{\Delta S_{CS}}{\Delta\bar{\kappa}} \leq 0$ still exhibited higher compressive strength than the control ($\Delta f_{CS} > 0$; see Figure 4-7 (b)). In case of the flexural strength, only 12% of $\frac{\Delta S_{FS}}{\Delta\bar{\kappa}} \leq 0$ for CNTs with $\bar{d}$ of Range 1 exhibited $\Delta f_{FS} > 0$ (see Figure 4-7 (d); 5 cases out of 42 total N_{obs}). Thus, CNTs with diameters of Range 1 tends to perform better for compressive strength than for flexural strength.

CNTs with $20\ nm \leq \bar{d} \leq 45\ nm$ for compressive strength and $15\ nm \leq \bar{d} \leq 32.5\ nm$ for flexural strength (Range 2) dramatically reduced the cases that exhibited lower strength than the control for Δf_{CS} and Δf_{FS}, as highlighted in Figure 4-7 (b) and (d), respectively. For example, 51% and 91% of the total N_{obs} of Δf_{FS} were positive for CNTs within Ranges 1 and 2, respectively. When considering the dispersion quality, within the optimum range of $\bar{d}$ (Range 2), although 38 cases showed poor dispersion quality (see Figure 4-7 (a)), but only 17 cases exhibited lower compressive strength than the control (see Figure 4-7 (b)). CNTs with $\bar{d}$ of Range 3 degraded the strength gain in both compressive and flexural strengths. This might be explained by the effect of CNT diameter on the pore structure of the cement matrix (see Figure 2-2 in Chapter 2). Pore sizes greater than 50 *nm* (referred to as macro-pores) have been reported to have adverse effects on the strength [160].

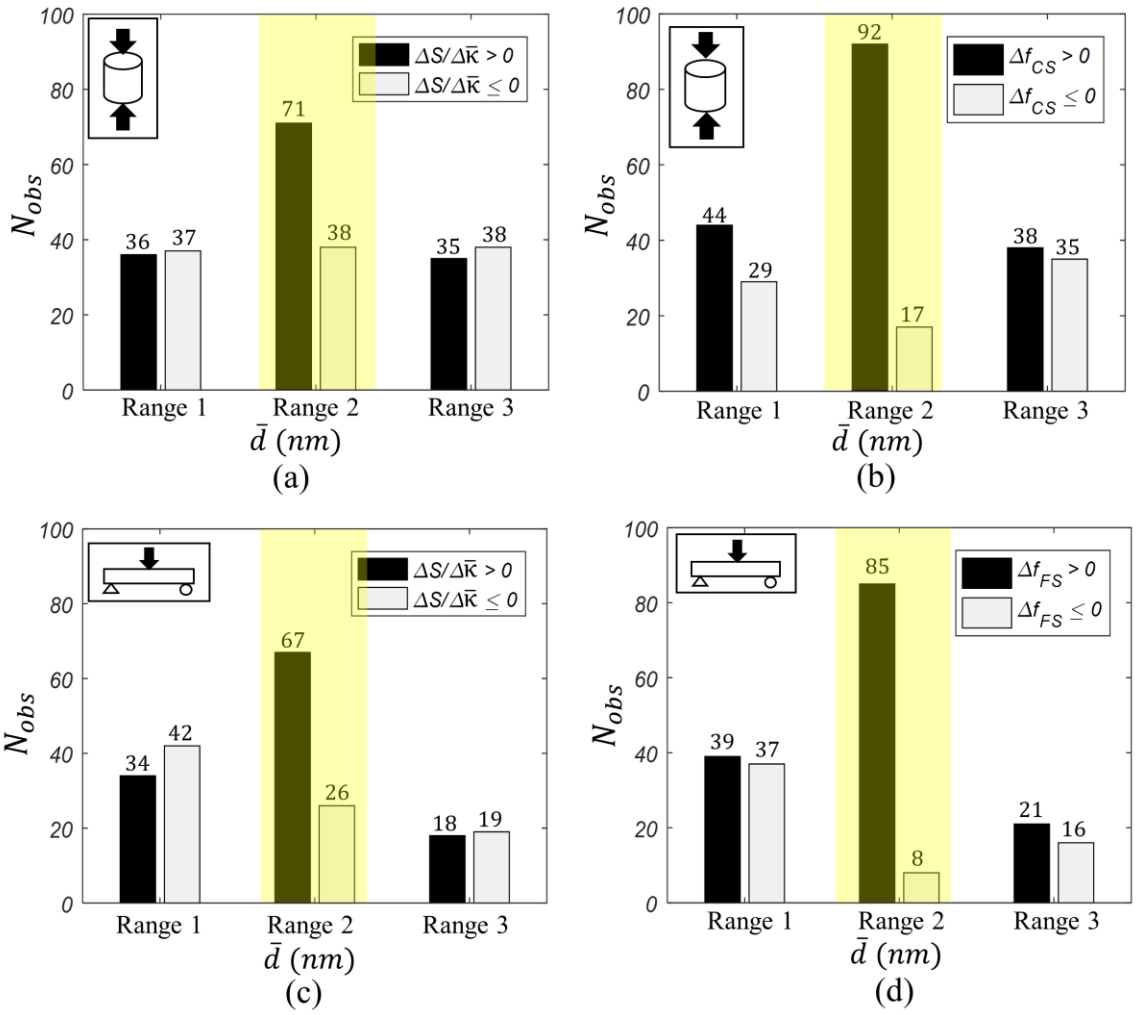

Figure 4-7. Effect of $\bar{d}$ of CNTs on quality of dispersion ($\frac{\Delta S}{\Delta \bar{\kappa}}$) and strength gain/loss (Δf) for compressive and flexural strengths

It was found that CNTs with smaller diameters had a more positive influence on the compressive strength than the flexural strength. This might be explained by different mechanisms of CNTs in terms of compressive and flexural strengths. In case of the compressive strength, CNTs with small diameters, even when clumped together, can still act as fillers and contribute to the refinement of pore structures. However, premature debonding of agglomerated CNTs adversely affects the load transfer mechanism between the cement matrix and CNTs, degrading the flexural strength. Generally, CNTs with $\bar{d}$

between 20 and 32.5 *nm* may be considered as the best range for increasing both compressive and flexural strengths.

4.6.3. Effect of CNT Aspect Ratio

Figure 4-8 shows the effect of CNT $\overline{AR}$ on the N_{obs} of $\Delta S/\Delta\bar{\kappa}$ and Δf for both compressive and flexural strengths. Figure 4-8 (b) and (d) show the high likelihood of obtaining negative Δf_{CS} and Δf_{FS}, respectively, in either $\overline{AR}$ of Range 1 or Range 3. For example, there were 22 N_{obs} of $\Delta f_{FS} \leq 0$, while there were only 29 N_{obs} of $\Delta f_{FS} > 0$ for CNTs with $\overline{AR}$ within Range 1 (see Figure 4-8 (d)). Also, the N_{obs} of negative Δf_{FS} was 52% of the total N_{obs} for CNTs with $\overline{AR}$ within Range 3. Thus, incorporating CNTs with $\overline{AR}$ of Ranges 1 and 3 is not recommended. Note that CNTs with high $\overline{AR}$ (Range 3) had very small diameters ($\bar{d} < 8\ nm$). Consequently, these CNTs even when agglomerated were still capable of acting as fillers, benefiting the compressive strength (see Figure 4-8 (b); CNTs with $\overline{AR}$ of Range 3 exhibited 25 N_{obs} of positive Δf_{CS} vs. 17 N_{obs} of negative Δf_{CS}). However, lower bond strength between agglomerated CNTs and cement matrix might lead to their premature debonding from the matrix, weakened their contribution to the flexural performance. Thus, CNTs with $\overline{AR}$ of Range 3 seem to exhibit better performance in compressive strength than flexural strength.

In Range 2 (compressive and flexural strengths), although a lot of cases showed poor dispersion ($\frac{\Delta S}{\Delta\bar{\kappa}} \leq 0$), but most of the data exhibited higher strength than the control (Δf_{CS} and $\Delta f_{FS} > 0$). This Range of CNTs provides more benefits to the flexural than compressive strength, which could be attributed to the higher surface area of CNTs (higher $\overline{AR}$) that provides better bonding between CNTs and cement matrix.

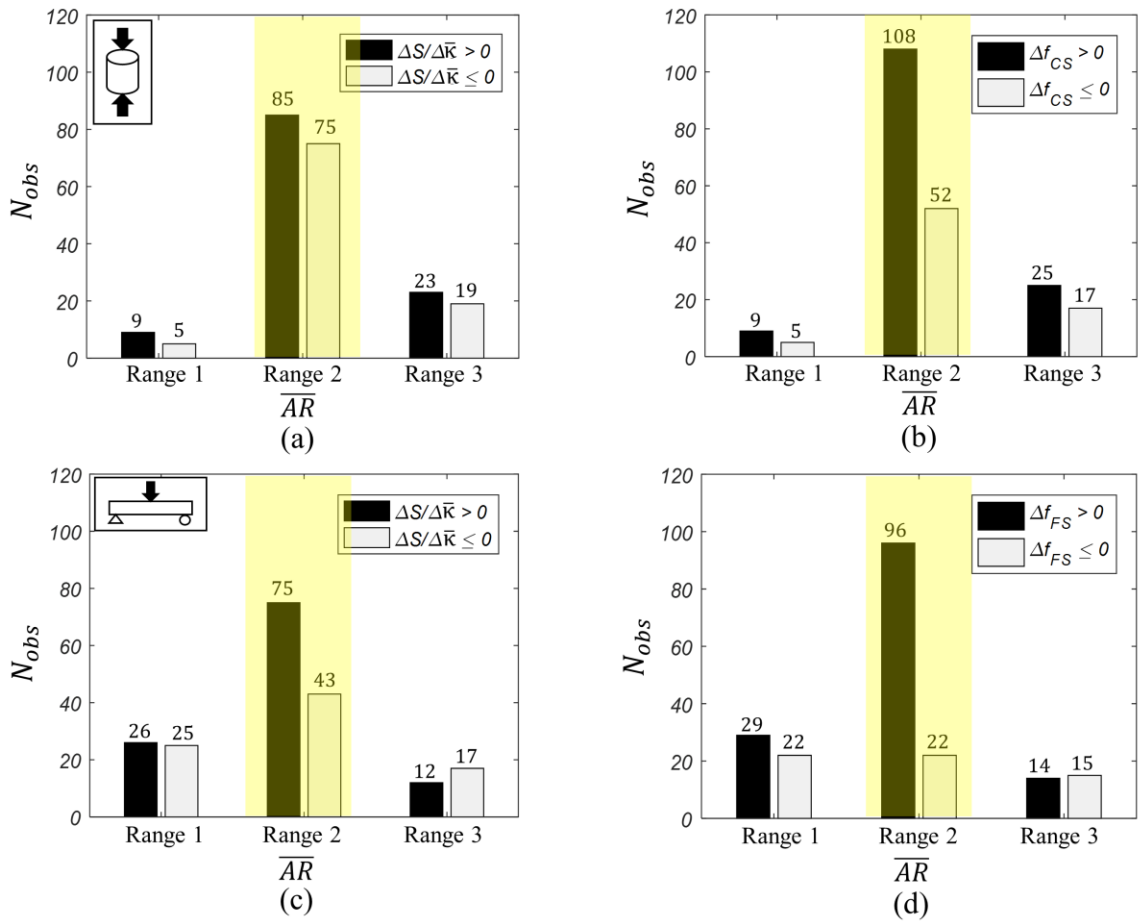

Figure 4-8. Effect of $\overline{AR}$ of CNTs on quality of dispersion ($\frac{\Delta S}{\Delta\bar{\kappa}}$) and strength gain/loss (Δf) for compressive and flexural strengths

When considering the obtained optimum length (see Section 4.6.1) and diameter (see Section 4.6.2) of CNTs, the optimum range for CNT aspect ratio between 300 and 1000 is suggested based on the database. This is in a good agreement with the findings regarding the effect of CNT aspect ratio on both compressive and flexural strengths obtained in this section.

4.6.4. Effect of CNT Concentration

Figure 4-9 shows the effect of the concentration of CNTs on the N_{obs} of $\Delta S/\Delta\bar{\kappa}$ and Δf for both compressive and flexural strengths. In Range 1 of Figure 4-9 (a) ($\bar{\kappa} \leq 0.2$ *c-wt%*), the N_{obs} of uniform dispersion (98 N_{obs} for $\frac{\Delta S_{CS}}{\Delta\bar{\kappa}} > 0$) is 2.2 times more than that of

poor dispersion (44 N_{obs} for $\frac{\Delta S_{CS}}{\Delta \bar{\kappa}} \leq 0$). The similar trend was also observed for the flexural strength, where the N_{obs} of uniform and poor dispersion for Range 1 ($\bar{\kappa} \leq 0.15$ *c-wt*%) were 91 and 50, respectively (see Figure 4-9 (c)). In addition, Figure 4-9 (b) and (d) show that there are many cases of higher strength than the control in Range 1, as highlighted in Figure 4-9. This indicates that the dispersion quality is highly correlated with the strength gain/loss compared with the control.

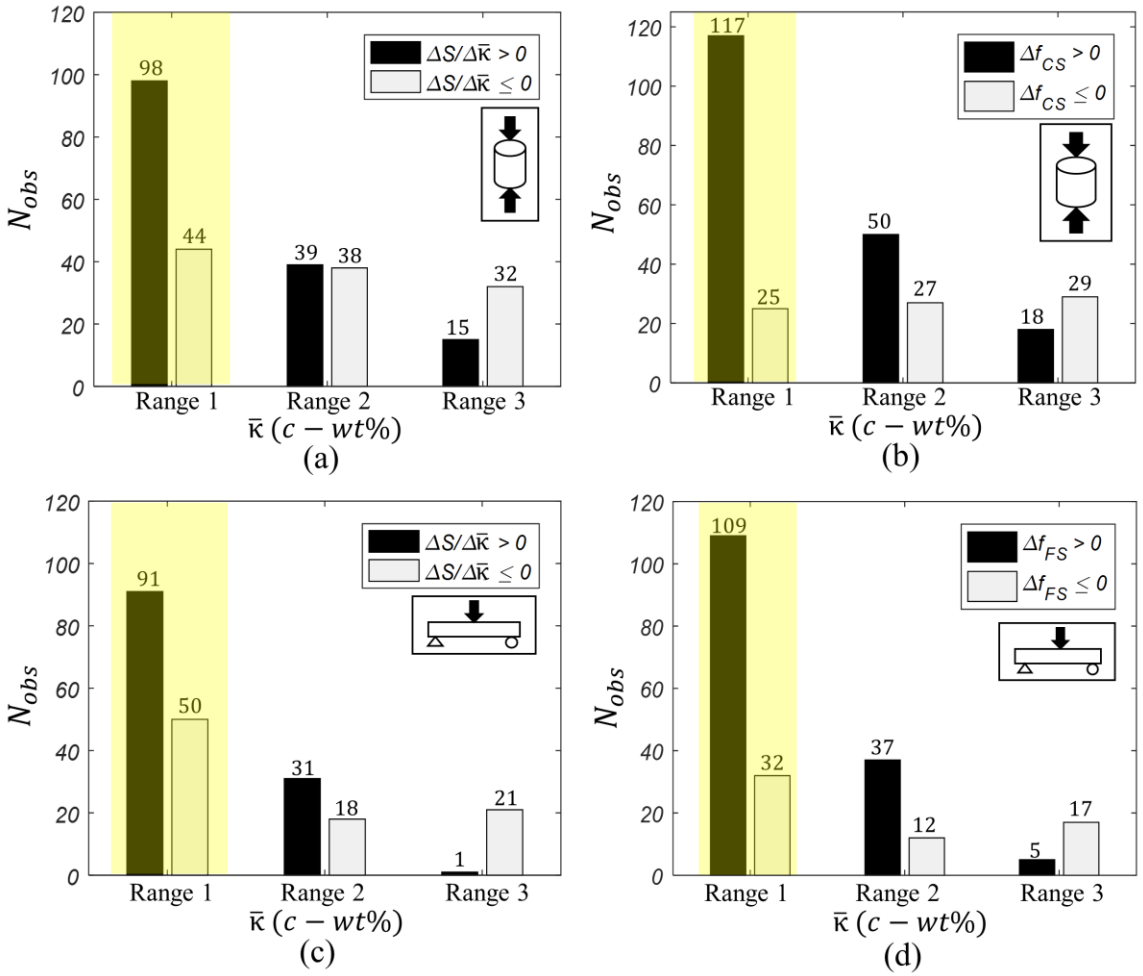

Figure 4-9. Effect of $\bar{\kappa}$ of CNTs on quality of dispersion ($\frac{\Delta S}{\Delta \bar{\kappa}}$) and strength gain/loss (Δf) for compressive and flexural strengths

Beyond Range 1, increasing the CNT concentration considerably increased the probability of getting lower strength than the control. For example, in Range 2, 35% of the

overall N_{obs} exhibited lower compressive strength than the control. This was even worse for CNTs with $\bar{\kappa}$ of Range 3 which showed 29 N_{obs} of $\Delta f_{CS} \leq 0$, while there were only 18 N_{obs} of $\Delta f_{CS} > 0$ (see Figure 4-9 (b)). The similar trend can be observed for the flexural strength (see Figure 4-9 (d)).

There are two different thresholds of CNT concentration for the compressive and flexural strengths. As seen in Figure 4-5 and Figure 4-9, the threshold concentration for flexural strength ($\bar{\kappa}$ = 0.15 *c-wt*%) is slightly lower than that of the compressive strength ($\bar{\kappa}$ = 0.2 *c-wt*%). When the concentration of CNTs exceeds the threshold, both compressive and flexural strengths decreased with an increase in CNT concentration. The different mechanisms of CNTs in compressive and flexural strengths could explain the different thresholds. In the threshold of 0.2 *c-wt*%, the agglomerated CNTs can degrade the bond strength between cement matrix and CNTs, resulting in the reduction of the flexural strength, while the agglomerated CNTs can still be tolerable with respect to the compressive strength. Similarly, Danoglidis *et al*. [31] incorporated different concentrations of CNTs (in the range 0.08-0.5 *c-wt*%) to increase the mechanical properties of cement mortars. Their results indicated that, beyond $\bar{\kappa}$ = 0.1 *c-wt*%, the flexural strength degraded with an increase in CNT concentration, whereas the compressive strength was not reduced with a higher CNT concentration (this study was not included in the data analysis).

4.7. Detailed Analysis of Identifying Different Ranges

This Section presents the detailed analysis of identifying three different ranges for each CNT property for compressive strength (Section 4.7.1) and flexural (Section 4.7.2) strengths (see Table 4-7).

4.7.1. Compressive Strength

Figure 4-10 shows the boxplots of $\Delta f_{CS}(\%)$ concerning different CNT properties. Figure 4-10 (a) shows the analysis of the impact of $\bar{L}$ of CNTs on $\Delta f_{CS}(\%)$. The range for $\bar{L}$ was varied between 2.5 and 25 μm. The ranges of each CNT property in the boxplots (herein, $\bar{L}$) is not the absolute value obtained from individual studies. For example, $\bar{L}$ = 7.5 μm in the boxplot includes any $\bar{L}$ between 6.25 and 8.75 μm. The median value of $\Delta f_{CS}(\%)$ varied between -2.1% and 12.4% for the entire data except for $\bar{L}$ = 5 μm, which showed the median value of -55.7% [117]. The poor compressive performance of CNTs with $\bar{L}$ = 5 μm could be related to the method used to pre-dispersed CNTs in acetone via ultrasonication process, resulted in partial hydration of cement [117]. Therefore, $\bar{L}$ = 5 μm is not considered for the analysis. As the length of CNTs increases from 7.5 to 25 μm, the first quartiles and medians gradually decrease, except for $\bar{L}$ of 17.5 and 20 μm (see arrow *a* in Figure 4-10 (a)). Note that $\bar{L}$ of 17.5 and 20 μm had small diameters to compensate for the poor compressive performance (see the positive first quartiles of data in Figure 4-10 (a)). For example, CNTs having $\bar{L}$ of 17.5 μm had $\bar{d}$ of 1.5 *nm* [93]. In contrast, third quartiles indicates the limited contribution of CNT length on the compressive strength (see arrow *b* in Figure 4-10 (a)). Similarly, Kumar *et al*. [186] observed that compressive strength had not been affected by the variations in carbon fiber length in the polymer matrix. In general, shorter CNTs ranging from the length of 2.5 μm to 12.5 μm exhibited positive impact on $\Delta f_{CS}(\%)$ (see Range 1 in Figure 4-10 (a)). As $\bar{L}$ increases to Range 2 (15 $\mu m \leq \bar{L} \leq 20$ μm), many data points exhibited $\Delta f_{CS}(\%) < 0$, however, the median value was still positive. In Range 3 ($\bar{L} > 20$ μm), most of the data showed $\Delta f_{CS}(\%) < 0$ and the median value fell in the negative zone.

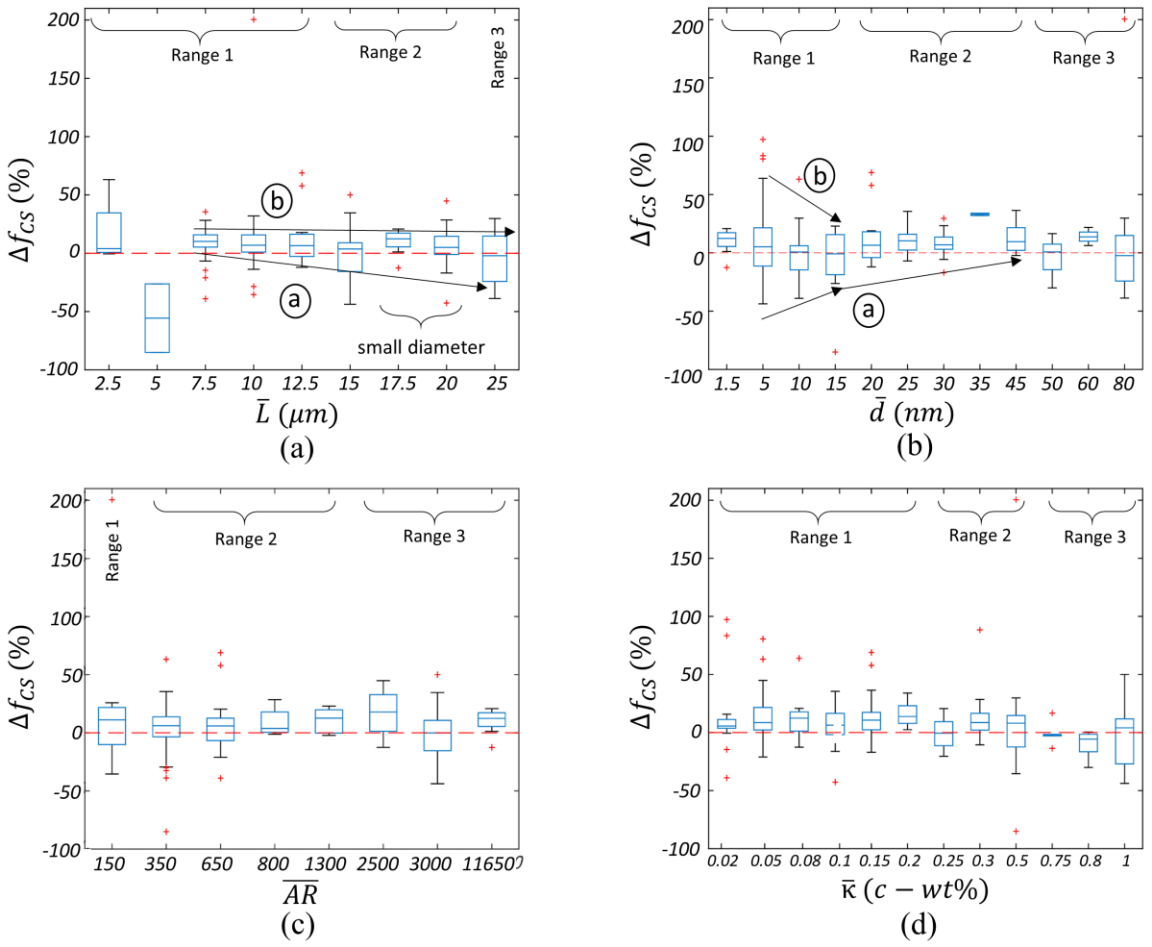

Figure 4-10. $\Delta f_{CS}(\%)$ as a function of CNT properties: (a) $\bar{L}$ (b) $\bar{d}$ (c) $\overline{AR}$ (d) $\bar{\kappa}$

Figure 4-10 (b) shows the boxplot of $\Delta f_{CS}(\%)$ with respect to various $\bar{d}$ ranging from 1.5 to 80 *nm*. The diameter of CNTs seems to be critical to maximize the likelihood of obtaining improved compressive performance. There are three ranges for $\bar{d}$ to characterize the effect of diameter of CNTs on $\Delta f_{CS}(\%)$: 1) $\bar{d} < 20$ *nm* (Range 1), 2) 20 *nm* $\leq \bar{d} \leq 45$ *nm* (Range 2), and 3) $\bar{d} \geq 50$ *nm* (Range 3). The minimum values of Δf_{CS} (%) gradually increase up to $\bar{d}$ of 45 *nm* (see arrow *a* in Ranges 1 and 2 in Figure 4-10 (b)). Also, the first quartiles continuously increased for CNTs having $\bar{d}$ between 15 and 30 *nm*, whereas, the third quartile values remained with minimal changes (13.5% ~18%). In Range 1, both the gain and loss in $\Delta f_{CS}(\%)$ are more pronounced compared with other ranges (see

arrows *a* and *b* in Figure 4-10 (b)). Incorporating CNTs with $\bar{d}$ of 5 *nm* resulted in the highest maximum and third quartile values of $\Delta f_{CS}(\%)$. However, the greatest minimum value was also observed for $\bar{d}$ = 5 *nm*, most probably due to the dispersion issues of CNTs with small diameters [184]. CNTs within Range 2 exhibited more cases of positive $\Delta f_{CS}(\%)$. However, their contribution is limited. In Range 3, most cases had the compressive strength lower than that of the control.

Figure 4-10 (c) shows the effect of $\overline{AR}$ of CNTs on $\Delta f_{CS}(\%)$. It indicates that there is no noticeable impact of aspect ratio on $\Delta f_{CS}(\%)$. In general, the median values of $\Delta f_{CS}(\%)$ of various $\overline{AR}$ are greater than zero. CNTs with $350 \leq \overline{AR} \leq 1300$ (Range 2) exhibited lower level of variations between the first and third quartile values. Beyond and below this range, CNTs with Ranges 1 and 3 exhibited high variations of compressive strength. Note that the acceptable compressive performance of CNTs with $\overline{AR}$ of 11650 could be attributed to their very small diameter ($\bar{d}$ = 1.5 *nm* in Figure 4-10 (b)).

Figure 4-10 (d) shows the impact of $\bar{\kappa}$ of CNTs on $\Delta f_{CS}(\%)$. The $\bar{\kappa}$ of CNTs is critical for the dispersion quality and the mechanical properties. Three ranges of $\bar{\kappa}$ can be defined: 1) $\bar{\kappa} \leq 0.2$ *c-wt*% (Range 1), 2) $0.2 < \bar{\kappa} \leq 0.5$ *c-wt*% (Range 2), and 3) $\bar{\kappa} > 0.5$ *c-wt*% (Range 3). The dominant data of $\Delta f_{CS}(\%)$ falls in the positive zone for $\bar{\kappa}$ within Range 1. The median and first quartile values of each group (within Range 1) had positive values, except for the $\bar{\kappa}$ = 0.1 *c-wt*% with the first quartile value of slightly below zero (-1.8%). In Range 2, the first quartile values mostly fall in the negative zone. However, the median values of each group still fall in the positive zone. Incorporating CNTs with $\bar{\kappa}$ within Range 2 degrades the compressive strength compared with Range 1. When incorporating CNTs within Range 3 concentration, most of the data falls in the negative zone. Furthermore, the

highest difference between the first and third quartiles was achieved for $\bar{\kappa}$ = 1 *c-wt*% (38.8%). These indicate the very high uncertainty while using excessive CNT concentrations.

4.7.2. Flexural Strength

Figure 4-11 shows the effect of CNT $\bar{L}$, $\bar{d}$, $\overline{AR}$, and $\bar{\kappa}$ on $\Delta f_{FS}(\%)$. Figure 4-11 (a) shows the effect of $\bar{L}$ on $\Delta f_{FS}(\%)$. It indicates that being different from the compressive strength, short CNTs (Range 1: $\bar{L} < 10$ μm) have limited contribution to the flexural strength. In Range 1, most of the data exhibits $\Delta f_{FS} \leq 0$. On the other side, when $\bar{L}$ ranges between 10 and 20 μm (Range 2), most of the data falls in the positive zone. The minimum and first quartile values showed a continuous increase for $\bar{L}$ between 2.5 and 12.5 μm, beyond which it started to decrease (see arrow *a* in Figure 4-11 (a)). Also, the median value of $\Delta f_{FS}(\%)$ increased for $\bar{L}$ between 5 and 12.5 μm and remained acceptable for $\bar{L}$ of 20 μm (see arrow *b* in Figure 4-11 (a)). However, when using CNTs with $\bar{L} > 20$ μm (Range 3), $\Delta f_{FS}(\%)$ is lower than Range 2. The good flexural performance for $\bar{L}$ of 55 μm, on the other side, can be explained by the wide range of CNT length (10 $\mu m \leq L \leq 100$ μm) [11, 16]. Thus, $\bar{L}$ of 55 μm cannot be considered as a good indicator.

Figure 4-11 (b) shows the effect of CNT $\bar{d}$ on $\Delta f_{FS}(\%)$. Despite the acceptable performance of CNTs with small $\bar{d}$ in the compressive strength (see Figure 4-11 (b)), CNTs having $\bar{d} < 15$ *nm* (Range 1) did not show a clear positive impact on getting higher $\Delta f_{FS}(\%)$. This could be confirmed by the increase in the maximum, third quartile, and median values of CNTs having $\bar{d}$ ranging from 5 to 15 *nm*. In Range 2 (15 *nm* $\leq \bar{d} \leq$ 30 *nm*), the likelihood of achieving positive $\Delta f_{FS}(\%)$ was significantly increased. The median value showed a continuous increase for $\bar{d}$ between 5 and 20 *nm* and remained almost

identical for $\bar{d}$ of 30 *nm* (see the arrow in Figure 4-11 (b)). The undesirable flexural performance of CNTs with $\bar{d}$ of 25 *nm* could be explained by their very large length (100-300 μm) [60]. The $\Delta f_{FS}(\%)$ for $\bar{d} = 25$ *nm*, at worst case, showed 10% reduction compared with the control. This further confirms the lower sensitivity of CNTs having $\bar{d}$ in Range 2 to other variables. The median value of CNTs within Range 3 ($\bar{d} \geq 50$ *nm*) showed degradation compared with Range 2. When incorporating CNTs with diameters within Range 3, the median values were mostly below zero. Although special care was taken for uniform dispersion of CNTs with $\bar{d}$ of 60 *nm* (repeated ultrasonication and centrifugation) [25], it did not show further improvement comparaed with Range 2 CNTs.

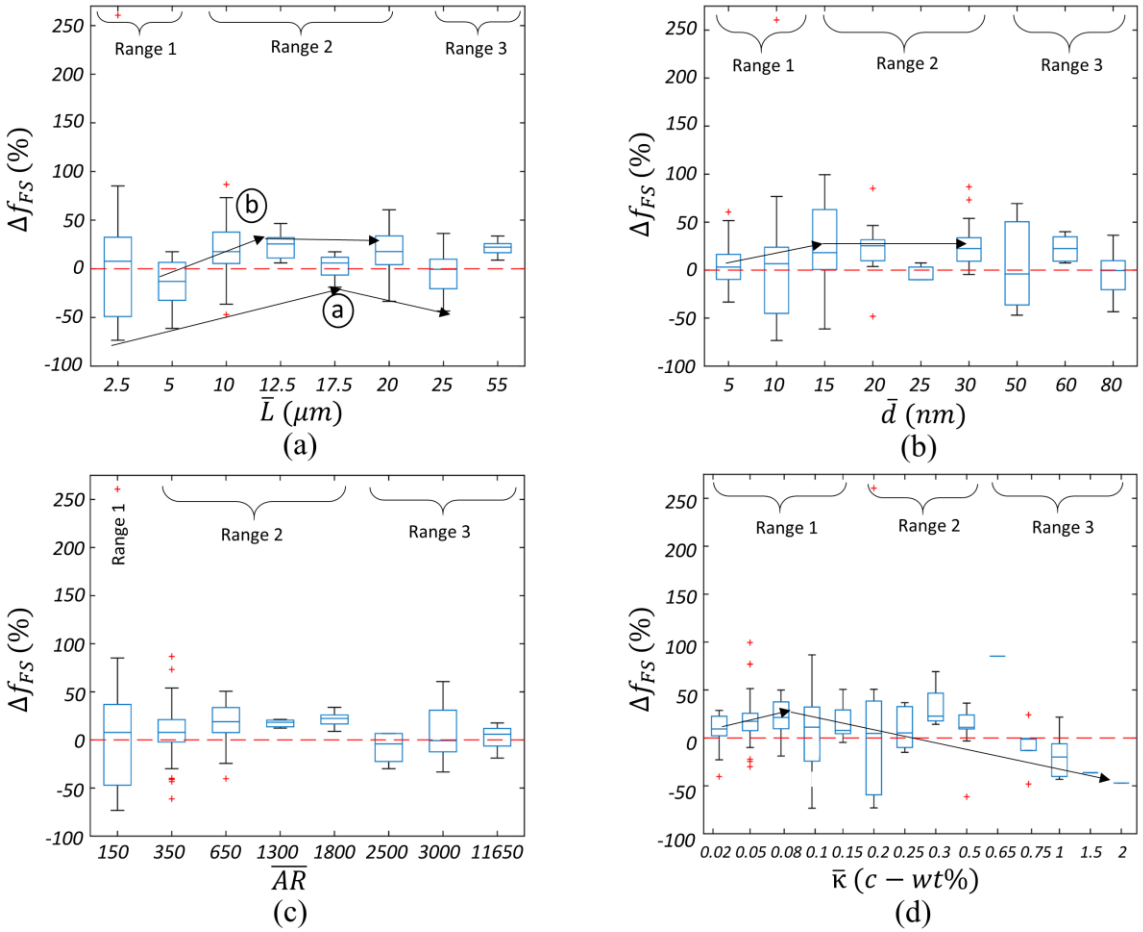

Figure 4-11. $\Delta f_{FS}(\%)$ as a function of CNT properties: (a) $\bar{L}$ (b) $\bar{d}$ (c) $\overline{AR}$ (d) $\bar{\kappa}$

Figure 4-11 (c) shows the effect of CNT $\overline{AR}$ on $\Delta f_{FS}(\%)$. CNTs having $\overline{AR}$ < 350 (Range 1) exhibited the high likelihood of obtaining negative $\Delta f_{FS}(\%)$. Both the lowest minimum and first quartile values of $\Delta f_{FS}(\%)$ were achieved for CNTs with $\overline{AR}$ of Range 1. The likelihood of obtaining positive $\Delta f_{FS}(\%)$ was increased for CNTs with $350 \leq \overline{AR} \leq 1800$ (Range 2). The median value of $\Delta f_{FS}(\%)$ showed continuous increase for $\overline{AR}$ between 150 and 1800. This confirms the better performance of CNTs with higher $\overline{AR}$, if selected from the optimum range. In Range 3 ($\overline{AR} \geq 2500$), the improvement in the flexural strength dropped dramatically.

Figure 4-11 (d) shows the effect of $\bar{\kappa}$ on $\Delta f_{FS}(\%)$. There are three identifiable ranges for CNT concentration: 1) $\bar{\kappa} \leq 0.15$ *c-wt*% (Range 1), 2) 0.15 *c-wt*% < $\bar{\kappa} \leq 0.5$ *c-wt*% (Range 2), and 3) $\bar{\kappa} > 0.5$ *c-wt*% (Range 3). The median value of $\Delta f_{FS}(\%)$ varied between -20% and 22.7% for the entire data, except for three $\bar{\kappa}$ of 0.65, 1.5, and 2 *c-wt*%. These $\bar{\kappa}$ lack the adequate number of experiments (only one experiment). In Range 1, most of the data falls in the positive zone of the diagram. The medians and first quartiles of all groups within Range 1 were greater than the control specimens except for $\bar{\kappa}$ of 0.1 *c-wt*%, which exhibited negative first quartile value. As $\bar{\kappa}$ increased up to 0.08 *c-wt*%, the median values of $\Delta f_{FS}(\%)$ increased. Thereafter, the median values continuously decreased by adding additional CNTs except for $\bar{\kappa}$ of 0.3 and 0.5 *c-wt*% (see the arrow in Figure 4-11 (d)). The improved flexural strength by increasing in $\bar{\kappa}$ up to certain limits have also been reported by other researchers [11, 16, 23]. In Range 2, the first quartiles for $\bar{\kappa}$ of 0.2 and 0.25 *c-wt*% exhibited negative values. Also, the median values were only marginally increased (about 6%), resulted from the excessive $\bar{\kappa}$ that degraded the quality of dispersion. The better performance of CNTs having $\bar{\kappa}$ = 0.3 *c-wt*% can be attributed to the direct

synthesis of CNTs onto the cement particles [75]. The direct growth of CNTs onto the surface of cement is a promising method that can be utilized to eliminate the tedious procedure of CNT dispersion within the cement matrix [74, 78]. In addition, although $\bar{\kappa}$ of 0.5 *c-wt*% showed good flexural performance, but the level of improvement in $\Delta f_{FS}(\%)$ was still lower than $\bar{\kappa}$ within Range 1 [97, 185]. When incorporating CNTs with concentrations within Range 3, the dominant data of $\Delta f_{FS}(\%)$ falls in the negative zone. Thus, this range of CNT concentration is not recommended.

4.8. Effect of CNT on the Elastic Modulus

The elastic modulus of CNT-cement nanocomposites is determined by the elastic properties of its components, CNT aspect ratio, and concentration. Figure 4-12 shows the influence of CNT $\bar{L}$, $\bar{d}$, $\overline{AR}$, and $\bar{\kappa}$ on the elastic modulus percent change ($\Delta f_E(\%)$) that can be defined as $\Delta f_E(\%) = \frac{f_{E\,(CNTs)} - f_{E\,(control)}}{f_{E\,(control)}} \times 100\%$.

Figure 4-12 (a) shows that the elastic modulus increases by increasing in CNT $\bar{L}$ up to 10 μm, beyond which $\Delta f_E(\%)$ degrades. The median value of $\Delta f_E(\%)$ increased from 4% to 68.7% by increasing in $\bar{L}$ from 1.5 to 10 μm. Thereafter, the reduction in $\Delta f_E(\%)$ was obvious for CNTs with $\bar{L}$ of 20 and 21 μm, most probably due to dificulty in achieving uniform dispersion. The acceptable performance of CNTs with $\bar{L}$ = 55 μm can be explained by the wide range of CNT length (10 μm < L < 100 μm) [11, 16].

Figure 4-12 (b) shows the continuous increase in $\Delta f_E(\%)$ by increasing in CNT $\bar{d}$. The median value of $\Delta f_E(\%)$ increased from -12.1% to 33% by increasing in $\bar{d}$ up to 30 *nm*. Considering the stronger interfacial bond strength between smaller diameter CNTs and cement matrix, this might seem the oposite conclusion. This could be explained by dificulty

in getting a uniform dispersion of CNTs having small diameters ($\bar{d} \leq 10\ nm$).

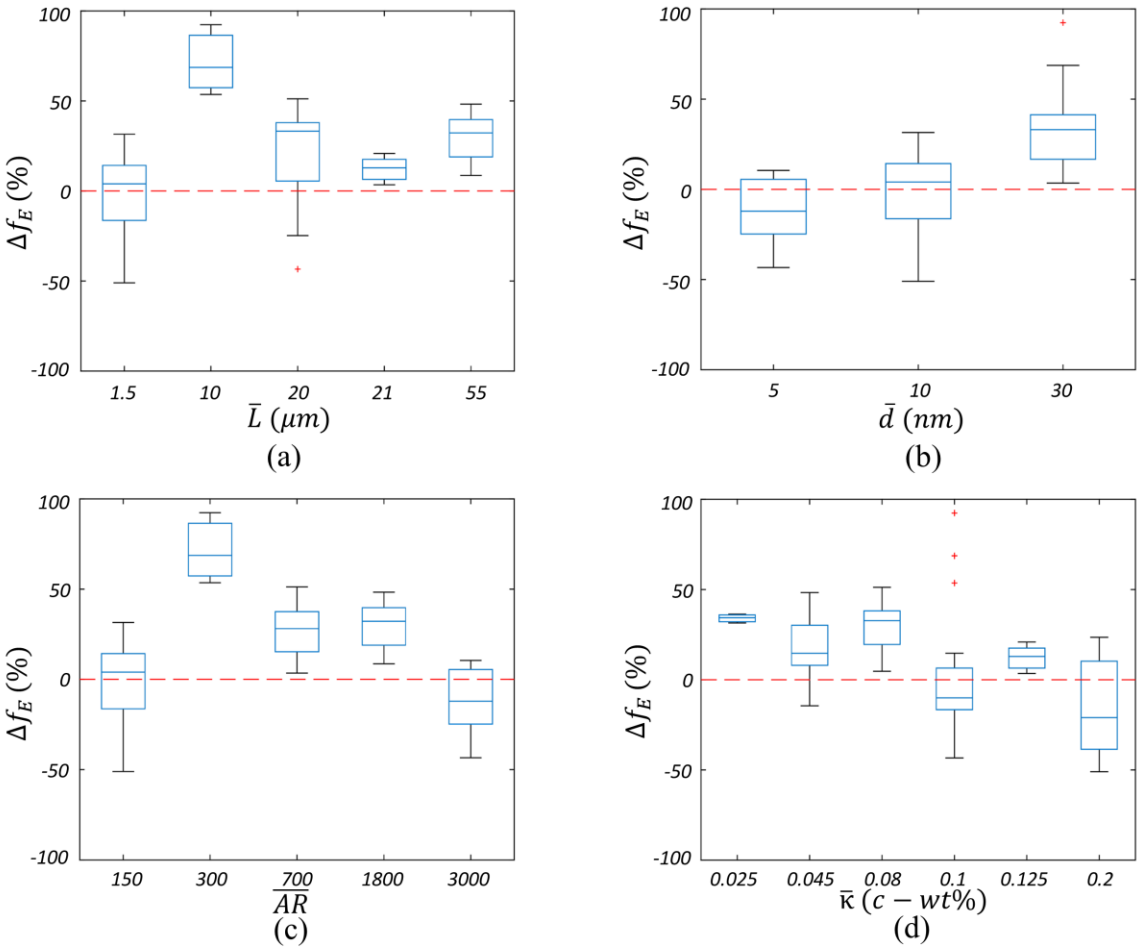

Figure 4-12. Effect of CNT properties on elastic modulus: (a) $\bar{L}$ (b) $\bar{d}$ (c) $\overline{AR}$ (d) $\bar{\kappa}$

Figure 4-12 (c) shows the very high probability of obtaining $\Delta f_E(\%) \leq 0$ in $\overline{AR}$ of either 150 or 3000. The lowest median and first quartile values of $\Delta f_E(\%)$ were correlated with $\overline{AR}$ of 3000 by -12.1% and -24.8%, respectively. Also, CNTs with $\overline{AR}$ of 150 resulted in the second lowest median and first quartile values by 4% and -16.4%, respectively. CNTs with $\overline{AR}$ between 300 and 1800 always exhibited a higher elastic modulus than the control. These findings are in good agreement with the findings in Figure 4-12 (a) and (b).

Figure 4-12 (d) shows the effect of $\bar{\kappa}$ of CNTs on $\Delta f_E(\%)$. Below CNT $\bar{\kappa}$ of 0.1 *c-wt%*, most of the data shows positive $\Delta f_E(\%)$. However, for CNTs having $\bar{\kappa} \geq 0.1$ *c-wt%*,

the dominant data shows degradation in elastic modulus compared with the control. Therefore, $\bar{\kappa} = 0.1$ *c-wt*% can be set as the percolation threshold, beyond which CNTs tend to agglomerate, acting as mechanical defects.

4.9. Effect of CNT on the Toughness

Figure 4-13 shows the influence of CNT $\bar{L}$,$\bar{d}$, $\overline{AR}$, and $\bar{\kappa}$ on the toughness percent change ($\Delta f_T(\%)$) where $\Delta f_T(\%) = \frac{f_{T\,(CNTs)} - f_{T\,(control)}}{f_{T\,(control)}} \times 100\%$.

CNTs with $\bar{L}$ of 1.5 μm resulted in the lowest minimum (-77.8%) and first quartile (-32.2%) values of $\Delta f_T(\%)$. This might be explained by limited crack bridging of short CNTs. Thus, they debonded prematurely and $\Delta f_T(\%)$ did not increase greatly, indicating short CNTs had limited post-cracking load carrying capacity [187]. The median value of $\Delta f_T(\%)$ varied between 19.6% and 56% and showed an increase by increasing in $\bar{L}$ up to 17.5 μm (see Figure 4-13 (a)). The higher pull-out strength of CNTs is the main contribution of longer CNTs. However, CNTs having $\bar{L}$ of 20 μm degraded $\Delta f_T(\%)$, most probably due to the dispersion issues, which led to the premature debonding of CNTs from the matrix. Another possible reason could be the transition in the failure mode of long CNTs, resulting in the reduction of $\Delta f_T(\%)$. Chen *et al*. [187] concluded that in case of a strong CNT-matrix bond, the failure mode of CNTs was changed from debond failure to breakage of CNTs by increasing in CNT length, resulted in lower toughness.

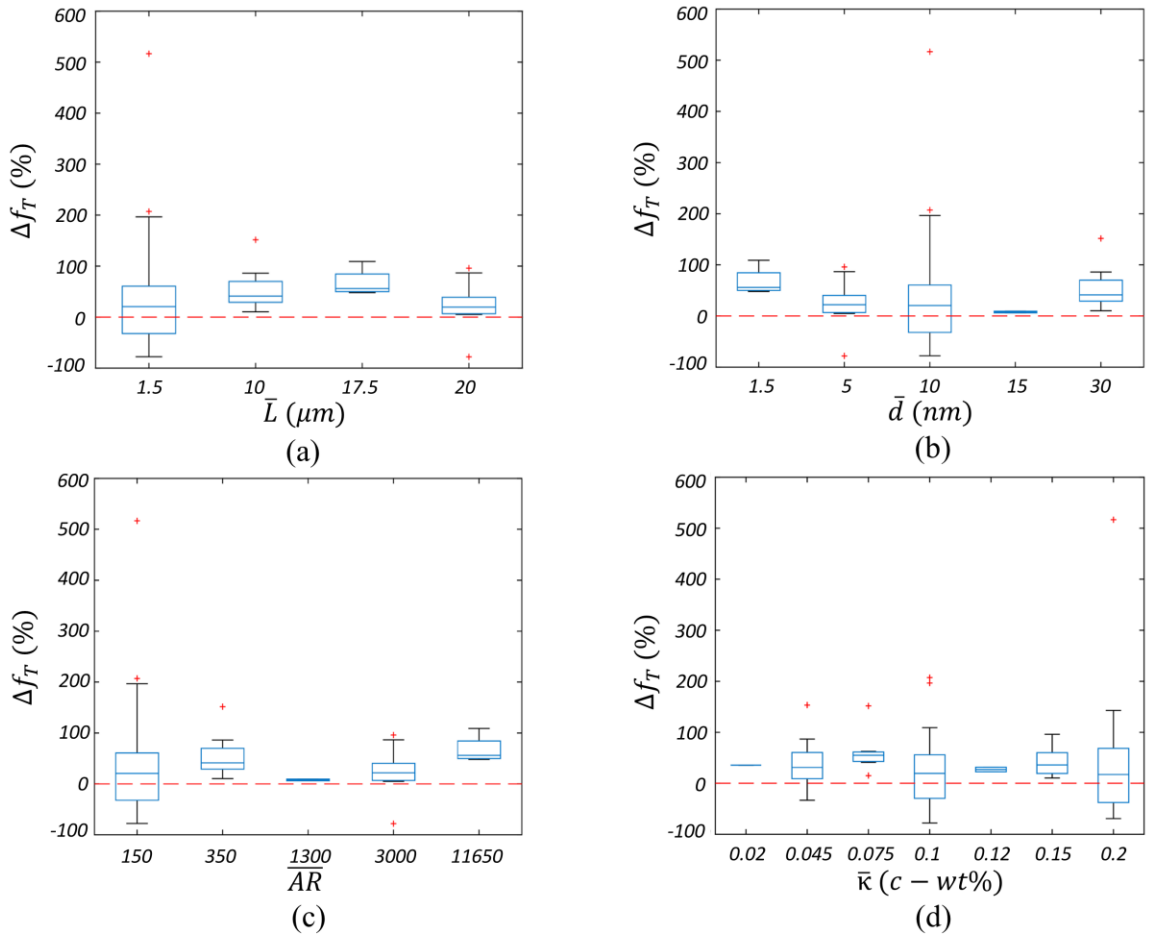

Figure 4-13. Effect of CNT properties on the toughness: (a) $\bar{L}$ (b) $\bar{d}$ (c) $\overline{AR}$ (d) $\bar{\kappa}$

Figure 4-13 (b) shows that CNTs with the smallest diameter ($\bar{d}$ = 1.5 *nm*) outperforms with respect to the toughness. This might be explained by the higher surface area of smaller diameter CNTs, resulting in higher interfacial bond strength between CNTs and cement matrix. The median value of $\Delta f_T(\%)$ decreased from 56% to 7.8% by increasing in CNT $\bar{d}$ up to 15 *nm*. On the other side, CNTs with $\bar{d}$ of 30 *nm* had the second highest minimum, first quartile, median, and third quartile values of toughness, due to their higher flexural strength (see Figure 4-13 (b)).

Figure 4-13 (c) suggests the better performance of CNTs with higher $\overline{AR}$ in terms of toughness. Also, CNTs with $\overline{AR}$ of 11650 outperformed compared with other groups.

This can support the earlier analysis that showed CNTs with longer $\bar{L}$ and smaller $\bar{d}$ had positive impacts on the toughness (see Figure 4-13 (a) and (b)). Similarly, toughness of polymers containing CNTs with high aspect ratios was found to be significantly increased [188].

If CNTs are well dispersed, the higher $\bar{\kappa}$ of CNTs decreases the fiber free area, resulting in higher $\Delta f_T(\%)$. In contrast, the excessive amount of CNTs increases the chance of interface defects between CNTs and cement hydration products, resulting in hindering of cracks coalescene [30]. Figure 4-13 (d) shows $\Delta f_T(\%)$ of all experiments was above the control for CNTs with $\bar{\kappa} \leq 0.075$ *c-wt*%, except for one data point ($\bar{\kappa} = 0.045$ *c-wt*%) that exhibited 33% reduction in the toughness. Also, the median value increased from 31% to 55.1% for the $\bar{\kappa}$ ranging from 0.045 to 0.075 *c-wt*%. The concentration of 0.1 *c-wt*% seems to be the threshold for getting the higher toughness level.

4.10. Other Important Variables and their Interactions

In addition to the proposed optimum ranges, there are other important variables that affect the mechanical properties such as testing age, cement matrix composition, dispersion procedure, etc. Therefore, further research is needed to investigate the possible interactions between these variables affecting the mechanical properties. Through analyzing the extensive literature data, five main interactions affecting the dispersion quality and the mechanical properties were identified as follows:

1. CNT concentration and aspect ratio
2. ultrasonication energy and amplitude
3. ultrasonication energy and surfactant
4. *w/c* ratio and *s/c* ratio

5. CNT concentration and hydration age

4.10.1. CNT Concentration and Aspect Ratio (Interaction *I*)

The concentration of CNTs (κ) influences both the dispersion quality and the mechanical properties. The concentrations of CNTs ranged from 0.007 *c-wt*% [92] to 2 *c-wt*% [94]. The mechanical properties improve as κ increases up to a certain limit, beyond which the mechanical properties degrade due to the dispersion issues [28, 31, 110, 174, 189]. Besides, due to the different mechanisms of CNTs affecting the compressive and flexural strengths (see Section 2.6.1), although excessive κ hurts the flexural strength, it might be tolerable in terms of the compressive strength (at certain ranges of CNT length and diameter). For example, Dangolidis *et al*. [31] incorporated different κ ranging from 0.08 to 0.5 *c-wt*% to increase the mechanical properties of cement mortars. The results indicated that beyond κ = 0.1 *c-wt*%, the flexural strength degraded by adding additional CNTs, whereas the compressive strength did not experience reduction by adding higher CNT concentration.

Also, the optimum κ is correlated with CNT aspect ratio (*AR*). The higher concentration of short CNTs exhibited comparable mechanical properties as lower concentration of long CNTs did [16, 23, 170].

4.10.2. Ultrasonication Energy and Amplitude (Interaction *II*)

Amongst various dispersion techniques, pre-dispersion of CNTs in water using a surfactant assisted ultrasonication procedure (US+S) is the most common route. Therefore, this research focuses on US+S technique for CNT dispersion.

In an ultrasonication process, the ultrasonication amplitude (*UA*) governs the amount of energy delivered to the solution within a designated time (i.e., the intensity of

ultrasonication energy). Although a high *UA* might help CNT dispersion [190], it may cause more damage to CNTs [191]. Conversely, a low *UA* might minimize the breakage of CNTs, but it significantly increases the duration of an ultrasonication process. Therefore, the duration of an ultrasonication process (t_s) should be adjusted depending on *UA* to yield the required total ultrasonication energy (UE_T) to overcome the VdW forces. When excessive UE_T is induced, CNTs would be broken into shorter tubes [192]. Therefore, an optimized threshold of UE_T is critical. For example, Konsta-Gdoutos *et al*. [11] and Zou *et al*. [12] achieved comparable improvement in the mechanical properties (flexural strength and elastic modulus) of CNT-cement pastes using UE_T of 2800 *J/ml* (*UA* = 50%) and 150 *J/ml* (*UA* = 100%), respectively. This indicates that lower threshold of UE_T might be used when using higher *UA*. When a high *UA* of 100% was used, increasing UE_T from 75 to 400 *J/ml* resulted in the reduction of CNT average length from 661 to 392 *nm* [192]. This may degrade the interfacial bond strength, due to the lower bond capacity of shorter CNTs [122, 188].

4.10.3. Ultrasonication Energy and Surfactant (Interaction *III*)

The surfactant-to-CNTs ratio (by mass) is often used to retain stable CNT dispersion over time [16, 60]. The surfactant-to-CNTs ratio in cementitious materials ranged from zero (i.e., no surfactant used) to 90 [62, 64, 92, 94, 115]. However, an excessive surfactant-to-CNTs ratio resulted in the re-agglomeration of CNTs [16, 60]. Also, either lower UE_T with higher surfactant-to-CNTs ratio or higher UE_T with lower surfactant-to-CNTs ratio might be used to achieve comparable CNT dispersion [176]. Similarly, utilizing lower UE_T with higher surfactant-to-CNTs ratio produced comparable mechanical properties as incorporating higher UE_T with lower surfactant-to-CNTs ratio

did [12, 16]. This indicates that there might be an interaction between UE_T and surfactant-to-CNTs ratio.

4.10.4. *w/c* and *s/c* Ratios (Interaction *IV*)

As discussed in Section 2.5, in cementitious materials containing CNTs, SP has two functions: surfactant for CNT dispersion and admixture to enhance the flowability of cement matrix. If improperly designed, there is a possibility for cement grains to intake the part of the SP leaving insufficient SP to function as a surfactant on CNT surface which may lead to re-agglomoration [94, 193, 194], degrading the mechanical properties. Therefore, the cement matrix composition (e.g., *w/c* and *s/c* ratios) can be another important consideration for proper CNT dispersion. The lower *w/c* ratio and/or higher *s/c* ratio (denser material) may limit the free movements of CNTs, reducing re-agglomeration. Similarly, fly ash or silica fume mitigated the agglomeration by blocking CNT movement in the mixture [20, 62, 65]. Ahmed *et al*. [170] also found similar trends when incorporating various types of CNTs in cement mortars with *w/c* ratios ranged from 0.35 to 0.55. The highest increase in the flexural strength compared with the control was achieved when using the lowest *w/c* ratio. Also, in most cases, *w/c* = 0.55 exhibited the lowest enhancement in the flexural strength [170]. The similar trend was also observed in [11, 16].

4.10.5. CNT Concentration and Hydration Age (Interaction *V*)

The hydration process of cement might be influenced by CNT concentration (κ). As κ increased, the rate of the gain in the compressive strength [174] , splitting-tensile strength [116], and flexural strength [31] was found to be higher over time. This indicates that there might be an interaction between κ and age of specimen (*t*) to achieve superior mechanical properties. The slower hydration process of cement when using high κ might

be attributed to covering the surface of cement powders by CNTs, limiting the access of water for cement [76]. This effect might be aggravated when COOH functional groups are attached to the surface of CNTs [93]. The COOH-CNTs becomes hydrophilic which tends to absorb water and slowly release the retained water over time [93]. Therefore, they absorb more water at higher κ, resulting in slower progress in the hydration process of cement. Musso *et al*. [117] performed TGA after grinding the 28-day specimens to investigate the effect of COOH-CNTs on cement hydration. The results showed the significant reduction of tobermorite gel in the presence of 0.5 *c-wt*% COOH-CNTs compared with the control specimen. On the other side, in some cases (e.g., certain ranges of κ, type, and dosage of surfactant, etc.), CNTs might work as nucleation sites and increase the rate of hydration at early ages [72]. However, this phenomena is beyond the scope of this study, and therefore is neglected.

4.11. Summary

Through extensive data analysis, this chapter provided guidelines for future researchers and engineers to select the correct type of CNTs to tailor the mechanical properties for various structural applications based on different strengthening mechanisms. To identify the optimum ranges, a total of 2363 experimental data (44 studies) from the literature was used. The analyses revealed that CNT properties contributed differently to the mechanical properties. The following conclusions were drawn:

1. The length of CNTs was found to have minimal influence on the compressive strength. Whereas, relatively longer CNTs outperformed in the flexural strength, elastic modulus, and toughness.

2. CNTs with small diameters benefited the compressive strength and toughness. However, they adversely affected the flexural strength and elastic modulus.
3. Generally, average length and diameter ranging from 10 to 20 μm and 20 to 32.5 *nm*, respectively, significantly contributed to obtaining higher mechanical properties (compressive strength, flexural strength, elastic modulus, and toughness). This corresponds to CNT aspect ratio between 300 and 1000.
4. Concerning CNT concentration, the optimal upper limit of 0.15 *c-wt*% and 0.2 *c-wt*% were obtained for flexural and compressive strengths, respectively. Also, CNT concentration of 0.1 *c-wt*% was found to be the threshold limit for the elastic modulus and toughness.
5. Besides CNT intrinsic properties, other potential variables and five main interactions between them need to be considered to make stronger and stiffer concrete. The most important interactions affecting the mechanical properties are: *I*) interaction between CNT concentration and aspect ratio, *II*) interaction between ultrasonication energy and amplitude, *III*) interaction between ultrasonication energy and surfactant, *IV*) interaction between *w/c* and *s/c* ratios, and *V*) interaction between CNT concentration and hydration age. To date, the contributions of most of these interactions to the mechanical properties were not quantified using a prediction model. Therefore, this study aims to develop prediction models that can capture these interactions.

CHAPTER 5. EXPERIMENTAL PROGRAM

5.1. General

This chapter presents the raw materials (Section 5.2), mix proportions and sample preparations (Section 5.3), as well as test procedures (Section 5.4) used for experimental investigation on flowability, mechanical properties, and durability of CNT-cement nanocomposites (pastes and mortars). In the following chapter (Chapter 6), experimental test results will be discussed.

5.2. Raw Materials

This section describes the raw materials used throughout the experimental program of this research.

5.2.1. Cement

Type I/II ordinary Portland cement conforming to ASTM C150-09 [195], "Standard Specification for Portland Cement," was used in this study. The average size of cement grains was 11.4 μm which was measured via laser particle size analyzer. The Blaine surface area of this cement was 400.8 m^2/kg. Table 5-1 lists the chemical compositions of the cement determined through X-ray Fluorescence (XRF) provided by the manufacturer (CEMEX, Louisville plant, KY, USA). Also, the mineral compositions of the cement were assessed using the Bogue's equation [196] and are presented in Table 5-2.

Table 5-1. Chemical Composition of Type I/II Ordinary Portland Cement

Compound	SiO_2	AL_2O_3	Fe_2O_3	CaO	MgO	SO_3	Na_2O	K_2O	LoI
wt%	19.7	4.84	3.05	62.62	4	3.23	0.15	0.49	1.21

LoI: loss on ignition

Table 5-2. Mineral Composition of Type I/II Ordinary Portland Cement

Compound	C_3S	C_2S	C_3A	C_4AF
wt%	59.1	11.9	7.67	9.3

5.2.2. CNTs

Two types of CNTs synthesized using a CVD technique denoted as Type I (manufacturer: Nanostructured & Amorphous Materials) and II (manufacturer: US Research Nanomaterials) were used in this research. Both types of CNTs had the same average length ($\bar{L}$) of 20 μm (10 < L < 30 μm). The outside diameter of Type I CNTs was smaller than 8 *nm*, whereas the outside diameter of Type II CNTs ranged between 20 and 30 *nm* ($\bar{d} = 25$ *nm*). This resulted in the average aspect ratios ($\overline{AR}$) of 2500 and 800 for Type I and II CNTs, respectively. Also, Type I CNTs possess COOH functional groups covalently bonded to their sidewalls, while Type II CNTs are pristine (without covalently bonded functional groups on their surface). The physical properties of CNTs are listed in Table 5-3.

Table 5-3. Physical Properties of CNTs

Type	Outside diameter (*nm*)	Inside diameter (*nm*)	Length (μm)	$\overline{AR}$ (unitless)	Surface area (m^2/gr)	Purity (%)
I	< 8	2-5	10-30	2500	> 500	> 95
II	20-30	5-10	10-30	800	> 500	> 95

Type I CNT is COOH functionalized (3.67-4.05 *wt*%)

5.2.3. Surfactant and Water

A commercially available poly-carboxylate based superplasticizer (SP) conforming to Types A and F in ASTM C494-05 [197], "Standard Specification for Chemical Admixtures for Concrete," and Type I in ASTM C1017-03 [198], "Standard Specification for Chemical Admixtures for Use in Producing Flowing Concrete" was used as a surfactant

for CNT dispersion. The density of the superplasticizer was 1.1 *kg/l* (8.9 *lb/gal*). Tap water was used to fabricate the specimens.

5.2.4. Sodium Hydroxide

Pure sodium hydroxide pellets with a molecular weight of 39.997 *g*/*mol* were used to prepare sodium hydroxide solution in accordance with ASTM C1260-14 [199], "Standard Test Method for Potential Alkali Reactivity of Aggregates (Mortar-Bar Method)."

5.2.5. Sand

A 20-30 silica sand conforming to ASTM C778-06 [200], "Standard Specification for Standard Sand" was used as aggregate. Also, local river sand was obtained in accordance with ASTM C33-13 [201], "Standard Specification for Concrete Aggregates." The fineness modulus of the river sand was 2.92. The specific gravity of the river sand was 2.69 and 2.66 at oven dry and saturated surface dry conditions, respectively. The absorption capacity of the river sand was 0.775%.

For durability tests, concrete sandstone (chemical name: quartz) from central city sand plant (Pennsylvania, USA) was used as aggregate. This sand is considered to be ASR reactive according to Pennsylvania Department of Transportation (PennDOT). The fineness modulus of the sandstone was 2.90. The specific gravity of sandstone was 2.8 and 2.76 at oven dry and saturated surface dry conditions, respectively. The absorption capacity of the sandstone was 0.943%. The grading curves of river sand and sandstone are shown in Figure 5-1.

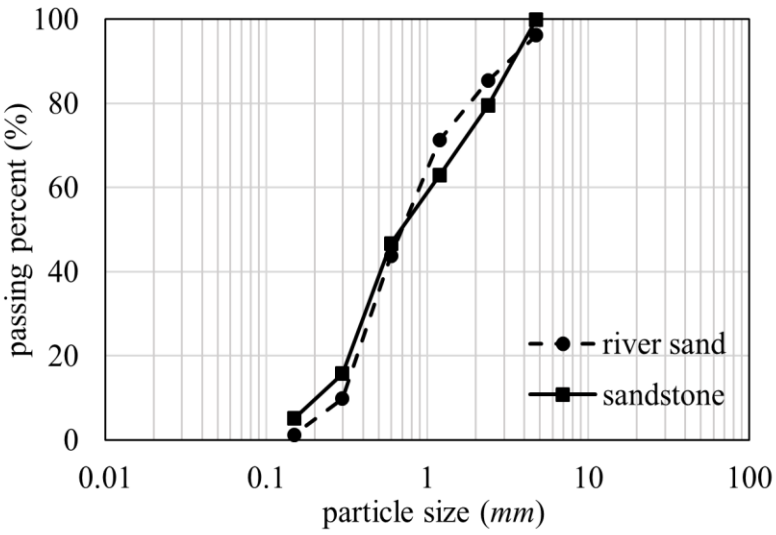

Figure 5-1. Grading curves of river sand and sandstone

In this research, both river sand and sandstone were graded such that 10% of the total mass retained on sieve No. 8, 25% retained on sieve Nos. 16, 30 and 50, and 15% retained on sieve No. 100 in accordance with ASTM C1260-14 [199] (see Table 5-4).

Table 5-4. River Sand and Sandstone Grading

Sieve size		Mass, %
Passing	Retained	
4.75 *mm* (No. 4)	2.36 *mm* (No. 8)	10
2.36 *mm* (No. 8)	1.18 *mm* (No. 16)	25
1.18 *mm* (No. 16)	600 *μm* (No. 30)	25
600 *μm* (No. 30)	300 *μm* (No. 50)	25
300 *μm* (No. 50)	150 *μm* (No. 100)	15

5.3. Mix Proportions and Sample Preparations

This section presents the mix proportions and sample preparations used for the experimental investigation on flow (Section 5.3.1), mechanical (Section 5.3.2), and durability (Section 5.3.3) properties of cement pastes and mortars.

5.3.1. Flow Properties (*C* and *M* series)

The mix proportions (Section 5.3.1.1) and sample preparations (Section 5.3.1.2) for the flow properties is discussed as follows.

5.3.1.1. Mix Proportions

In case of cement pastes, three different *w/c* ratios of 0.35, 0.45 and 0.6 were employed and for each *w/c* ratio, four different SP dosages were used to study their influences on flowability. The concentration of CNTs for all paste specimens was 0.1 *c-wt*% of Type I CNTs. Mix proportions of paste samples are listed in Table 5-5.

Table 5-5. Test Identifications and Mix Proportions for Cement Pastes (*C* series)

Test ID	*w/c* ratio	SP (*c-wt*%)	CNTs (*c-wt*%)	*SP/CNTs* ratio
*C*1	0.35	0.3	0.1	3
*C*2		0.4		4
*C*3		0.6		6
*C*4		0.9		9
*C*5*		0.3	-	-
*C*6	0.45	0.3	0.1	3
*C*7		0.4		4
*C*8		0.5		5
*C*9		0.6		6
*C*10*		0.3	-	-
*C*11	0.6	0.1	0.1	1
*C*12		0.2		2
*C*13		0.3		3
*C*14		0.4		4
*C*15*		0.3	-	-

Note: *indicates the control mix (without CNTs) for each *w/c* ratio

For cement mortars, three different *w/c* ratios of 0.35, 0.45 and 0.6 were used. For each *w/c* ratio, three different concentrations of Type I CNTs were employed (0.05, 0.1, and 0.15 *c-wt*%). For all of the listed test identifications (IDs) in Table 5-6, silica sand was used and its volume was fixed at 60% of the total volume. Also, a fixed dosage of SP was used for each *w/c* ratio.

Table 5-6. Test Identifications and Mix Proportions for Cement Mortars (*M* series)

Test ID	water:cement:sand (ratio by volume)	SP (*c-wt*%)	CNTs (*c-wt*%)	*SP/CNTs* ratio
*M*1	0.35:1:2.6	0.6	0.05	12
*M*2			0.1	6
*M*3			0.15	4
*M*4*			-	-
*M*5	0.45:1:3.0	0.4	0.05	8
*M*6			0.1	4
*M*7			0.15	2.7
*M*8*			-	-
*M*9	0.6:1:3.6	0.2	0.05	4
*M*10			0.1	2
*M*11			0.15	1.3
*M*12*			-	-

Note: *indicates the control mix (without CNTs) for each *w/c* ratio

5.3.1.2. Sample Preparations

For the control pastes (*C*5, *C*10 and *C*15; see Table 5-5), a mixture of water and SP was gradually added to the cement over the first minute of mixing and then continued to mix for two additional minutes at a speed of 136 *rpm* using a kitchen mixer (Model: Kitchen Aid Pro Line Stand Mixer). The sample was then allowed to rest for two minutes, which was followed by a mixing of another three minutes at a high speed of 195 *rpm*.

In case of CNT-cement pastes, water and SP were first mixed with a glass stirring rod. Then, CNTs were added to the aqueous solution (i.e., water + SP) and sonicated for 25 minutes at room temperature with 75% of the maximum amplitude of a 500 *W* ultrasonic processor having a probe tip of 12 *mm* (1/2 *in.*) (see Figure 5-2 (a)). The sonication was done at cycle intervals of 25 seconds in order to prevent overheating of CNTs. After sonication, the temperature of the prepared suspension (i.e., CNTs + water + SP) was gradually decreased to reach the ambient room temperature of 25 ℃ (77 ℉) using a water

circulator prior to mixing with cement (see Figure 5-2 (b)). The cement and the prepared suspension were mixed with the same procedure of control mixes.

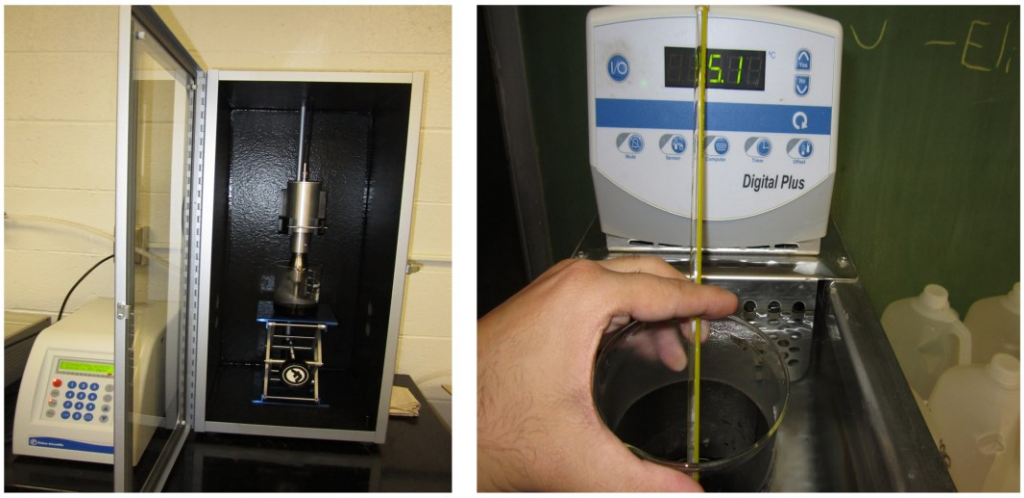

(a) (b)

Figure 5-2. Test equipment: (a) tip horn ultrasonicator (b) water circulator

For mortar samples, first, cement and the first half of the silica sand were mixed. Then, water (or the prepared suspension) and the rest of silica sand were gradually added to the mixture over the first minute of mixing, followed by the same mixing procedure as of cement pastes. For each test ID, at least two batches were prepared to measure the average flow diameter of CNT-cement mortars.

5.3.2. Mechanical Properties (*I~V* and *R* series)

This section provides mix proportions (Section 5.3.2.1) and sample preparations (Section 5.3.2.2) used for the mechanical properties.

5.3.2.1. Mix Proportions

The mix proportions of CNT-cement nanocomposites (pastes and mortars) used for mechanical property tests are presented in Table 5-7. The mix proportions were varied to investigate the interactions between two experimental variables on the mechanical properties (see the bolded variables for each interaction in Table 5-7); interaction between

AR and κ (interaction *I*), interaction between UE_T and *UA* (interaction *II*), interaction between UE_T and *SP/CNTs* ratio (interaction *III*), interaction between *w/c* and *s/c* ratios (interaction *IV*), and interaction between κ and *t* (interaction *V*).

In the test ID (see the third column in Table 5-7), the first letter stands for the interaction number followed by the amount of two experimental variables that are investigated. For example, test ID *I*-800/0.05 is used for interaction *I* (interaction between *AR* and κ) having *AR* and κ of 800 and 0.05 *c-wt*%, respectively. Also, the control specimens used for different interactions are listed in Table 5-8. In the *s/c* ratio columns in Table 5-7 and Table 5-8, the letters *R* and *S* reflect the type of sand (*R*: river sand and *S*: silica sand) followed by mixing procedure (*A* or *B*) used. The mixing procedures *A* and *B* are presented in Section 5.3.2.2.

Table 5-7. Test Identifications and Mix Proportions for CNT-Cement Nanocomposites (*I*~*V* series)

Interaction #	Interaction Variables	Test ID	*w/c* ratio	*s/c* ratio	*AR*	κ (*c*-*wt*%)	UE_T (*J/ml*)	UE_m (*J/ml/min*)	*UA* (%)	*SP/CNTs ratio*	*t* (days)
I	*AR* & κ	*I*-800/0.05	0.35	2 (*S*-*A*)	**800**	**0.05**	2610 ± 15	9.4± 0.2	57	6	28
		I-800/0.1‡				**0.1**					
		I-800/0.3 +				**0.3**					
		I-2500/0.05			**2500**	**0.05**					
		I-2500/0.1				**0.1**					
		I-2500/0.3				**0.3**					
II	UE_T & *UA*	*II*-500/50	0.45	2.25 (*R*-*B*)	800	0.1	**500**	6.5± 0.2	**50**	3	7
		II-1000/50					**1000**				
		II-1500/50					**1500**				
		II-200/75					**200**	13.5± 0.2	**75**		
		II-300/75					**300**				
		II-500/75					**500**				
		II-1000/75					**1000**				
III	UE_T & *SP/CNTs*	*III*-500/4	0.45	2.25 (*R*-*B*)	800	0.025	**500**	6.5± 0.2	50	**4**	7
		III-500/12								**12**	
		III-1500/4					**1500**			**4**	
		III-1216/6		3 (*S*-*A*)		0.1	**1216**	9.4± 0.2	57	**6**	28
		III-1850/12					**1850**			**12**	
		III-2733/6 *					**2733**			**6**	
IV	$^{w}/_{c}$ & $^{s}/_{c}$	*IV*-0.35/2‡	**0.35**	**2**(*S*-*A*)	800	0.1	2610 ± 15[a]	9.4± 0.2	57	6	28
		IV-0.45/0	**0.45**	**0** (*A*)			2218 [a]	7.8			
		IV-0.45/3 *		**3**(*S*-*A*)			2733 [a]	9.4± 0.2			
		IV-0.6/2	**0.6**	**2**(*S*-*A*)			2523 [a]	8.9			
V	κ & *t*	*V*-0.1/3‡	0.35	2 (*S*-*A*)	800	**0.1**	2610 ± 15	9.4± 0.2	57	6	**3**
		V-0.3/3 +				**0.3**					
		V-0.1/28‡				**0.1**					**28**
		V-0.3/28 +				**0.3**					

Note: *, ‡, and + indicate the same mix proportions. [a]Ultrasonication Energy Indicator (UEI) = $\left(\frac{UE_T}{UE_m}\right)^{UA}$ = 25 (see Chapter 8)

Table 5-8. Test Identifications and Mix Proportions for Control Specimens (*R* series)

Test ID	*w/c* ratio	*s/c* ratio	*t* (days)	Interaction
*R*1	0.35	2 (*S-A*)	28	*I & IV & V*
*R*2	0.45	2.25 (*R-B*)	7	*II & III*
*R*3	0.45	3 (*S-A*)	28	*III & IV*
*R*4	0.45	0 (*A*)	28	*IV*
*R*5	0.6	2 (*S-A*)	28	*IV*
*R*6	0.35	2 (*S-A*)	3	*V*

In interaction *I*, two levels of *AR* (Type I: *AR* of 2500 and Type II: *AR* of 800) were employed, and for each *AR*, three different κ ranging from 0.05 to 0.3 *c-wt*% were used. The *UA* and UE_T were fixed at 57% and 2610 ± 15 *J/ml*, respectively, for all the investigated test IDs within interaction *I*. Although Type I and II CNTs are COOH-functionalized and pristine, respectively, this study did not consider CNT chemical functionalization as an important variable to affect the mechanical properties. Similarly, previous studies found that the impact of chemical functionalization on the mechanical properties was minimal compared to other CNT properties [28, 170].

In interaction *II,* two levels of *UA* (50 and 75%) were used. Also, UE_T was varied between 200 and 1500 *J/ml*. When investigating the effects of the studied experimental variables on 7-day mechanical properties within interaction *II*, other experimental variables were kept constant. The *w/c* and *s/c* ratios were 0.45 and 2.25, respectively. In addition, all of the test IDs had 0.1 *c-wt*% of type II CNTs (*AR* = 800) with *SP/CNTs* = 3.

In interaction *III*, half of the test IDs used river sand in which two levels of UE_T (500 and 1500 *J/ml*) and *SP/CNTs* ratio (4 and 12) were used for 7-day testing. The other half used silica sand in which three levels of UE_T (ranging from 1216 to 2733 *J/ml*) and two levels of *SP/CNTs* ratio (6 and 12) were used for 28-day testing. Note that CNT concentration of 0.025 and 0.1 *c-wt*% were used for 7-day and 28-day mechanical testing, respectively.

In interaction *IV,* three levels of *w/c* ratios ranging from 0.35 to 0.6 and three levels of *s/c* ratios ranging from 0 to 3 were employed. Note that although UE_T was not the same for the test IDs within interaction *IV*, but all of them had the same Ultrasonication Energy Indicator (*UEI*) which will be defined in Chapter 8. The *UEI* is to express the relationship between UE_T and *UA* to yield the same degree of CNT dispersion and comparable mechanical improvement. Therefore, the effect of *w/c* and *s/c* ratios on the mechanical properties are investigated in comparable conditions.

In interaction *V,* two levels of κ (0.1 and 0.3 *c-wt%*) of Type II CNTs (*AR* = 800) were tested at 3 and 28 days. Note that UE_T and *UA* were 2610 ± 15 *J/ml* and 57%, respectively. Also, *w/c*, *s/c*, and *SP/CNTs* ratios were fixed at 0.35, 2, and 6, respectively, for all the investigated test IDs within interaction *V*.

5.3.2.2. Sample Preparations

Before mixing the paste or mortar, 315 to 400 grams of tap water and the required *SP* dosage were mixed with a glass stirring rod. Then, CNTs were added to the aqueous solution and sonicated at room temperature with a 500 *W* ultrasonic processor having a probe tip of 19 *mm* (3/4 *in.*). The ultrasonication was done at a cycle interval of 20 seconds, and the beaker containing CNTs was placed in a water bath to prevent overheating of water. After ultrasonication process, cement and sand were added to the prepared suspension to fabricate CNT-cement nanocomposites.

For mixing procedure *A*, a standard Hobart mixer was used to fabricate cement pastes and mortars in accordance with ASTM C305-06 [202], "Standard Practice for Mechanical Mixing of Hydraulic Cement Pastes and Mortars of Plastic Consistency." For mixing procedure *B*, cement and first half of the sand were mixed by a spatula. Then, water

(or the prepared suspension as mentioned above) and the rest of the sand were gradually added to the mixture over the first minute of mixing, followed by the same mixing procedure as discussed in Section 5.3.1.2. Note that different mixing procedures and equipment were used to investigate their potential influence on the mechanical properties of the final nanocomposites.

After mixing, at least three beam specimens of 25×25×285 *mm* (1×1×11.25 *in.*) were cast for measuring the flexural strength and elastic modulus. Also, three cube specimens of size 50 *mm* (2 *in.*) were cast for measuring the compressive strength. After pouring the material in the molds (see Figure 5-3), the shaking table was used to reduce the air voids and entrapped air bubbles within the specimens. All specimens were cured for 24±2 hours at room temperature (20 to 25 ℃ [68 to 77 °F]) under a sealed plastic bag to minimize any moisture loss, followed by demolding. Then, the specimens were stored in the moisture room (23±2 ℃ [73.4±3.6 °F]) and at least 95% relative humidity) till testing.

(a) (b)

Figure 5-3. Sample preparation: (a) compressive strength (b) flexural strength

5.3.3. Durability: Alkali-Silica Reaction (*D* series)

This section provides mix proportions (Section 5.3.3.1) and sample preparations (Section 5.3.3.2) used for ASR tests.

5.3.3.1. Mix Proportions

The mix proportions of cement mortars for ASR tests are provided in Table 5-9. The mix proportions were varied to study the influences of different CNT types, concentrations, and dispersion procedures on the properties of cement mortars affected by ASR. Two different *w/c* ratios of 0.35 (with *s/c* ratio of 2) and 0.45 (with *s/c* ratio of 3) were prepared. Also, two different CNT concentrations of 0.1 and 0.3 *c-wt*% were used. These values were selected to yield a wide range of ASR performance based on the findings from the mechanical test results. In the test IDs for CNT-cement mortars, I or II reflects the type of CNTs followed by its concentration (0.1% or 0.3% *c-wt*%). For example, *D*1/I0.1 is used for cement mortars having *w/c* and *s/c* ratios of 0.35 and 2, respectively, strengthened with 0.1 *c-wt*% of type I CNTs. To study the influence of dispersion procedure, two different ultrasonication procedure denoted as *A* and *B* were used. For those test IDs related to *w/c* ratio of 0.45 (*D*2 series), *A* and *B* reflects the ultrasonication procedure used. For example, *D*2/II0.1-*A* is used for CNT-cement mortars having *w/c* and *s/c* ratios of 0.45 and 3, respectively, strengthened with 0.1 *c-wt*% of type II CNTs, in which ultrasonication procedure *A* was used.

Table 5-9. Test Identifications and Mix Proportions (*D* series)

Test ID	*w/c* ratio	*s/c* ratio	κ *(c-wt%)*	CNT type	Ultrasonication procedure
*D*1/I0.1	0.35	2	0.1	I	*A*
*D*1/II0.1				II	
*D*1/I0.3			0.3	I	
*D*1/II0.3				II	
*D*2/II0.1-*A*	0.45	3	0.1	II	
*D*2/II0.1-*B*					*B*
*D*1	0.35	2	-	-	-
*D*2	0.45	3	-	-	-

5.3.3.2. Sample Preparations

To properly disperse CNTs, 340 *gr* of tap water and superplasticizer (*SP/CNTs* = 6) were first mixed with a glass stirring rod. Then, CNTs were added to the aqueous solution, and the resulting suspension was sonicated using the same procedure discussed in Section 5.3.2.2. For type *A* ultrasonication procedure, ultrasonication amplitude was fixed at 57% and the total ultrasonication energy of 2610 ± 15 *J/ml* was delivered. For type *B* ultrasonication procedure, a total ultrasonication energy of 200 *J/ml* was delivered while ultrasonication amplitude was fixed at 50%.

After ultrasonication process, cement and sand were added to the prepared suspension (or tap water for control specimens) to fabricate cement mortars in accordance with ASTM C305-06 [202]. After mixing, five beam specimens of 25×25×285 *mm* (1×1×11.25 *in.*) and three cube specimens of the size 50 *mm* (2 *in.*) were cast. All specimens were cured for 24±2 hours at room temperature (20 to 25 ℃; 68 to 77 ℉) under a sealed plastic bag to minimize any moisture loss, followed by demolding. Then, the specimens were placed in tap water at 80±2 ℃ (176±3.6 ℉) for 24 hours (zero reading) after which they were submerged in 1N NaOH solution at 80±2 ℃ (176±3.6 ℉) in accordance with ASTM C1260-14 [199].

5.4. Test Procedures

This section describes the test procedures for flow (Section 5.4.1), mechanical (Section 5.4.2), and durability (Section 5.4.3) properties.

5.4.1. Flow Properties

In this section, mini-cone slump (Section 5.4.1.1) and rheology (Section 5.4.1.2) test procedures are discussed.

5.4.1.1. Mini-Cone Slump Test

The mini-cone slump test was conducted to measure the flow diameter. For cement pastes, the average of the flow diameter in two perpendicular directions was used to represent the flow diameter (see Figure 5-4 (a)). For cement mortars, flow table test in accordance with ASTM C1437-07 [203], "Standard Test Method for Flow of Hydraulic Cement Mortar" was used to calculate the flow diameter of the mortar samples (see Figure 5-4 (b)).

(a) (b)

Figure 5-4. Mini-cone slump test: (a) paste samples (b) mortar samples

5.4.1.2. Rheology Test and Models

The rheometer (Model: Anton Paar MCR 502) with concentric cylinders having conical end geometry (cup and bob; gap size of 1.6 *mm*; 0.063 *in.*) was used to measure the rheological properties of cement pastes (see Figure 5-5). During the tests, cement pastes were pre-sheared at a shear rate of 600 s^{-1} for 10 seconds and then let rest for three minutes. After that, samples were sheared at seven different shear rates (600, 500, 400, 300, 200, 100, and 10 s^{-1}). Each shear rate was maintained for 10 seconds and 60 data points were collected (each at 0.167 second intervals). For data analysis, the last 20 data points corresponding to shear stress were averaged for each shear rate.

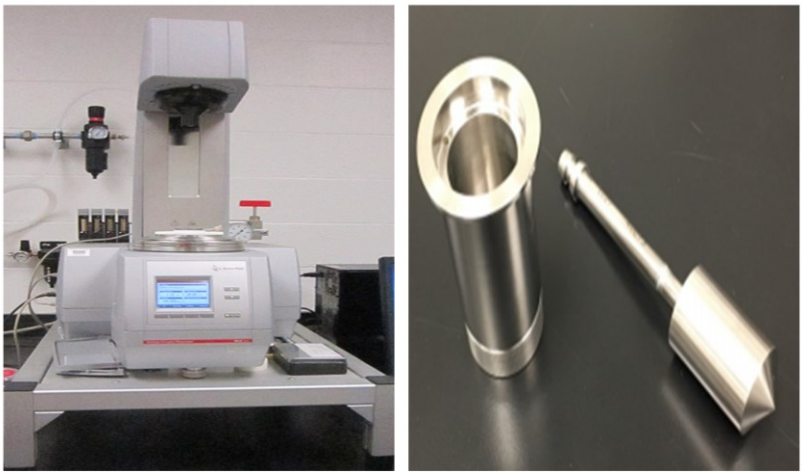

(a) (b)

Figure 5-5. (a) Rheometer Anton Paar MCR 502 (b) concentric cylinders

To determine the rheological properties, Bingham and Herschel-Bulkley models were used. Bingham model (Equation 4-1) uses linear regression to find the yield stress and plastic viscosity [204, 205]. Hershchel-Bulkley model, on the other side, uses nonlinear regression (Equation 4-2). The flow index ($\dot{n}$) in Herschel-Bulkley model was used as an indication of the shear behavior of cement pastes. When flow index is larger than one, the material exhibits shear thickening behavior, and a shear thinning behavior corresponds to a flow index smaller than one [205, 206].

$$\tau = \tau_0 + \mu_P . \dot{\gamma} \tag{4-1}$$

$$\tau = \tau_0 + K . \dot{\gamma}^{\dot{n}} \tag{4-2}$$

where τ is the shear stress (Pa), τ_0 is the yield stress (Pa), μ_P is the plastic viscosity ($Pa.s$), $\dot{\gamma}$ is the shear rate (s^{-1}), K is consistency ($Pa.s^n$), and $\dot{n}$ is the flow index.

5.4.2. Mechanical Properties

This section describes the test procedures for compressive strength (Section 5.4.2.1), flexural strength and static elastic modulus (Section 5.4.2.2), and dynamic elastic modulus (Section 5.4.2.3).

5.4.2.1. Compressive Strength

The compressive strength of cement pastes and mortars was measured using a 60 *Kips* Universal Testing Machine (UTM) in accordance with ASTM C109-08 [207], "Standard Test Method for Compressive Strength of Hydraulic Cement Mortars (Using 2-*in.* or [50-*mm*] Cube Specimens)." The average compressive strength of three specimens was used as a representative value. The compressive strength was calculated by dividing the maximum load obtained using the UTM (see Figure 5-6) by the cross sectional area of the cube as follows:

$$f_{cs} = \frac{P_{cs}}{A} \tag{4-3}$$

where f_{cs} is the compressive strength (*MPa* or *psi*), P_{cs} is the maximum compression load applied (*N* or *lbf*), and *A* is the cross sectional area of the cube (mm^2or in^2).

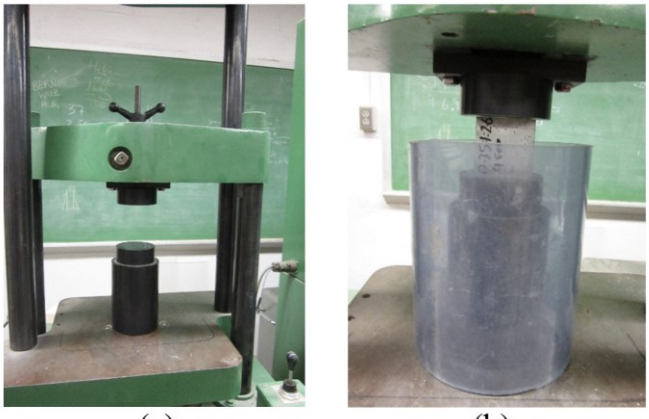

(a) (b)

Figure 5-6. Compressive strength test configuration: (a) upper bearing and seated blocks (b) experimental setup

5.4.2.2. Flexural Strength and Elastic Modulus

For the evaluation of the flexural strength and elastic modulus, a three-point bending test was performed using a UTM (60 *kips* [≅ 267 *kN*] capacity). The shear span was 117.5 *mm* (4.63 *in.*) to obtain a representative average value of at least three beam specimens. The outliers (differing by more than 10% from the average value of all test specimens) were discarded in accordance with ASTM C348-08 [208], "Standard Test Method for Flexural Strength of Hydraulic-Cement Mortars." To measure the applied load, a load cell with the maximum capacity of ≅ 3336 *N* (750 *lbf*) was used. The accuracy of the load cell was 0.037% of the full-scale. The rate of loading was maintained at 5.75±0.25 *N/sec* (≅ 1.29±0.06 *lbf /sec*). A Linear Variable Differential Transducer (LVDT) with the range of ±5 *mm* (±0.2 *in.*) range (0.02% of the full-scale accuracy) was used to measure the deflection at mid-span (see Figure 5-7 (a)). The sampling rate of the data was per second. Figure 5-7 (a) and (b) show a simply supported beam under a three-point bending test configuration. A load bearing apparatus was used to avoid failure due to stress concentration and to ensure that forces were perpendicular to the face of the beam specimens and were applied without eccentricity (see Figure 5-7 (b)). A typical load-deflection curve (for test ID: *R*1; see Table 5-8) is shown in Figure 5-7 (c). The flexural strength was calculated as follows:

$$f_{FS} = \frac{3P_{FS}L}{2bd^2} \tag{4-4}$$

where f_{FS} is the flexural strength (*MPa* or *psi*), P_{FS} is the maximum flexural load applied (*N* or *lbf*), *b*, *d*, and *L* are the width, depth, and length (i.e., 2 × shear span) of a specimen, respectively (*mm* or *in.*). A caliper with the accuracy of 0.01 *mm* (0.0001 *in.*) was used to

measure the average b, d, and L with three measurements for each dimension. The elastic modulus, E_F, was calculated from the following equation:

$$E_F = \frac{L^3}{48I} \times \frac{\bar{P}}{\bar{\Delta}} \tag{4-5}$$

where E_F is the flexural elastic modulus (*GPa* or *ksi*), I is the second moment of inertia (mm^4 or $in.^4$), and $\frac{\bar{P}}{\bar{\Delta}}$ is the slope of a flexural load-deflection curve ranging from 15 to 40% of P_f (see Figure 5-7 (d)).

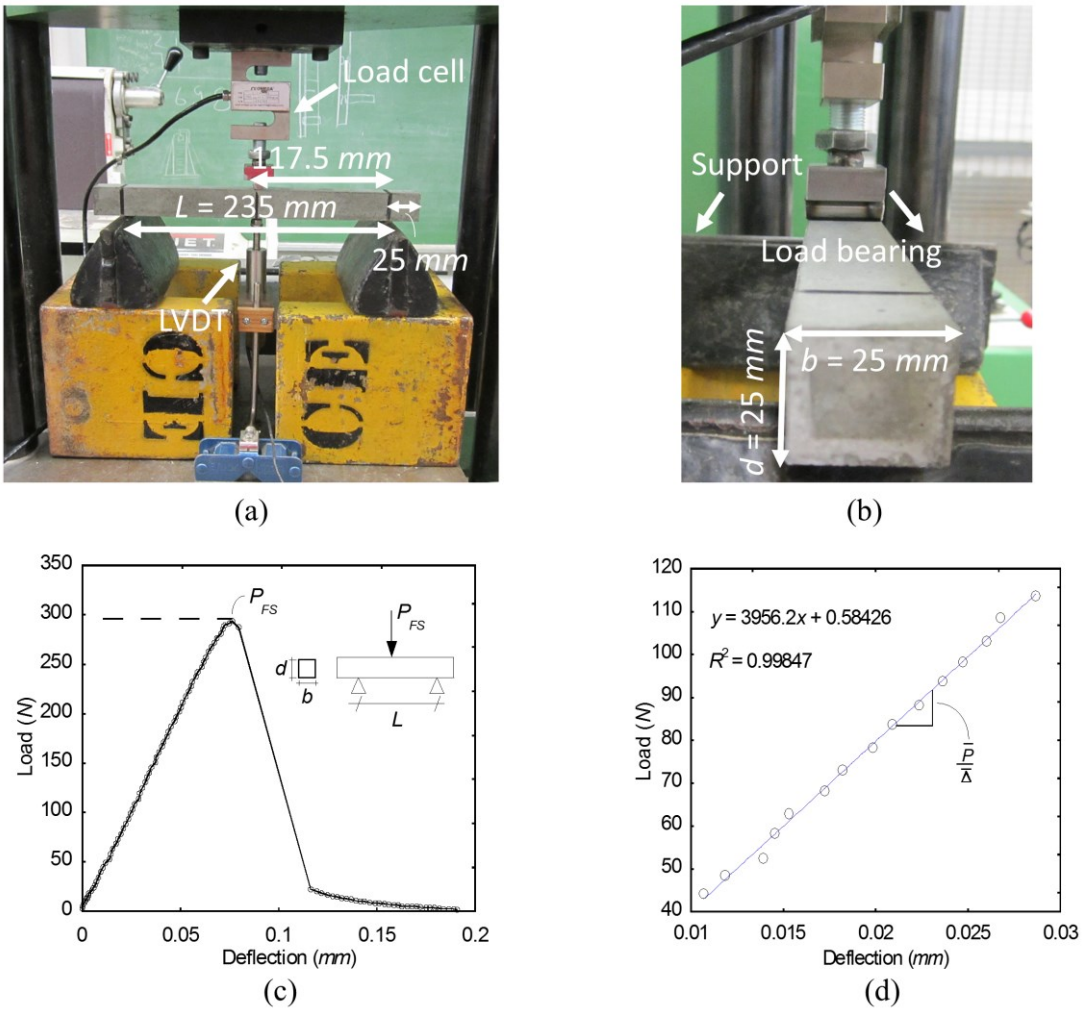

Figure 5-7. Three-point bending test: (a) experimental setup (front view) (b) experimental setup (side view) (c) typical load-deflection curve (d) load-deflection curve used to calculate the elastic modulus
Note: 1 *in.* = 25.4 *mm*

5.4.2.3. Dynamic Elastic Modulus

The dynamic elastic modulus (average of two beam specimens) was measured in accordance with ASTM C215-02 [209], "Standard Test Method for Fundamental transverse, Longitudinal, and Torsional Resonant Frequencies of Concrete Specimens." The longitudinal resonant frequencies were determined using the impact resonant method. The beam specimens were supported at the center of the beam length so that they could freely vibrate in longitudinal mode. An accelerometer (frequency range: 0.5-10 *kHz*) was attached at the center of one end of the beam specimen and a rigid plastic impactor with a spherical shape was used to strike the other end of the specimen to generate vibration as shown in Figure 5-8 (a). The longitudinal resonant frequencies (highest peak in the amplitude spectrum) were obtained from the fast Fourier transform of the recorded accelerometer signal using a data acquisition system. Figure 5-8 (b) shows a typical longitudinal resonant frequency (for test ID: *D*1 at age of 1 day; see Table 5-9). The dynamic elastic modulus, E_d, was calculated from the following equation:

$$E_d = DM(n')^2 \tag{4-6}$$

where E_d is the dynamic elastic modulus (*GPa* or *ksi*), M is the mass of the beam specimen (kg), n' is the longitudinal resonant frequency (Hz), and $D = 4(L/bd)$.

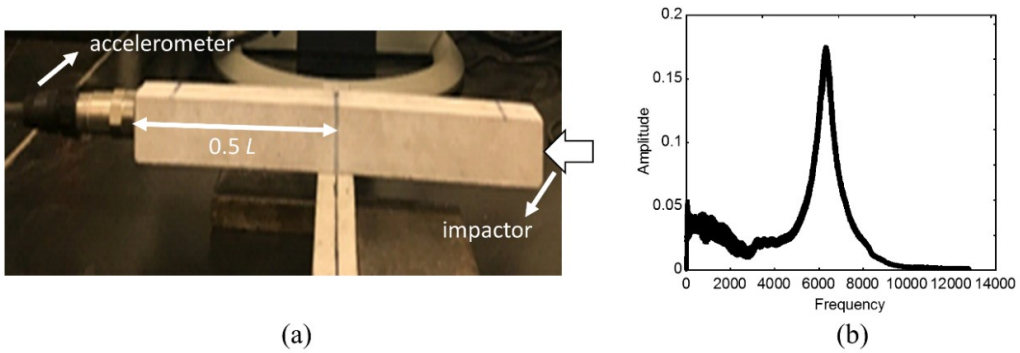

Figure 5-8. (a) Locations of impactor and accelerometer to generate random vibration (b) typical longitudinal resonant frequency

The dynamic elastic modulus was performed on two beam specimens for each test ID at ages of 1, 2, 3, 7, 14, 21, and 28 days after casting.

5.4.3. Durability: Alkali-Silica Reaction

The linear expansion of mortar bars in accordance with ASTM C1260-14 [199] is discussed in this section.

5.4.3.1. Linear Expansion

To measure the length change of cement mortars subjected to ASR (average of three specimens), mortar bars with embedded gauge studs were cast in accordance with ASTM C 1260-14 [199] (see Figure 5-9 (a)). A dial gauge length comparator with an accuracy of 0.0001 *in.* was used to measure the time-dependent expansion as seen in Figure 5-9 (b). The expansion measurements were performed after 1, 2, 3, 7, 10, 14, 21, and 28 days of submersion in 1N NaOH solution at 80±2 ℃ (176±3.6 ℉). According to ASTM C1260-14 [199], cement mortars expanding less than 0.1% after 16 days of casting (14 days in NaOH solution) have a low risk of ASR expansion under field conditions. While cement mortars that expand more than 0.2% after 14 days in 1N NaOH solution at 80±2 ℃ (176±3.6 ℉) have a high risk of ASR expansion under field conditions.

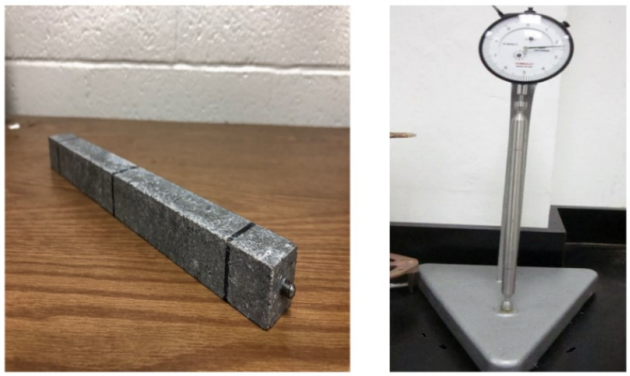

(a) (b)

Figure 5-9. (a) Beam specimen with embedded gauge studs (b) dial gauge length comparator

5.5. Summary

This chapter presented raw materials, mix proportions, and test procedures used in this study.

A total of 27 mix proportions were used to investigate the influence of CNTs on flowability of cement pastes and mortars. To evaluate the flow properties, mini-cone slump (for both pastes and mortars) and rheology (for pastes only) tests were performed.

A total of 28 mix proportions were used to study the contributions of multiple experimental variables and their interactions to the mechanical properties of cement pastes and mortars at different ages (3, 7, and 28 days). The investigated mechanical properties included compressive strength, flexural strength, static elastic modulus (using flexural test), and dynamic elastic modulus.

A total of 8 mix proportions were used to study the possible contribution of CNTs to mitigate ASR in cement mortars subjected to severe ASTM C1260 test conditions. To characterize the influence of CNTs, linear expansion and dynamic elastic modulus tests were performed over time. After 28 days of exposure to extreme ASR conditions, the compressive strength, flexural strength, and static elastic modulus were also measured.

CHAPTER 6. EXPERIMENTAL TEST RESULTS AND ANALYSIS

6.1. General

In this chapter, the contribution of CNTs to fresh (Section 6.2), mechanical (Section 6.3), and durability (Section 6.4) properties of cement pastes and mortars are investigated. The details are discussed in the following sections.

6.2. Flow Properties*

Flow properties are affected by particle dispersion in cementitious materials. Flowability and rheological properties also govern the stability of the material, which eventually affect the mechanical properties. Therefore, flow properties should be controlled during the fabrication process. In this section, the influence of *w/c* ratio, CNT concentration, and *SP/CNTs* ratio on flowability of cement pastes (Section 6.2.1) and mortars (Section 6.2.2) are investigated.

6.2.1. Cement Paste Test Results

Both mini-cone slump (Section 6.2.1.1) and rheology (Section 6.2.1.2) tests were performed to study the influence of solid concentration and *SP/CNTs* ratio on the workability of cement pastes.

* The main part of this section is published in SCC 2016
Ramezani, M., Kim, Y.H., Hasanzadehm B., and Sun, Z. "*Influence of Carbon Nanotubes on SCC Flowability*." In 8th Int. RILEM Symp. Self-Compacting Concr., Washington DC, USA 15-18 May (2016): 397-406

6.2.1.1. Mini-Cone Slump Test

Figure 6-1 compares the flow diameters of cement pastes having different *w/c* ratios with and without inclusion of 0.1 *c-wt*% Type I CNTs and *SP/CNTs* = 3. By comparing the flow diameters, it is evident that adding CNTs would reduce the flowability of the paste. The flow diameter decreased by 13.7%, 11.8%, and 12.2% for *w/c* ratios of 0.35, 0.45, and 0.6, respectively. Also, as *w/c* ratio increased, the flow diameter increased for both the control specimens (without CNTs) and those pastes containing CNTs. This can be visually observed in Figure 6-2, which shows the mini-cone slump tests for cement pastes containing CNTs.

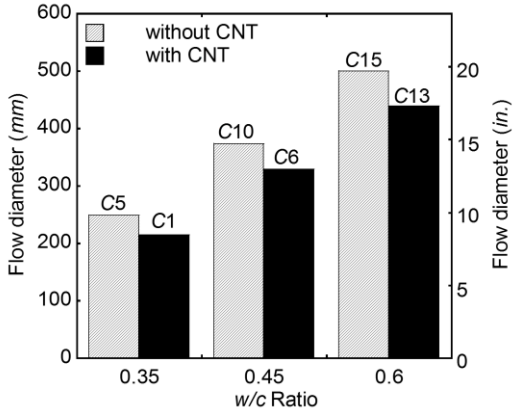

Figure 6-1. Influence of CNTs on flowability of cement paste

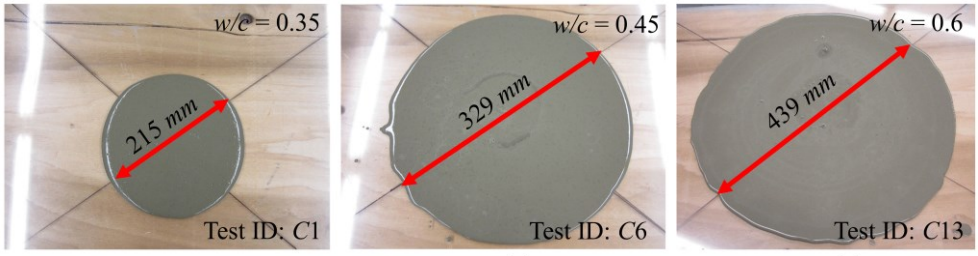

(a) (b) (c)

Figure 6-2. Mini-cone slump test for cement pastes containing 0.1 *c-wt*% of Type I CNTs: (a) *w/c* = 0.35 (b) *w/c* = 0.45 (c) *w/c* = 0.6

Note: 1 *in.* = 25.4 *mm*

Figure 6-3 shows the influence of *SP/CNTs* ratio on the flow diameter of cement pastes at different *w/c* ratios. Increasing *SP/CNT*s ratio from 3 to 4 caused the flow diameter to increase by 23%, 17% and 6% for *w/c* ratios of 0.35, 0.45 and 0.6, respectively, and it continued to increase by keep adding more SP dosage (i.e., higher *SP/CNTs* ratio). However, as *SP/CNTs* ratio increases, the potential of bleeding could increase.

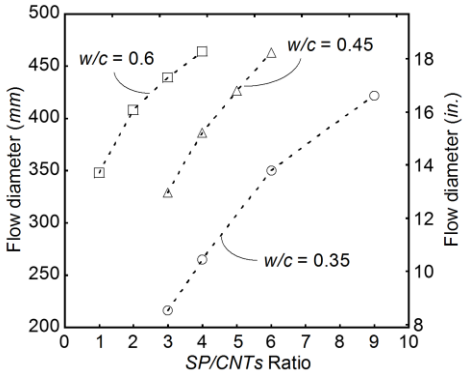

Figure 6-3. Influence of *SP/CNTs* ratio on flowability of cement paste

Figure 6-4 shows pictures of two pastes with *w/c* = 0.6 and *SP/CNTs* = 3 on the flow table after 30 minutes of the mini-cone slump test. Figure 6-4 (a) shows the control (test ID *C*15) and Figure 6-4 (b) shows the specimen containing 0.1 *c-wt*% CNTs (test ID *C*13). Bleeding issue was observed for the control paste. However, a clear layer of water was not seen for paste containing 0.1 *c-wt*% CNTs, which must be related to the change in its rheological properties.

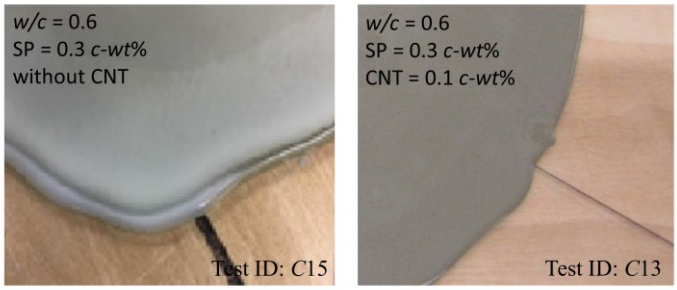

(a) (b)

Figure 6-4. Cement pastes after 30 minutes on flow table test (a) without CNT (b) with CNT

6.2.1.2. Rheology Test

Table 6-1 summarizes flow diameters of mini-cone slump and rheology tests for cement pastes with and without incorporating CNTs. The yield stress and the viscosity of each test ID were obtained from two rheological models (Bingham and Herschel-Bulkley models). There was a substantial difference in yield stresses and viscosities between the two rheological models. As it is clear from Table 6-1, SP dosage has an influence on the shear behavior of the material. *C*5, *C*10 and *C*15 are control samples with SP dosage of 0.3 *c-wt*% and *w/c* ratios of 0.35, 0.45 and 0.6, respectively. It is clearly shown that the higher the *w/c* ratio, the lower the influence of SP on shear behavior of the material is. It can also be seen that the flow index value for all test IDs is greater than one which represents the shear thickening behavior, except for test ID *C*11 which has a flow index value of 0.738. This might be attributed to the mix proportion of test ID *C*11; the highest *w/c* ratio and the lowest SP dosage (SP = 0.1 *c-wt*%). In this case, SP dosage is not high enough, therefore, the paste behaves in a shear thinning manner.

Table 6-1. Cement Paste Test Results

Test ID	*w/c* ratio	SP (*c-wt*%)	Flow diameter (*mm*)	Bingham		Herschel-Bulkley		
				Yield stress (*Pa*)	Viscosity (*Pa.s*)	Yield stress (*Pa*)	Viscosity (*Pa.s*)	Flow index
*C*1	0.35	0.3	215	-1.447	0.429	14.040	0.076	1.267
*C*2		0.4	265	-14.005	0.391	6.823	0.022	1.447
*C*3		0.6	350	-15.622	0.306	3.707	0.008	1.573
*C*4		0.9	422	-14.118	0.270	2.186	0.009	1.534
*C*5*		0.3	249	-14.547	0.440	9.343	0.023	1.458
*C*6	0.45	0.3	329	0.586	0.072	2.101	0.029	1.142
*C*7		0.4	386	-0.790	0.066	0.882	0.021	1.174
*C*8		0.5	426	-1.046	0.056	0.677	0.014	1.218
*C*9		0.6	463	-1.101	0.054	0.642	0.012	1.233
*C*10*		0.3	373	-1.205	0.075	1.232	0.017	1.234
*C*11	0.6	0.1	348	5.556	0.023	4.193	0.130	0.738
*C*12		0.2	408	0.892	0.018	0.962	0.016	1.023
*C*13		0.3	439	0.181	0.016	0.236	0.014	1.020
*C*14		0.4	464	0.015	0.015	0.059	0.013	1.018
*C*15*		0.3	500	-0.050	0.015	0.172	0.008	1.098

Note: *indicates the control mix (without CNTs) for different *w/c* ratios

Figure 6-5 (a) and (b) show viscosity and yield stress versus *SP/CNTs* ratio obtained from Bingham model, respectively. It can be seen that viscosity decreases by the increase in *SP/CNTs* ratio for all the *w/c* ratios. Also, for a given *SP/CNTs* ratio, the higher the *w/c* ratio, the lower the viscosity is. The yield stresses obtained from Bingham model are negative in most cases (except for *w/c* ratio of 0.6) that are practically infeasible. Also, by increasing the *w/c* ratio, the yield stress is unexpectedly increasing for a given *SP/CNTs* ratio. This could be an indication of the non-linear behavior of the material flow. Therefore, Bingham model probably is not a good indication for the pastes with the *w/c* ratios of 0.35 and 0.45. Other researchers have also reported shear thickening effect of superplasticizers on cement pastes which caused the Bingham yield stress to become negative [210, 211].

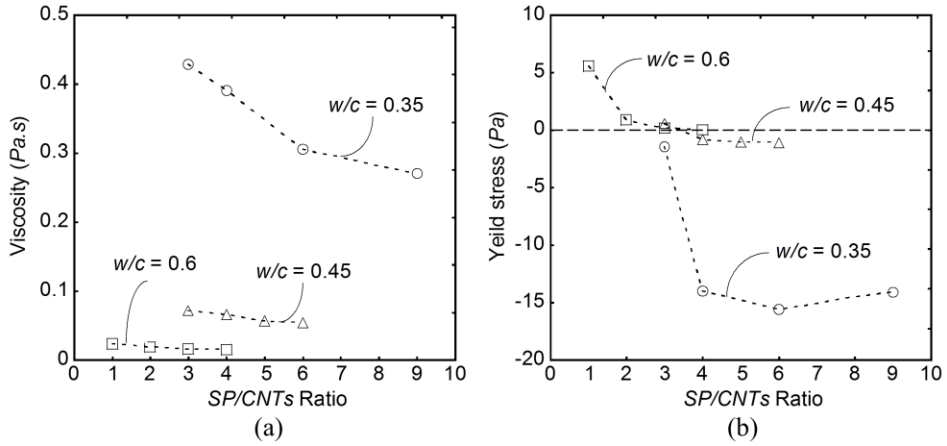

Figure 6-5. Influence of *SP/CNTs* ratio: (a) viscosity (b) yield stress (Bingham model)

The shear stress (τ)-shear strain ($\dot{\gamma}$) curves for different *w/c* ratios using Bingham model is shown in Figure 6-6. It is clear that Bingham model uses the linear regression and the value of yield stress is negative for *w/c* ratios of 0.35 (see Figure 6-6 (a)) and 0.45 (see Figure 6-6 (b)). In case of *w/c* = 0.6, although the control mix (test ID *C*15) exhibited the negative yield stress of -0.05 (see Figure 6-6 (c)), the CNT-cement pastes (test IDs *C*11 through *C*14) showed positive values of yield stress. This indicates that adding CNTs would increase the yield stress. Also, as *SP/CNTs* ratio decreased, the value of yield stress increased.

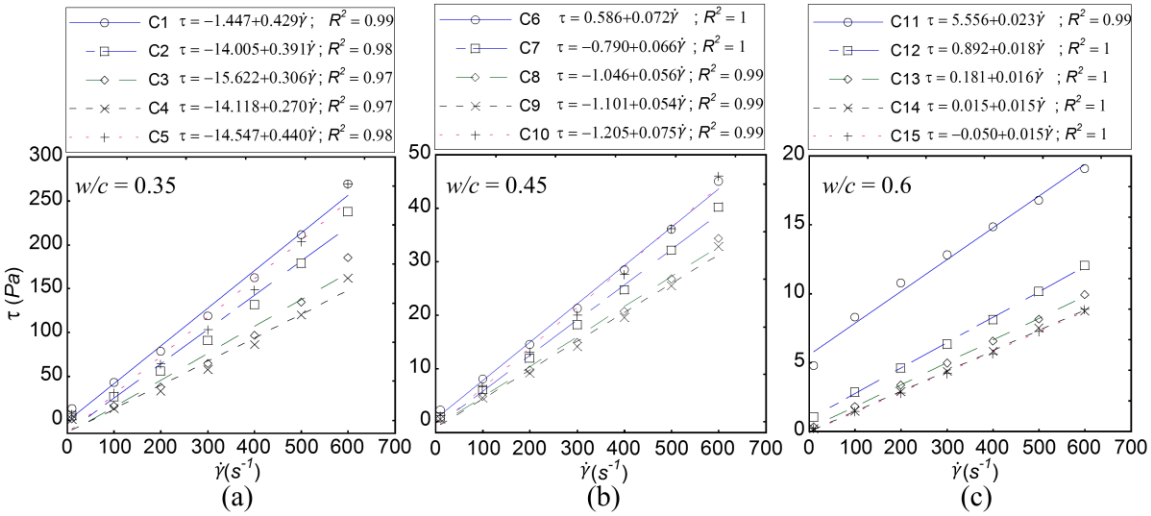

Figure 6-6. Shear stress (τ)-shear strain ($\dot{\gamma}$) curves for Bingham model: (a) *w/c* = 0.35 (b) *w/c* = 0.45 (c) *w/c* = 0.6

To rationally quantify the rheological properties of the pastes, Herschel-Bulkley model is used. Figure 6-7 shows τ versus $\dot{\gamma}$ curves of different test IDs using Herschel-Bulkley model. Note that Herschel-Bulkley uses the nonlinear regression to find the yield stress and viscosity. Despite Bingham model, the values of yield stress obtained from Herschel-Bulkley model for different test IDs are positive. Also, the flow index values are greater than one except for test ID *C*11 that exhibits a flow index of 0.738 (see different behavior of τ-$\dot{\gamma}$ curve for *C*11 compared with other test IDs in Figure 6-7 (c)). This might be attributed to the low *SP/CNTs* ratio (*SP/CNTs* = 1) of *C*11, causing it to behave in a shear thinning manner.

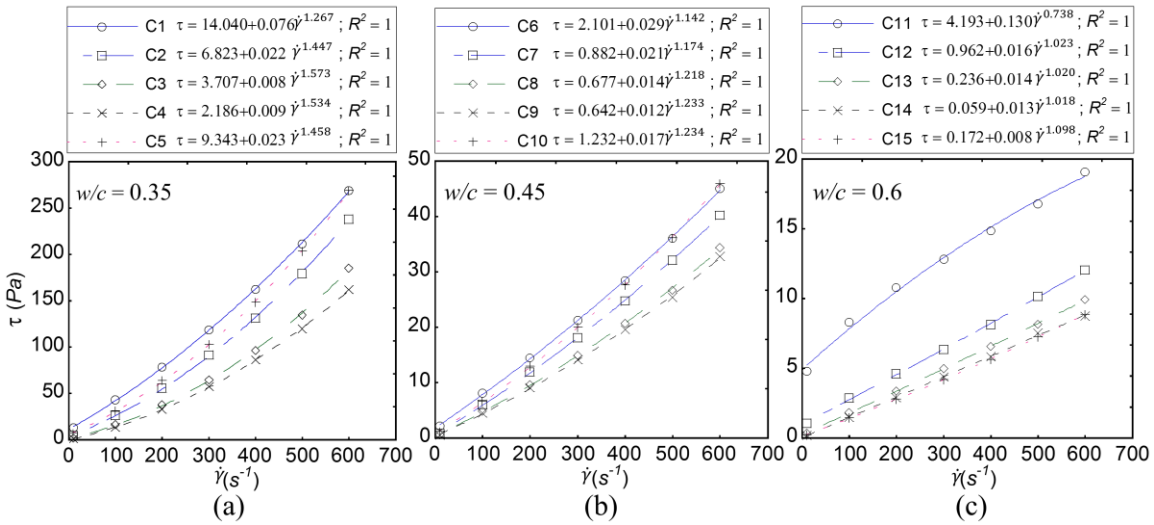

Figure 6-7. Shear stress (τ)-shear strain ($\dot{\gamma}$) curves for Herschel-Bulkley model: (a) *w/c* = 0.35 (b) *w/c* = 0.45 (c) *w/c* = 0.6

Figure 6-8 (a) shows the flow index values versus *w/c* ratios obtained from Herschel-Bulkley model for cement pastes with and without CNTs. The SP and CNT concentrations are constant for all the *w/c* ratios. It is evident that using CNTs in cement pastes decreases the flow index for all the *w/c* ratios. Therefore, CNTs effectively decrease the shear thickening behavior of cement pastes, which is beneficial to high shear rate

applications such as high speed mixing and pumping.

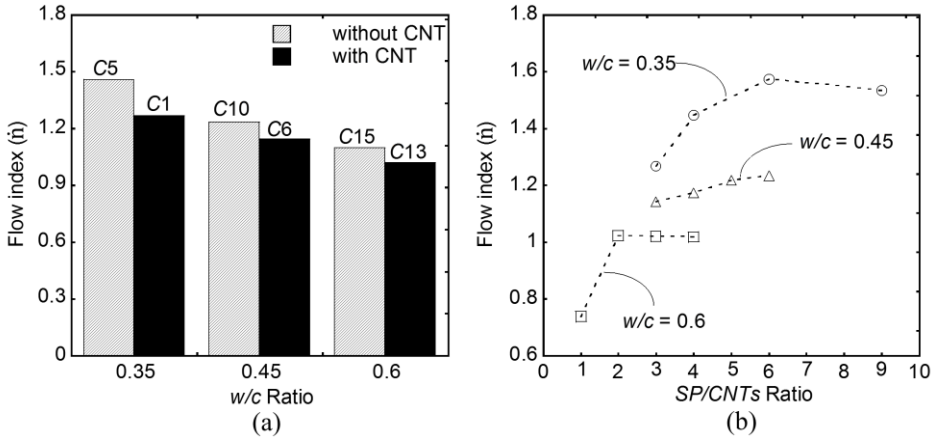

Figure 6-8. Flow index versus: (a) *w/c* ratio (b) *SP/CNTs* ratio

Figure 6-8 (b) shows the influence of *SP/CNTs* ratio on the flow index of cement pastes. By increasing the *SP/CNTs* ratio from 1 to 2 for *w/c* of 0.6, the flow index increases by approximately 40% (See Figure 6-8 (b)). However, once this threshold is passed, higher *SP/CNTs* ratio has no significant effect on cement pastes shear behavior for *w/c* = 0.6. The same trend is observed for other *w/c* ratios. Therefore, it is evident that after a certain *SP/CNTs* ratio for each specific *w/c* ratio, adding more SP has minimum effect on cement pastes' shear behavior. These threshold *SP/CNTs* ratios are found to be 2, 4, and 6 for *w/c* ratios of 0.6, 0.45, and 0.35, respectively. The higher the *w/c* ratio, the less sensitivity of the material's shear behavior to *SP/CNTs* ratio. This is the observation in the range of *SP/CNTs* ratio between 3 and 4.

Figure 6-9 (a) and (b) show the viscosity and yield stress obtained from Herschel-Bulkley model, respectively, of cement pastes with and without CNTs with respect to *w/c* ratios. The *SP/CNTs* ratio is kept constant for all mixes in order to investigate the influence of CNT addition on pastes' rheological properties. It is clear that CNTs can increase viscosity greatly compared with plain cement pastes. Using 0.1 *c-wt*% of CNTs in cement pastes increased the viscosity by about 230%, 75% and 85% for *w/c* ratios of 0.35, 0.45,

and 0.6, respectively. The addition of CNTs also increased yield stress. By incorporating 0.1 *c-wt*% of CNTs, the yield stress increased by 50%, 70% and 35% compared with plain cement pastes for *w/c* ratios of 0.35, 0.45, and 0.6, respectively. The increased viscosity and yield stress in cement pastes containing CNTs also clearly tied with the observation of bleeding in cement pastes (See Figure 6-4).

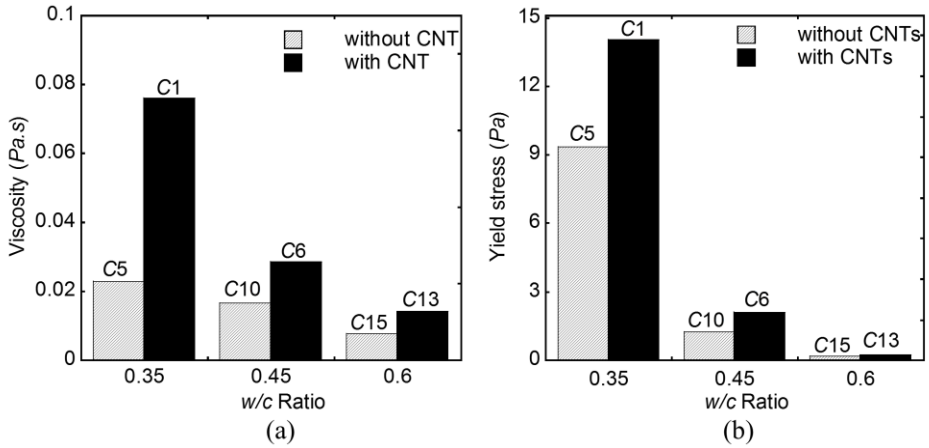

Figure 6-9. Effect of *w/c* ratio: (a) viscosity (b) yield stress (Herschel-Bulkley model)

6.2.2. Cement Mortar Mini-Cone Slump Test

To investigate the influence of CNTs on flow diameter of cement mortars, three different *w/c* ratios ranging from 0.35 to 0.6 were used. The *s/c* ratio was fixed at 60% of the total volume for each *w/c* ratio. Also, the fixed SP dosage of 0.6, 0.4, and 0.2 *c-wt*% for *w/c* ratios of 0.35, 0.45, and 0.6, respectively, were used. These SP dosages were based on the earlier analysis concerning cement pastes that revealed shear behavior did not significantly changed beyond these threshold values for each specific *w/c* ratio (see Figure 6-8 (b)).

Figure 6-10 shows the results of flow table test for cement mortars containing three different concentrations of CNTs (0.05, 0.1, and 0.15 *c-wt*%) at various *w/c* ratios. The standard deviation between different batches for each mix proportion is also included. As

it is clear, adding higher CNT concentration resulted in lower flow diameter for each *w/c* ratio. For example, concerning *w/c* ratio of 0.6, the flow diameter decreased by 6.60%, 10.1%, and 12.1%, compared with the control cement mortar, when incorporating 0.05, 0.1, and 0.15 *c-wt*% Type I CNTs, respectively. The flow table test results of cement mortars are listed in Table B-1 in the Appendix.

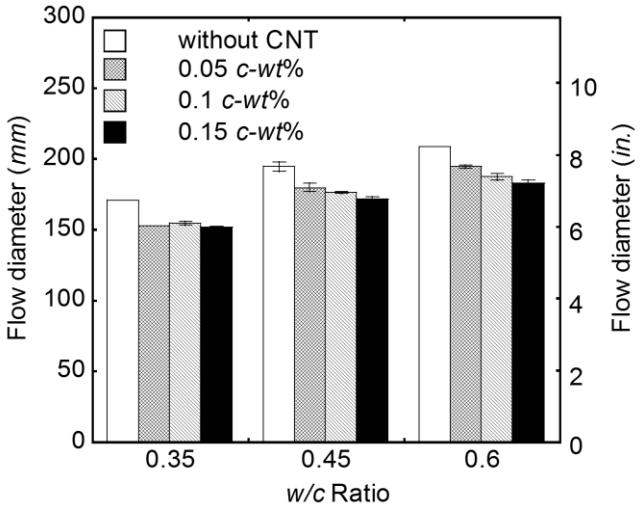

Figure 6-10. Influence of CNT concentration on flowability of cement mortar

Figure 6-11 shows the visual observation of the mini-cone slump test for control cement mortars and those containing 0.05, 0.1, and 0.15 *c-wt*% Type I CNTs at different *w/c* ratios. As it can be seen from Figure 6-11, the flow diameter of CNT cement mortars decreased compared with the control cement mortars for each *w/c* ratio. In addition, cement mortars appear to lose flowability at higher CNT concentrations (see Figure 6-11). This might be attributed to the fact that as CNT concentration increases, more SP is adsorbed on their surface, and the remaining SP in the mix is not effective on getting higher level of flowability.

To further confirm the influence of CNT concentration on the flowability of cement mortars, the ANOVA test was performed and the *p*-values between different mix

proportions are listed in Table C-1 in the Appendix. The *p*-values between the control specimens (without CNTs) and different concentrations of CNTs at each specific *w/c* ratio are smaller than 0.05, except for CNT concentration of 0.1 *c-wt%* at *w/c* ratio of 0.35 (*p*-value = 0.05169 > 0.05). This suggests that addition of CNTs significantly reduces the flowability of cement mortars. Also, as CNT concentration increases from 0.05 to 0.15 *c-wt%*, the *p*-values are lower than 0.05 at *w/c* ratios of 0.45 and 0.6. However, the similar trend was not observed for *w/c* ratio of 0.35 (*p*-value = 0.12995 > 0.05).

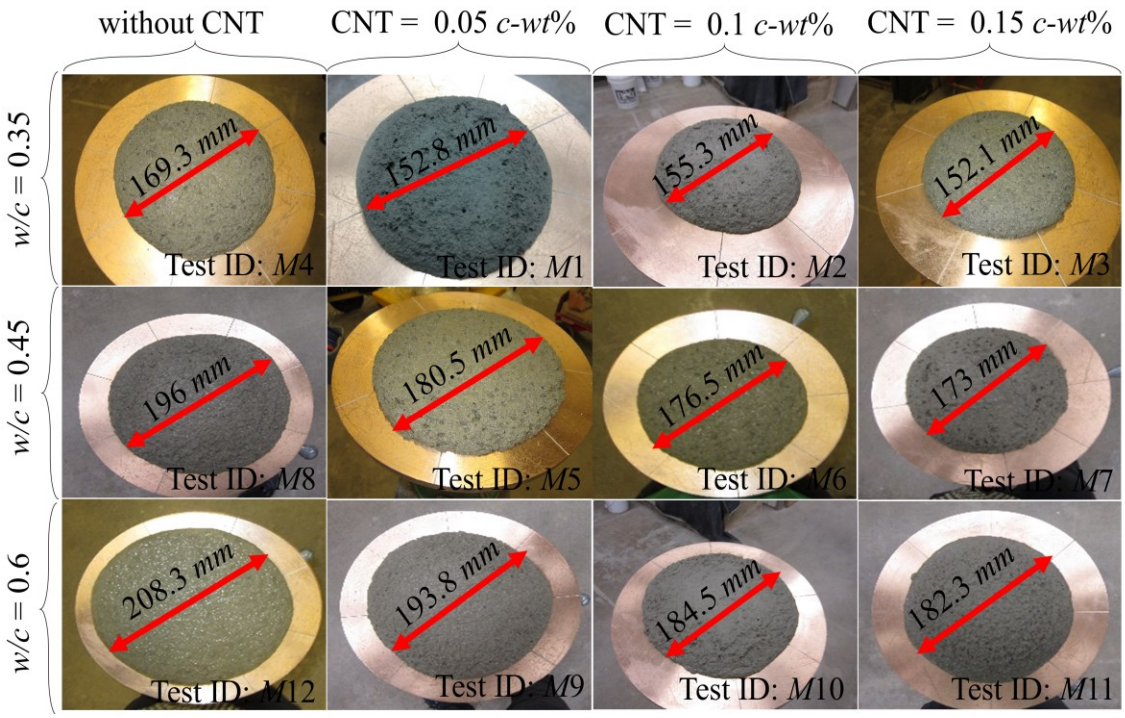

Figure 6-11. Mini-cone slump test for cement mortars containing different CNT concentrations
Note: 1 *in.* = 25.4 *mm*

6.2.3. Summary: Flow Properties

Flowability and rheological properties are closely related to the construction and early age behaviors of cementitious materials. From the test results, the following conclusions were drawn:

1. For cement pastes, addition of 0.1 *c-wt*% CNTs significantly increased the yield stress and viscosity compared with the control pastes. These improvements in rheological properties may help to reduce the bleeding issue.
2. Most of the studied cement pastes indicated shear thickening behavior. The *SP/CNTs* ratio was found to be critical to determine the shear behavior of the material. Adding more *SP* dosage will decrease the viscosity and the yield stress (for a given *w/c* ratio). The threshold values of *SP/CNTs* ratio of 2, 4, and 6 were found for cement pastes with *w/c* ratios of 0.6, 0.45, and 0.35, respectively. Once this threshold value is surpassed, the flow behaviors of the material are not significantly influenced by *SP/CNTs* ratio.
3. Addition of only small amount of CNTs (0.05-0.15 *c-wt*%) was found to significantly reduce the flowability of cement mortars. And, as CNT concentration increased, the flowability of cement mortars further decreased. This might be attributed to the adsorption of higher SP dosage on CNT surface to facilitate their dispersion, resulted in lower available SP to interact with cement.

In this section, flow properties of CNT-cement nanocomposites were experimentally studied to find a good mix design for superior mechanical properties. However, no clear correlations were found between the fresh and mechanical properties (mechanical properties test results can be found in Table B-2 (for cement pastes) and Table B-3 (for cement mortars) in the Appendix. In Section 6.3, the influences of the studied important variables and their interactions affecting the mechanical properties are discussed.

6.3. Mechanical Properties*

To re-examine the interactions between the important variables discussed in Section 4.10, the compressive strength (f_{CS}), flexural strength (f_{FS}), and elastic modulus (E_F) of CNT-cement nanocomposites (paste and mortar) were evaluated. Section 6.3.1 studies the interaction between CNT concentration (κ) and aspect ratio (*AR*). Section 6.3.2 studies the interaction between ultrasonication energy (UE_T) and amplitude (*UA*). The interaction between UE_T and *SP/CNTs* ratio is investigated in Section 6.3.3. The interaction between *w/c* ratio and *s/c* ratio is presented in Section 6.3.4. Also, Section 6.3.5 investigates the interaction between κ and hydration age (*t*). The influence of CNTs on the dynamic elastic modulus (E_d) is presented in Section 6.3.6. The mechanical properties test results are listed in Table B-4 (for f_{CS}, f_{FS}, and E_F) and Table B-5 (for E_d) in the Appendix.

6.3.1. Interaction between κ and *AR* (Interaction *I*)

Figure 6-12 (a-*i*), (a-*ii*), and (a-*iii*) show f_{CS}, f_{FS}, and E_F, respectively, for *AR* = 800 (*I*-800/*κ* series). Figure 6-12 (b-*i*), (b-*ii*), and (b-*iii*) show f_{CS}, f_{FS}, and E_F, respectively, for *AR* = 2500 (*I*-2500/κ series).

In case of *I*-800/κ series, the increase in κ from 0.05 to 0.1 *c-wt*% exhibited approximately 18% increase in f_{CS} and about 30% increase in both f_{FS} and E_F. However, κ = 0.3 *c-wt*% (test ID *I*-800/0.3) exhibited lower mechanical properties than κ = 0.1 *c-wt*% (test ID *I*-800/0.1). This might be attributed to the poor dispersion quality of CNTs. This was also confirmed using ANOVA test results. The *p*-values < 0.05 between *I*-800/0.1 and

* The main part of this section is published in Cement and Concrete Composites
Ramezani, M., Kim, Y.H., and Sun, Z. "*Modeling the Mechanical Properties of Cementitious Materials containing CNTs*." Cement and Concrete Composites 104 (2019): 1-21

the other two test IDs (*I*-800/0.05 or *I*-800/0.3) indicated a significant difference between the mean of the investigated groups (see Table C-2 in the Appendix).

In case of *I*-2500/κ series, the mechanical properties degraded gradually as κ increased from 0.05 to 0.3 *c-wt*% by showing the *p*-value < 0.05 between κ of 0.05 and 0.3 *c-wt*% (see Table C-2 in the Appendix).

Comparing the trends between *AR* of 800 and 2500 concerning the change of κ, the threshold κ to increase the mechanical properties were varied depending on *AR*. Beyond the threshold of κ, the mechanical properties gradually decreased as κ increased. Other researchers have also reported similar findings [16, 23, 170]. Comparing between *AR* of 800 and 2500, it can be found that the highest mechanical properties were obtained using CNTs with 0.1 *c-wt*% of *AR* = 800 followed by 0.05 *c-wt*% of *AR* = 2500.

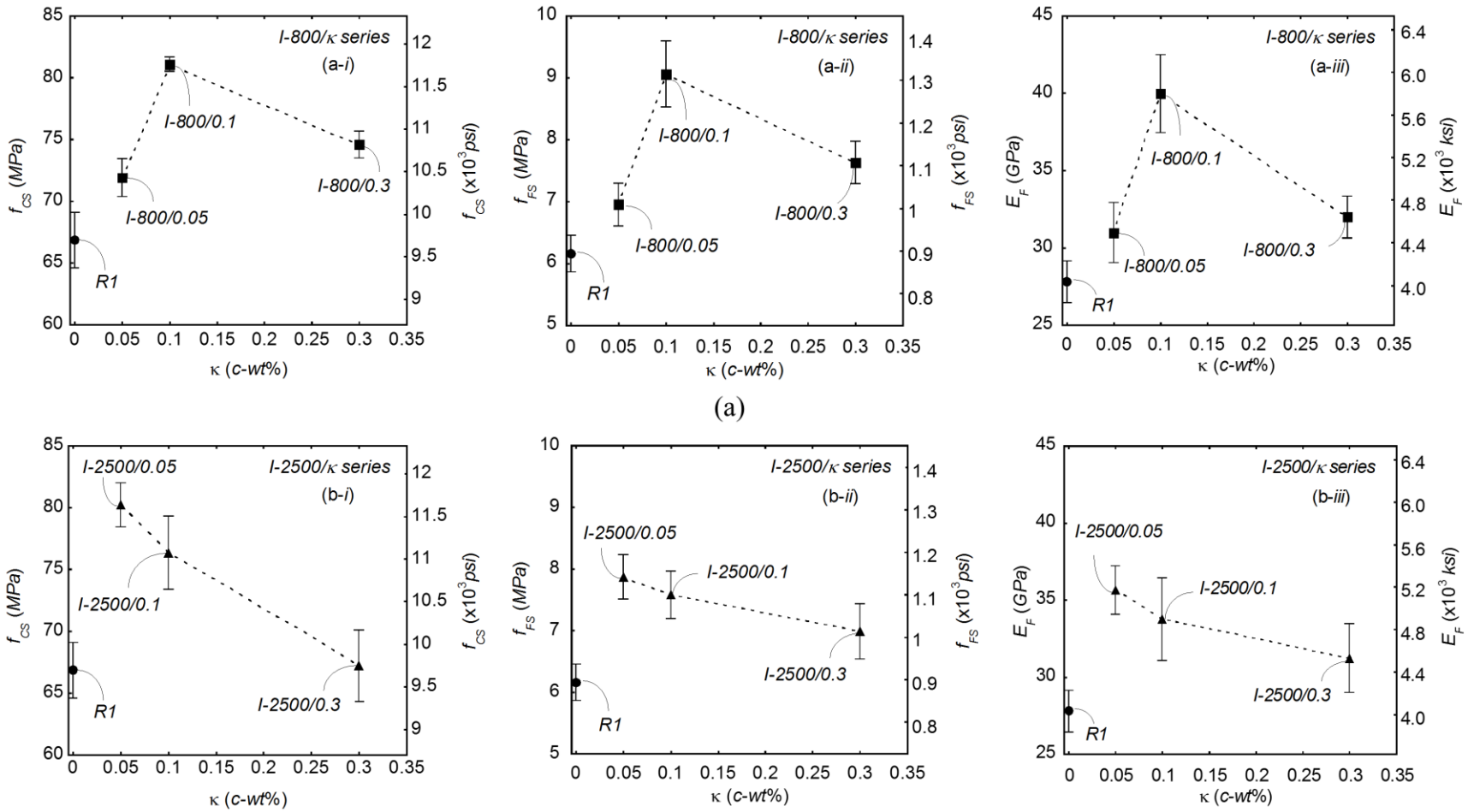

Figure 6-12. Effect of κ on f_{CS}, f_{FS}, and E_F: (a) *I*-800/κ series (b) *I*-2500/κ series

In addition, to experimentally confirm different contributions of CNT properties to the compressive and flexural strengths (see Section 2.6.1), *I*-800/κ and *I*-2500/κ series are further analyzed. Figure 6-13 shows the influence of CNT diameter and concentration on the 28 day f_{CS} (Figure 6-13 (a)) and f_{FS} (Figure 6-13 (b)), with the other experimental variables fixed. When type II CNTs (*I*-800/κ) with the optimum diameter (20 *nm* < *d* < 30 *nm*) was used, both f_{CS} and f_{FS} increased by increasing the CNT concentration from 0.05 to 0.1 *c-wt*%, which was within the optimal upper limit for CNT concentration found using the statistical analysis in Chapter 4 (as shown by the vertical dashed lines in Figure 6-13). However, beyond the threshold concentrations, the mechanical properties degraded by increasing the CNT dosage to κ = 0.3 *c-wt*%.

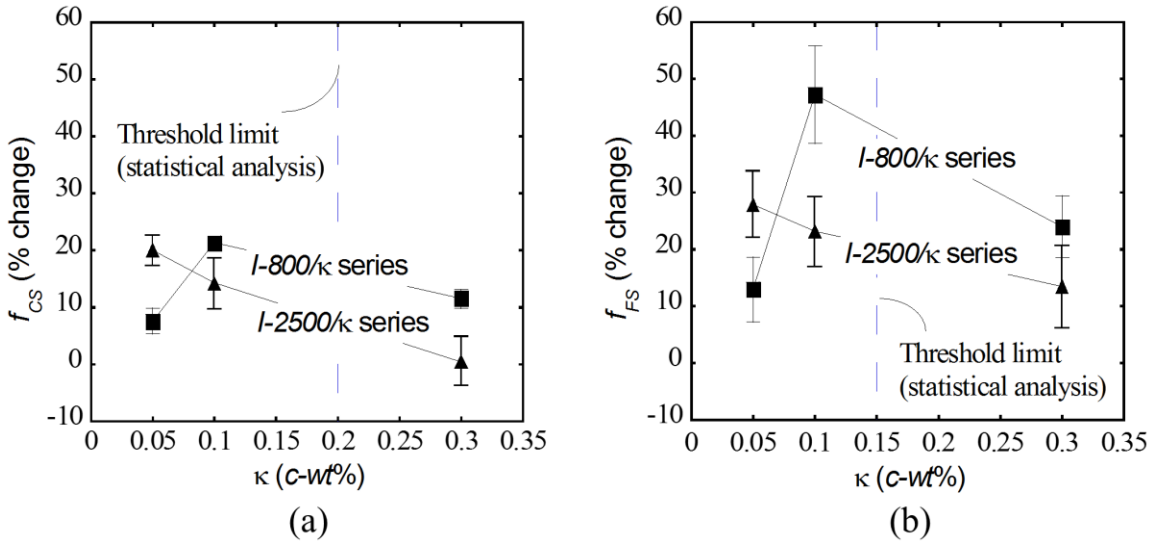

Figure 6-13. Influence of CNT diameter and concentration: (a) f_{CS} (b) f_{FS}

When Type I CNTs was used (*I*-2500/κ; *d* < 8 *nm*), the mechanical properties decreased with an increase in CNT concentration. However, *p*-values suggest that, within the threshold limits of concentration, the change in the mechanical properties from 0.05 to 0.10 *c-wt*% was not significant (*p*-values of 0.12609 and 0.35316 for f_{CS} and f_{FS},

respectively). Beyond the threshold concentrations, the mechanical properties degraded with the use of additional CNTs.

Within the threshold concentrations, the smaller diameter CNTs (Type I) were beneficial in increasing f_{CS}, while the larger diameter CNTs (Type II) benefited f_{FS}. For example, when using κ = 0.1 *c-wt*%, utilizing either Type I or II CNTs had no significant influence on f_{CS} (p-value > 0.05). On the other hand, Type II CNTs contributed significantly to higher f_{FS} compared with the Type I CNTs (p-value = 0.0039 < 0.05).

6.3.2. Interaction between UE_T and UA (Interaction *II*)

Figure 6-14 presents the contributions of UE_T and UA to f_{CS}, f_{FS}, and E_F. Figure 6-14 (a-*i*), (a-*ii*), and (a-*iii*) show f_{CS}, f_{FS}, and E_F, respectively, for UA = 50% (*II-*UE_T*/*50 series). Figure 6-14 (b-*i*), (b-*ii*), and (b-*iii*) show f_{CS}, f_{FS}, and E_F, respectively, for UA = 75% (*II-*UE_T*/*75 series).

In case of *II-*UE_T*/*50 series, as UE_T increased, the mechanical properties increased. When UE_T increased from 500 to 1000 *J/ml*, the p-value indicated that there was no difference between the mean of the investigated groups (p-value = 0.38, 0.16, and 0.43 for f_{CS}, f_{FS}, and E_F, respectively). However, $UE_T = 1500$ *J/ml* resulted in a significant increase in the mechanical properties compared with the lower UE_T (500 and 1000 *J/ml*) with the p-values < 0.05 (see Table C-3 in the Appendix).

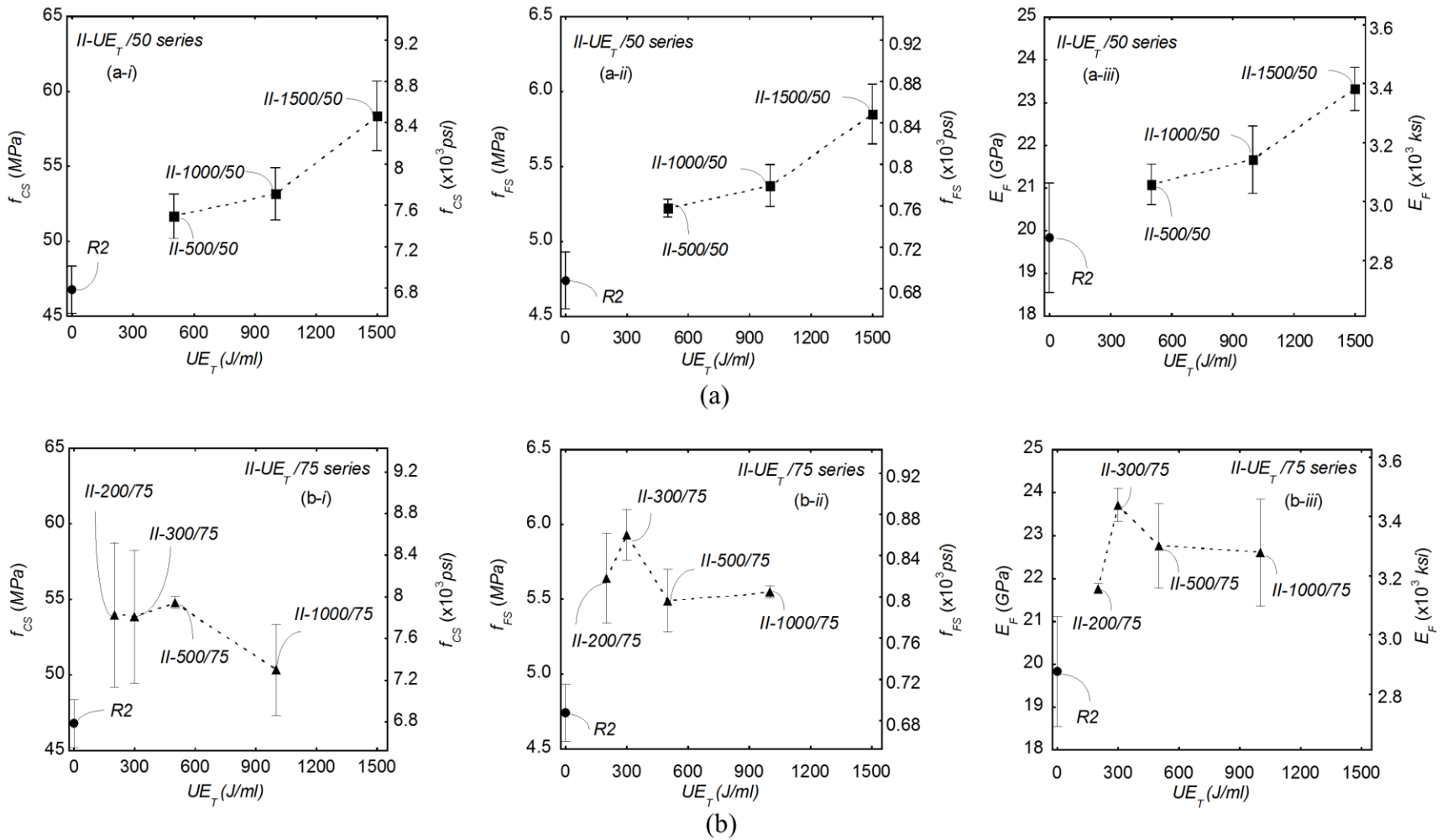

Figure 6-14. Effect of UE_T on f_{CS}, f_{FS}, and E_F: (a) *II-*UE_T*/*50 series (b) *II-*UE_T*/*75 series

In case of *II*-UE_T/75 series, both f_{FS} and E_F increased as UE_T increased from 200 to 300 *J/ml* (see Figure 6-14 (b-*ii*) and (b-*iii*)). However, the *p*-value of 0.22 indicated that the effect of UE_T was not significant to change f_{FS} ranging between 200 and 300 *J/ml*. Conversely, E_F increased significantly as UE_T increased from 200 to 300 *J/ml* (*p*-value = 0.0011 < 0.05; see Table C-3 in the Appendix). This might be attributed to the higher standard deviation in f_{FS} test results (see Figure 6-14 (b-*ii*)). Conversely, in terms of f_{CS}, the increase in UE_T from 200 to 300 *J/ml* did not exhibit a difference between the mean of the investigated groups (*p*-value = 0.98 between *II*-200/75 and *II*-300/75). When using $UE_T = 500$ and 1000 *J/ml*, the average values of the mechanical properties were lower than $UE_T = 300$ *J/ml* (see Figure 6-14 (b)). However, the difference was not significant at 95% confidence level (*p*-value > 0.05; see Table C-3). The *p*-values between *II*-300/75 and *II*-1000/75 were 0.32, 0.06, and 0.22 for f_{CS}, f_{FS}, and E_F, respectively. The smaller *p*-value for f_{FS} (0.06) compared with those of f_{CS} and E_F might be related to the adverse effect of high *UA* which might shorten CNTs [192]. Therefore, the bond capacity of CNTs decreased by shorter length, resulting in the premature debonding of CNTs [122, 188]. This indicates that the threshold of UE_T is lower in this group (*II*-UE_T/75 series) as opposed to the group of *II*-UE_T/50 series. Meanwhile, the bond capacity is not an important factor to increase the compressive strength. Therefore, f_{CS} did not degraded.

When comparing test IDs *II*-1500/50 with *II*-300/75, different combinations of UE_T and *UA* yielded similar f_{FS} (5.85 vs. 5.93 *MPa* [848.5 vs. 860.1 *psi*]) and E_F (23.3 vs. 23.7 *GPa* [3379.4 vs. 3437.4 *ksi*]). Also, f_{CS} exhibited a difference of only 8% (58.35 vs. 53.84 *MPa* [8463 vs. 7809 *psi*]) between the two groups with the *p*-value = 0.19. This indicates

that certain combinations of UE_T and *UA* is needed to yield comparable mechanical properties. In addition, when higher *UA* is used, the lower threshold of UE_T should be used.

6.3.3. Interaction between UE_T and *SP/CNTs* Ratio (Interaction *III*)

Figure 6-15 and Figure 6-16 show the contributions of UE_T and *SP/CNTs* ratio to f_{CS}, f_{FS}, and E_F. The mechanical properties were investigated in two levels of κ (0.025 and 0.1 *c-wt*% for Figure 6-15 and Figure 6-16, respectively).

Figure 6-15 (a-*i*), (a-*ii*), and (a-*iii*) show the effect of UE_T on f_{CS}, f_{FS}, and E_F, respectively, at constant *SP/CNTs* = 4 and κ = 0.025 *c-wt*% (*III*-UE_T/4 series). Figure 6-15 (b-*i*), (b-*ii*), and (b-*iii*) show the effect of *SP/CNTs* ratio on f_{CS}, f_{FS}, and E_F, respectively, at constant UE_T = 500 *J/ml* and κ = 0.025 *c-wt*% (*III*-500/*SP/CNTs* series).

When UE_T increased from 500 to 1500 *J/ml*, test ID *III*-1500/4 yielded approximately 15% higher f_{CS} and 10% higher f_{FS} and E_F than test ID *III*-500/4. When *SP/CNTs* ratio increased from 4 to 12 (see Figure 6-15 (b); *III*-500/*SP/CNTs* series), test ID *III*-500/12 exhibited about 18%, 10%, and 13% increase in f_{CS}, f_{FS}, and E_F, respectively, higher than test ID *III*-500/4. This might be related to a better dispersion of CNTs using higher *SP/CNTs* ratio.

As it can be seen in Figure 6-15 (a-*ii*) and (b-*ii*), the combination of UE_T = 1500 *J/ml* and *SP/CNTs* = 4 (*III*-1500/4) yielded the similar f_{FS} as the combination of UE_T = 500 *J/ml* and *SP/CNTs* = 12 (*III*-500/12) did (p-value = 0.882 > 0.05; see Table C-4 in the Appendix). The similar trend can also be found in f_{CS} (see Figure 6-14 (a-*i*) and (b-*i*); 58.2 vs. 59.7 *MPa* [8441.2 vs. 8658.8 *psi*]) and E_F (see Figure 6-14 (a-*iii*) and (b-*iii*); 22.7 vs. 23.6 *GPa* [3292.4 vs. 3422.9 *ksi*]).

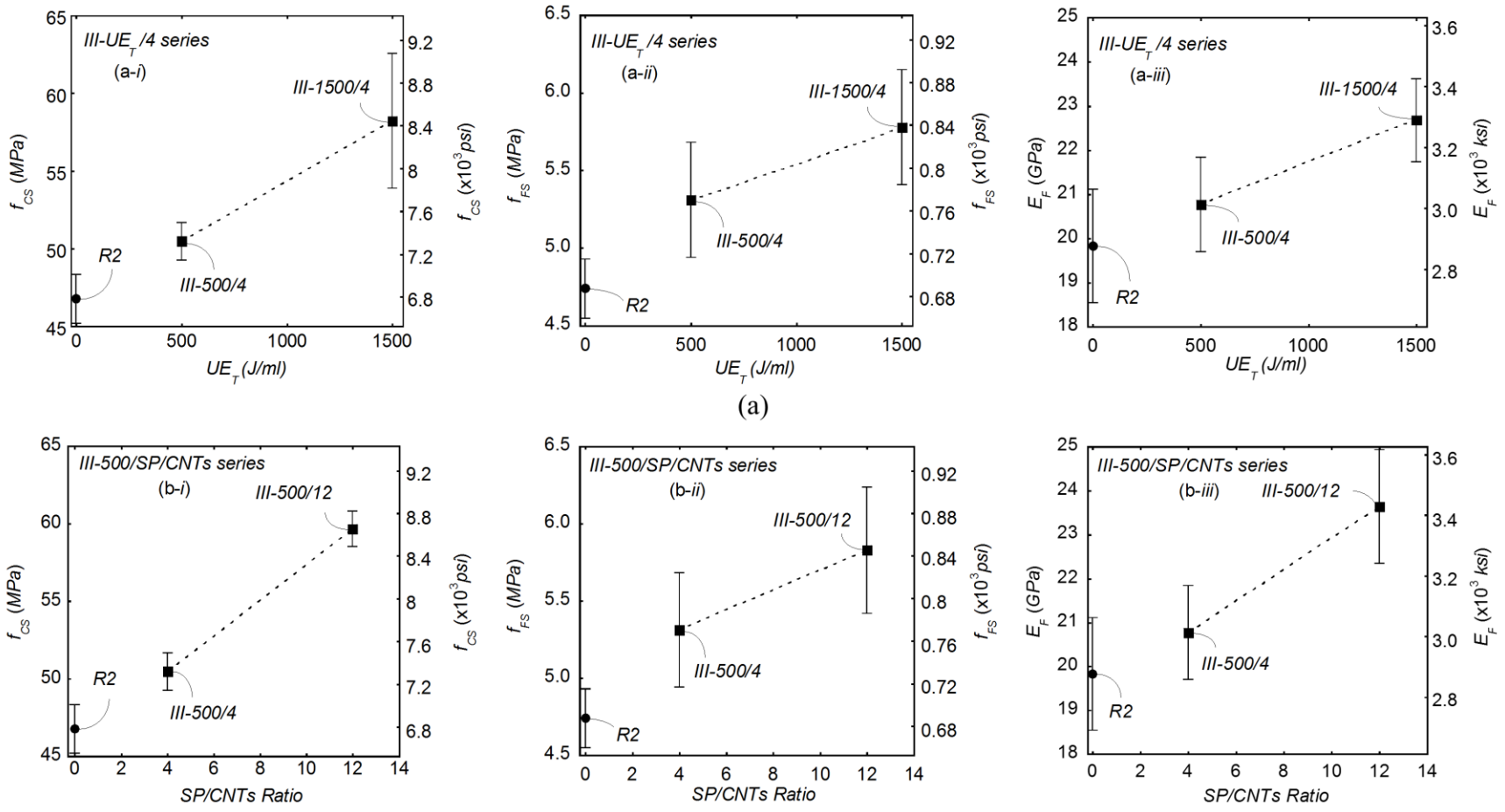

Figure 6-15. Effect of UE_T and *SP/CNTs* ratio on f_{CS}, f_{FS}, and E_F: (a) *III*-UE_T/4 series (b) *III*-500/*SP/CNTs* series

Similarly, in case of κ = 0.1 *c-wt*% (see Figure 6-16), increasing UE_T from 1216 to 2733 *J/ml* resulted in the increase in f_{CS}, f_{FS}, and E_F by 11.1%, 18.5% and 26.1%, respectively (p-values < 0.05; see Table C-4). In addition, test ID *III*-1850/12 produced comparable mechanical properties with test ID *III*-2733/6 (p-value > 0.05).

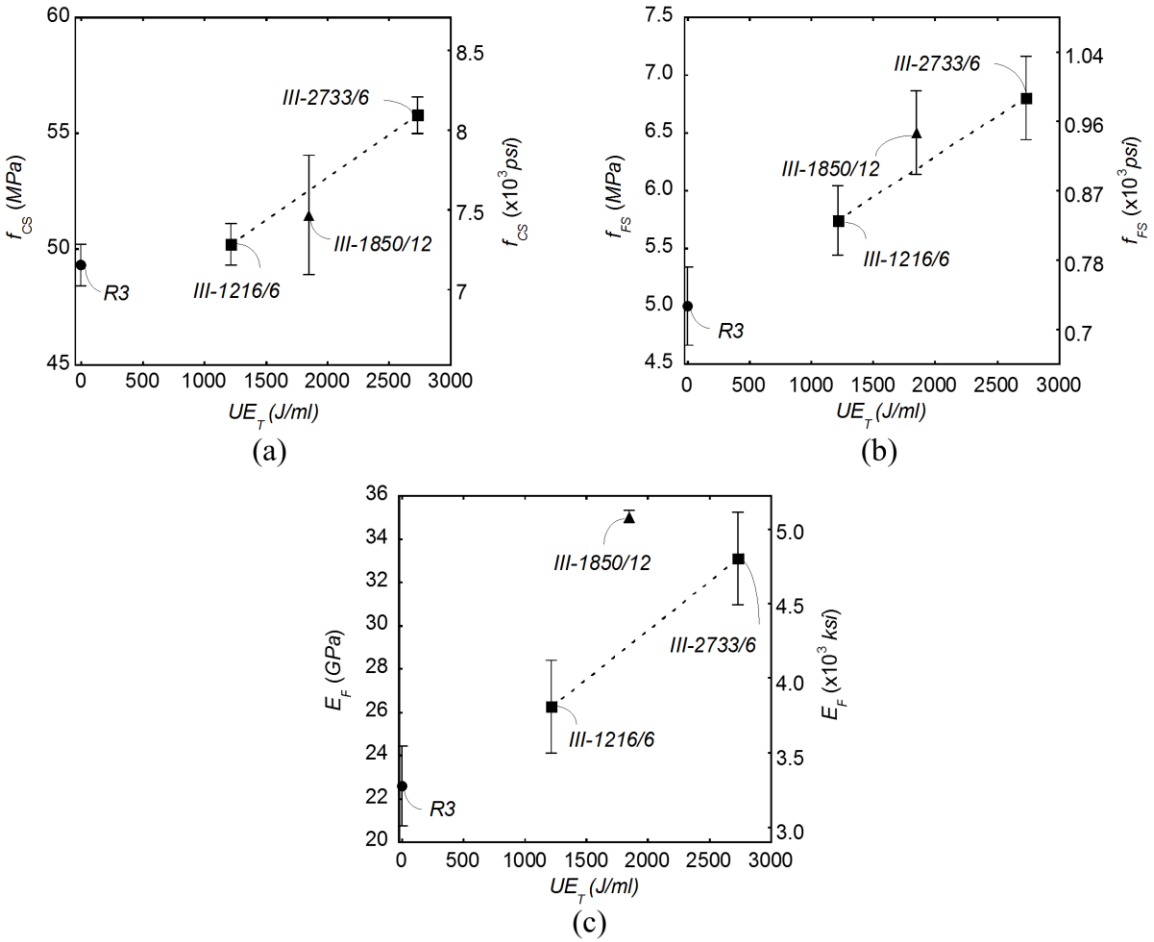

Figure 6-16. Effect of UE_T and *SP/CNTs* ratio at κ = 0.1 *c-wt*%: (a) f_{CS} (b) f_{FS} (c) E_F

Note that in case of κ = 0.025 *c-wt*% (see Figure 6-15), p-values suggested that there was no significant difference between different test IDs for f_{FS} and E_F (p-value > 0.05). This might be attributed to the low concentration of CNTs. As mentioned earlier, mechanical properties increase as κ increases up to its optimal upper limit, beyond which the mechanical properties degrade due to the dispersion issues. Therefore, the effects of

UE_T and *SP/CNTs* ratio in low CNT concentration (κ = 0.025 *c-wt*%) is not obvious. However, the similar trend was not observed in terms of f_{CS} (p-value = 0.04033 (*III*-500/4 vs. *III*-1500/4) and 0.00066 (*III*-500/4 vs. *III*-500/12)).

6.3.4. Interaction between *w/c* and *s/c* Ratios (Interaction *IV*)

Figure 6-17 shows the contributions of *w/c* and *s/c* ratios to the relative mechanical properties that can be defined as follows:

$$P_R = \frac{P_c}{P_m} \tag{5-1}$$

where P_R is the relative mechanical properties of CNT-cement mortars (herein, C_R, F_R, and E_R), P_c is the mechanical properties of CNT-cement nanocomposite, and P_m is the mechanical properties of the matrix (i.e., control specimen without CNTs). Note that C_R is the relative compressive strength (unitless), F_R is the relative flexural strength (unitless), and E_R is the relative elastic modulus (unitless). Figure 6-17 (a) shows the effect of *w/c* ratio on the values of C_R, F_R and E_R, respectively, at *s/c* = 2 (*IV-w/c/*2 series). Figure 6-17 (b) shows the effect of *s/c* ratio on the values of C_R, F_R, and E_R, respectively, at *w/c* = 0.45 (*IV*-0.45/*s/c* series).

In case of *IV-w/c/*2 series, the increase in *w/c* ratio from 0.35 to 0.6 reduced the values of C_R from 1.27 to 1.21 (see Figure 6-17 (a-*i*)), F_R from 1.47 to 1.20 (see Figure 6-17 (a-*ii*)), and E_R from 1.44 to 1.18 (see Figure 6-17 (a-*iii*)). In case of *IV-0.45/s/c* series, the increase in *s/c* from 0 (i.e., paste) to 3 increased the values of C_R from 1.08 to 1.13 (see Figure 6-17 (b-*i*)), F_R from 1.23 to 1.36 (see Figure 6-17 (b-*ii*)), and E_R from 1.22 to 1.47 (see Figure 6-17 (b-*iii*)).

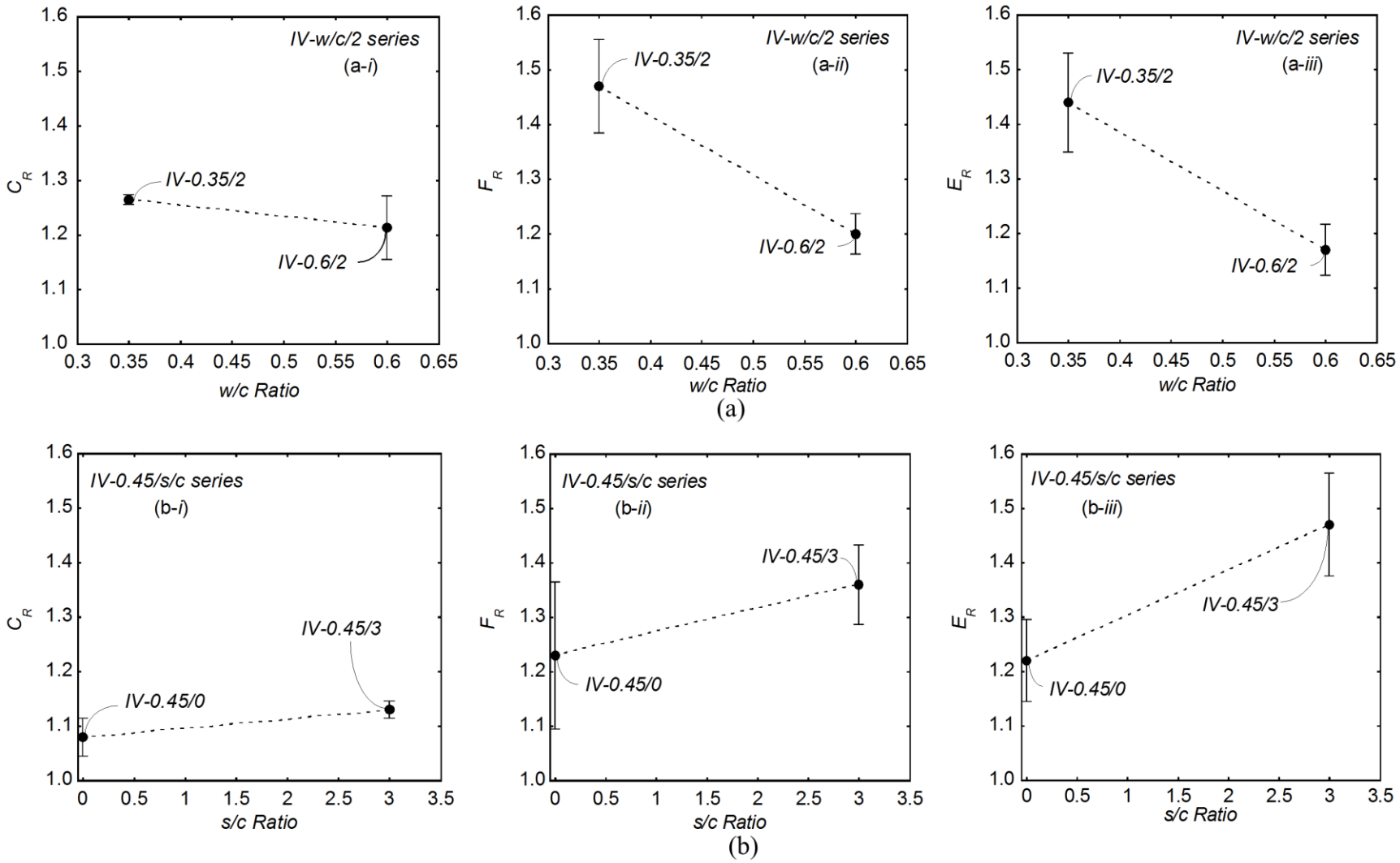

Figure 6-17. Effect of *w/c* ratio and *s/c* ratio on C_R, F_R, and E_R: (a) *IV*-*w/c*/2 series (b) *IV*-0.45/*s/c* series

Generally, lower *w/c* or higher *s/c* ratios (i.e., denser cement matrix) exhibited superior mechanical properties. The statistical analyses also confirmed that the effects of *w/c* and *s/c* ratios are significant in terms of F_R and E_R (p-values < 0.05; see Table C-5 in the Appendix). This can possibly be related to the superior bonding and dispersion of CNTs within a denser cement matrix. Katz *et al*. [212] also found that cement matrix densified by silica fume or the low water-to-binder (*w/b*) ratio resulted in higher interfacial bond strength (50-100%) between carbon fibers and cement matrix. However, in terms of C_R, the p-values of greater than 0.05 indicated that there were no significant differences between *IV*-0.35/2 and *IV*-0.6/2 (p-value = 0.20945) and *IV*-0.45/0 and *IV*-0.45/3 (p-value = 0.08193). This again confirms that bond capacity is not an important factor affecting the compressive strength.

It can also be seen that there is a relationship between *w/c* and *s/c* ratios to achieve superior mechanical properties. For example, the value of E_R was approximately 1.45 when using either test ID *IV*-0.35/2 (1.44) or *IV-0.45/3* (1.47). The similar trend can also be found in F_R where the p-value = 0.13 > 0.05 suggests that there is no significant difference between test IDs *IV*-0.45/3 and *IV*-0.35/2. However, the similar trend was not observed in C_R (p-value = 0.00022).

6.3.5. Interaction between κ and *t* (Interaction *V*)

Figure 6-18 (a), (b), and (c) shows the contributions of κ and *t* of CNT-cement mortars to the values of C_R, F_R and E_R, respectively.

In case of κ = 0.1 *c-wt*% (*V*-0.1/*t* series), F_R and E_R did not exhibit any further improvement at different testing ages of 3 and 28 days (p-value > 0.05; see Table C-6 in the Appendix). For example, 3-day and 28-day values of F_R were 1.48 and 1.47,

respectively. However, C_R degraded from 1.35 to 1.27 (p-value = 0.00751 < 0.05; significant decrease in C_R for V-0.1/t series in a period from 3 days to 28 days).

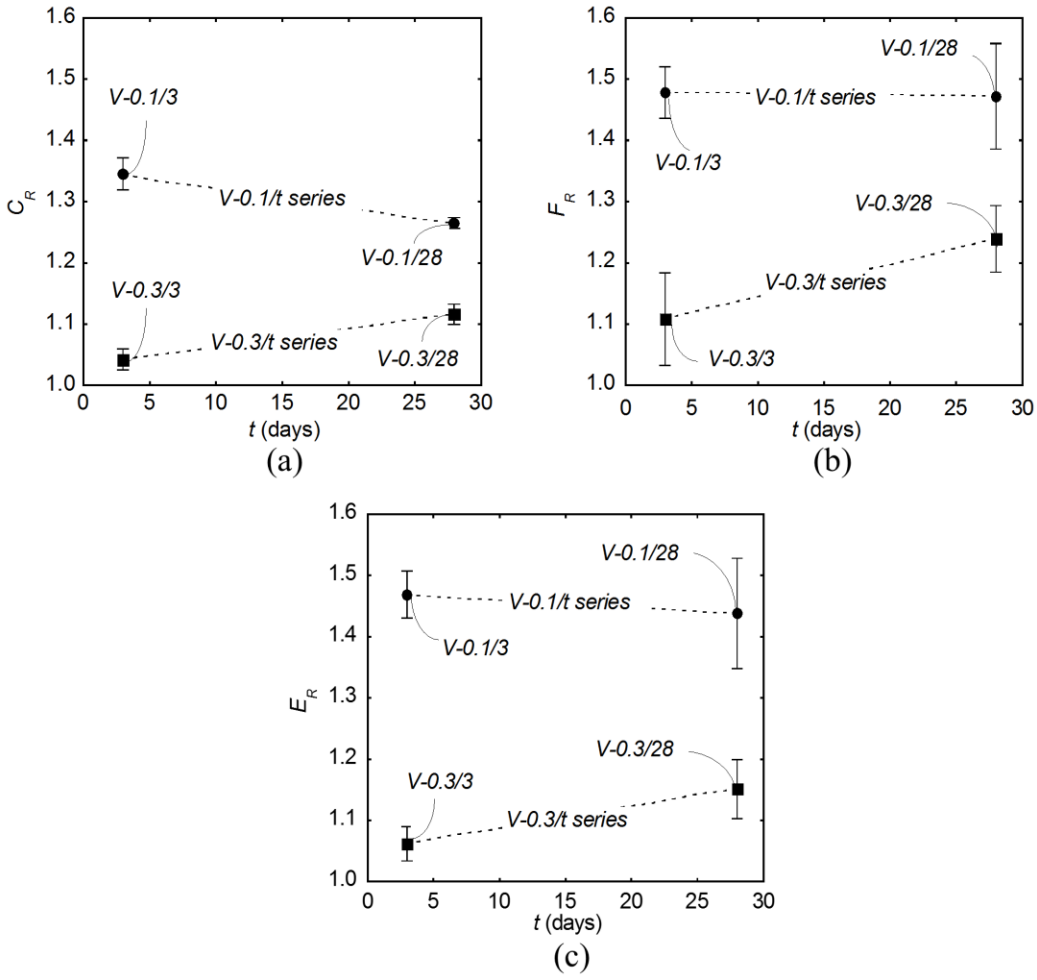

Figure 6-18. Effect of κ and t on (a) C_R (b) F_R (c) E_R

In case of κ = 0.3 *c-wt*% (V-0.3/t series), C_R, F_R and, E_R values at the age of 3 days were 1.04, 1.11, and 1.06, respectively. The 28-day values of C_R, F_R and E_R, however, increased to 1.12, 1.24 and 1.15, respectively (p-value < 0.05). The similar trend could also be observed in [11].

Besides the studied interactions between the experimental variables (see Sections 6.3.1 through 6.3.5), a limited study was conducted to investigate the influence of the sand gradation and mixing procedure on 7-day mechanical properties of CNT-cement mortars

(see Figure B-1 and Figure B-2 in the Appendix). The experimental results exhibited that neither sand gradation nor mixing procedure affected the mechanical properties of CNT-cement nanocomposites. Therefore, they are not considered as important variables in the modeling process, presented in Chapter 8.

6.3.6. Effect of CNTs on the Dynamic Elastic Modulus

In this section, the contributions of κ and *AR* (interaction *I*; see Section 6.3.6.1), UE_T and *SP/CNTs* ratio (interaction *III*; see Section 6.3.6.2), *w/c* and *s/c* ratios (interaction *IV*; see Section 6.3.6.3), and κ and *t* (interaction *V*; see Section 6.3.6.4) to dynamic elastic modulus (E_d) are discussed. Note that this section presents the 28-day (and 1-day for interaction *V*) test results. The general trend of E_d over time is discussed in Figure B-3 through Figure B-5, presented in the Appendix.

6.3.6.1. Interactions between κ and *AR* (Interaction *I*)

Figure 6-19 shows E_d at age of 28 days for *AR* = 800 (*I*-800/κ series; Figure 6-19 (a)) and *AR* = 2500 (*I*-2500/κ series; Figure 6-19 (b)).

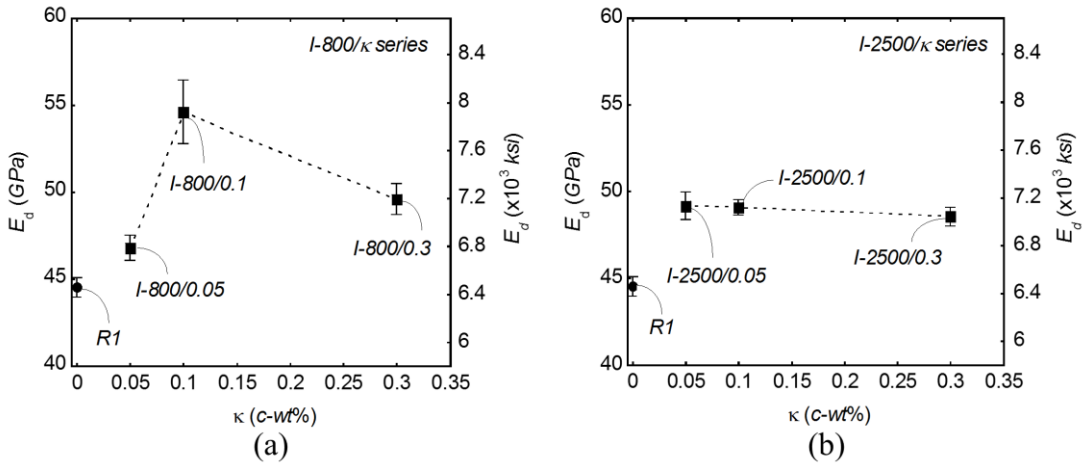

Figure 6-19. Effect of κ on E_d (a) *I*-800/κ series (b) *I*-2500/κ series

In case of *I*-800/κ series (see Figure 6-19 (a)), test ID *I*-800/0.1 yielded the maximum increase in E_d by 22.6%, compared with the control specimen (*R1*). The

contribution of CNTs (κ = 0.1 *c-wt*%) to increase E_d is much lower than E_F (see Figure 6-12 (a-*iii*)) which exhibited 43.7% increase compared with the control. The superior performance of CNTs in terms of E_F than E_d might be explained by the crack bridging ability of CNTs when the specimens are under flexural load. On the other hand, the contribution of CNTs to increase E_d is only limited to the reduced porosity which makes the material denser. In addition, the increase in κ from 0.05 to 0.1 *c-wt*% exhibited 16.7% increase in E_d. However, κ = 0.3 *c-wt*% (test ID *I*-800/0.3) exhibited lower E_d than κ = 0.1 *c-wt*% (test ID *I*-800/0.1), most probably due to the degraded dispersion quality. However, this was not confirmed using the ANOVA test results (p-values = 0.0735 between *I*-800/0.1 and *I*-800/0.3).

In case of *I*-2500/κ series, different concentrations of CNTs exhibited similar E_d of around 49 *GPa* (≅ 7107 *ksi*) which yielded an increase of about 10% compared with the control (E_d = 44.53 *GPa* [6459 *ksi*]). The p-values between different test IDs are listed in Table C-7 in the Appendix.

6.3.6.2. Interactions between UE_T and *SP/CNTs* Ratio (Interaction *III*)

Figure 6-20 shows the influence of UE_T and *SP/CNTs* ratio on E_d. The increase in UE_T from 1216 to 2733 *J/ml*, yielded approximately 9% higher E_d. This might be explained by a better dispersion of CNTs using higher UE_T. However, p-value > 0.05 between *III*-1216/6 and *III*-2733/6 did not confirm this (see Table C-8 in the Appendix). This might be attributed to utilizing uncracked beam specimens in terms of E_d, limiting the contribution of CNTs [213]. In addition, test ID *III*-1850/12 (see the solid triangle in Figure 6-20) exhibited comparable E_d with test ID *III*-2733/6 (p-value = 0.24076; see Table C-8).

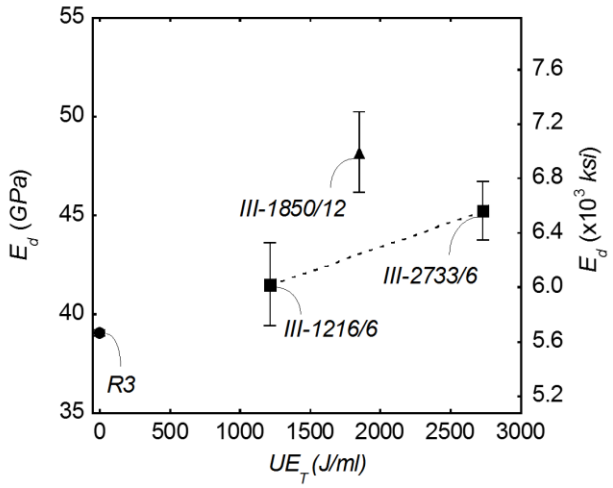

Figure 6-20. Effect of UE_T and *SP/CNTs* Ratio on E_d

6.3.6.3. Interactions between *w/c* and *s/c* ratios (Interaction *IV*)

Figure 6-21 (a) and (b) show the influence of *w/c* and *s/c* ratios, respectively, on the relative E_d (E_d of CNT-cement nanocomposites over the control specimen) at age of 28 days. Generally, CNTs exhibited higher contribution to increase E_d in denser cement matrix (i.e., lower *w/c* ratio or higher *s/c* ratio). Ahmed *et al*. [213] also reported the higher influence of CNTs on the increase in E_d for cement pastes with lower *w/c* ratio. However, the contribution of CNTs to increase the relative E_d is much smaller than their contribution to increase the relative static elastic modulus (E_R; see Figure 6-17 (a-*iii*) and (b-*iii*)). This might be attributed to the limited contribution of CNT crack bridging in uncracked specimens, in terms of E_d.

In case of *IV-w/c/*2 series (see Figure 6-21 (a)), utilizing either *w/c* ratio of 0.35 or 0.6 exhibited similar relative E_d (p-value > 0.05; see Table C-9 in the Appendix).

In case of *IV-0.45/s/c* series (see Figure 6-21 (b)), the increase in *s/c* from 0 to 3 increased the relative E_d from 1.07 to 1.16. However, p-value > 0.05 suggests that the effect of *s/c* ratio on the relative E_d is negligible (see Table C-9).

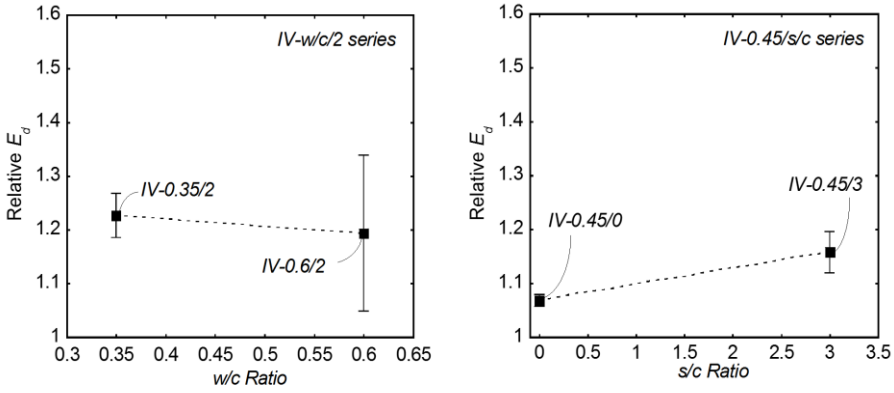

(a) (b)

Figure 6-21. Effect of *w/c* ratio and *s/c* ratio on the relative E_d: (a) *IV-w/c*/2 series (b) *IV*-0.45/*s/c* series

6.3.6.4. Interactions between κ and *t* (Interaction *V*)

Figure 6-22 shows the interactions between κ and *t* affecting the relative E_d for CNTs with *AR* = 800.

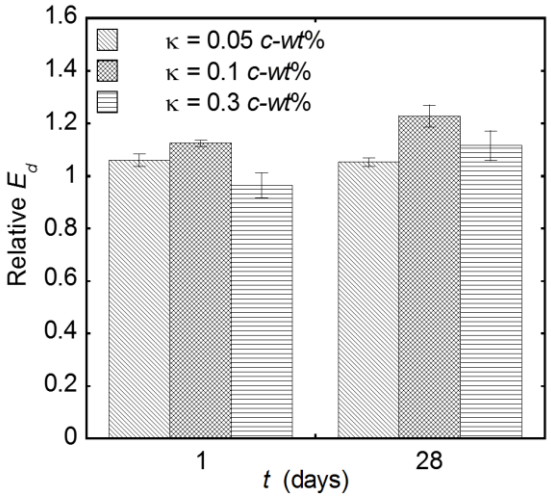

Figure 6-22. Effects of κ and t on the relative E_d

When using either κ = 0.05 or 0.1 *c-wt*%, the relative E_d did not exhibit any further improvement at different testing ages of 1 and 28 days (*p*-value > 0.05; see Table C-10 in the Appendix). For example, in case of κ = 0.1 *c-wt*%, the relative E_d exhibited the values of 1.12 and 1.23 at age of 1 and 28 days, respectively (*p*-value = 0.076 > 0.05). Conversely, in case of κ = 0.3 *c-wt*%, the relative E_d exhibited a significant increase from 0.96 to 1.11

in a period of 1 to 28 days (p-value = 0.0381 < 0.05). This might be explained by the lower rate of cement hydration at early ages when using high CNT concentrations [31, 116, 174].

6.3.7. Summary: Mechanical Properties

CNTs have the potential to increase the mechanical properties of cementitious materials significantly. However, due to the complex interactions between multiple variables, conflicting results have been reported. Therefore, through experimental investigation, this research program re-examined five main interactions between multiple experimental variables affecting the mechanical properties (compressive strength, flexural strength, static elastic modulus, and dynamic elastic modulus) of CNT-cement pastes and mortars. The controlled experimental variables were CNT aspect ratio (*AR*), concentration (κ), total ultrasonication energy (UE_T), ultrasonication amplitude (*UA*), superplasticizer-to-CNTs (*SP/CNTs*) ratio, hydration age (*t*), water-to-cement (*w/c*) ratio, sand-to-cement (*s/c*) ratio, sand gradation, and mixing procedure. The following conclusions were drawn.

1. There is a threshold CNT concentration beyond which the mechanical properties degraded, and this threshold concentration depended on *AR*. Higher concentration of CNTs with smaller *AR* produced comparable mechanical properties as lower concentration of larger *AR* CNTs did. The threshold CNT concentration was found to be 0.05 and 0.1 *c-wt*% at *AR* of 2500 and 800, respectively.
2. When using ultrasonication procedure to disperse CNTs, UE_T, *UA*, and *SP/CNTs* ratio are critical variables to affect the mechanical properties. When using high *UA*, lower threshold of UE_T should be used, to eliminate the risk of CNT breakage. Also, as *SP/CNTs* ratio increases, lower amount of UE_T could be utilized to attain comparable mechanical performance. For example, using UE_T and *SP/CNTs* ratio

of 1500 *J/ml* and 4 or 500 *J/ml* and 12, respectively, produced comparable mechanical properties.

3. The contribution of CNTs to increase the mechanical properties becomes more pronounced when using a denser cement matrix (lower *w/c* ratio and/or higher *s/c* ratio). This might be attributed to the superior dispersion and interfacial bond strength between CNTs and denser cement matrix. In addition, certain combinations of *w/c* and *s/c* ratios could be used to produce comparable mechanical properties. For example, *w/c* and *s/c* ratios of either 0.35 and 2 or 0.45 and 3, respectively, exhibited comparable enhancements in the mechanical properties.
4. At low CNT concentrations ($\kappa \leq 0.1$ *c-wt*%), the hydration age is not an important factor to affect the mechanical properties. Conversely, as CNT concentration increased, the contribution of CNTs to increase the mechanical properties at early ages decreased. However, the rate of increase in mechanical properties increased over time.
5. Generally, the contribution of CNTs to increase the dynamic elastic modulus (E_d) was less than the static elastic modulus measured from the flexural test. This might be explained by using the uncracked and unloaded beam specimens for E_d testing. Therefore, the contribution of CNTs to increase E_d was limited to filling the micro-pores and densifying the cement matrix. On the other side, the crack bridging ability of CNTs could be utilized in terms of the static elastic modulus, resulting in higher improvement.

6.4. Durability: Alkali-Silica Reaction

A total of 8 mix proportions were tested to investigate the influence of CNT type, its concentration, and ultrasonication procedure on the properties of ASR-affected cement mortars. The mix proportions were selected to cover the extreme cases based on the findings from the experimental test results of mechanical properties (see Section 6.3). Besides the evaluation of mortar bar expansion and E_d over time (Section 6.4.1), the 28-day f_{CS}, f_{FS}, and E_F (after submersion in 1N NaOH at 80±2 ℃ [176±3.6 ℉]) were also examined in Section 6.4.2. The details are discussed as follows.

6.4.1. Effect of CNTs on Expansion and E_d of ASR-affected Cement Mortars

This section discusses the influence of CNT concentration (Section 6.4.1.1), aspect ratio (Section 6.4.1.2), cement matrix composition (Section 6.4.1.3), and ultrasonication procedure (Section 6.4.1.4) on the expansion and E_d of mortar bars after 14 and 28 days exposure to 1N NaOH at 80±2 ℃ (176±3.6 ℉). The detailed analysis of the contributions of these variables on the expansion and E_d of mortar bars over time is presented in Figure B-6 through Figure B-9 in the Appendix).

6.4.1.1. Effect of CNT Concentration

Figure 6-23 shows the influence of different concentrations of CNTs with *AR* of 800 (Type II CNTs) on average expansion (see Figure 6-23 (a)) and E_d (see Figure 6-23 (b)) of ASR-affected mortar bars (*w/c* = 0.35) after 14- and 28-day exposure to ASR conditions. The standard deviation of different mixtures is also included. The dashed line in Figure 6-23 (a) represents ASTM C1260 non-reactive limit of 0.1% (low risk of ASR expansion under field conditions). The dashed-dotted line in Figure 6-23 (a), on the other

hand, represents ASTM C1260 ASR reactive limit of 0.2% (high risk of ASR expansion under field conditions).

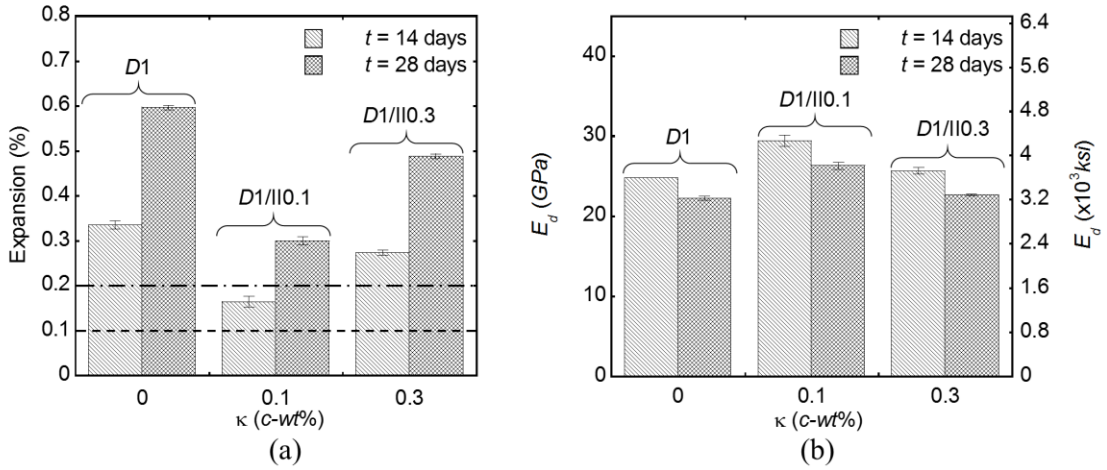

Figure 6-23. Effect of κ: (a) expansion (b) E_d (*w/c* = 0.35)

Note: dashed line represents ASTM C1260 non-reactive limit, dashed-dotted line represents ASTM reactive limit

Figure 6-23 (a) shows that the control cement mortar (test ID *D*1) expanded by 0.34% after 14 days in 1N NaOH solution which exceeded 0.2% expansion limit of ASTM C1260 (see dashed-dotted line in Figure 6-23 (a)). The average expansion of *D*1 increased to 0.6% at 28 days. Utilizing 0.1 *c-wt*% of Type II CNTs (test ID *D*1/II0.1) significantly contributed to lower expansions. The 14- and 28-day average expansion of *D*1/II0.1 decreased by 50% compared with *D*1 (average expansion of 0.17% and 0.3% at 14 and 28 days, respectively). In case of using 0.3 *c-wt*% Type II CNTs (test ID *D*1/II0.3), the efficiency of CNTs in controlling ASR expansion decreased considerably. The average expansion of *D*1/II0.3 was 0.27 and 0.49 at 14 and 28 days, respectively. Although *D*1/II0.3 exhibited around 20% decrease in the average expansion compared with *D*1, it expanded more than ASTM C1260 expansion limit of 0.2% at 14 days (see dashed-dotted line in Figure 6-23 (a)). This might be attributed to the improper dispersion when using high CNT concentration. Improper dispersion of CNTs (CNT agglomeration) could create defects

such as increased permeability and decreased load carrying capacity [24, 66]. Therefore, alkali ions penetrated easier into the interior of the mortar bars, accelerated ASR and caused more internal cracks within the specimens. Thereafter, the lower load carrying capacity of agglomerated CNTs was less effective to delay the crack propagation, resulted in higher expansion than *D*1/II0.1. This might explain the lower rate of increase in the expansion of *D*1/II0.1 compared with *D*1/II0.3. Considering the period between 14 and 28 days, the rate of increase in the expansion for *D*1/II0.1 (0.0193) was 37% lower than *D*1/II0.3 (0.0306).

Figure 6-23 (b) shows the contributions of *D*1/II0.1 and *D*1/II0.3 to controlling ASR cracks by showing the average E_d of two mortar bars after 14-day and 28-day exposure to extreme ASR conditions. Dynamic elastic modulus has been extensively used in the literature to evaluate the damage associated with durability issues including freeze and thaw and ASR [214].

As ASR progressed, E_d of *D*1 decreased from 24.9 *GPa* (3611.4 *ksi*) to 22.3 *GPa* (3234.3 *ksi*) in a period between 14 and 28 days. In case of *D*1/II0.1, E_d exhibited higher values than *D*1. *D*1/II0.1 exhibited almost 20% higher values of E_d at 14 and 28 days compared with *D*1. This indicates that incorporating CNTs might restrain the propagation of internal cracks due to ASR. Even though *D*1/II0.3 outperformed compared with *D*1 in the expansion test results (see Figure 6-23 (a)), the average E_d exhibited marginal difference by showing *p*-values > 0.05 (See Table C-11 in the Appendix). Nevertheless, *D*1/II0.3 delayed the propagation of internal cracks compared with *D*1 which was confirmed using ANOVA test results (see Table C-16 in the Appendix).

6.4.1.2. Effect of CNT Aspect Ratio

Figure 6-24 (a) presents the influence of *AR* on 14- and 28-day relative expansion (average expansion of CNT-cement mortars over the control) at κ = 0.1 *c-wt*% (see Figure 6-24 (a-*i*)) and 0.3 *c-wt*% (see Figure 6-24 (a-*ii*)). Figure 6-24 (b) shows the influence of *AR* on the relative E_d at κ = 0.1 *c-wt*% (see Figure 6-24 (b-*i*)) and 0.3 *c-wt*% (see Figure 6-24 (b-*ii*)) at ages of 14 and 28 days. The dashed lines indicate the relative properties of the control specimen (*D*1).

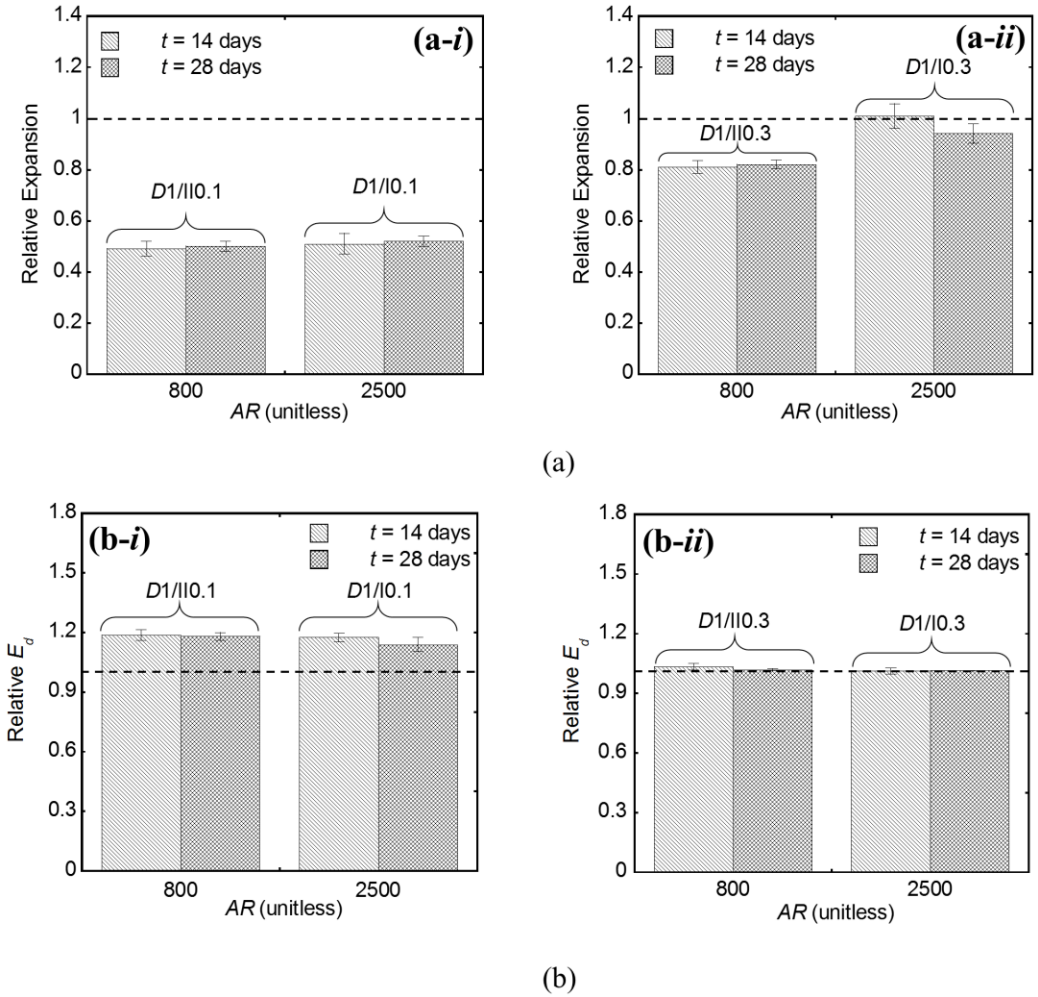

(a)

(b)

Figure 6-24. Effect of *AR*: (a) relative expansion (b) relative E_d (*w/c* = 0.35)

Figure 6-24 (a) shows that when using κ = 0.1 *c-wt*% (see Figure 6-24 (a-*i*)), the relative expansion of either *AR* = 800 (*D*1/II0.1) or *AR* = 2500 (*D*1/I0.1) was around 0.5

(i.e., the expansion of CNT-cement mortars decreased by 50% compared with the control). However, in case of κ = 0.3 *c-wt*% (see Figure 6-24 (a-*ii*)), 14-day relative expansion of *D*1/II0.3 (*AR* = 800) was 0.81, while it was around 1.01 for *D*1/I0.3 (*AR* = 2500). Therefore, *D*1/II0.3 outperformed by 24.7% compared with *D*1/I0.3. Similar trend could also be observed at 28 days where the percent difference of the relative expansion between *AR* = 800 and 2500 was 14.7%.

Note that when using 0.3 *c-wt*% CNT concentration (see Figure 6-24 (a-*ii*)), the percent difference of the relative expansion between *D*1/I0.3 and *D*1/II0.3 decreased by 8.4% in a period from 14 to 28 days (from 22.0% to 13.6%). This might be attributed to the presence of COOH functional groups on the surface of Type I CNTs (*AR* = 2500). COOH-CNTs might provide stronger engagement with C-S-H [166], decreasing the ion diffusion within the cement hydrates and lowering the rate of ASR. In addition, COOH-CNTs might absorb higher amount of water at higher concentrations [93]. Therefore, they released more water over time, resulting in higher progress in the hydration process. As a result, the bond between Type I CNTs and hydration products increased, delaying the propagation of internal cracks. Further study is needed to confirm this trend.

Despite the different trends in the relative expansion between 0.1 and 0.3 *c-wt*% of CNTs with *AR* of 800 and 2500 (see Figure 6-24 (a)), the relative E_d exhibited similar trend. The 14- and 28-day relative E_d of 0.1 (see Figure 6-24 (b-*i*)) and 0.3 (see Figure 6-24 (b-*ii*)) *c-wt*% of either *AR* = 800 or 2500 were very close to each other. For example, the 14-day relative E_d of *D*1/I0.1 and *D*1/II0.1 were 1.18 and 1.19, respectively. The 14-day relative E_d of *D*1/I0.3 and *D*1/II0.3 were 1.01 and 1.03, respectively.

6.4.1.3. Effect of Cement Matrix Composition

Despite the notable benefits of CNTs in reducing the ASR expansion at 0.1 *c-wt*% concentration, the 14-day expansion was above the ASTM C1260 non-reactive limit of 0.1% (see the dashed line in Figure 6-23 (a)). This might be explained by the lower *w/c* ratio used in this study (*w/c* = 0.35) compared with ASTM C1260 (*w/c* = 0.47). The lower *w/c* ratio might result in higher expansion rate due to the higher alkali concentration in the pore solution [215]. Therefore, to allow a more subjective comparison between the results of this experimental study and ASTM C1260 expansion limits, a limited study was conducted using the *w/c* ratio of 0.45.

Figure 6-25 (a-*i*) and (a-*ii*) show the influence of cement matrix composition (*w/c* = 0.35 (*s/c* = 2) vs. *w/c* = 0.45 (*s/c* = 3)) on the average expansion of cement mortars with and without inclusion of 0.1 *c-wt*% Type II CNTs (*AR* = 800) after 14- and 28-day exposure to ASR conditions, respectively. Also, Figure 6-25 (b-*i*) and (b-*ii*) show the influence of cement matrix composition on 14- and 28-day E_d of ASR-affected cement mortars, respectively. Note that ultrasonication procedure *A* was used to fabricate CNT-cement mortars (see Section 5.3.3.2).

Figure 6-25 (a-*i*) shows that although *D*1/II0.1 (*w/c* = 0.35) passed ASTM C1260 non-reactive limit of 0.1% at 14 days (see the dashed line in Figure 6-25 (a-*i*)), *D*2/II0.1-*A* (*w/c* = 0.45) exhibited lower expansion than 0.1% at 14 days. The control cement mortar (test ID *D*2) exhibited the average expansion of 0.22%, which was beyond the reactive limit of ASTM C1260. Conversely, *D*2/II0.1-*A* significantly reduced the expansion by 72.7% (expansion of 0.06%) compared with *D*2. After 28 days of exposure to extreme ASR conditions (see Figure 6-25 (a-*ii*)), *D*2/II0.1-*A* yielded a reduction of 65.7% compared with

*D*2. The 28-day average expansions of *D*2 and *D*2/II0.1-*A* were 0.35% and 0.12%, respectively. This suggests that adding CNTs (up to threshold concentration of 0.1 *c-wt*% in this research) might mitigate the ASR expansion under field conditions.

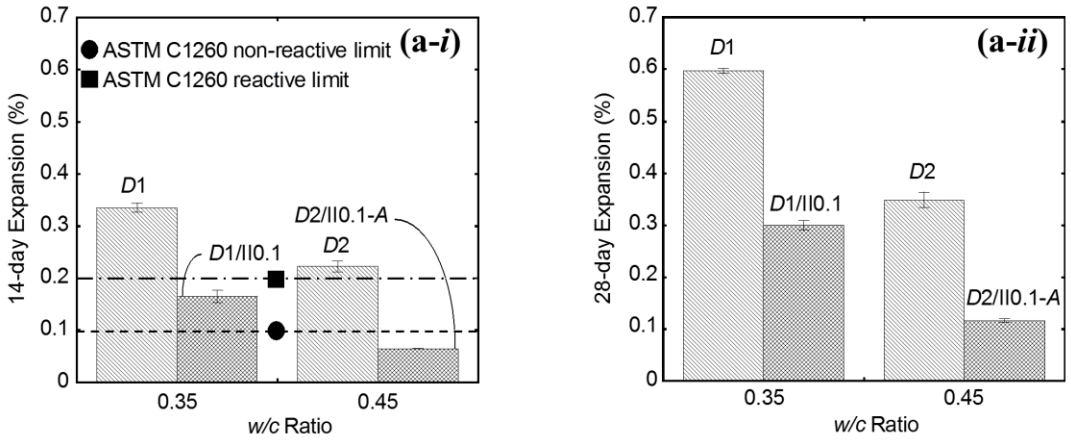

(a)

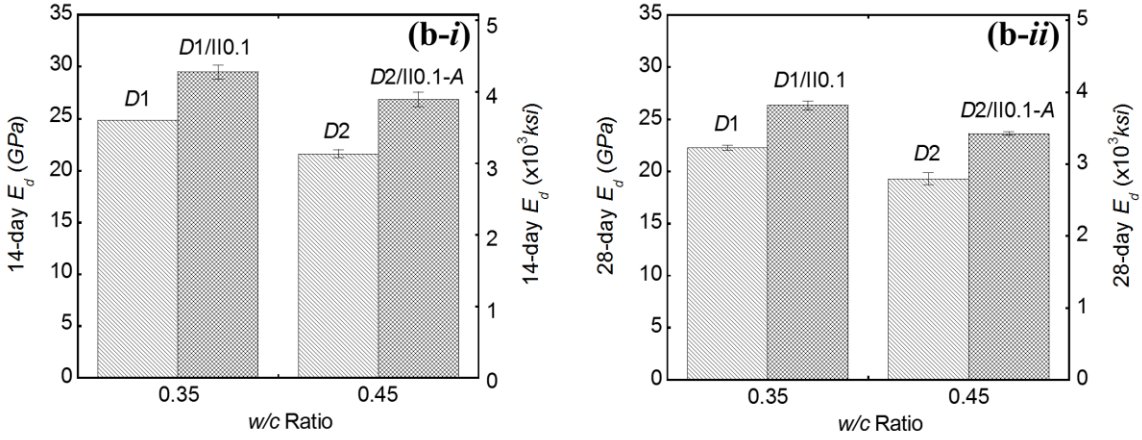

(b)

Figure 6-25. Influence of cement matrix composition: (a) expansion (b) E_d

Figure 6-25 (b-*i*) and (b-*ii*) show the contributions of *D*1/II0.1 and *D*2/II0.1-*A* on E_d after 14- and 28-day exposure to ASR conditions, respectively. Incorporating 0.1 *c-wt*% CNTs resulted in an increase in the average E_d at different *w/c* ratios. For example, *D*2/II0.1-*A* exhibited 24.3% increase in the 14-day E_d compared with *D*2 (see Figure 6-25 (b-*i*)). This might be attributed to a good degree of CNT dispersion. The well-dispersed

CNTs might reduce the permeability as well as delaying the propagation of cracks by bridging between them. The similar trend can also be observed at 28-day (see Figure 6-25 (b-*ii*)).

6.4.1.4. Effect of Ultrasonication Procedure

To investigate the influence of ultrasonication procedure on the performance of cement mortars affected by ASR, two same mix proportion were prepared (*D*2/II0.1) using different ultrasonication procedures denoted as procedure *A* ($UE_T = 2610 \pm 15$ *J/ml* with *UA* = 57%; *D*2/II0.1-*A*) and *B* ($UE_T = 200$ *J/ml* with *UA* = 50%; *D*2/II0.1-*B*).

Figure 6-26 (a) and (b) show the contributions of *D*2/II0.1-*A* and *D*2/II0.1-*B* on the relative expansion and relative E_d, respectively.

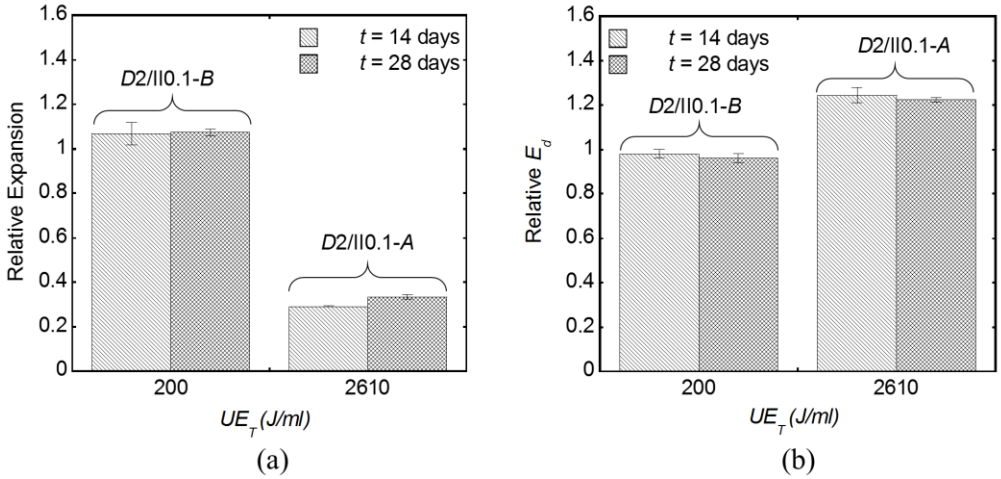

Figure 6-26. Effect of UE_T (a) relative expansion (b) relative E_d

Figure 6-26 (a) shows that despite the exceptional performance of *D*2/II0.1-*A* in reducing ASR expansion (relative expansion of 0.29 and 0.33 at 14- and 28-day, respectively), *D*2/II0.1-*B* exhibited 14- and 28-day relative average expansion of 1.068 (6.8% higher than *D*2) and 1.074 (7.4% higher than *D*2), respectively. The *p*-values > 0.05 suggest that there is no significant difference between *D*2 and *D*2/II0.1-*B*.

In terms of the relative E_d (see Figure 6-26 (b)), *D*2/II0.1-*B* exhibited no difference compared with *D*2 (p-value > 0.05; see Table C-11). While, *D*2/II0.1-*A* exhibited about 23% increase compared with *D2* (relative E_d of 1.24 and 1.22 at 14- and 28-day, respectively). These results indicate that to exploit CNT advantages to control ASR progress, their proper dispersion is vital. The optimum range of UE_T found from mechanical properties test results can also have positive impact on mitigating ASR damages.

6.4.2. Effect of CNTs on ASR-affected Cement Mortars (f_{CS}, f_{FS}, E_F)

After 28-days exposure to extreme ASR conditions, the mechanical properties of ASR-affected cement mortars; namely, f_{FS} (Section 6.4.2.1), E_F (Section 6.4.2.2), and f_{CS} (Section 6.4.2.3) were evaluated and test results were compared with those of the control specimens. The test results are listed in Table B-7 in the Appendix.

6.4.2.1. Flexural Strength

Figure 6-27 (a) and (b) present the flexural load-deflection curves for the *w/c* ratio of 0.35 and 0.45, respectively, with and without inclusion of 0.1 *c-wt*% of Type II CNTs (ultrasonication procedure *A* was used). The flexural load-deflection curves were plotted using one specimen graph (out of 5 mortar bars for each test ID) which represented closet to the average mechanical performance of all the specimens. The different shapes of the load-deflection relations between the control and CNT-cement mortars were observed, for both *w/c* ratios. The control specimens showed a more gradual softening branch than CNT-cement mortars. This might be attributed to the greater meandering and branching of the cracks within the control specimens affected by ASR [216, 217].

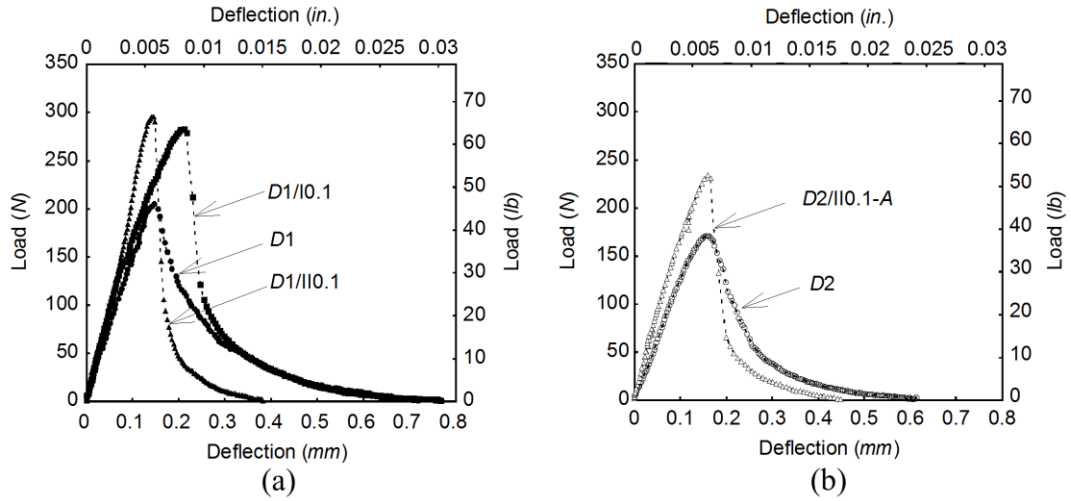

Figure 6-27. Flexural load-deflection relations of mortar bars with and without using CNTs: (a) *w/c* = 0.35 (b) *w/c* = 0.45

Figure 6-28 shows the flexural strength (f_{FS}) of mortar bars after 28 days exposure to ASR conditions at different *w/c* ratios of 0.35 (see Figure 6-28 (a)) and 0.45 (see Figure 6-28 (b)).

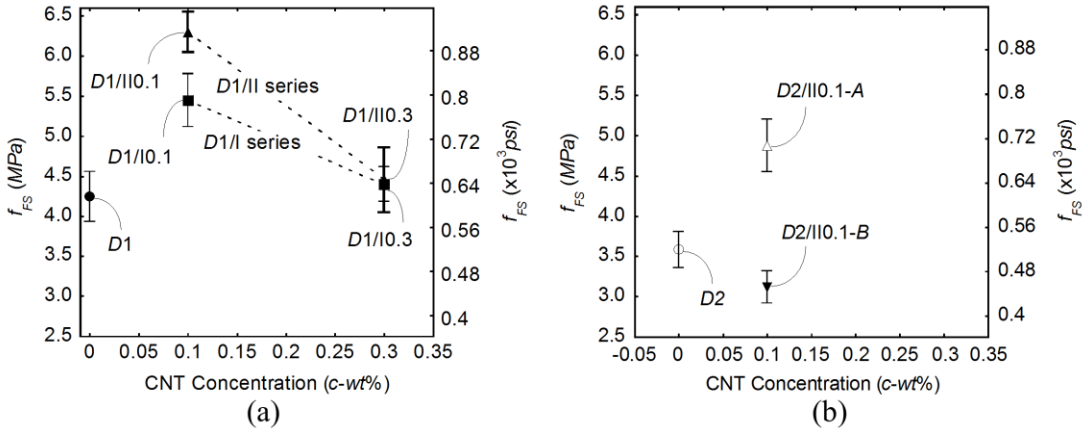

Figure 6-28. Influence of CNTs on 28-day f_{FS} of ASR affected cement mortars: (a) *w/c* = 0.35 (b) *w/c* = 0.45

Figure 6-28 (a) shows that the average f_{FS} of *D*1/II0.1 increased by 49% compared with *D*1 which exhibited an average f_{FS} of 4.24 *MPa* (615 *psi*). However, *D*1/II0.3 did not show a positive influence on increasing f_{FS} compared with *D*1 (*p*-value = 0.38256 > 0.05; see Table C-13 in the Appendix). The decrease in f_{FS} by the increase in CNT concentration

from 0.1 to 0.3 *c-wt*% might be attributed to the ASR cracks due to the expansion pressure (see Figure 6-23 (a)). When using Type I CNTs (*D*1/I series), the average f_{FS} of *D*1/I0.1 exhibited 29% increase compared with *D*1. Conversely, *D*1/I0.3 exhibited no increase in the flexural strength compared with *D*1 by showing *p*-value > 0.05 (see Table C-13).

In case of *w/c* ratio of 0.45 (see Figure 6-28 (b)), the average f_{FS} of *D*2/II0.1-*A* was 4.88 *MPa* (707.8 *psi*) which exhibited 36.1% increase compared with *D*2 (3.58 *MPa* [519.2 *psi*]). This can also be statistically confirmed by showing *p*-value < 0.05 between *D*2 and *D*2/II0.1-*A* (see Table C-13). However, when using ultrasonication procedure *B* to disperse CNTs (*D*2/II0.1-*B*), the average f_{FS} was 3.12 *MPa* (452.5 *psi*) which showed 13% decrease compared with *D*2 (*p*-value = 0.02566). This is in good agreement with the findings in expansion and E_d test results (see Figure 6-26).

6.4.2.2. Elastic Modulus

Figure 6-29 shows the 28-day elastic modulus (E_F) of mortar bars at different *w/c* ratios of 0.35 (see Figure 6-29 (a)) and 0.45 (see Figure 6-29 (b)).

Figure 6-29 (a) shows that in case of *D*1/II series, the average E_F exhibited 46.7% and 35.1% increase compared with *D*1 for *D*1/II0.1 and *D*1/II0.3, respectively. In case of *D*1/I series, the average E_F exhibited 36.8% and 25.4% increase using *D*1/I0.1 and *D*1/I0.3, respectively, compared with *D*1.

In case of *w/c* ratio of 0.45 (see Figure 6-29 (b)), the average E_F of *D*2/II0.1-*A* exhibited 54.2% increase compared with *D*2. Whereas, *D*2/II0.1-*B* exhibited 16.4% decrease compared with *D*2. However, the *p*-value of 0.26587 between *D*2 and *D*2/II0.1-*B* indicates no significant difference (see Table C-14). This shows similar trend with the findings in Figure 6-26 (b).

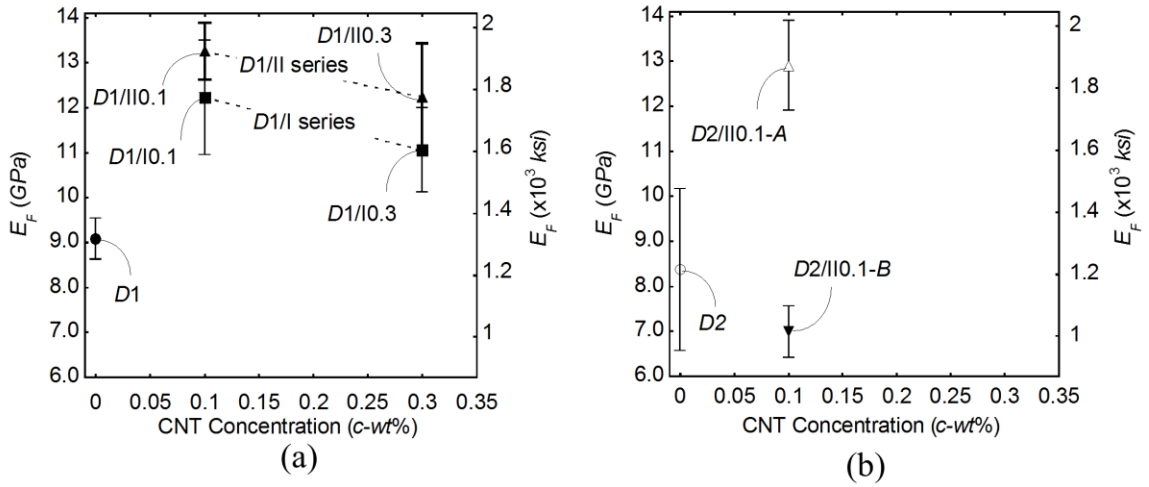

Figure 6-29. Influence of CNTs on 28-day E_F of ASR affected cement mortars: (a) *w/c* = 0.35 (b) *w/c* = 0.45

6.4.2.3. Compressive Strength

Figure 6-30 (a) and (b) present the 28-day compressive strength (f_{CS}) of cement mortars at different *w/c* ratios of 0.35 and 0.45, respectively.

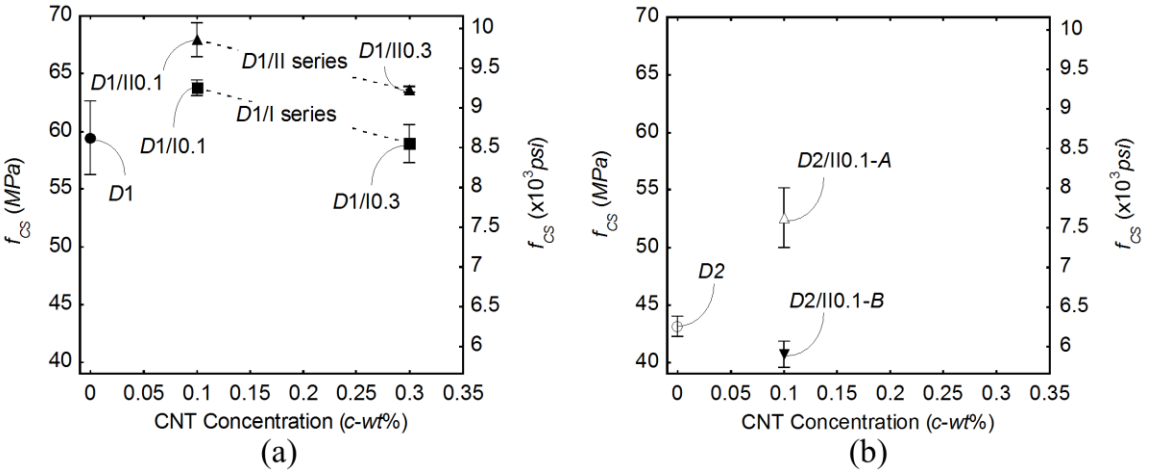

Figure 6-30. Influence of CNTs on 28-day f_{CS} of ASR affected cement mortars: (a) *w/c* = 0.35 (b) *w/c* = 0.45

Figure 6-30 (a) shows that the average f_{CS} of *D*1 was 59.4 *MPa* (8615.2 *psi*) and it increased by 14.3% (67.9 *MP*a; 9848.1 *psi*) and 7.1% (63.6 *MP*a; 9224.4 *psi*) when using CNT concentration of 0.1 and 0.3 *c-wt*% of *D*1/II series, respectively. However, *p*-values

> 0.05 between *D*1 and *D*1/II0.1 or *D*1/II0.3 suggest that there are no significant differences between the mean of the compressive strength of the control (*D*1) and CNT-reinforced cement mortars (*D*1/II series). Similarly, in case of *D*1/I series, f_{CS} exhibited no significant difference between *D*1 and *D*1/I0.1 or *D*1/I0.3 by showing p-values > 0.05 (see Table C-15 in the Appendix).

When using *w/c* ratio of 0.45 (see Figure 6-30 (b)), the average f_{CS} of *D*2/II0.1-*A* increased by 21.9% compared with *D*2. However, *D*2/II0.1-*B* degraded the compressive strength compared with *D*2.

Generally, addition of CNTs contributed to higher f_{FS} and E_F than f_{CS}. The similar trend was also observed in the study performed by Park and Lee [218]. In their study, polypropylene fibers resulted in larger increase in the flexural strength than compressive strength of ASR-affected cement mortars.

6.4.3. Summary: Durability Property

Crack bridging ability and reduced permeability by adding CNTs might help to reduce the ASR progress. However, to exploit the full advantage of CNTs, their proper dispersion within the cement matrix is very important. If CNTs lack proper dispersion, they might even accelerate the ASR progress. From the test results, the following conclusions were drawn:

1. Incorporating CNTs could significantly contribute to lowering the ASR-induced damages. The highest reduction in expansion was obtained using 0.1 *c-wt*% Type II CNTs (*AR* = 800) which exhibited 73% lower expansion than control specimen without CNTs. Also, the dynamic elastic modulus yielded 24% increase compared

with the control. The effectiveness of CNTs to mitigate ASR damages significantly decreased at concentration of 0.3 *c-wt*%.

2. At the optimum CNT concentration (0.1 *c-wt*%), both types of CNTs (Type I and II with aspect ratios of 2500 and 800, respectively) exhibited similar results in reducing the ASR expansion. At high concentration (0.3 *c-wt*%), the effectiveness of Type I CNTs was significantly reduced compared with Type II CNTs, most probably due to dispersion issues. The 14- and 28-day expansion of mortar bars reinforced with 0.3 *c-wt*% of Type II CNTs was 24% and 15% higher than Type I CNTs. Despite linear expansion test results, dynamic elastic modulus did not show clear differences when using 0.3 *c-wt*% concentration of either Type I or II CNTs.
3. Although optimum ultrasonication energy significantly contributed to mitigate ASR, utilizing low ultrasonication energy did not improve the properties of ASR-affected CNT-cement mortars (compared with the control specimen).
4. The test results indicated that even though ASR damage was observed in all the specimens, CNTs could act as reinforcement and did not lose their load carrying capacity. For example, when using 0.1 *c-wt*% of Type II CNTs (*w/c* = 0.35), flexural strength and static elastic modulus exhibited approximately 50% increase compared with the control specimens in both ASR and normal curing conditions.

CHAPTER 7. MODELING PROCEDURE: PROBABILISTIC APPROACH

7.1. General

Because of the high degree of uncertainty while incorporating CNTs, a probabilistic approach is used (Section 7.2) to predict the mechanical properties (flexural strength and static elastic modulus). The sources of uncertainty are from the intrinsic properties of CNTs (e.g., amount of structural defects on CNT surface, number of walls, material properties, etc.) as well as statistical uncertainty in the estimation of the unknown model parameters, model error associated with the inexact form of the models, and missing of the possible influential variables. A Bayesian methodology is adopted and the unknown model parameters are calibrated with extensive experimental test data from this research and the literature (Section 7.3). The proposed probabilistic model provides valuable information for engineers and designers to determine and optimize the most critical variables and the interactions between them to achieve the desired mechanical properties through computing the probability of failure (Section 7.4). Finally, sensitivity and importance analyses are presented in Section 7.5 to determine the effect of variables on probability estimates.

7.2. Formulation of the Probabilistic Model

The probabilistic approach is used based on the available deterministic models (Kelly-Tyson model for flexural strength and Halpin-Tsai model for elastic modulus; see Section 2.6.2). Then, additional correction terms and model errors are introduced to the deterministic expressions to account for inherent bias and to capture the remaining variability in the residuals, respectively [219].

The probabilistic models relate the quantity of interest (flexural strength (f_{FS-c}; herein, σ_c) and elastic modulus (E_{F-c}; herein, E_c) of CNT-cement nanocomposites) to a set of measurable variables (defined as $\boldsymbol{x} = (x_1, x_2, x_3, x_4, \dots)$) such as *AR*, κ, *UEI*, *SP/CNTs* ratio, *w/c* ratio, *s/c* ratio, *t*, etc. The probabilistic capacity model can be written as follows:

$$C(\boldsymbol{x}, \boldsymbol{\Theta}) = C(\boldsymbol{x}) + \gamma(x, \Theta) + \partial\varepsilon \tag{6-1}$$

where $C(\boldsymbol{x}, \boldsymbol{\Theta})$ is the capacity model of interest, $\boldsymbol{x}$ is a set of measurable variables, $\boldsymbol{\Theta} = (\theta, \partial)$, $\theta = (\theta_1, \theta_2, \theta_3, \dots)$ denotes a set of unknown model parameters used to fit the data, $C(\boldsymbol{x})$ is the selected deterministic model, $\gamma(x, \theta)$ is the correction term (herein, η_D, η_H, and η_M; these will be defined in Chapter 8), ∂ is a standard deviation of the error term taken from Var $[C(\boldsymbol{x}, \boldsymbol{\Theta})] = \partial^2$, ε is a random variable with zero mean and unit variance, and $\partial\varepsilon$ is the error term of the model. There are two assumptions in the formulation of the probabilistic model: 1) ∂ is assumed to be independent of $\boldsymbol{x} = (x_1, x_2, x_3, \dots)$ (i.e., homoscedasticity assumption), and 2) ε has the normal distribution (i.e., normality assumption).

7.3. Bayesian Methodology

Generally, there are two subfields of probability: frequentist and Bayesian methodologies [220]. In frequentist methodology, the probability is defined as the long-term relative frequency of occurrence of an event. In Bayesian methodology, however, the concept of probability is interpreted as the degree of belief of a likelihood of an event by bringing prior knowledge into consideration. Therefore, a Bayesian methodology is used to correct the impact of each variable in a probabilistic manner. The unknown model

parameters in Bayesian approach depend on the values of the experimental data and are estimated using the following updating rule [221]:

$$f(\boldsymbol{\Theta}) = \lambda L(\boldsymbol{\Theta}) p(\boldsymbol{\Theta}) \tag{6-2}$$

where $\boldsymbol{\Theta}$ is a vector of unknown model parameters, $p(\boldsymbol{\Theta})$ is prior distribution of $\boldsymbol{\Theta}$ based on knowledge about $\boldsymbol{\Theta}$ that represents the information available before collecting the data D of size n, $L(\boldsymbol{\Theta})$ is the likelihood function that captures the information on $\boldsymbol{\Theta}$ from data D which is proportional to the conditional probability $P(D|\boldsymbol{\Theta})$ of observing D for given values of $\boldsymbol{\Theta}$, $\lambda = [\int L(\boldsymbol{\Theta}) p(\boldsymbol{\Theta})\, d(\boldsymbol{\Theta})]^{-1}$ is a normalizing factor, and $f(\boldsymbol{\Theta})$ is the posterior distribution that shows the updated state of information about $\boldsymbol{\Theta}$. Note that $f(\boldsymbol{\Theta})$ represents a compromise between the prior knowledge and the observed data. For large or even moderate data size, a substantial modification of $p(\boldsymbol{\Theta})$ may only lead to a minor modification of $f(\boldsymbol{\Theta})$ [221].

Once $f(\boldsymbol{\Theta})$ is known, the posterior mean vector ($M_{\boldsymbol{\Theta}}$) and the covariance matrix ($\Sigma_{\boldsymbol{\Theta\Theta}}$) could be obtained. Because there is no prior information about $\boldsymbol{\Theta}$ before collecting data D, a non-informative prior distribution $p(\boldsymbol{\Theta}) \propto \frac{1}{\partial}$ is used [219]. If new data becomes available in the future, Equation 6-2 can still be used to update the estimates of the unknown model parameters by using the current $f(\boldsymbol{\Theta})$ as a new previous distribution [222].

7.4. Probability of Failure

After calibrating the unknown model parameters using experimental test data, the proposed probabilistic models will be used to optimize each variable to maximize the mechanical properties. This could be achieved by computing the probability of not meeting a specified mechanical properties requirement (probability of failure; P_f).

Every structure has a capacity (C) and is subjected to some sort of demand (D) where both of them depend on random variables. Therefore, each of C and D has a probability distribution ($f_D(D)$ and $f_C(C)$) which could be combined to form a joint probability density function ($f_{CD}(C,D)$; see Figure 7-1). If the joint probability density function is known, the probability of failure could be easily determined by $P_f = \int_{-\infty}^{\infty}\int_{-\infty}^{C\leq D} f_{CD}(C,D)dC\,dD$. However, because of the large number of variables, the probability of failure cannot be determined in a mathematical way and therefore might be estimated using simulation-based analyses.

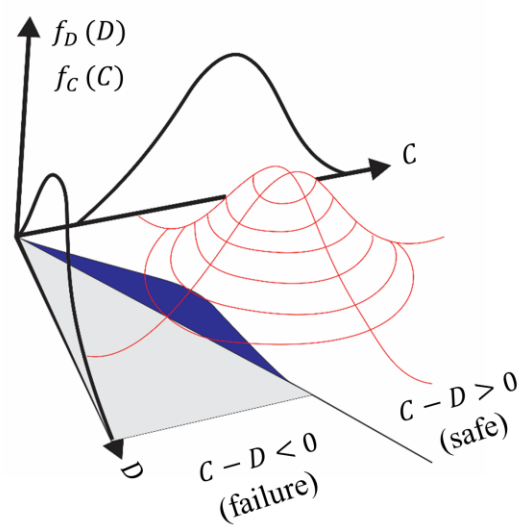

Figure 7-1. Joint probability density function (modified from [223])

Following the conventional notation in structural reliability theory [224], a limit state function $g(\cdot)$ is introduced such that the event $[g(\cdot) \leq 0]$ denotes not meeting the specified capacity requirements [224]. For the determination of the structural reliability, the probability of failure can be derived considering the probability density functions of C and D in the limit state function. If the capacity is greater than the demand (i.e., $C - D > 0$), the structure is safe. Conversely, if the demand exceeds the capacity ($C - D < 0$), the

structure fails. The probability of failure could be visualized as the overlapping area of the normally distributed capacity and demand curves (see Figure 7-1).

In this research, because there is no code or requirement criteria available in the literature, the minimum mechanical properties requirement (demand) of cementitious materials containing CNTs (f_{FS-c} (herein, σ_c) and E_{F-c} (herein, E_c)) is set to the deterministic value of 50% increase compared with the control specimen without CNTs (f_{FS-m} (herein, σ_m) and E_{F-m} (herein, E_m)). Using the proposed probabilistic models, the limit state function can be written as follows:

$$g(\psi\sigma_m(\text{or } E_m), \boldsymbol{x}, \boldsymbol{\Theta}) = C(\boldsymbol{x}, \boldsymbol{\Theta}) - \psi\sigma_m(\text{or } E_m) \quad (6\text{-}3)$$

where ψ is the minimum design requirement (herein, ψ = 1.5), σ_m and E_m are the flexural strength and elastic modulus of the control specimen without CNTs. The probability of not meeting the specified mechanical properties requirement can be given by:

$$P(\boldsymbol{\Theta}) = P[g(\psi\sigma_m(\text{or } E_m), \boldsymbol{x}, \boldsymbol{\Theta}) \leq 0 \mid \boldsymbol{\Theta}] \quad (6\text{-}4)$$

where $P(\cdot \mid \cdot)$ denotes the conditional probability of $g(\psi\sigma_m(\text{or } E_m), \boldsymbol{x}, \boldsymbol{\Theta}) \leq 0$ for given values of $\boldsymbol{\Theta}$.

The probability of failure is visualized using the isoprobability lines which connect pairs of values of different variables corresponding to the same probability of failure (see Figure 7-2; $p[g(\psi\sigma_m(\text{or } E_m), \boldsymbol{x}, \boldsymbol{\Theta}) \leq 0]$). The lower values of probability of failure (P_f) indicates that the likelihood of $C - D > 0$ is higher (i.e., the flexural strength or elastic modulus meets the design requirement).

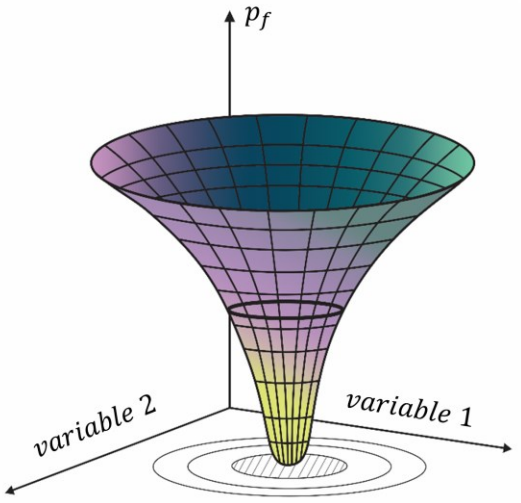

Figure 7-2. Visualization of probability of failure using isoprobability lines

7.5. Sensitivity and Importance Measures

This section presents the sensitivity and importance analyses for different variables in the limit state function (see Equation 6-3) to assess their effect on the probability estimates, helping researchers to minimize P_f by designing more efficiently.

The sensitivity analysis is performed to investigate what variables are most sensitive to the change in mechanical properties [225]. By computing sensitivity measures, researchers could determine variable(s) to be changed to make stronger CNT-cement nanocomposites. To compare the sensitivity measures of all the variables, the vector $\boldsymbol{\delta}$ is computed as follows:

$$\boldsymbol{\delta} = \boldsymbol{\sigma_s} \boldsymbol{\nabla_{\Theta_f}} \beta \tag{6-5}$$

where $\boldsymbol{\sigma_s}$ is the diagonal matrix with diagonal elements given by the standard deviation of each random variable in $\boldsymbol{x}$, $\boldsymbol{\nabla_{\Theta_f}} \beta$ is the gradient vector of β with respect to $\boldsymbol{\Theta}_f$ computed at the mean point, and β is the reliability index from the first order reliability method (FORM) analysis.

Although the sensitivity measures provide information on how sensitive the variables are with respect to the changes in mechanical properties, they cannot be compared because they have different units [226]. The importance measure can be used to rank the importance of different variables with respect to their effects on the variability of the limit state function.

In the limit state function (see Equation 6-3), important variables have larger impacts on the variability of the limit state function and less important variables have smaller impacts. In this research, an importance analysis is conducted to obtain the vector of importance measures ($\boldsymbol{\gamma}$) as follows [227]:

$$\boldsymbol{\gamma}^T = \frac{\boldsymbol{\alpha}^T \boldsymbol{J}_{\boldsymbol{u}^*\boldsymbol{z}^*} \boldsymbol{SD}'}{\|\boldsymbol{\alpha}^T \boldsymbol{J}_{\boldsymbol{u}^*\boldsymbol{z}^*} \boldsymbol{SD}'\|} \tag{6-6}$$

where $\boldsymbol{\alpha}$ is a row vector of the negative normalized gradient of the limit state function evaluated at the design point in standard normal space, $\boldsymbol{z}$ is vector of random variables ($\boldsymbol{z} = (x_p, \boldsymbol{\Theta})$), $\boldsymbol{J}_{\boldsymbol{u}^*\boldsymbol{z}^*}$ is Jacobian of the probability transformation from the original space (i.e., $\boldsymbol{z}$) to the standard normal space (i.e., $\boldsymbol{u}$) with respect to the coordinates of the most likely failure point (i.e., design point, $\boldsymbol{z}^*$), and $\boldsymbol{SD}'$ is the standard deviation diagonal matrix of equivalent normal variables $\boldsymbol{z}'$ defined by the linearized inverse transformation $\boldsymbol{z}' = \boldsymbol{z}^* + \boldsymbol{J}_{\boldsymbol{z}^*\boldsymbol{u}^*}(\boldsymbol{u} - \boldsymbol{u}^*)$ at the design point. The elements in the matrix $\boldsymbol{SD}'$ are the square root of the corresponding diagonal elements of the covariance matrix $\Sigma' = \boldsymbol{J}_{\boldsymbol{z}^*\boldsymbol{u}^*} \boldsymbol{J}^T_{\boldsymbol{z}^*\boldsymbol{u}^*}$ of the variables in the $\boldsymbol{z}'$.

CHAPTER 8. MODELING THE MECHANICAL PROPERTIES: FLEXURAL STRENGTH AND ELASTIC MODULUS

8.1. General

Based on the extensive experimental test data from this research and the literature, analytical models are developed to predict the mechanical properties (flexural strength and elastic modulus) of CNT-cement nanocomposites (pastes and mortars). In Section 8.2, three critical relations affecting the mechanical properties are proposed. The proposed critical relations are then used to predict the mechanical properties and validate their applicability using a regression equation (see Section 8.3). In Section 8.4, the proposed critical relations are added to available theoretical models in the literature (see Section 2.6.2). The models are formulated using a probabilistic approach as discussed in Chapter 7 to reliably predict the mechanical properties of CNT-cement nanocomposites (Section 8.4). Then, the optimum ranges of variables are identified through computing the failure probability (Section 8.4.4). Finally, the effect of changes in different variables on the probability estimates is examined using sensitivity and importance analyses, guiding future researchers and engineers to design more efficiently (Section 8.4.5).

8.2. Critical Relations affecting the Mechanical Properties*

Because of the complex interactions between multiple experimental variables affecting the mechanical properties, theoretical models to include these interactions are not

* Section 8.2 and Section 8.3 are published in Cement and Concrete Composites
Ramezani, M., Kim, Y.H., and Sun, Z. "*Modeling the Mechanical Properties of Cementitious Materials containing CNTs.*" Cement and Concrete Composites 104 (2019):1-21

available in the literature. Therefore, an intuitive approach is adopted to find the relations between the experimental variables. This approach is widely used in mathematics such as Bayesian approach and other domains including, but not limited to, physics, biology, and psychology [228]. To capture the most important interactions, three analytical relations are proposed: 1) dispersion relation (η_D; Section 8.2.1), 2) matrix relation (η_M; Section 8.2.2), and 3) hydration age relation (η_H; Section 8.2.3).

8.2.1. Dispersion Relation (η_D)

Researchers tried to indirectly evaluate CNT dispersion by measuring the mechanical [16] or electrical [229, 230] properties. However, due to the complex dispersion procedure of CNTs using a surfactant-assisted ultrasonication procedure, analytical equations to quantify the degree of CNT dispersion is vaguely defined in the literature [174]. Therefore, this section focuses on the effects of AR, v_f, UE_T, UA, and *SP/CNTs* ratio to correlate CNT dispersion with the mechanical properties by proposing the dispersion relation (η_D).

8.2.1.1. Ultrasonication Energy Indicator (*UEI*)

As discussed in Section 4.10.2, *UA* governs the amount of energy delivered to the solution within a designated time (i.e., the intensity of ultrasonication energy). Besides, the intensity of ultrasonication energy which determines CNT dispersion quality was found to be depended on horn tip depth [231, 232]. To obtain a relationship between the intensity of ultrasonication energy (UE_m; energy delivered to the solution in a minute) and UA, 300 *ml* of a prepared suspension (i.e., water + SP + CNTs) was sonicated at different horn immersion depths of 1.5, 2.5, 3.5 and 5 *cm* (0.59, 0.98, 1.38, and 1.97 *in*.) and various *UA* ranging from 20% to 100%. Figure 8-1 (a) shows the relationship between *UA* (normalized

between 0 and 1) and UE_m (*J/ml/min*). As *UA* increased, the amount of UE_m increased. Also, it can be observed that the larger depth of the horn tip in the suspension resulted in higher UE_m. Based on the results, the relationship between *UA* and UE_m can be formulated as follows:

$$UE_m = 22.15 \times UA^{1.45} \tag{7-1}$$

To confirm this relationship, the predicted UE_m is compared with the reported UE_m in this research and the literature [1,2]. As shown in Figure 8-1 (b), the reported UE_m shows a good correlation with the predicted UE_m using Equation 7-1. The mean and median values of the ratio of predicted to reported UE_m are 1.11 and 1.07, respectively, with small variations (standard deviation (*SD*) of 0.08 and coefficient of variance (*COV*) of 0.07).

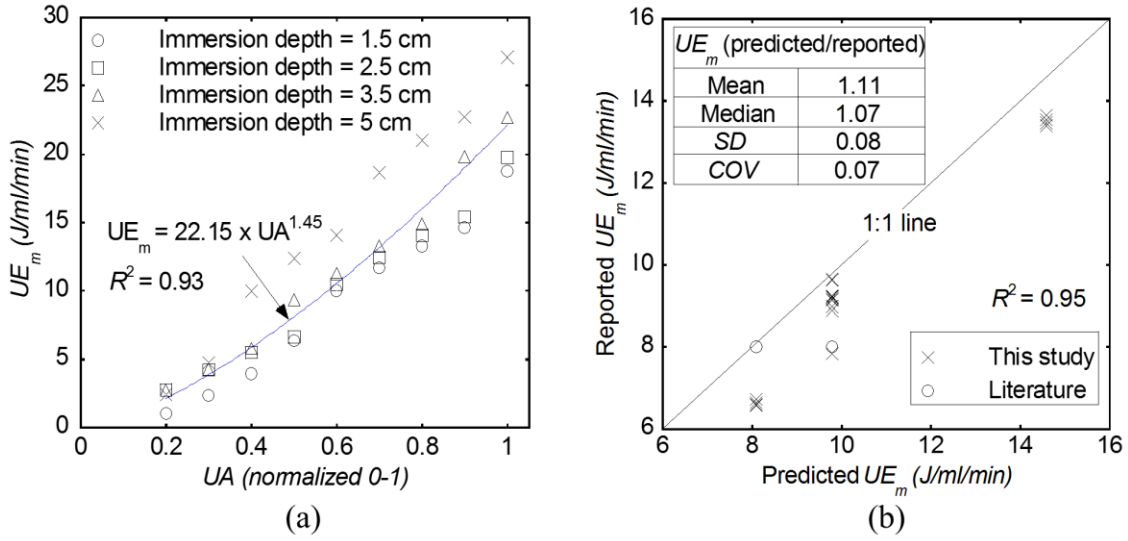

Figure 8-1. (a) Relationship between UE_m and *UA* (b) Predicted versus reported UE_m

The total amount of ultrasonication energy (UE_T) can therefore be obtained as follows, in which t_s is the duration of the ultrasonication process (*min.*).

$$UE_T = t_s \times UE_m \tag{7-2}$$

Nevertheless, as discussed in Section 6.3.2, the same UE_T does not yield the similar level of improvement in the mechanical properties. On the other side, as shown in Table 8-1, two different levels of UE_T (500 and 1500 *J/ml*) exhibited the similar relative mechanical properties (mechanical property of CNT reinforced cementitious material over the control): C_R (p-value = 0.06 > 0.05), F_R (p-value = 0.15 > 0.05), and E_R (p-value = 0.45 > 0.05).

Table 8-1. *UEI* and its Contribution to the Mechanical Properties

Test ID	UE_T *(j/ml)*	UE_m *(j/ml/min)*	*UA* (%)	C_R	F_R	E_R
II-500/75 (see Figure 8-2, ○)	500	13.7	75	1.17	1.16	1.15
II-1500/50 (see Figure 8-2, Δ)	1500	6.6	50	1.24	1.23	1.18

C_R: relative compressive strength, F_R: relative flexural strength, E_R: relative elastic modulus

Therefore, the Ultrasonication Energy Indicator (*UEI*) is proposed to quantify the effectiveness of the ultrasonication process related to the mechanical properties:

$$UEI = \left(\frac{UE_T}{UE_m}\right)^{UA} = (t_s)^{UA} \tag{7-3}$$

Figure 8-2 shows the relationship between *UEI* and UE_T at different *UA*. To achieve the same *UEI*, there are various options to determine the ultrasonication process. The same *UEI* (*y*-axis) can be attained by different combinations of UE_T and *UA*. For example, the experimental test results showed that using different combinations of $UE_T = 500$ *J/ml* with *UA* = 75% (see the circle in Figure 8-2) or $UE_T = 1500$ *J/ml* with *UA* = 50% (see the triangle in Figure 8-2) produced comparable *UEI* of around 15 and mechanical properties (see Table 8-1).

The mechanical properties increase as *UEI* increases up to its optimum value corresponding to different *UA*, beyond which mechanical properties do not exhibit further

improvement. Similar trends were also observed in [12, 176, 177]. However, Equation 7-3 has a limitation: *UEI* increases rapidly with higher *UA* (e.g., *UA* ≥ 70%). Therefore, special care should be taken when using this equation with high *UA*. Figure 8-3 (a) and (b) show the relationship between *UEI* and the values of F_R and E_R, respectively, obtained from the experimental test results in this research (see the circles in Figure 8-3; *UA* = 75%) and the literature (see the squares in Figure 8-3; *UA* = 100%) [12]. Based on these results, when using high *UA*, the practical limit of *UEI* = 15 is suggested, beyond which the mechanical properties do not exhibit further improvement. Note that a slightly lower *UEI* practical limit at *UA* = 100% [12] might be attributed to utilizing lower CNT concentration (κ = 0.075 *c-wt*%).

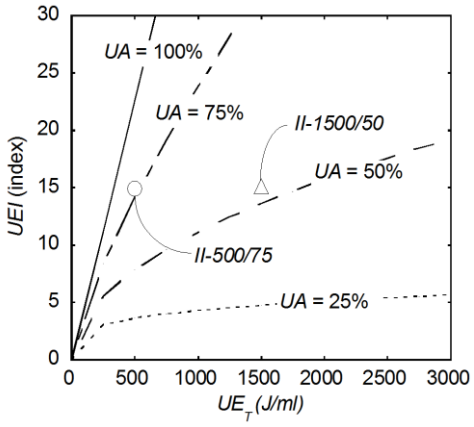

Figure 8-2. Relationship between UE_T and *UEI* at different *UA*

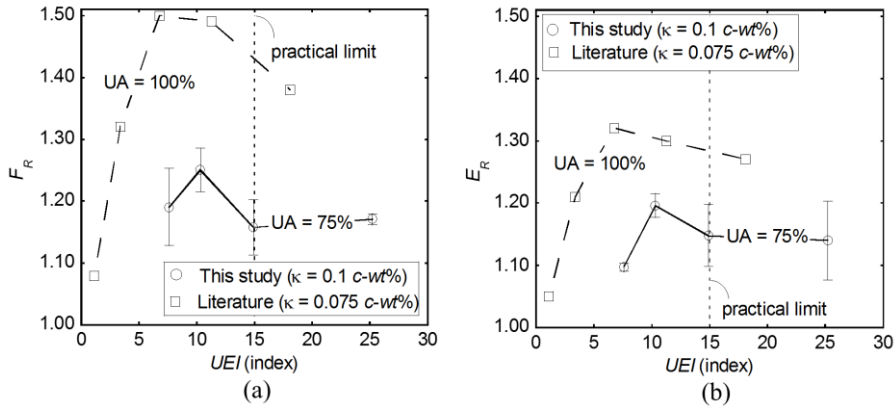

Figure 8-3. Relationship between: (a) *UEI* and F_R (b) *UEI* and E_R

8.2.1.2. Formulation of η_D

In the experimental part of this research (see Section 6.3.1), mechanical properties degraded beyond the threshold values of κ (or v_f) depending on *AR* (κ = 0.05 *c-wt*% for *AR* = 2500 and κ = 0.1 *c-wt*% for *AR* = 800). Generally, the higher v_f of CNTs with lower *AR* can be used to produce comparable mechanical properties as the lower v_f of CNTs with higher *AR* does [16, 23, 170].

Besides, as discussed in Section 6.3.3, as *UEI* increased (at constant *SP/CNTs* ratio), mechanical properties also increased. In addition, higher values of *SP/CNTs* ratio (at constant *UEI*) resulted in higher mechanical properties. Meanwhile, to achieve comparable mechanical properties, it was feasible to adjust *UEI* and *SP/CNTs* ratio, simultaneously (see Section 6.3.3). The increase in mechanical properties by increasing in *UEI* or *SP/CNTs* ratio might be related to a better dispersion quality of CNTs. However, beyond certain values of these variables, the higher values of *UEI* and/or *SP/CNTs* ratio does not lead to a better dispersion quality [16, 176].

Based on these findings and to correlate the degree of CNT dispersion using an ultrasonication procedure with the mechanical properties, the dispersion relation (η_D) which considers the correlations between *AR,* v_{f-w} (CNT volume fraction in aqueous solution), *UEI,* and *SP/CNTs* ratio is proposed as follows:

$$\eta_D = \left[1 - \left(\frac{AR \times v_{f-w}}{UEI \times ({}^{SP}/_{CNTs})}\right)\right] \tag{7-4}$$

Figure 8-4 (a) shows the contributions of *AR* and v_{f-w} to η_D, when using fixed values of *UEI* = 10 and *SP/CNTs* = 2. The maximum value of η_D is 1 (i.e., perfect

dispersion quality). As *AR* and/or v_{f-w} increases, η_D gets smaller (i.e., poor dispersion quality). Figure 8-4 (b) shows the contributions of *UEI* and *SP/CNTs* ratio to η_D, when using fixed values of *AR* = 800 and v_{f-w} = 0.001. As *UEI* and/or *SP/CNTs* ratio increases, η_D approaches to the unity ($\eta_D = 1$). However, beyond certain values of UEI and/or *SP/CNTs* ratio, η_D reaches a plateau. Therefore, optimization of these variables is important. For example, concerning *SP/CNTs* ratio, if too less is used, the solid particles may flocculate and agglomerate; and if too much is used, the cement paste may start to bleed to lose the material integrity.

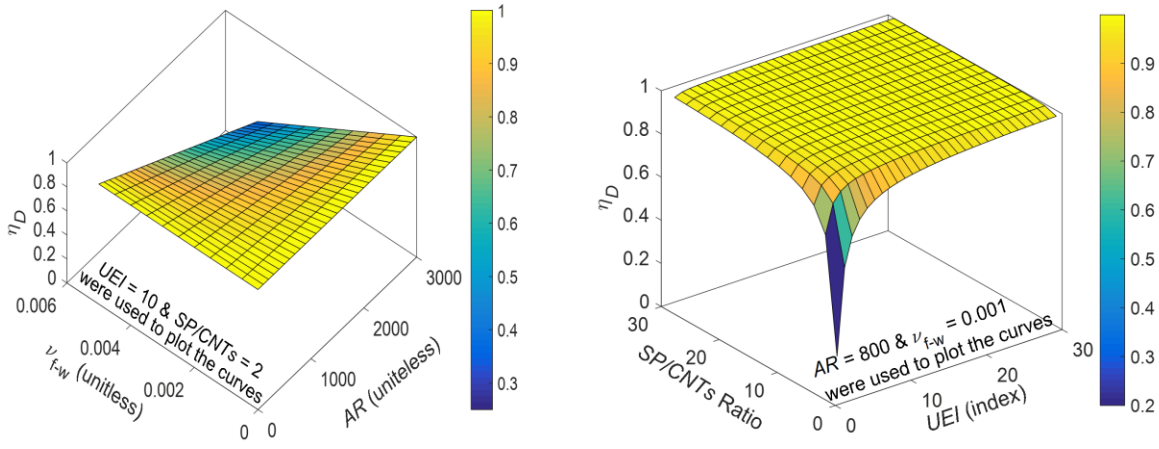

(a) (b)

Figure 8-4. Influence of (a) *AR* and v_{f-w} on η_D (b) *UEI* and *SP/CNTs* ratio on η_D

8.2.2. Matrix Relation (η_M)

To consider the effects of *w/c* and *s/c* ratios on mechanical properties, the matrix relation (η_M) is proposed as follows:

$$\eta_M = \frac{(1 + {}^{s}/_{c})}{({}^{w}/_{c})} \tag{7-5}$$

The effect of *w/c* and *s/c* ratios on the value of η_M is presented in Figure 8-5. When using a constant *w/c* ratio, higher *s/c* ratio results in the increase in the value of η_M. Also, when using a constant *s/c* ratio, the lower *w/c* ratio leads to an increase in the value of η_M. This is in a good agreement with the mechanical properties experimetal test results (see Section 6.3.4).

Note that mechanical properties are also dependent on the grading characteristics of particles and packing density. However, this is not the primary interest of this study. The developed model is examined and seems to be valid regardless of the solid particle characteristics and packing density for *w/c* ratio ranges between 0.3 and 0.6 and *s/c* ratio ranges between 0 and 3.

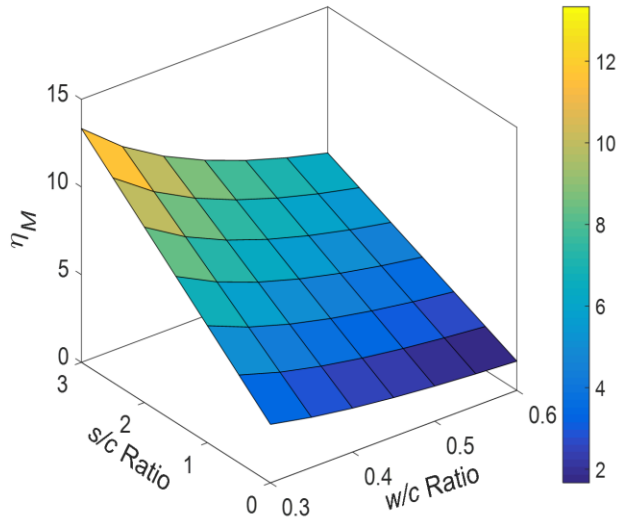

Figure 8-5. Influence of *w/c* and *s/c* ratios on η_M

8.2.3. Hydration Age Relation (η_H)

According to the ACI committee 209.2R-08 [233], "Guide for Modeling and Calculating Shrinkage and Creep in Hardened Concrete," the time-strength relationship of the moist cured concrete made with normal Portland cement can be estimated as follows:

$$f_{CS}(t) = f_{CS28}\left(\frac{t}{4 + 0.85t}\right) \tag{7-6}$$

where $f_{CS}(t)$ is the compressive strength at age t (days), f_{CS28} is the 28-day compressive strength, and t is the time in days.

In this research, to account for the influence of κ and *t* on mechanical properties of CNT-cement nanocomposites, the hydration age relation (η_H) is proposed as follows:

$$\eta_H = \left(\frac{t}{4 + 0.85t}\right)^{\kappa} \tag{7-7}$$

Figure 8-6 shows the influences of *t* and κ on η_H. At low concentrations ($\kappa \leq 0.1$ *c-wt%*), the effect of hydration age (*t*) is minimal. However, as κ increases, the effect of *t* on η_H becomes more pronounced and η_H reaches a plateau at later ages. This shows good agreement with the experimental test results in the literature [31, 116, 174] and this research (see Section 6.3.5).

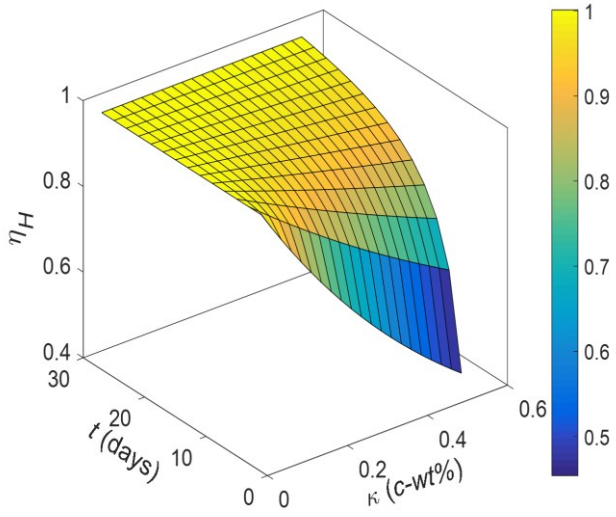

Figure 8-6. Influence of κ and *t* on η_H

8.3. Regression Model*

To investigate the influence of the proposed critical relations on mechanical properties of CNT-cement nanocomposites (pastes and mortars), a simple equation is used as shown below:

$$P_c = \eta_D{}^X \eta_H{}^Y \eta_M{}^Z P_m \quad (7\text{-}8)$$

where P_c is the mechanical properties of CNT-cement nanocomposites (flexural strength; f_{FS-c} (herein, σ_c) or elastic modulus; E_{F-c} (herein, E_c)), P_m is the mechanical properties of control specimens (flexural strength; f_{FS-m} (herein, σ_m) or elastic modulus; E_{F-m} (herein, E_m)), and X, Y, Z are unknown model parameters to fit the data. The unknown model parameters were obtained using the maximum likelihood parameter estimation function. Table 8-2 lists the mean, standard deviation (*SD*), and coefficient of variance (*COV*) of the calibrated unknown model parameters based on the experimental test data from this study and the literature [11, 12, 16, 28, 30, 31, 111, 112] for both σ_c and E_c.

Table 8-2. Unknown Model Parameters for σ_c and E_c

Unknown model parameters	Flexural strength (σ_c)			Elastic modulus (E_c)		
	Mean	*SD*	*COV*	Mean	*SD*	*COV*
X	4.91	1.68	0.34	6.32	2.30	0.36
Y	0.59	0.29	0.50	0.43	0.37	0.87
Z	0.20	0.01	0.07	0.22	0.02	0.10

SD: standard deviation, *COV*: coefficient of variance

The comparison between the predicted and experimental σ_c and E_c is shown in Figure 8-7 (a) and (b), respectively. The 1:1 lines (dashed lines in Figure 8-7) indicate that the predicted value of mechanical properties is identical to its experimental value. Using

* Section 8.2 and Section 8.3 are published in Cement and Concrete Composites
Ramezani, M., Kim, Y.H., and Sun, Z. "*Modeling the Mechanical Properties of Cementitious Materials containing CNTs*." Cement and Concrete Composites 104 (2019): 1-21

the estimated unknown model parameters shown in Table 8-2, the predicted σ_c (see Figure 8-7 (a)) and E_c (see Figure 8-7 (b)) show desirable accuracy within the solid lines (±20% error). Also, the mean and median values of the predicted to the experimental mechanical properties are close to 1.00 with small variations (COV = 0.14 for σ_c and 0.17 for E_c), indicating a good performance of the proposed model.

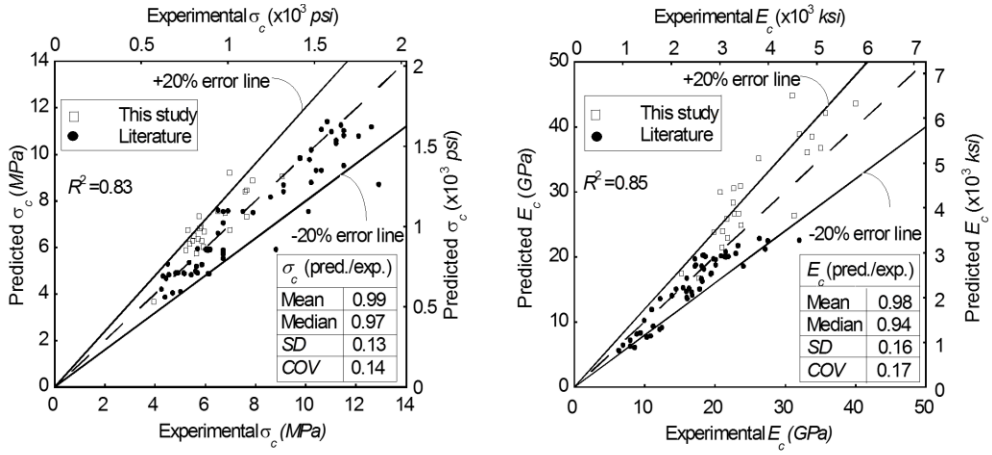

(a) (b)

Figure 8-7. Experimental vs. predicted mechanical properties: (a) σ_c (b) E_c

8.3.1. Applicability of the Proposed Critical Relations

To validate the applicability of the proposed critical relations, the corrected relations (η_D^X, η_H^Y, and η_M^Z) are further analyzed by comparing the estimated with measured values. The estimated value is obtained by plugging in the value of experimental variables in corresponding equations. For example, the estimated value of ${\eta_M}^Z$ is calculated using $\eta_M^Z = \left[\frac{1+s/c}{w/c}\right]^Z$. The measured value is back calculated using Equation 7-8 and experimental test results (${\sigma_c}^{exp.}$ or ${E_c}^{exp.}$), assuming that η_D^X, η_H^Y, and η_M^Z are not correlated. For example, the measured value of ${\eta_M}^Z$ can be expressed as $\eta_M^Z = \frac{{\sigma_c}^{exp.}}{\sigma_m \times \eta_D^X \times \eta_H^Y}$ in which estimated values of η_D^X and η_H^Y are used (see Table A-2 in the Appendix).

To visualize the influences of variables on the response (η_D^X, η_H^Y, and η_M^Z), each critical relation is plotted as a function of a main variable and its interaction with another variable (two ranges are used as shown in Table 8-3); Range 1 (*R1*) and Range 2 (*R2*) for experimental variable below and above the mean value, respectively.

Table 8-3. Ranges used for each Critical Relation

Critical relation (*y*-axis)	Main variable (*x*-axis)	Range (based on mean values of data)	
		*R*1	*R*2
η_D^X	*AR*	$v_f \leq 0.0012$	$v_f > 0.0012$
η_D^X	*UEI*	*SP/CNTs* ≤ 6	*SP/CNTs* > 6
η_H^Y	*t*	$\kappa \leq 0.11$	$\kappa > 0.11$
η_M^Z	*s/c ratio*	*w/c* ≤ 0.43	*w/c* > 0.43

Figure 8-8 through Figure 8-10 demonstrate the influences of the main variables (*x*-axis) on the critical relations (*y*-axis; η_D^X, η_H^Y, and η_M^Z) for both σ_c and E_c . Each plot describes how the response (*y*-axis) varies as a function of two variables. The solid lines in each plot represent the estimated values of ηs. To plot the solid lines, the mean value of other variables is used except for the main variable (*x*-axis). Also, the dashed lines represent ±*SD* of the model error. The open circles are the measured values of ηs. Figure 8-8 (a) and (b) show the influence of changes in *AR* and its interaction with another independent variable (v_{f-w}) on η_D^X for σ_c and E_c, respectively. Figure 8-8 (c) and (d) show the influence of *UEI* and *SP/CNTs* ratio on η_D^X for σ_c and E_c, respectively. Figure 8-9 (a) and (b) demonstrate the influence of *t* and its interaction with κ on η_H^Y for σ_c and E_c, respectively. And, Figure 8-10 (a) and (b) show the contribution of *s/c* ratio and its interaction with *w/c* ratio to η_M^Z for σ_c and E_c, respectively.

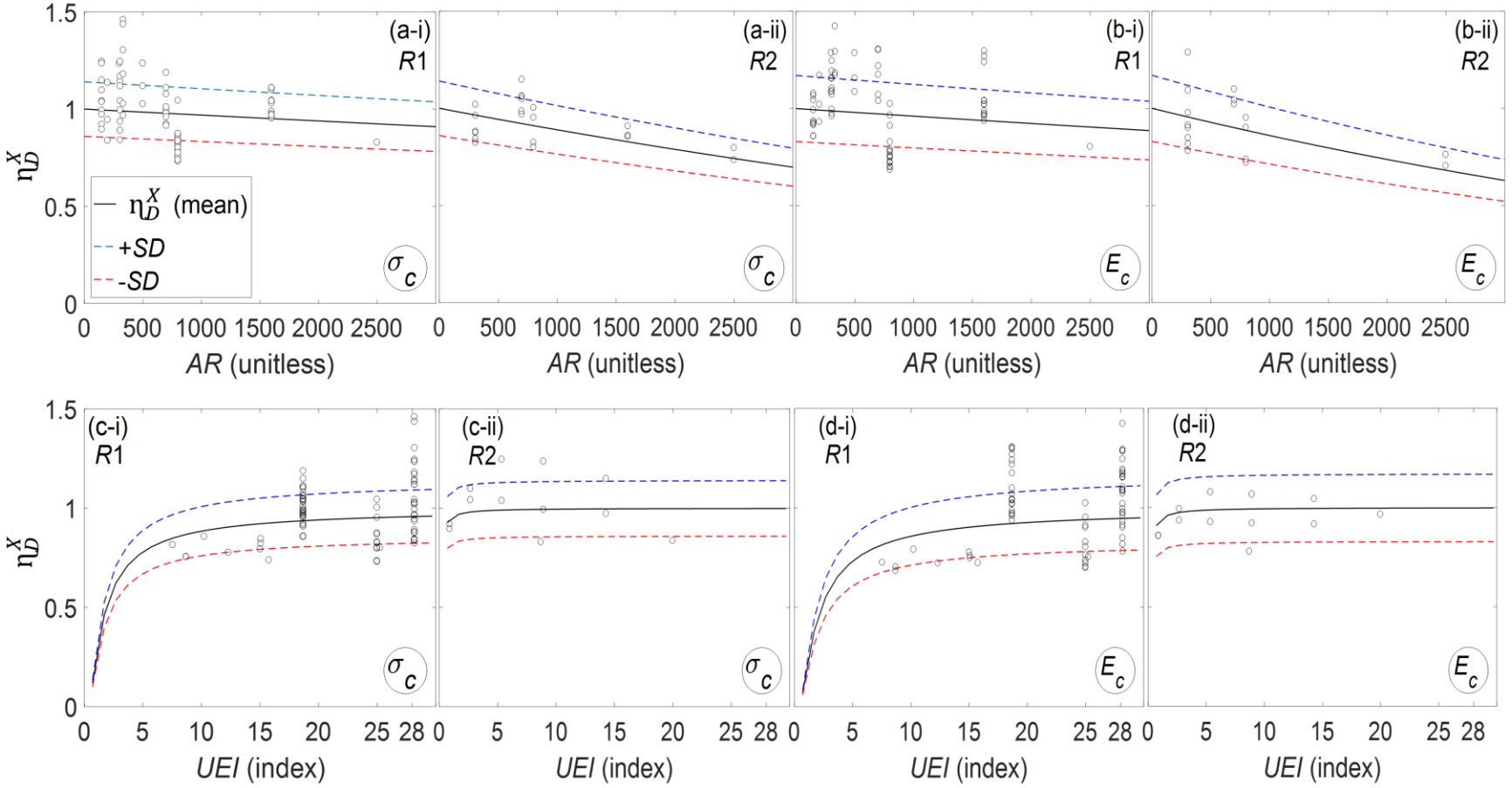

Figure 8-8. Estimated vs. measured η_D^X as a function of: (a) *AR* for σ_c (b) *AR* for E_c (c) *UEI* for σ_c (d) *UEI* for E_c

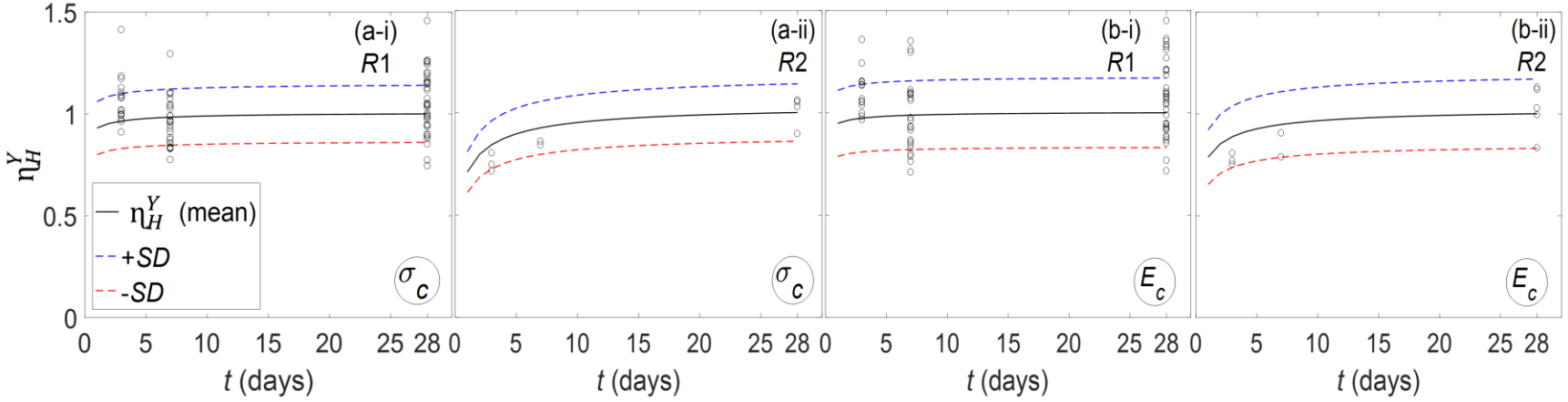

Figure 8-9. Estimated vs. measured η_H^Y as a function of *t*: (a) σ_c (b) E_c

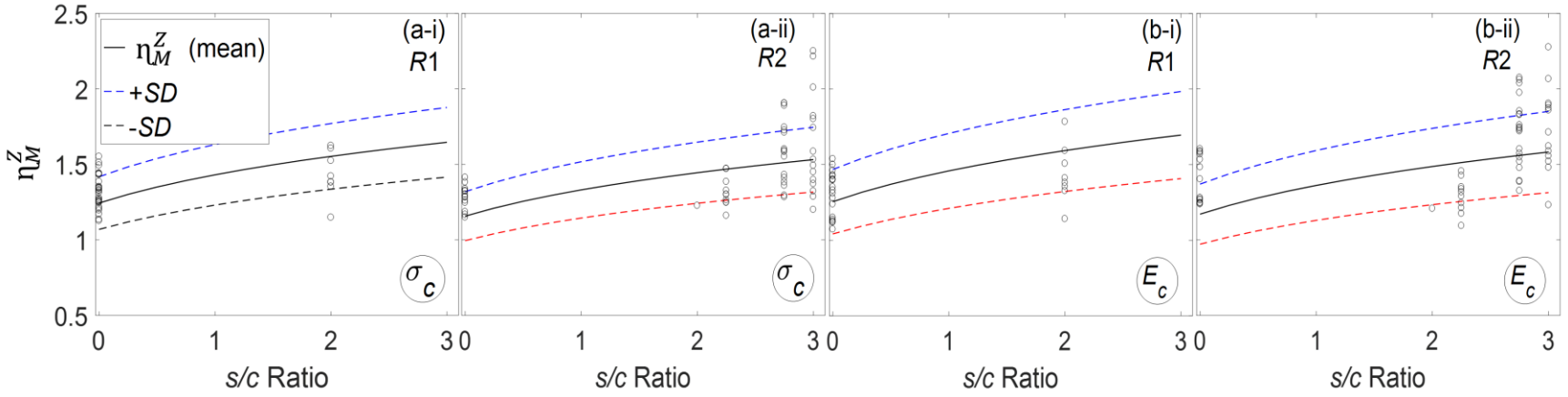

Figure 8-10. Estimated vs. measured η_M^Z as a function of *s/c* ratio: (a) σ_c (b) E_c

Figure 8-8 through Figure 8-10 exhibit that most of the measured ηs are within ±*SD* and they follow similar trends. For example, Comparing Figure 8-8 (b-*i*; for *R*1) with (b-*ii*; for *R*2), it is obvious that the influence of *AR* on the value of η_D^X becomes more pronounced as v_f increases. Note that those circles that fall outside the boundary (±*SD*) might be attributed to utilizing the mean values of other variables in the estimated ηs. This might explain the superior performance of data within *R*2 compared with *R*1, in which the mean values are closer to the actual values of most of the data. Table 8-4 shows the statistics of the ratio of the measured to the estimated ηs for each data point (the exact values). The mean and median values of the ratio of the measured to the estimated ηs for both σ_c and E_c are close to 1.00 with small variations (*COV* ranges between 0.08 and 0.17), indicating that the proposed critical relations exhibit good correlations between the measured and estimated values.

Table 8-4. Statistics of the Ratio of Measured to Estimated Corrected Critical Relations (Regression Model)

Critical relation	Main variable	Statistics	σ_c		E_c	
			*R*1	*R*2	*R*1	*R*2
η_D^X	*AR*	Mean	1.04	1.00	1.06	1.00
		Median	1.03	1.03	1.07	0.99
		Standard deviation	0.15	0.09	0.18	0.14
		Coefficient of variance	0.15	0.09	0.17	0.14
η_D^X	*UEI*	Mean	1.03	1.03	1.06	0.96
		Median	1.03	1.02	1.08	0.94
		Standard deviation	0.14	0.14	0.18	0.09
		Coefficient of variance	0.14	0.13	0.17	0.09
η_H^Y	*t*	Mean	1.04	0.95	1.06	0.95
		Median	1.04	0.92	1.07	0.92
		Standard deviation	0.15	0.07	0.17	0.11
		Coefficient of variance	0.14	0.08	0.16	0.12
η_M^Z	*s/c* ratio	Mean	1.03	1.04	1.00	1.07
		Median	1.03	1.03	1.01	1.07
		Standard deviation	0.11	0.16	0.12	0.19
		Coefficient of variance	0.10	0.16	0.12	0.17

Figure 8-11 shows contour plots of the corrected critical relations (η_D^X, η_H^Y, and η_M^Z) as a function of important variables for both σ_c (Figure 8-11 (a)) and E_c (Figure 8-11 (b)). Each contour plot describes how the response (η_D^X, η_H^Y, and η_M^Z; see the lines in contour plots) varies as a function of two variabless (*x* and *y* axes). For example, Figure 8-11 (a-*i*) and (b-*i*) show a quantitative visualization of the influences of changes in v_{f-w} (*x*-axis) and its interaction with *AR* (*y*-axis) on η_D^X for σ_c and E_c, respectively. Also, Figure 8-11 (a-*ii*) and (b-*ii*) quantify the effects of changes in κ (*x*-axis) and *t* (*y*-axis) on η_H^Y for σ_c and E_c, respectively. Besides, Figure 8-11 (a-*iii*) and (b-*iii*) show a quantification of η_M^Z as a function of *w/c* (*x*-axis) and *s/c* (*y*-axis) ratios for for σ_c and E_c, respectively.

The contour plots are a useful tool for designers and engineers to allocate resources for practical applications using proposed equations. For example, to achieve a 44% increase in 28-day flexural strength ($^{\sigma_c}/_{\sigma_m} = 1.44$), the product of $\eta_D^X \eta_M^Z$ = 1.44 could be used ($\eta_H^Y = 1$ for different κ at 28 days; see Figure 8-11 (a-*ii*) and (b-*ii*)). There are several options to achieve $\eta_D^X \eta_M^Z$ = 1.44 by various combinations of the critical relations; η_D^X and η_M^Z of either 0.93 and 1.55 or 0.96 and 1.50, respectively, could be used. Also, different combinations of the experimental variables might be used to achieve the same value for each of these critical relations. For example, incorporating CNTs with *AR* and v_{f-w} of either 1200 and 0.001 or 600 and 0.002, respectively, results in $\eta_D^X = 0.93$ (see the solid circles in Figure 8-11 (a-*i*)). Note that fixed values of *UEI* = 20 and *SP/CNTs* = 4 were used to plot η_D^X (see Figure 8-11 (a-*i*) and (b-*i*)).

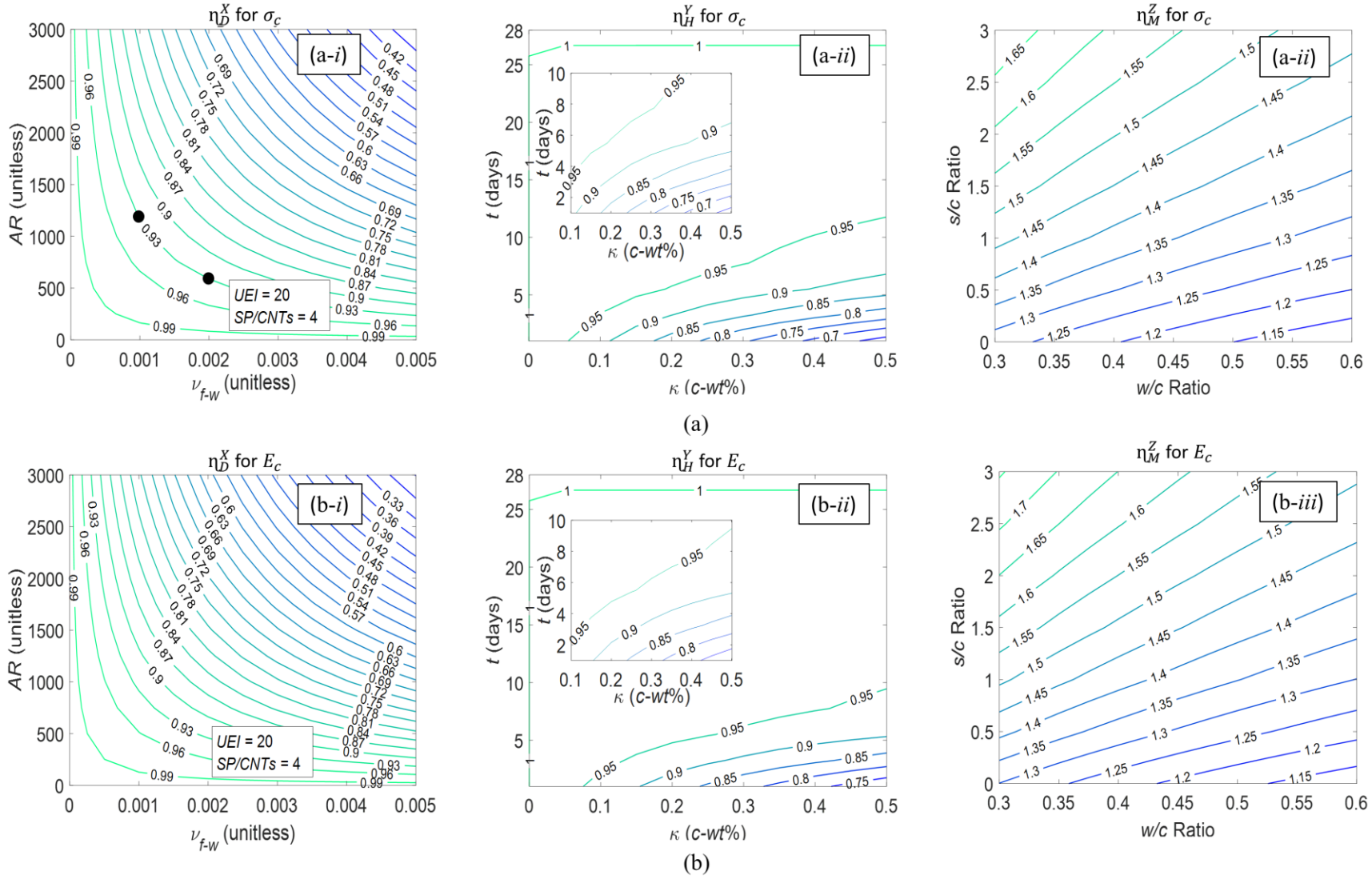

Figure 8-11. Corrected critical relations as a function of important variables for σ_c and E_c: (a) η_D^X (b) η_H^Y (c) η_M^Z

8.3.2. Limitations of the Regression Model

Although the regression model (Equation 7-8) exhibited an acceptable performance to predict the mechanical properties of the investigated data in Section 8.3 (see solid circles in Figure 8-12), it is unable to reliably predict the mechanical properties of new dataset (see open triangles in Figure 8-12). Therefore, the model is not robust.

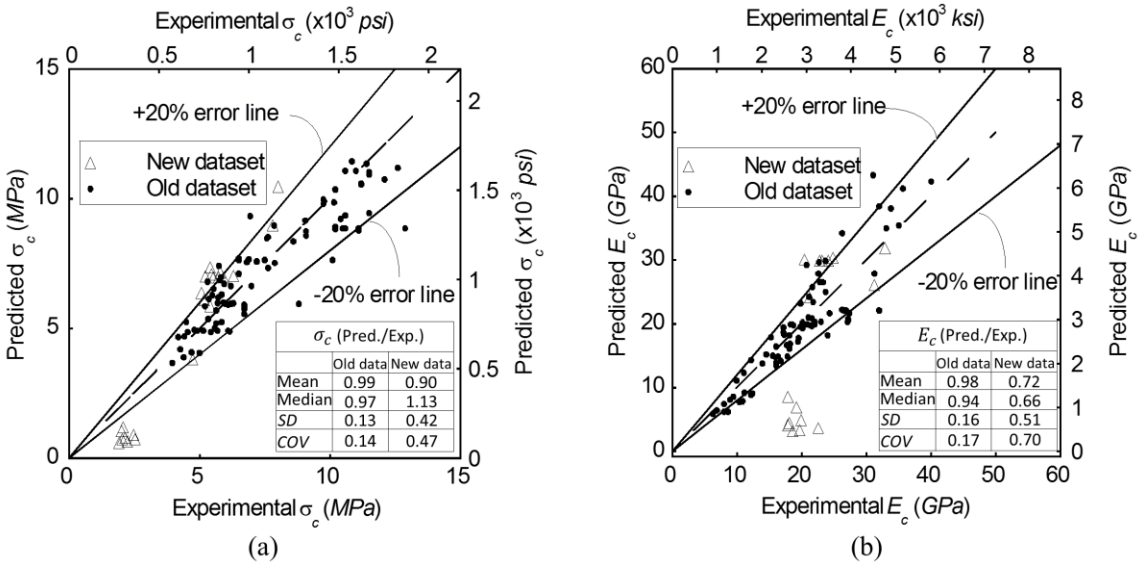

Figure 8-12. Performance of regression model after adding new dataset

Besides, the regression model cannot capture the mechanisms of CNTs affecting the mechanical properties. In real applications, mechanical properties increase as CNT aspect ratio and/or concentration (or volume fraction) increases up to certain thresholds, beyond which mechanical properties degrade due to the dispersion issues. However, when using the regression model, the predicted mechanical properties tend to be higher at lower *AR* and/or v_{f-w}. This could be explained by the fact that as *AR* and/or v_{f-w} decreases, the value of η_D becomes larger (see Figure 8-4 (a)).

To overcome these limitations, the proposed critical relations will be added to available theoretical models in the literature to predict the mechanical properties of CNT-

cement nanocomposites (see Section 8.4). In addition, as discussed in Chapter 7 (see Equation 6-1), the new models are formulated in a probabilistic manner (see Equations 7-9 and 7-10 for σ_c and E_c, respectively) to account for the high degree of uncertainty while incorporating CNTs, statistical uncertainty in estimation of the unknown model parameters, model error associated with inexact form of the model, and missing of the possible influential variables that might influence the mechanical properties [222, 234].

$$\sigma_c = \eta_D(x_D, \theta_D) \times \eta_H(x_H, \theta_H) \times \eta_M(x_M, \theta_M) \times \Big[1/6\tau_i(AR){v_{f-m}}^{2/3} + \sigma_m\big(1 - {v_{f-m}}^{2/3}\big)\Big] + \partial_1\varepsilon_1 \quad (7\text{-}9)$$

$$E_c = \eta_D(x_D, \theta_D) \times \eta_H(x_H, \theta_H) \times \eta_M(x_M, \theta_M) \times \frac{1 + \xi E_{f'} {v_{f-m}}^{\theta_8}}{1 - E_{f'} {v_{f-m}}^{\theta_8}} E_m + \partial_2\varepsilon_2 \quad (7\text{-}10)$$

where $\eta_D(x_D, \theta_D)$, $\eta_H(x_H, \theta_H)$, and $\eta_M(x_M, \theta_M)$ are dispersion relation, hydration age relation, and matrix relation, respectively, v_{f-m} is the volume fraction of CNTs within the cement matrix, and θ . Note that because v_{f-m} used in cementitious materials is very low (0.000038-0.001277; based on the database), the predicted elastic modulus of CNT-cement nanocomposites is almost the same as the matrix elastic modulus. Therefore, ${v_{f-m}}^{\theta_8}$ is used to fit the data. The final form of the proposed probabilistic models after adding the experimental variables and their corresponding unknown model parameters to predict σ_c (Equation 7-11) and E_c (Equation 7-12) are as follows:

$$\sigma_c = \left[1 - \left(\frac{AR^{\theta_1} \times {v_{f-w}}^{\theta_3}}{UEI^{\theta_2} \times \left({SP}/{CNTs}\right)^{\theta_4}}\right)\right] \times \left(\frac{t}{4 + 0.85t}\right)^{\kappa\theta_5} \times \frac{(1 + {S}/{C})^{\theta_6}}{({W}/{C})^{\theta_7}} \times \Big[1/6\tau_i(AR){v_{f-m}}^{2/3} + \sigma_m\big(1 - {v_{f-m}}^{2/3}\big)\Big] + \partial_1\varepsilon_1 \quad (7\text{-}11)$$

$$E_c = \left[1 - \left(\frac{AR^{\theta_9} \times {v_{f-w}}^{\theta_{11}}}{UEI^{\theta_{10}} \times \left({SP}/{CNTs}\right)^{\theta_{12}}}\right)\right] \times \left(\frac{t}{4 + 0.85t}\right)^{\kappa\theta_{13}} \times \frac{(1 + {s}/{c})^{\theta_{14}}}{({w}/{c})^{\theta_{15}}} \quad (7\text{-}12)$$

$$\times \frac{1 + \xi E_{f'} {v_{f-m}}^{\theta_8}}{1 - E_{f'} {v_{f-m}}^{\theta_8}} E_m + \partial_2 \varepsilon_2$$

8.4. Probabilistic Models

This section first presents the database used to develop the probabilistic models (Section 8.4.1). The performance of the probabilistic models are assessed against extensive experimental test data from both the literature and this research program (Section 8.4.2). In Section 8.4.3, the performance of various models containing different subsets of the proposed critical relations are assessed to select the best model by taking both model accuracy and complexity into account. Then, the best model is used to optimize the experimental variables to maximize the mechanical properties through computing the conditional probability of not meeting a specified design requirement (Section 8.4.4). Finally, the effect of changes in the experimental variables on the probability estimates are determined by performing sensitivity and importance analysis (Section 8.4.5).

8.4.1. Database for Constructing Probabilistic Models

A total of 105 data was collected from several literature [11, 12, 16, 28-30, 111-113, 142] and this research study to calibrate the unknown model parameters in Equations 7-11 and 7-12 using a Bayesian methodology.

To evaluate the robustness of the models, the total database was not used for the development of the probabilistic models due to two fundamental issues: overfitting and being overly optimistic on model error [235]. Therefore, the database was split into two sets of data using random selection for both σ_c and E_c; 80% of the data (84 data points)

was used to develop the models (Dataset I) and the remaining 20% (21 data points) was used to validate the proposed probabilistic models (Dataset II). Table 8-5 and Table 8-6 show the statistics of different variables used to develop the probabilistic models (Dataset I) for σ_c and E_c, respectively. Note that the average values of CNT length, diameter, and aspect ratio were used in the probabilistic models.

Table 8-5. Range of Variables to Develop Probabilistic Model using Dataset I for σ_c

Variables	Minimum	Maximum	Mean	Median	Standard deviation
κ (*c-wt%*)	0.0125	0.5	0.1033	0.09	0.0987
L (μm)	1.5	55	21.7	20	13.45
d (nm)	8	32.5	25.29	27.5	7.58
AR (unitless)	157.89	2500	902.83	800	622.28
SP/CNTs	1.32	24	6.4	4	5.26
w/c	0.3	0.6	0.426	0.45	0.0748
s/c	0	3	1.527	2.25	1.235
t (days)	3	28	14.643	7	11.18
$\sigma_m(MPa)$	1.94	9.3	5.36	4.88	1.91
UE_t (*J/ml*)	25	2800	1703.65	2612.5	1208.2
UE_m (*J/ml/min*)	3.95	28	9.21	8	5.998
UA (%)	30	100	55.63	50	15.63

Table 8-6. Range of Variables to Develop Probabilistic Model using Dataset I for E_c

Variables	Minimum	Maximum	Mean	Median	Standard deviation
κ (*c-wt%*)	0.0125	0.5	0.1164	0.1	0.1079
L (μm)	1.5	55	20.48	20	12.54
d (nm)	8	32.5	26.86	30	6.72
AR (unitless)	157.89	2500	791.02	670.83	536.49
SP/CNTs	1.32	24	5.78	4	4.57
w/c	0.3	0.6	0.445	0.485	0.0667
s/c	0	3	1.844	2.25	1.18
t (days)	3	28	15.44	7	11.24
$E_m(GPa)$	5.8	27.81	15.24	14.33	5.45
UE_t (*J/ml*)	25	2800	1991.85	2800	1119.32
UE_m (*J/ml/min*)	3.95	28	9.26	8	5.15
UA (%)	30	100	56.44	57	13.78

8.4.2. Probabilistic Models Assessment

Table 8-7 and Table 8-8 show the posterior statistics of **Θ** estimated using Dataset I for σ_c and E_c, respectively. Also, Figure 8-13 (a) and (b) show the performance of the probabilistic models for σ_c and E_c, respectively, versus the experimental test data. The solid circles are the data used to develop the model (Dataset I) and the open triangles are the data used to validate the model (Dataset II). The robustness of the proposed probabilistic model was validated using Dataset II which was not used for model development, indicating the accuracy of the proposed probabilistic model by showing desirable performance (i.e., within ± standard deviation of the error term in the proposed model; ∂_1 = 15% and $\partial_2 = 18\%$ for σ_c and E_c, respectively). Note that three data points inscribed within the oval in Figure 8-13 are related to the flexural strength of cement mortar reinforced with mechanical functionalized CNTs at different ages (3, 7, and 28 days). The mechanical functionalized CNTs provided superior bond properties [28], resulted in under-prediction of the flexural strength.

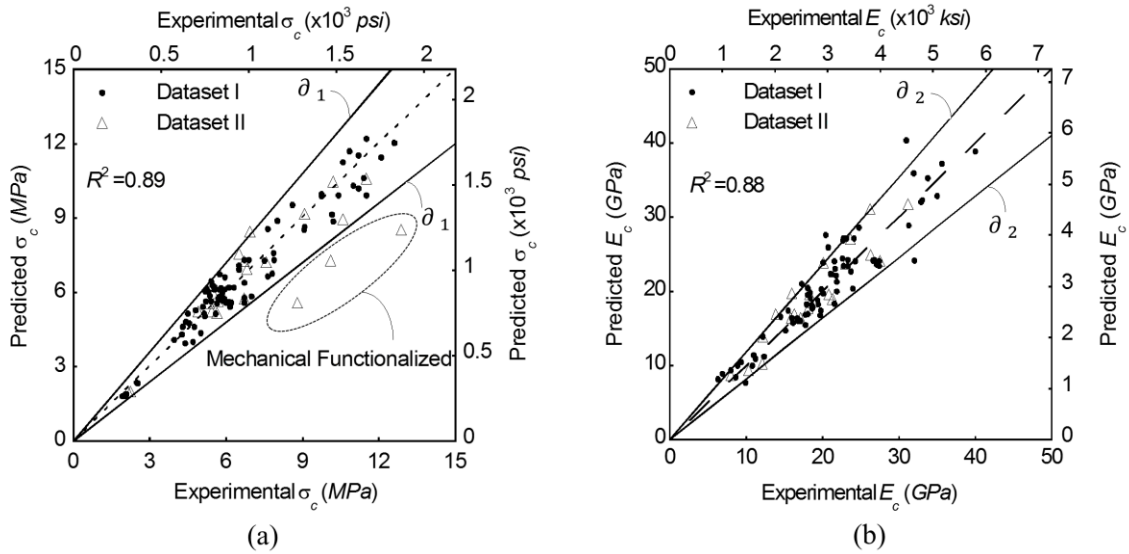

Figure 8-13. Predicted value of mechanical properties versus experimental test results: (a) σ_c (b) E_c

Note: Dataset I was used for model development and Dataset II was used for model validation

Table 8-7. Posterior Statistics of the Unknown Model Parameters using Dataset I for σ_c

Unknown parameter	Mean	Standard deviation	Correlation matrix							
			θ_1	θ_2	θ_3	θ_4	θ_5	θ_6	θ_7	∂_1
θ_1	0.3925	0.0280	1	-0.5390	0.9981	0.9495	0.8606	-0.5683	-0.9771	0.6282
θ_2	0.2798	0.0086		1	-0.5713	-0.6965	-0.6583	-0.0396	0.6082	-0.4281
θ_3	0.4806	0.0299			1	0.9483	0.8541	-0.5671	-0.9786	0.6275
θ_4	0.1317	0.0369				1	0.9458	-0.3876	-0.9627	0.6753
θ_5	1.0589	0.0575					1	-0.2129	-0.8844	0.5981
θ_6	0.1730	0.0046						1	0.4226	-0.5294
θ_7	0.1269	0.0146							1	-0.6007
∂_1	0.1491	0.0008								1

Table 8-8. Posterior Statistics of the Unknown Model Parameters using Dataset I for E_c

Unknown parameter	Mean	Standard deviation	Correlation matrix								
			θ_8	θ_9	θ_{10}	θ_{11}	θ_{12}	θ_{13}	θ_{14}	θ_{15}	∂_2
θ_8	0.2912	0.0230	1	0.6634	0.6766	0.8013	0.0488	-0.3253	-0.5609	-0.3456	0.0676
θ_9	0.0249	0.0089		1	0.6663	0.9061	-0.0037	-0.2431	-0.5304	-0.2254	0.0735
θ_{10}	0.0257	0.0094			1	0.6288	-0.0826	0.0248	-0.5707	-0.3499	0.1259
θ_{11}	0.0502	0.0112				1	0.0246	-0.2923	-0.6398	-0.4807	0.0755
θ_{12}	0.0166	0.0114					1	-0.0709	-0.1251	-0.4773	-0.0311
θ_{13}	2.5572	0.3296						1	0.2247	0.0285	0.0286
θ_{14}	0.4624	0.0341							1	0.3828	-0.0304
θ_{15}	0.8091	0.1121								1	-0.0629
∂_2	0.1803	0.0149									1

Also, Figure 8-14 through Figure 8-16 are plotted to validate the applicability of $\eta_D\ (x_D, \theta_D)$, $\eta_H\ (x_H, \theta_H)$, and $\eta_M\ (x_M, \theta_M)$, respectively, for both σ_c and E_c. Each critical relation was plotted as a function of a main variable and its interaction with another independent variable in two different ranges: $R1$ and $R2$ (see Table 8-3). The solid lines represent the estimated critical relations. The dashed lines represent the standard deviations of the model errors ($\pm\partial$), and the open circles represent the measured values of the critical relations, as described in Section 8.3.1.

Comparing Figure 8-14 through Figure 8-16 with those of the regression model (Figure 8-8 through Figure 8-10), it can be seen that more measured data (see open circles) fall within $\pm\partial$. This indicates that the proposed critical relations outperform in the probabilistic models than regression model. In Figure 8-16 (a-*ii*), three data points that fell outside the boundary are related to utilizing mechanical functionalized CNTs (see the inscribed data in the oval in Figure 8-13). The superior performance of the critical relations in probabilistic models can also be statistically confirmed by showing that the mean and median values of the ratio between the measured and the estimated critical relations are closer to the unity for the probabilistic models (see Table 8-9) compared with the regression model (see Table 8-4).

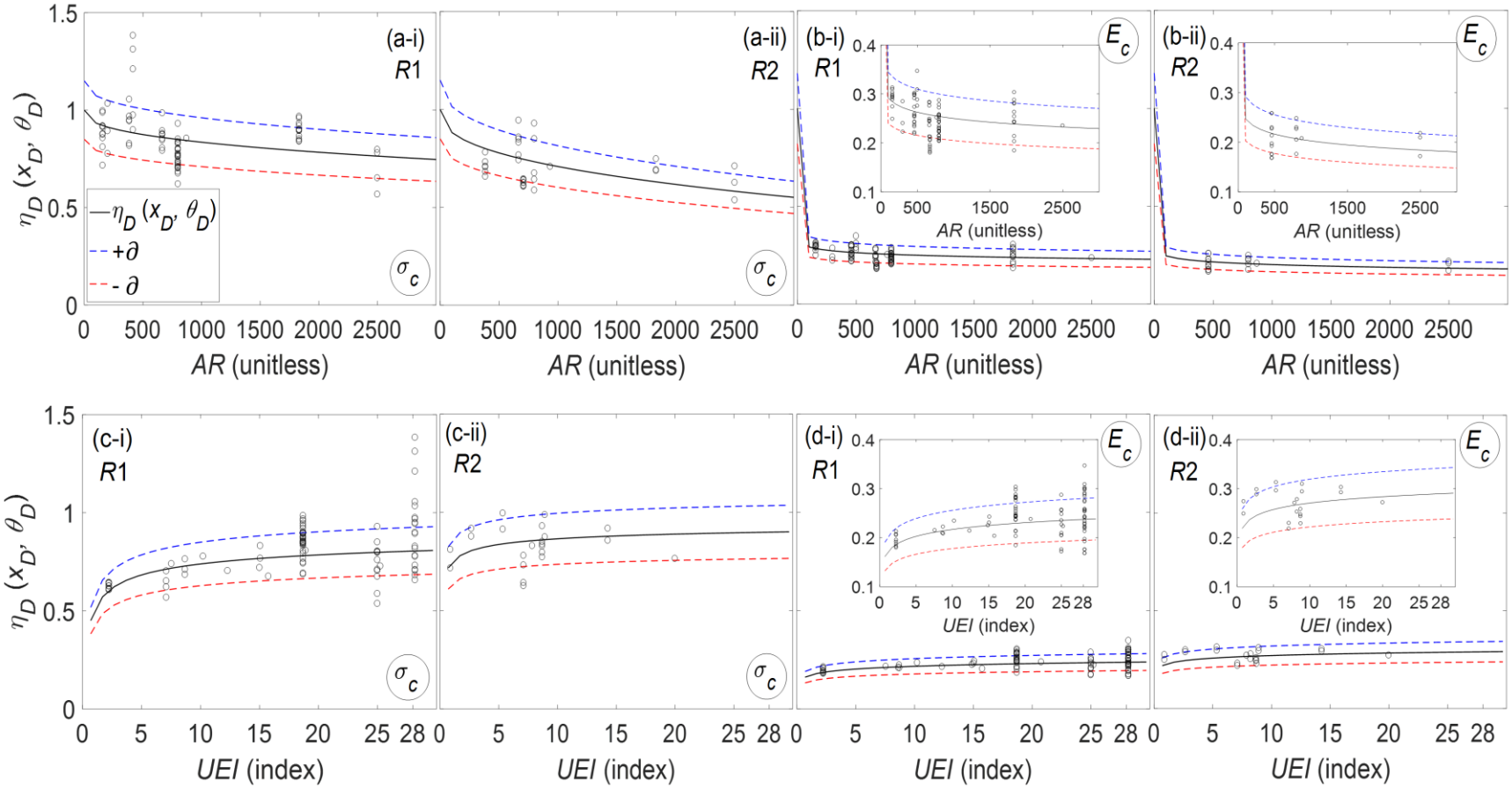

Figure 8-14. Estimated vs. measured $\eta_D(x_D, \theta_D)$ as a function of: (a) *AR* for σ_c (b) *AR* for E_c (c) *UEI* for σ_c (d) *UEI* for E_c

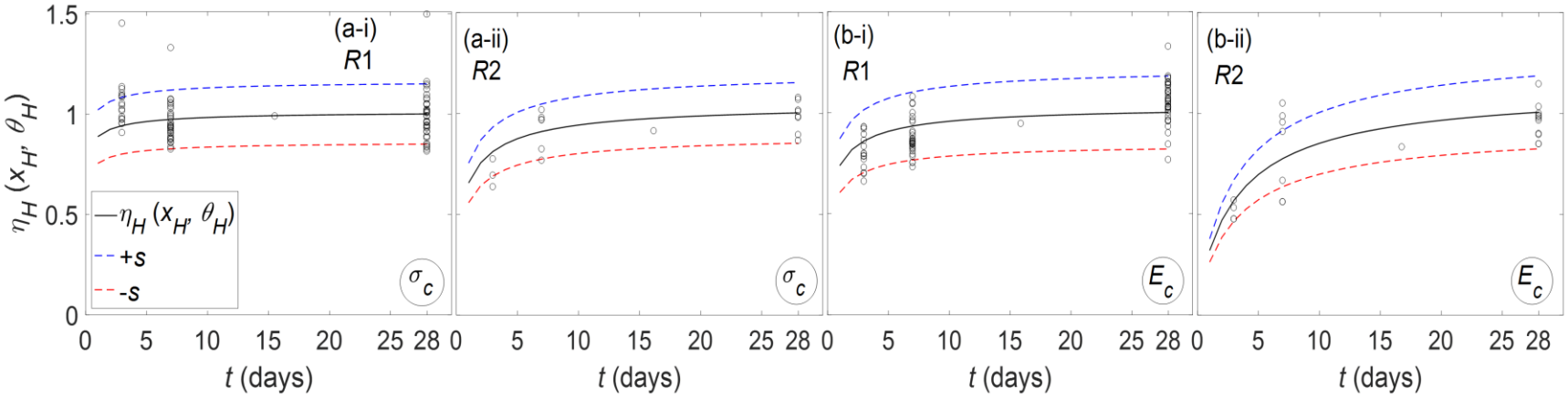

Figure 8-15. Estimated vs. measured η_H (x_H, θ_H) as a function of t: (a) σ_c (b) E_c

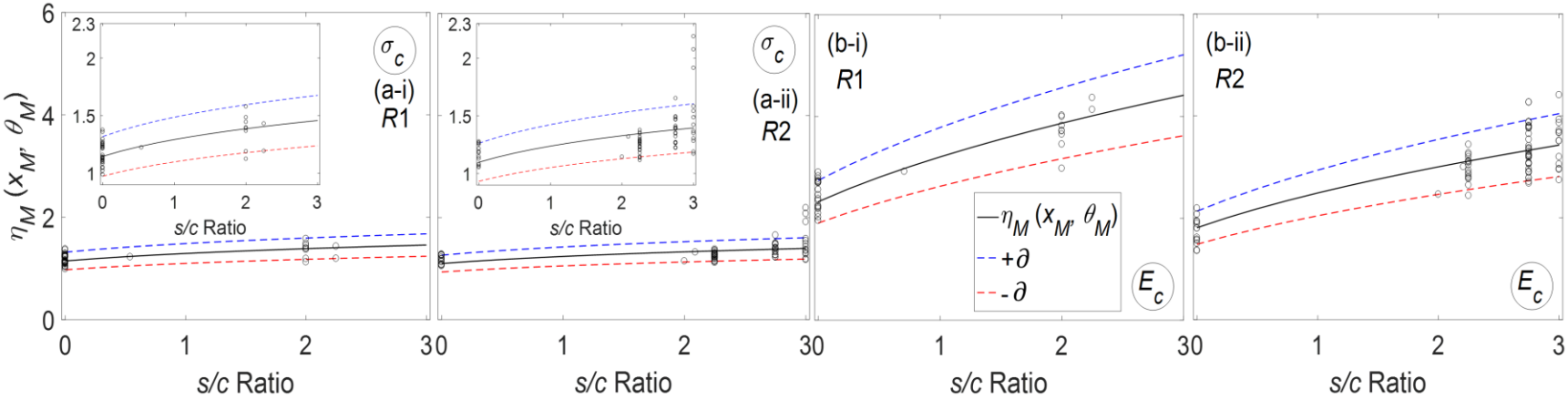

Figure 8-16. Estimated vs. measured η_M (x_M, θ_M) as a function of *s/c* ratio: (a) σ_c (b) E_c

Table 8-9. Statistics of the Ratio of Measured to Estimated Corrected Critical Relations (Probabilistic Models)

Critical relation	Main variable	Statistics	σ_c		E_c	
			*R*1	*R*2	*R*1	*R*2
$\eta_D(x_D, \theta_D)$	*AR*	Mean	1.01	1.00	1.00	0.98
		Median	0.99	1.01	1.01	0.96
		Standard deviation	0.14	0.07	0.12	0.13
		Coefficient of variance	0.14	0.07	0.12	0.13
$\eta_D(x_D, \theta_D)$	*UEI*	Mean	1.02	0.95	0.99	0.99
		Median	1.01	0.94	0.98	1.03
		Standard deviation	0.13	0.08	0.12	0.12
		Coefficient of variance	0.13	0.08	0.12	0.12
$\eta_H(x_H, \theta_H)$	*t*	Mean	1.01	0.98	0.99	1.00
		Median	0.99	0.99	1.00	0.98
		Standard deviation	0.13	0.07	0.12	0.13
		Coefficient of variance	0.13	0.07	0.12	0.13
$\eta_M(x_M, \theta_M)$	*s/c* ratio	Mean	1.01	1.00	1.02	0.98
		Median	1.01	0.98	1.03	0.97
		Standard deviation	0.09	0.14	0.08	0.13
		Coefficient of variance	0.09	0.14	0.08	0.13

8.4.3. Model Selection Criteria

The most complicated model with the highest accuracy is not always the best model. Generally, it is accepted that there is a single correct model (or at least the best model) that tradeoffs between goodness of fit and parsimony (i.e., preserves the model accuracy while using less variables). In this regard, the two most commonly used penalized likelihood information criteria, Akaike Information Criterion (*AIC*) and Bayesian Information Criterion (*BIC*), were used to take both model accuracy and parsimony into account. The *AIC* and *BIC* can be determined as follows:

$$AIC = -2\ log\ L(\boldsymbol{\Theta}) + 2N_p \tag{7-13}$$

$$BIC = -2\ log\ L(\boldsymbol{\Theta}) + N_p log N_s \tag{7-14}$$

where $log\ L(\boldsymbol{\Theta})$ is a measure of model fit, N_p is the number of unknown model parameters included in $\boldsymbol{\Theta}$, and N_s is the number of samples.

The best model is selected from a set of candidate models containing different subsets of the critical relations as listed in Table 8-10 (for σ_c) and Table 8-11 (for E_c). For example, model III has only the critical relation of η_D with the unity of η_M and η_H (i.e., $\eta_M = \eta_H = 1$). The best model is the one that neither under-fits nor over-fits (i.e., the model with the smallest approximated values of *AIC* and *BIC*). As seen in Table 8-10 and Table 8-11, Both *AIC* and *BIC* estimated values are smallest for model IX compared with other competing models, indicating that including all critical relations is best to accurately predict the mechanical properties.

Table 8-10. Model Selection Criteria using Dataset I for σ_c

Model		N_p	Information criteria			R-squared
#	Critical relations		*AIC*	*BIC*	Δ*AIC*	
I (Equation 2-5)	Deterministic	0	-18.73	-18.73	25.02	0.79
II (Equation 7-8)	Regression	3	-13.33	-13.27	30.42	0.83
III	η_D	4	-8.014	-8.317	31.40	0.84
IV	η_M	2	-11.15	-11.30	28.26	0.86
V	η_H	1	-17.58	-17.66	21.83	0.87
VI	$\eta_D \times \eta_M$	6	-6.434	-6.889	32.98	0.86
VII	$\eta_D \times \eta_H$	5	-11.80	-12.18	27.61	0.86
VIII	$\eta_M \times \eta_H$	3	-16.43	-16.66	22.98	0.87
IX (Equation 7-11)	$\eta_D \times \eta_M \times \eta_H$	7	-39.41	-39.94	0	0.95

Table 8-11. Model Selection Criteria using Dataset I for E_c

Model		N_p	Information criteria			R-squared
#	Critical relations		*AIC*	*BIC*	Δ*AIC*	
I (Equation 2-14)	Deterministic*	1	28.19	28.09	31.17	0.63
II (Equation 7-8)	Regression	3	10.31	10.34	13.29	0.85
III	η_D	5	31.78	31.29	34.76	0.70
IV	η_M	3	19.05	18.76	22.03	0.73
V	η_H	2	23.74	23.55	26.72	0.69
VI	$\eta_D \times \eta_M$	7	7.088	6.410	10.07	0.78
VII	$\eta_D \times \eta_H$	6	31.08	30.50	34.06	0.73
VIII	$\eta_M \times \eta_H$	4	15.79	15.41	18.77	0.76
IX (Equation 7-12)	$\eta_D \times \eta_M \times \eta_H$	8	-2.98	-3.76	0	0.88

*Halpin-Tsai model with raising factor θ_8 for v_{f-m}

In addition, ΔAIC score which is defined as the difference between *AIC* values of the best model (AIC_{min}) and other competing models (AIC_i) were calculated:

$$\Delta AIC = AIC_i - AIC_{min} \quad (7\text{-}15)$$

The models with $\Delta AIC \leq 2$ have substantial evidence of better performance. The models with $4 \leq \Delta AIC \leq 7$ have less evidence, and those models having $\Delta AIC > 10$ have no evidence [236]. It can be seen that all competing models have ΔAIC value of greater than 10. This further confirms the superior performance of model IX compared with other candidate models. Also, the *R*-squared value for model IX is higher than other candidate models, confirming the superior performance of the proposed probabilistic models (Equation 7-11 for σ_c and Equation 7-12 for E_c).

8.4.4. Probability of Failure: Optimization of Variables

After estimating the unknown model parameters (see Table 8-7 and Table 8-8), the proposed probabilistic models were used to optimize each variable to maximize the mechanical properties. This was done through computing the probability of not meeting the specified mechanical properties requirement of at least 50% increase compared with the control (probability of failure; P_f).

8.4.4.1. Relationship between Variables involved in Ultrasonication Procedure

Figure 8-17 (a-*i*) through (a-*iii*) show the contour plots of isoprobability lines as functions (*f*) of UEI versus κ (*f* (*UEI*, κ)), *AR* (*f* (*UEI*, *AR*)), and *SP/CNTs* ratio (*f* (*UEI*, *SP/CNTs*)), respectively, for σ_c. Figure 8-17 (b-*i*) through (b-*iii*) show the contour plots of *f* (*UEI*, κ), *f* (*UEI*, *AR*), and *f* (*UEI*, *SP/CNTs*), respectively, for E_c. Note that except for variables in the *x*-axis (e.g., κ in Figure 8-17 (a-*i*) and (b-*i*)), the mean value of other random

variables were used to plot the contours. The isoprobability lines connect pairs of values of different variables corresponding to the same probability of failure, as shown below:

$$P[g(1.5\sigma_m(\text{or } E_m), \boldsymbol{x}, \boldsymbol{\Theta}) \leq 0] \tag{7-16}$$

The lower value of isoprobability lines (i.e., P_f) indicates that the chance of obtaining the mechanical properties exceeding 50% larger than control is higher (lower value of P_f is desirable). The hatched areas in Figure 8-17 specify the optimum ranges of variables for superior mechanical properties.

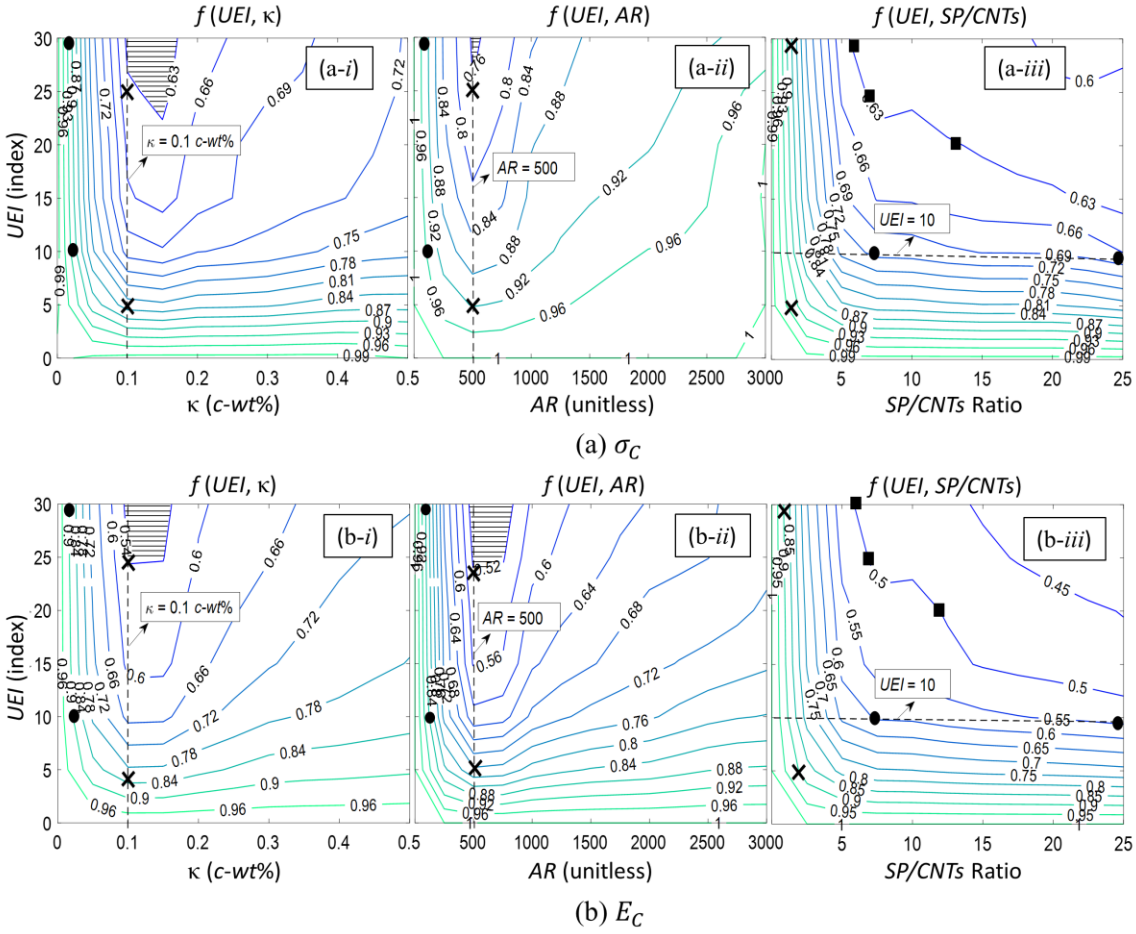

Figure 8-17. Contour plots of the failure probability: (a) σ_c (b) E_c

Figure 8-17 (a-*i*) and (b-*i*) show the relationship between *UEI* and κ (f (*UEI*, κ)) for σ_c and E_c, respectively. When κ is below approximately 0.05 *c-wt*%, increasing *UEI* has

negligible influence on obtaining higher probability of getting at least 50% increase in mechanical properties. For example, in case of κ = 0.02 *c-wt*%, the increase in *UEI* from 10 to 30 results in a constant P_f of 0.93 for σ_c and 0.90 for E_c (see the solid circles on the same failure probability line in Figure 8-17 (a-*i*) and (b-*i*)). As κ increases, P_f decreases by increasing in *UEI*. For example, in case of κ = 0.1 *c-wt*%, increasing *UEI* from 5 to 25 minimizes P_f from 0.84 to 0.65 for σ_c and from 0.84 to 0.54 for E_c (see the crosses on the dashed lines in Figure 8-17 (a-*i*) and (b-*i*)). Generally, P_f is lowest when UEI is above 25 and κ is between 0.1 and 0.15 *c-wt*% (see the hatched areas in Figure 8-17 (a-*i*) and (b-*i*)).

Figure 8-17 (a-*ii*) and (b-*ii*) show the relationship between *UEI* and *AR* (*f* (*UEI*, *AR*)) for σ_c and E_c, respectively. As *AR* increases, the influence of *UEI* on probability estimates becomes more pronounced. For example, when *AR* = 100, increasing *UEI* from 10 to 30 does not contribute to minimizing P_f (i.e., constant P_f of 0.96 and 0.88 for σ_c and E_c, respectively; see the solid circles on the same failure probability lines in Figure 8-17 (a-*ii*) and (b-*ii*)). However, when *AR* = 500, increasing *UEI* from 5 to 24 exhibited the reduction in P_f from 0.92 to 0.77 for σ_c and from 0.80 to 0.52 for E_c (see the crosses on the dashed lines in Figure 8-17 (a-*ii*) and (b-*ii*)). Beyond *AR* of 1500 for σ_c and 2500 for E_c, the increase in *UEI* could reduce P_f, however, its contribution is not significant. Generally, utilizing UEI of above 25 with *AR* between 400 and 800 results in the lowest P_f (see the hatched areas in Figure 8-17 (a-*ii*) and (b-*ii*)).

Figure 8-17 (a-*iii*) and (b-*iii*) show the relationship between UEI and *SP/CNTs* ratio (*f* (*UEI*, *SP/CNTs*)) for σ_c and E_c, respectively, by using contour plot of isoprobability lines. When *SP/CNTs* < 3, the increase in UEI has negligible effect on decreasing P_f. This might be attributed to the insufficient *SP* dosage to coat the entire surface of CNTs [60].

For example, when *SP/CNTs* = 2, the increase in *UEI* from 10 to 30 results in the same P_f of 0.96 for σ_c and 0.90 for E_c (see the crosses on the same failure probability lines in Figure 8-17 (a-*iii*) and (b-*iii*)). In addition, when *UEI* < 10 (see the dashed lines in Figure 8-17 (a-*iii*) and (b-*iii*)), the increase in *SP/CNTs* ratio has minimal influence on the change in P_f. Beyond *UEI* of 10, as *SP/CNTs* ratio increases, lower *UEI* is needed to produce similar P_f. For example, incorporating UEI and *SP/CNTs* ratio of 30 and 6, respectively, exhibits the same P_f as utilizing *UEI* and *SP/CNTs* ratio of either 25 and 7 or 20 and 12, respectively, does (see the solid squares on the same failure probability lines of $P_f = 0.63$ (for σ_c; see Figure 8-17 (a-*iii*)) and 0.50 (for E_c; see Figure 8-17 (b-*iii*))). In addition, when *UEI* is fixed, P_f becomes constant beyond certain *SP/CNTs* ratios, and the threshold *SP/CNTs* ratio achieves sooner at lower *UEI*s. For example, when *UEI* = 10, the increase in *SP/CNTs* ratio from 7 to 25 does not significantly affect P_f (see the solid circles on the dashed lines in Figure 8-17 (a-*iii*) and (b-*iii*)). The similar trend was also observed in the experimental studies showing that the excessive amount of surfactant-to-CNTs ratio (i.e., beyond their optimum ranges) did not yield a better dispersion quality [16, 60, 176].

8.4.4.2. Relationship between *w/c* and *s/c* Ratios

Figure 8-18 shows the contour plots as a function of *w/c* and *s/c* ratios *f* (*w/c*, *s/c*) based on the fixed values (mean values) of other variables for both σ_c (see Figure 8-18 (a)) and E_c (see Figure 8-18 (b)). The probability of failure decreases as *s/c* ratio increases. For example, in case of a constant *w/c* = 0.45 (see the dashed-dotted lines in Figure 8-18), the increase in *s/c* ratio from 0 (i.e., cement paste) to 3 results in decreasing P_f from 0.93 to 0.84 for σ_c and from 0.96 to 0.36 for E_c (see the solid squares in Figure 8-18). Conversely, P_f increases as *w/c* ratio increases. For example, in case of *s/c* = 2 (see the dashed lines in

Figure 8-18), the increase in *w/c* ratio from 0.4 to 0.6 results in the significant increase in P_f from 0.84 to 0.95 for σ_c and from 0.44 to 0.88 for E_c (see the solid circles on the dashed lines in Figure 8-18). In addition, there are several options to achieve the same P_f using certain combinations of *w/c* and *s/c* ratios. For example, in terms of σ_c, utilizing *w/c* and *s/c* ratios of 0.4 and 3, respectively, results in the same P_f as utilizing *w/c* and *s/c* ratios of 0.35 and 2, respectively, does (see the crosses on the same failure probability line of 0.8 in Figure 8-18 (a)). Similarly, concerning E_c (see Figure 8-18 (b), utilizing either *w/c* and *s/c* ratios of 0.4 and 3 or 0.35 and 2.25, respectively, results in the same $P_f = 0.24$.

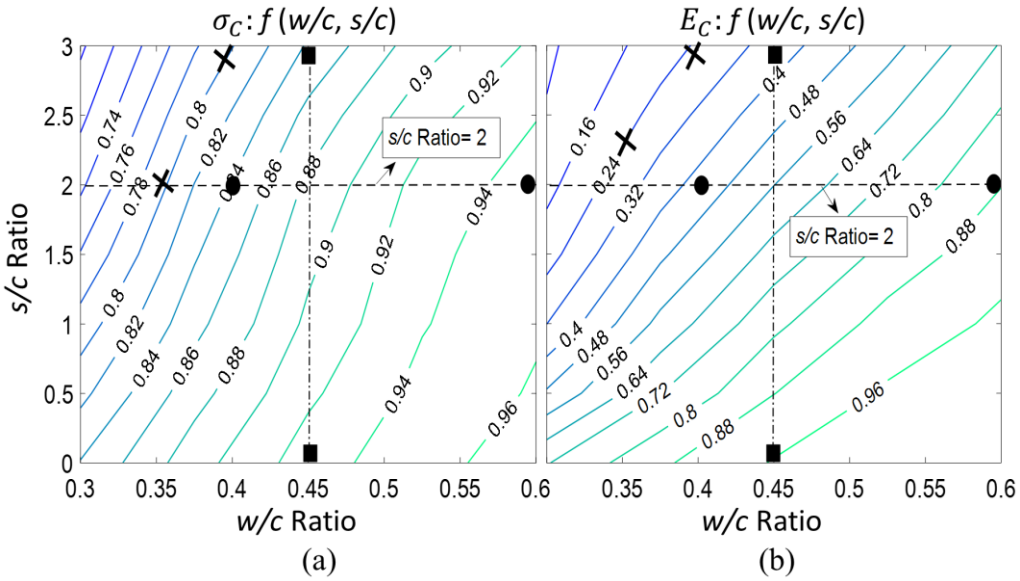

Figure 8-18. Contour plot of the failure probability; *f* (*w/c*, *s/c*): (a) σ_c (b) E_c

8.4.4.3. Relationship between κ and *t*

Figure 8-19 (a) and (b) show the relationship between κ and *t* (*f* (κ, *t*)) while incorporating mean of other variables for σ_c and E_c, respectively. When κ < 0.05 *c-wt*%, *t* has a negligible influence on minimizing P_f. For example, when κ = 0.05 *c-wt*% (see the dashed lines in Figure 8-19), P_f is not affected by the variation in *t* from 10 to 28 days (see the solid circles on the same failure probability lines of $P_f = 0.78$ (for σ_c) and 0.75 (for

E_c)). However, as κ increases, the contribution of t to P_f becomes more pronounced. For example, when κ = 0.1 *c-wt*%, the hydration age of t = 13 days is required to achieve the lowest P_f of 0.66 for σ_c and 0.55 for E_c, beyond which P_f does not change. Whereas, in case of utilizing κ = 0.35 *c-wt*%, t = 25 days is needed to achieve the same P_f (see the crosses on the same failure probability lines in Figure 8-19). Generally, at low κ, the concentration is the driving force to increase the mechanical properties rather than t. As κ increases, mechanical properties gradually increase against the control (i.e., without CNTs) over time.

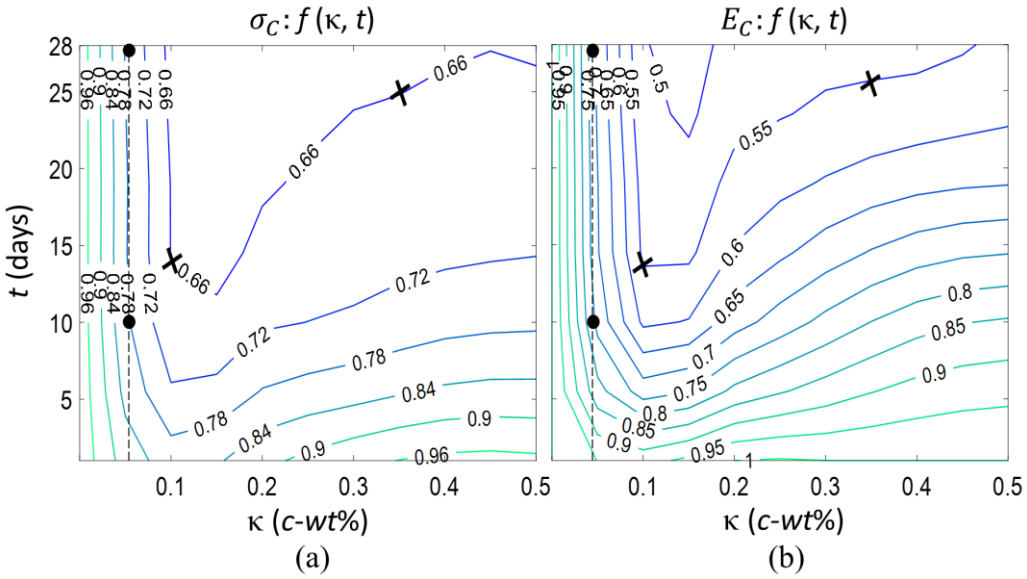

Figure 8-19. Contour plot of the failure probability; *f* (κ, *t*): (a) σ_c (b) E_c

8.4.4.4. Influence of Optimum Ranges of Variables on the Failure Probability

Figure 8-20 shows contour plots of isoprobability lines as a function of κ and *AR* (*f* (κ, *AR*)), while utilizing either mean of other variables (Figure 8-20 (a-*i*) and (b-*i*) for σ_c and E_c, respectively) or optimum values of each variable (Figure 8-20 (a-*ii*) and (b-*ii*) for σ_c and E_c, respectively). The optimum values of variables were obtained using Figure 8-17 (a-*iii*), Figure 8-17 (b-*iii*), and Figure 8-18 (deterministic values: *UEI* = 30, *SP/CNTs* = 6,

w/c = 0.4, *s/c* = 3). Generally, the value of P_f is very high while incorporating CNTs with high κ and *AR*. Besides, P_f decreases as κ increases up to 0.1 *c-wt*%, beyond which P_f increases, due to the dispersion issues (see the dashed lines in Figure 8-20). The lowest P_f is achieved when using CNTs with κ ranges from 0.08 to 0.18 *c-wt*% and *AR* between 400 and 800 (see the hatched areas in Figure 8-20).

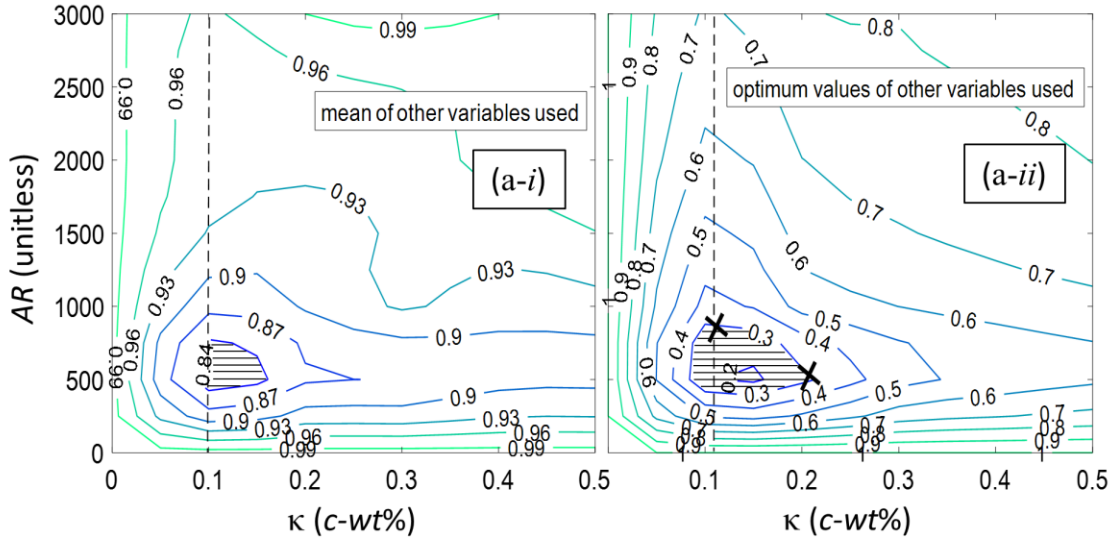

(a) $\sigma_C: f(\kappa, AR)$

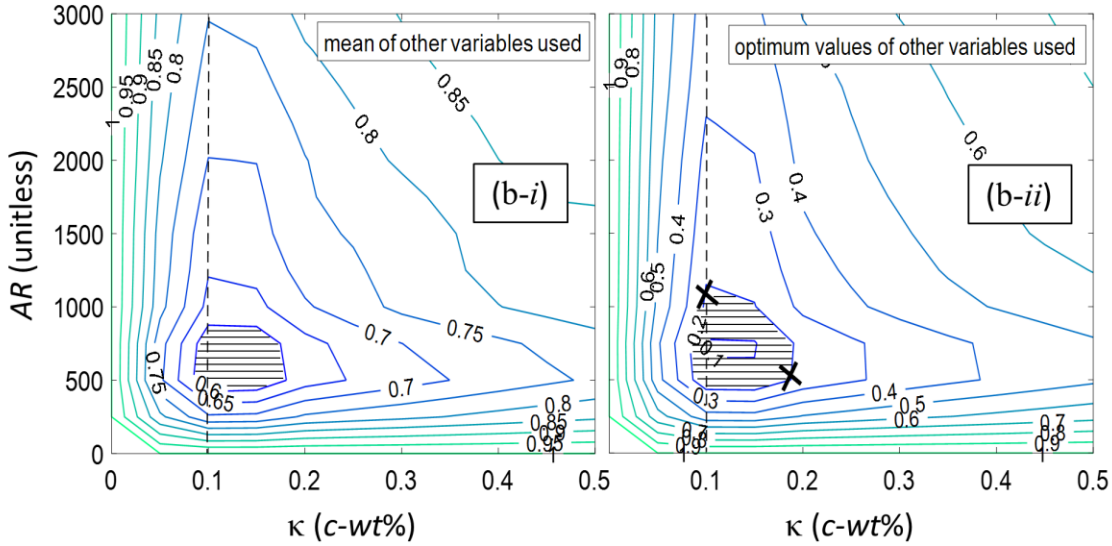

(b) $E_C: f(\kappa, AR)$

Figure 8-20. Contour plots of the failure probability; $f(\kappa, AR)$: (a) σ_c (b) E_c

In addition, comparing Figure 8-20 (a-*ii*) and (b-*ii*) with Figure 8-20 (a-*i*) and (b-*i*), respectively, it is obvious that utilizing optimum ranges of different variables significantly decreases P_f. For example, concerning σ_c, if using mean value of each variable (see Figure 8-20 (a-*i*)), the minimum P_f is 0.84 (see the hatched area in Figure 8-20 (a-*i*)). However, when using optimum values of different variables (i.e., deterministic values), P_f decreases to only 0.30 (see the hatched area in Figure 8-20 (a-*ii*)). Similar trend can also be observed in terms of E_c; utilizing optimum values of different variables (see Figure 8-20 (b-*ii*)) results in the reduction in P_f by 40% (from 0.60 to 0.20) compared with utilizing the mean values of the variables (see Figure 8-20 (b-*i*)).

Besides, using either low κ having high *AR* or high κ with low *AR* produces the similar P_f. For example, $P_f = 0.30$ can be attained when incorporating either κ = 0.1 *c-wt*% having *AR* = 800 or κ = 0.2 *c-wt*% having *AR* = 500 (see crosses on the same failure probability line of 0.30 in Figure 8-20 (a-*ii*)). This is in a good agreement with the trends observed in the experimental studies. Other researchers have reported that higher concentration of CNTs with smaller aspect ratios produced comparable mechanical properties as lower concentration of higher aspect ratio CNTs did [16, 23, 170].

8.4.5. Sensitivity and Importance Measures

Sensitivity and importance measures are performed to determine the effect of different variables on the probability estimates and to gain physical insights. Sensitivity and importance measures could be used to minimize the probability of failure to achieve certain required performance. In this section, the sensitivity (Section 8.4.5.1) and importance (Section 8.4.5.2) of each variable are measured with respect to three main

variables that are believed to significantly affect the mechanical properties: κ, *AR*, and *UEI*. The details are discussed as follow.

8.4.5.1. Sensitivity Measure

Figure 8-21 shows the sensitivity measure of each variable as a function of κ (see Figure 8-21 (a-*i*) and (b-*i*)), *AR* (see Figure 8-21 (a-*ii*) and (b-*ii*)), and *UEI* (see Figure 8-21 (a-*iii*) and (b-*iii*)) for σ_c and E_c, respectively. Note that the mean value of each variable was used to measure the sensitivity.

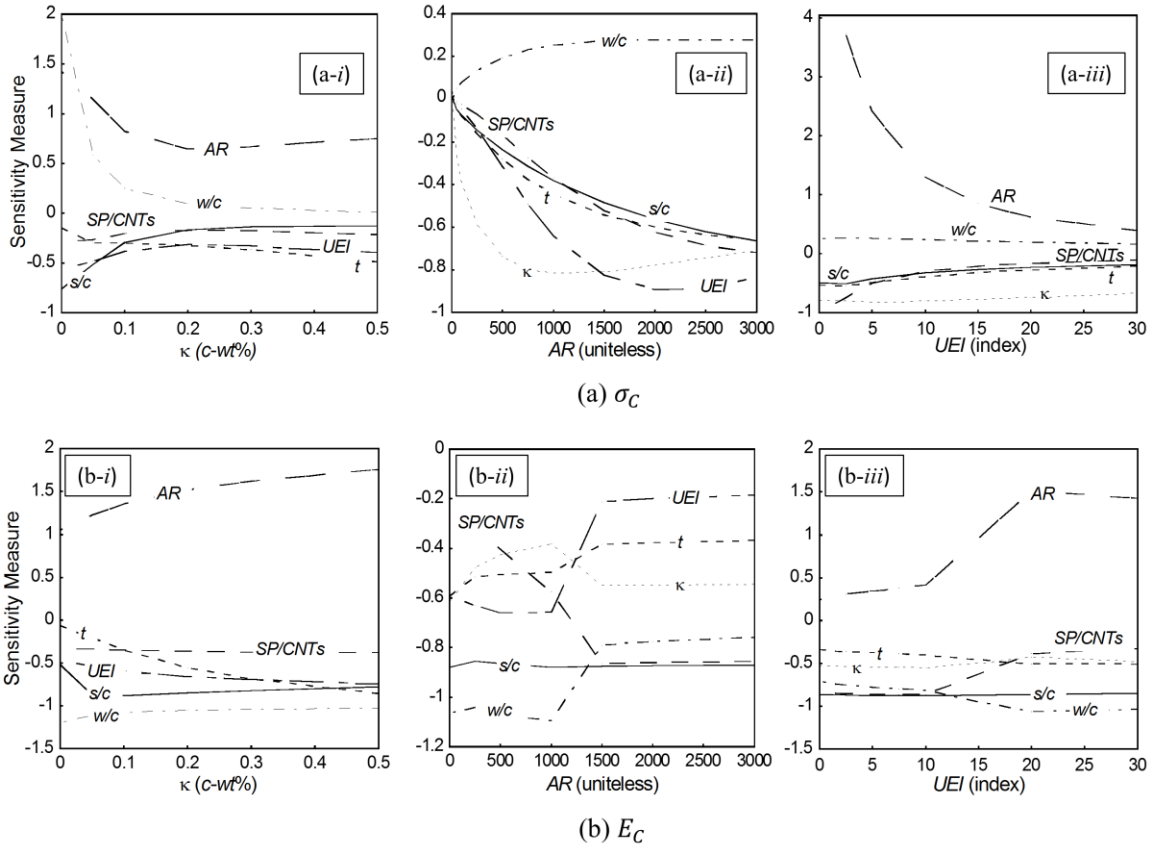

Figure 8-21. Sensitivity measure: (a) σ_c (b) E_c

The higher change in the sensitivity measure (*y*-axis) for each variable with respect to the main variable (*x*-axis) indicates the higher sensitivity of the mechanical properties to the variation in the amount of that variable (D = 1.5 σ_m (or E_m)).

Figure 8-21 (a-*i*) shows that up to κ = 0.2 *c-wt*%, the sensitivity measure of most variables changes significantly. However, the sensitivity measure remains almost constant beyond κ = 0.2 *c-wt*%. In case of κ ≤ 0.2 *c-wt*%, *w/c* ratio, *AR*, and *s/c* ratio are the most sensitive variables to the changes in P_f, respectively, while *SP/CNTs* ratio and *t* are the least sensitive variables. In case of κ > 0.2 *c-wt*%, P_f is most sensitive to the variation in *t*, followed by *AR*. Figure 8-21 (b-*i*) also shows that as κ increases (*x*-axis), *t* and *AR* have the largest slope amongst other variables, respectively, indicating that they are the most sensitive variables to the change in E_c.

When computing the sensitivity measures as a function of *AR* (see Figure 8-21 (a-*ii*) and (b-*ii*) for σ_c and E_c, respectively), κ is the most sensitive variable below *AR* of around 1000 beyond which the sensitivity of κ to change P_f gradually decreases. In contrast *w/c* ratio is the least sensitive variable to the change in P_f.

When computing the sensitivity measure with respect to the change in *UEI* (see Figure 8-21 (a-*iii*) and (b-*iii*) for σ_c and E_c, respectively), *AR* and *SP/CNTs* ratio are the most sensitive variables to the changes in P_f in terms of both σ_c and E_c.

In addition, the negative value of the sensitivity measure (*y*-axis) for variables indicates that P_f decreases as the amount of that variable increases. Conversely, the positive value of the sensitivity measure for each variable indicates that P_f increases as the value of the variable increases. For example, the value of the sensitivity measure for *AR* is positive for both σ_c and E_c. This indicates that P_f increases as the value of *AR* increases. Concerning σ_c, the positive values of the sensitivity measure for *w/c* ratio is also observed; indicating that P_f increases as *w/c* ratio increases. Conversely, P_f decreases (i.e., the chance of attaining at least 50% increase in mechanical properties increases) as the value of *t*, *UEI*,

s/c ratio, and *SP/CNTs* ratio increases. The different trend in the sensitivity measures for *w/c* ratio in terms of σ_c and E_c might be explained by the influence of *w/c* ratio on the bonding characteristics between CNTs and cement matrix. As *w/c* ratio increases, the interfacial bond strength between CNTs and cement matrix decreases. This might explain the positive value of the sensitivity measure for *w/c* ratio in σ_c, due to the fact that the interfacial bond strength is more important in the flexural strength than the elastic modulus.

As seen in Figure 8-21 (a-*iii*) and (b-*iii*), the negative values of the sensitivity measure for *SP/CNTs* ratio is observed. This shows that P_f decreases as *SP/CNTs* ratio increases. However, *SP/CNTs* ratio gets closer to zero as *UEI* increases. This suggests that lower amount of *SP/CNTs* ratio can be used when higher *UEI* is used. Konsta-Gdoutos *et al*. [16] also reported that excessive amount of surfactant (i.e., beyond optimum surfactant dosage) degraded the mechanical properties.

8.4.5.2. Importance Measure

Figure 8-22 shows the importance measures ($\boldsymbol{\gamma}$) of each variable as a function of κ (see Figure 8-22 (a-*i*) and (b-*i*)), *AR* (see Figure 8-22 (a-*ii*) and (b-*ii*)), and *UEI* (see Figure 8-22 (a-*iii*) and (b-*iii*)) for σ_c and E_c, respectively, while using the mean value of other variables. The importance measure is used to rank the importance of different variables on the variability of the limit state function. In importance analysis, the higher absolute value of the importance measure vector ($\boldsymbol{\gamma}$) for each variable indicates the higher importance of that variable.

When computing the importance measure with respect to the change in κ (see Figure 8-22 (a-*i*) and (b-*i*) for σ_c and E_c, respectively), Figure 8-22 (a-*i*) shows that *w/c* ratio is the most important variable at $\kappa \leq 0.05$ *c-wt*%. The importance of *w/c* ratio gradually

decreases as κ increases and beyond κ = 0.3 *c-wt*%, the *w/c* ratio is the least important variable to the variation in the limit state function (the smallest absolute value of importance measure (y-axis) amongst other variables). As κ increases, the importance of *AR*, *t*, and *UEI* also increases, while the importance of *SP/CNTs* ratio remains almost constant. For example, *t* is the least important variable at κ < 0.05 *c-wt*%. However, at κ = 0.5 *c-wt*%, *t* is the second most important variable, after *AR*. Similarly, Figure 8-22 (b-*ii*) shows that *s/c* and *w/c* ratios are the most important variables. Also, below κ of 0.1 *c-wt*%, *t* is the least important variable. However, the importance of *t* gradually and consistently increases as κ increases. Besides, as κ increases, the importance of *UEI* increases while the importance of *SP/CNTs* ratio and *w/c* ratio remains constant.

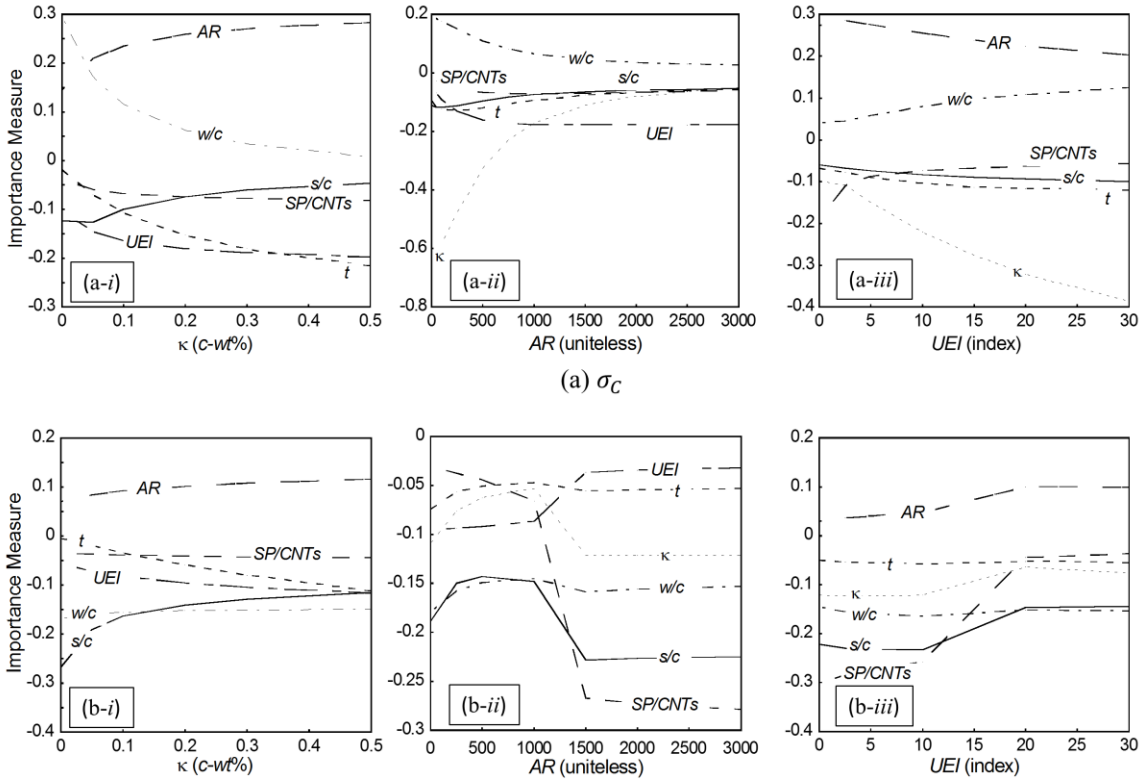

(a) σ_C

(b) E_C

Figure 8-22. Importance measure: (a) σ_c (b) E_c

Figure 8-22 (a-*ii*) shows that as *AR* increases, the importance of κ decreases. Below *AR* of around 1000, κ is the most important variable to the change in P_f. However, the importance of κ significantly decreases as *AR* increases. Also, Figure 8-22 (a-*ii*) and (b-*ii*) show that below *AR* of around 1000, *SP/CNTs* ratio is the least important variable. The importance of *SP/CNTs* ratio, however, increases as *AR* increases. Figure 8-22 (b-*ii*) shows that beyond *AR* = 1500, *SP/CNTs* ratio is the most important variable to the change in E_c.

When computing the importance measure with respect to the change in *UEI* (see Figure 8-22 (a-*iii*) and (b-*iii*) for σ_c and E_c, respectively), Figure 8-22 (a-*iii*) shows that when *UEI* < 5, *AR* and *SP/CNTs* ratio are the most important variables to the change in σ_c, respectively. However, the importance of *SP/CNTs* ratio decreases by increasing in *UEI* and it becomes the least important variable at *UEI* ≥ 10. In addition, as *UEI* increases, the importance of κ and *w/c* ratio increases. When *UEI* ≥ 15, κ is the most important variable to the variance of the limit state function. As seen in Figure 8-22 (b-*iii*), below *UEI* of around 12, *SP/CNTs* ratio is the most important variable to the change of E_c. However, the importance of *SP/CNTs* ratio decreases by increasing in *UEI* and it becomes the least important variable above *UEI* of 20 (i.e., the smallest absolute value of importance measure (*y*-axis) amongst other variables). It can also be seen that the importance of κ and *s/c* ratio decreases as *UEI* increases. On the other hand, the importance of *t* and *w/c* ratio remains constant.

8.5. Summary

Based on extensive experimental test results from this research and the literature, three critical relations were proposed: dispersion relation (η_D), hydration age relation (η_H), and matrix relation (η_M). The proposed critical relations were then used in a regression

equation to predict the mechanical properties (flexural strength (σ_c) and elastic modulus (E_c)) and showed a reasonable accuracy within ±20% error of the experimental observation. Nevertheless, the robustness of the regression model is questionable when using new dataset. Also, the regression model is not able to capture the nonlinear behavior of CNTs within nanocomposites; in real applications, mechanical properties increase as CNT aspect ratio and/or concentration (or volume fraction) increases up to certain limits, beyond which mechanical properties degrade, due to the dispersion issues. Therefore, the proposed critical relations were added to available theoretical models in the literature to predict the mechanical properties. Also, due to the inherent uncertainty while incorporating CNTs, the models were formulated in a probabilistic manner using a Bayesian methodology to predict σ_c and E_c. The probabilistic models could reliably predict the mechanical properties within ±15% (for σ_c) and ±18% (for E_c) error of the experimental test results. Then, the conditional probability of failure was used to identify the optimum ranges of the experimental variables. The recommended optimum ranges could help researchers to increase the mechanical properties. The following conclusions can be drawn:

1. The proposed critical relations were able to capture the contributions of the important variables and the interactions between them found in previous studies and this research.
2. To accurately predict the mechanical properties, including all three critical relations in the model is critical. The performance of the prediction model might be significantly degraded in the absence of any of these critical relations.

3. Incorporating CNTs with aspect ratio (*AR*) ranging from 400 to 800 and concentration (κ) between 0.08 and 0.18 *c-wt*% (based on the weight percent of cement powder) results in the highest improvement in the mechanical properties.
4. There are several options to attain the similar mechanical properties with varied combinations of the experimental variables. Certain combinations of the Ultrasonication Energy Indicator (*UEI*) and superplasticizer-to-CNTs (*SP/CNTs*) ratio or *w/c* and *s/c* ratios might be used to yield similar enhancement in the mechanical properties, when using constant values of other variables. Engineers and designers could use different combinations of suggested values in this research to attain the desired mechanical properties.
5. The hydration age of cement (*t*) is one of the most sensitive variables to change the mechanical properties as a function of CNT concentration (κ). However, when computing the sensitivity with respect to *UEI*, *t* is one of the least sensitive variables to affect the mechanical properties. Conversely, CNT aspect ratio (*AR*) and *SP/CNTs* ratio are the most sensitive variables to the change in mechanical properties with respect to *UEI*. As κ increases, the importance of *AR* and *t* increases, while the importance of *w/c* and *s/c* ratios decreases. In addition, as *UEI* increase, the importance of *SP/CNTs* ratio to attain the superior mechanical properties decreases.

CHAPTER 9. SUMMARY, CONCLUSIONS, RECOMMENDATIONS, AND FUTURE RESRACH

9.1. General

This chapter first discusses the key contributions of this research (Section 9.2 and Section 9.3). Based on the finding of this research, recommendations for incorporating CNTs in cementitious materials are given in Section 9.4. Finally, in Section 9.5, future research directions are recommended.

9.2. Summary

In this research, a comprehensive study was performed to provide a better understanding of the mechanisms of CNTs affecting different properties (flow, mechanical, and durability) of cementitious materials. Nevertheless, the focus of this study was on the contribution of CNTs to the mechanical properties. The main objective of this research was to propose reliable models to predict the flexural strength and elastic modulus of CNT-cement pastes and mortars. To achieve this objective, this study was conducted in three tracks as follows:

- Track 1 (mechanical properties)
    - Phase I: database and data analysis
    - Phase II: experimental study
    - Phase III: critical relations and regression model
    - Phase IV: probabilistic models
- Track 2 (flow properties)

- Track 3 (alkali-silica reaction)

In Track 1 (Phase I), extensive published data was analyzed to find the most important interactions between the experimental variables affecting the mechanical properties and select the correct type of CNTs for superior mechanical performance.

At the same time of conducting Phase I of Track 1, a total of 27 mix proportions were experimentally tested to find optimum mix proportions of CNT-cement pastes and mortars through relationship between the flow and mechanical properties. However, no clear correlations were found from this part of the research. This was the motivation to re-examine the possible interactions between multiple experimental variables in Phase II of Track 1.

In Phase II of Track 1, 28 mix proportions were tested to study the contributions of multiple experimental variables including CNT aspect ratio, concentration, total ultrasonication energy, ultrasonication amplitude, superplasticizer-to-CNTs ratio, hydration age, water-to-cement ratio, sand-to-cement ratio, sand gradation, and mixing procedure. The experimental results confirmed the interactions found in Phase I of Track 1.

In Phase III of Track 1, based on the findings from Phase I and Phase II, three critical relations were proposed to include the interactions between the important variables 1) dispersion relation (η_D), 2) hydration age relation (η_H), and 3) matrix relation (η_M). Then, the proposed critical relations were used in a regression equation to predict the flexural strength and elastic modulus.

In Phase IV of Track 1, to correct the bias observed in the regression equation, the proposed critical relations were added to available theoretical models in the literature to

predict the mechanical properties. Also, the developed models were formulated in a probabilistic manner to account for different sources of uncertainty. The developed probabilistic models provided guidelines for selecting the correct type of CNTs, mix design, and dispersion procedure for superior mechanical performance.

In Track 3, some cases were selected (a total of 8 mix proportions) to experimentally investigate the influence of adding CNTs on the durability (herein, alkali-silica reaction; ASR) of cement mortars.

The experimental study reported in this research included investigations on the following.

- mini-cone slump test
- rheological test (viscosity and yield stress)
- compressive strength
- flexural strength
- static elastic modulus (from flexural test)
- dynamic elastic modulus
- linear expansion

9.3. Conclusions

The following conclusions were drawn.

9.3.1. Flow Properties (Track 2)

1. Additions of small amounts of CNTs significantly decreased the flow diameter of cement pastes and mortars at various *w/c* ratios. Also, as CNT concentration increased, the flow diameter further decreased.

2. Addition of CNTs significantly increased the viscosity and yield stress of cement pastes. The improvements in rheological properties of cement pastes containing CNTs could help to reduce the bleeding issue.
3. Superplasticizer dosage was critical to determine the shear behavior of cement pastes. The flow index, which is a measure of the shear behavior, increased as superplasticizer dosage increased up to certain values, beyond which the flow index did not change. And, the threshold value of the superplasticizer dosage was higher at lower *w/c* ratios and vice versa.

9.3.2. Mechanical Properties (Track 1)

The mechanical properties are discussed in four different phases as mentioned in Section 9.2.

9.3.2.1. Phase I (Database and Data Analysis)

1. The contribution of CNT length to increase the compressive strength was found to be negligible, however, it significantly affected the flexural strength. Flexural strength increased by the increase in CNT length up to certain ranges, beyond which the flexural strength degraded due to the dispersion issues.
2. Smaller diameter CNTs outperformed in compressive strength than flexural strength and elastic modulus.
3. A threshold CNT concentration was found for superior mechanical properties, depending on CNT aspect ratio, beyond which the mechanical properties degraded. As CNT aspect ratio increased, its threshold concentration decreased.
4. Besides CNT intrinsic properties, there are other potential variables and interactions to affect the mechanical properties that need to be considered.

9.3.2.2. Phase II (Experimental Study)

1. The experimental study confirmed the contributions of the studied interactions to the mechanical properties.
2. Based on the experimental test results, the ultrasonication energy indicator (*UEI*) which quantifies the effectiveness of an ultrasonication process with the balance between the ultrasonication energy and amplitude was proposed. Despite total ultrasonication energy (UE_T), higher values of *UEI* yielded superior mechanical properties. However, when using high ultrasonication amplitude ($UA \geq 70\%$), the optimum value of $UEI = 15$ was suggested.
3. The lower *w/c* ratio and/or higher *s/c* ratio yielded superior enhancement. Also, certain combinations of *w/c* and *s/c* ratios exhibited comparable improvement in mechanical properties of CNT-cement nanocomposites compared with the control (without CNTs).
4. The contribution of hydration age to improve the mechanical properties increased as CNT concentration increased.
5. The contribution of CNTs to increase the static elastic modulus was found to be higher than the dynamic elastic modulus, which might be related to the crack bridging ability of CNTs when the specimen was cracked under flexural loading.

9.3.2.3. Phase III (Critical Relations and Regression Model)

1. The proposed critical relations in this research (dispersion relation (η_D), hydration age relation (η_H), and matrix relation (η_M)) were able to capture the interactions between the important variables affecting the mechanical properties.

2. There are various options to achieve comparable mechanical properties using different combinations of the experimental variables. Engineers and designers could use the contour plots provided in this research to yield the same level of improvement in mechanical properties.
3. The proposed critical relations enable to predict the mechanical properties using a simple regression model with reasonable accuracy (±20% error compared with the experimental test data). However, the regression model may only be applicable within the database that used to develop the best fit. Therefore, the robustness of the model is questionable.
4. The regression model is not able to capture the general trend observed in the experimental studies of this research and the literature.

9.3.2.4. Phase IV (Probabilistic Models)

1. The probabilistic models are robust to predict the mechanical properties of CNT-cement nanocomposites within ±15% error for flexural strength and ±18% for elastic modulus.
2. The probabilistic models indicated that the mechanical properties increased by the increase in CNT concentration and aspect ratio up to certain ranges, beyond which the mechanical properties degraded.
3. The inclusion of all three critical relations in the probabilistic models is critical to reliably predict the mechanical properties.

9.3.3. Durability: Alkali-Silica Reaction (Track 3)

1. CNT concentration of 0.1 *c-wt*% significantly decreased the progress of ASR in cement mortars, as compared with concentration of 0.3 *c-wt*%.

2. At high CNT concentrations, COOH functionalized CNTs decreased the rate of ASR expansion at later ages. This might be related to the release of the adsorbed water over time. Therefore, the bond between CNTs and cement matrix could be improved by the progress in the hydration process, delaying the propagation of internal cracks.
3. If optimum ranges of the experimental variables obtained from Phase II of Track 1 is used, well dispersed CNTs are able to significantly contribute to mitigate the progress of ASR.

9.4. Recommendations

Based on the findings from this research, the following recommendations are given for future researchers and engineers to exploit the full advantages of CNTs within cementitious materials.

1. For superior compressive strength, CNTs with length and diameter of smaller than 15 μm and 20 *nm*, respectively, might be considered as the best option.
2. For superior flexural strength, relatively longer CNTs (10-20 μm) with diameters ranging from 15 to 32.5 *nm* might be considered as the best option.
3. CNTs with aspect ratio ranging from 400 to 800 and concentration ranging from 0.08 to 0.18 *c-wt*% might be considered for superior mechanical performance.
4. Generally, denser cement matrix yield the highest improvement in the mechanical properties of CNT-cement nanocomposites. However, the optimum ranges of other potential variables must be used to maximize the mechanical properties.

5. COOH functionalized CNTs were found to have minimal contribution to the mechanical properties, compared with other potential variables. However, COOH-CNTs might be beneficial to lower the rate of ASR in the long run.
6. Engineers and designers may use the contour plots developed in this research to allocate resources for practical applications to achieve certain mechanical performance.

9.5. Future Research

The properties of CNT-cement nanocomposites rely on the mix proportions and material properties. However, as with most research, not all combinations of materials and mix proportions could be evaluated in this research. Therefore, the following research is recommended for future studies to supplement the current research and to provide further insight into the engineering applications of CNT-cement nanocomposites.

1. This research studied the influence of CNTs on properties of cement pastes and mortars. The research should be extended to concrete containing coarse aggregate to investigate how the addition of coarse aggregate might influence the studied properties in this research program. Also, the relationship between the properties of CNT reinforced cement paste, mortar, and concrete should be further studied.
2. This research investigated the properties of CNT-cement nanocomposites on the macroscopic scale. To fully understand the mechanisms of CNTs within nanocomposites, a microscopic study should be considered to provide further insights and to correlate between the microscopic and macroscopic aspects of cementitious materials reinforced with CNTs.

3. CNTs are not perfectly straight and have some sort of curvature. In this research, however, CNTs were considered as straight fiber. In future research, the proposed model in this study might be modified to consider the effect of CNT curvature on the mechanical properties of CNT-cement nanocomposites.
4. The proposed dispersion relation in this research was developed based on the surfactant-assisted ultrasonication procedure. The proposed model should be modified to predict the mechanical properties of CNT-cement nanocomposites when using other dispersion techniques. Further research is therefore needed to correlate the degree of CNT dispersion using other dispersion techniques with the proposed dispersion relation using a so-called correction factor.
5. The research showed that COOH functionalized CNTs might be able to lower the rate of ASR expansion at later ages. More focused study on the microstructure level concerning the influence of COOH functional groups covalently bonded to the surface of CNTs on the long-term progress of ASR is therefore needed.

REFERENCES

[1] Barros, J.A.O., Sena-Cruz, J., Fracture energy of steel fibre reinforced concrete, Journal of Mechanics of Composite Materials and Structures, 8 (2001) 29-45.

[2] Qian, C.X., Stroeven, P., Development of hybrid polypropylene-steel fibre-reinforced concrete, Cement and Concrete Research, 30 (2000) 63-69.

[3] Betterman, L.R., Ouyang, C., Shah, S.P., Fiber-matrix interaction in microfiber-reinforced mortar, Advanced Cement Based Materials, 2 (1995) 53-61.

[4] Banthia, N., Nandakumar, N., Crack growth resistance of hybrid fiber reinforced cement composites, Cement and Concrete Composites, 25 (2003) 3-9.

[5] Song, P.S., Hwang, S., Sheu, B.C., Strength properties of nylon-and polypropylene-fiber-reinforced concretes, Cement and Concrete Research, 35 (2005) 1546-1550.

[6] Song, P.S., Hwang, S., Mechanical properties of high-strength steel fiber-reinforced concrete, Construction and Building Materials, 18 (2004) 669-673.

[7] Akkaya, Y., Shah, S.P., Ghandehari, M., Influence of fiber dispersion on the performance of microfiber reinforced cement composites, ACI Special Publications 216: Innovations in Fiber-Reinforced Concrete 216 (2003) 1-18.

[8] Balaguru, P.N., Shah, S.P., Fiber-reinforced cement composites, McGraw-Hill Inc.,1992.

[9] Bentur, A., Mindess, S., Fibre reinforced cementitious composites, Taylor & Francis,2006.

[10] Ramezani, M., Kim, Y.H., Sun, Z., Mechanical properties of carbon nanotube reinforced cementitious materials: Database and statistical analysis, Magazine of Concrete Research, (2019) 1-62.

[11] Konsta-Gdoutos, M.S., Metaxa, Z.S., Shah, S.P., Multi-scale mechanical and fracture characteristics and early-age strain capacity of high performance carbon nanotube/cement nanocomposites, Cement and Concrete Composites, 32 (2010) 110-115.

[12] Zou, B., Chen, S.J., Korayem, A.H., Collins, F., Wang, C.M., Duan, W.H., Effect of ultrasonication energy on engineering properties of carbon nanotube reinforced cement pastes, Carbon, 85 (2015) 212-220.

[13] Tyson, B.M., Al-Rub, R.K.A., Yazdanbakhsh, A., Grasley, Z., Carbon nanotubes and carbon nanofibers for enhancing the mechanical properties of nanocomposite cementitious materials, Journal of Materials in Civil Engineering, 23 (2011) 1028-1035.

[14] Chuah, S., Pan, Z., Sanjayan, J.G., Wang, C.M., Duan, W.H., Nano reinforced cement and concrete composites and new perspective from graphene oxide, Construction and Building Materials, 73 (2014) 113-124.

[15] Lawler, J.S., Wilhelm, T., Zampini, D., Shah, S.P., Fracture processes of hybrid fiber-reinforced mortar, Materials and Structures, 36 (2003) 197-208.

[16] Konsta-Gdoutos, M.S., Metaxa, Z.S., Shah, S.P., Highly dispersed carbon nanotube reinforced cement based materials, Cement and Concrete Research, 40 (2010) 1052-1059.

[17] Raki, L., Beaudoin, J.J., Alizadeh, R., Makar, J.M., Sato, T., Cement and concrete nanoscience and nanotechnology, Materials, 3 (2010) 918-942.

[18] Kim, G., Naeem, F., Kim, H., Lee, H., Heating and heat-dependent mechanical characteristics of CNT-embedded cementitious composites, Composite Structures, 136 (2016) 162-170.

[19] Kim, H.-K., Chloride penetration monitoring in reinforced concrete structure using carbon nanotube/cement composite, Construction and Building Materials, 96 (2015) 29-36.

[20] Kim, H.K., Nam, I.W., Lee, H.K., Enhanced effect of carbon nanotube on mechanical and electrical properties of cement composites by incorporation of silica fume, Composite Structures, 107 (2014) 60-69.

[21] Yu, X., Kwon, E., A carbon nanotube/cement composite with piezoresistive properties, Smart Materials and Structures, 18 (2009) 055010.

[22] Ramezani, M., Kim, Y.H., Hasanzadeh, B., Sun, Z., Influence of carbon nanotubes on SCC flowability, 8th International RILEM Symposium on Self-Compacting Concrete, Washington DC, USA, (2016), pp. 397-406.

[23] Al-Rub, R.K.A., Ashour, A., Tyson, B.M., On the aspect ratio effect of multi-walled carbon nanotube reinforcements on the mechanical properties of cementitious nanocomposites, Construction and Building Materials, 35 (2012) 647-655.

[24] Wang, B., Han, Y., Pan, B., Zhang, T., Mechanical and morphological properties of highly dispersed carbon nanotubes reinforced cement based materials, Journal of Wuhan University of Technology-Mater. Sci. Ed., 28 (2013) 82-87.

[25] Xu, S., Liu, J., Li, Q., Mechanical properties and microstructure of multi-walled carbon nanotube-reinforced cement paste, Construction and Building Materials, 76 (2015) 16-23.

[26] Lu, L., Ouyang, D., Xu, W., Mechanical properties and durability of ultra high strength concrete incorporating multi-walled carbon nanotubes, Materials, 9 (2016) 1-11.

[27] Del Carmen Camacho, M., Galao, O., Baeza, F.J., Zornoza, E., Garcés, P., Mechanical properties and durability of CNT cement composites, Materials, 7 (2014) 1640-1651.

[28] Konsta-Gdoutos, M.S., Danoglidis, P.A., Falara, M.G., Nitodas, S.F., Fresh and mechanical properties, and strain sensing of nanomodified cement mortars: The effects of MWCNT aspect ratio, density and functionalization, Cement and Concrete Composites, 82 (2017) 137-151.

[29] Stynoski, P., Mondal, P., Marsh, C., Effects of silica additives on fracture properties of carbon nanotube and carbon fiber reinforced portland cement mortar, Cement and Concrete Composites, 55 (2015) 232-240.

[30] Gdoutos, E.E., Konsta-Gdoutos, M.S., Danoglidis, P.A., Portland cement mortar nanocomposites at low carbon nanotube and carbon nanofiber content: A fracture mechanics experimental study, Cement and Concrete Composites, 70 (2016) 110-118.

[31] Danoglidis, P.A., Konsta-Gdoutos, M.S., Gdoutos, E.E., Shah, S.P., Strength, energy absorption capability and self-sensing properties of multifunctional carbon nanotube reinforced mortars, Construction and Building Materials, 120 (2016) 265-274.

[32] Li, W.-W., Ji, Wei-Ming, Wang, Yao-Cheng, Liu, Yi, Shen, Ruo-Xu, Xing, Feng, Investigation on the mechanical properties of a cement-based material containing carbon nanotube under drying and freeze-thaw conditions, Materials, 8 (2015) 8780-8792.

[33] Shah, S.P., Hou, Pengkun, Konsta-Gdoutos, Maria S, Nano-modification of cementitious material: Toward a stronger and durable concrete, Journal of Sustainable Cement-Based Materials, (2015) 1-22.

[34] Sarkar, D., Xu, C., Li, H., Banerjee, K., High-frequency behavior of graphene-based interconnects—part i: Impedance modeling, IEEE Transactions on Electron Devices, 58 (2011) 843-852.

[35] Kaushik, B.K., Majumder, Manoj Kumar, Carbon nanotube: Properties and applications, Carbon nanotube based VLSI interconnects, Springer2015, pp. 17-37.

[36] Javey, A., Kong, J., Carbon nanotube electronics, Springer Science & Business Media2009.

[37] Vaisman, L., Wagner, H.D., Marom, G., The role of surfactants in dispersion of carbon nanotubes, Advances in colloid and interface science, 128 (2006) 37-46.

[38] Zhu, H.W., Xu, C.L., Wu, D.H., Wei, B.Q., Vajtai, R., Ajayan, P.M., Direct synthesis of long single-walled carbon nanotube strands, Science, 296 (2002) 884-886.

[39] Zheng, L.X., O'connell, M.J., Doorn, S.K., Liao, X.Z., Zhao, Y.H., Akhadov, E.A.*, et al.*, Ultralong single-wall carbon nanotubes, Nature materials, 3 (2004) 673-676.

[40] De Volder, M.F.L., Tawfick, S.H., Baughman, R.H., Hart, A.J., Carbon nanotubes: Present and future commercial applications, Science, 339 (2013) 535-539.

[41] Kim, S., Mulholland, G., Zachariah, M., Density measurement of size selected multiwalled carbon nanotubes by mobility-mass characterization, Carbon, 47 (2009) 1297-1302.

[42] Laurent, C., Flahaut, E., Peigney, A., The weight and density of carbon nanotubes versus the number of walls and diameter, Carbon, 48 (2010) 2994-2996.

[43] Poncharal, P., Wang, Z., Ugarte, D., De Heer, W.A., Electrostatic deflections and electromechanical resonances of carbon nanotubes, Science, 283 (1999) 1513-1516.

[44] Krishnan, A., Dujardin, E., Ebbesen, T., Yianilos, P., Treacy, M., Young's modulus of single-walled nanotubes, Physical Review B, 58 (1998) 14013.

[45] Lourie, O., Cox, DM, Wagner, HD, Buckling and collapse of embedded carbon nanotubes, Physical Review Letters, 81 (1998) 1638.

[46] Wagner, H., Lourie, O, Feldman, Y, Tenne, R, Stress-induced fragmentation of multiwall carbon nanotubes in a polymer matrix, Applied physics letters, 72 (1998) 188-190.

[47] Yu, M.F., Lourie, O., Dyer, M.J., Moloni, K., Kelly, T.F., Ruoff, R.S., Strength and breaking mechanism of multiwalled carbon nanotubes under tensile load, Science, 287 (2000) 637-640.

[48] Demczyk, B.G., Wang, Y.M., Cumings, J., Hetman, M., Han, W., Zettl, A.*, et al.*, Direct mechanical measurement of the tensile strength and elastic modulus of multiwalled carbon nanotubes, Materials Science and Engineering: A, 334 (2002) 173-178.

[49] Wong, E.W., Sheehan, P.E., Lieber, C.M., Nanobeam mechanics: Elasticity, strength, and toughness of nanorods and nanotubes, Science, 277 (1997) 1971-1975.

[50] Belytschko, T., Xiao, S., Schatz, G., Ruoff, R., Atomistic simulations of nanotube fracture, Physical Review B, 65 (2002) 235430.

[51] Wei, B., Vajtai, R, Ajayan, PM, Reliability and current carrying capacity of carbon nanotubes, Applied Physics Letters, 79 (2001) 1172-1174.

[52] Qiao, B., Xie, N., Meng, J., Yan, T., Feng, L., Zhong, J., Percolation effect on the piezoresistivity of carbon nanotube/cement composite as a stress self-sensing material, Journal of Testing and Evaluation, 44 (2016).

[53] Tombler, T.W., Zhou, C., Alexseyev, L., Kong, J., Dai, H., Liu, L.*, et al.*, Reversible electromechanical characteristics of carbon nanotubes under local-probe manipulation, Nature, 405 (2000) 769-772.

[54] Pop, E., Mann, David, Wang, Qian, Goodson, Kenneth, Dai, Hongjie, Thermal conductance of an individual single-wall carbon nanotube above room temperature, Nano letters, 6 (2006) 96-100.

[55] Kim, P., Shi, Li, Majumdar, A, McEuen, PL, Thermal transport measurements of individual multiwalled nanotubes, Physical review letters, 87 (2001) 215502.

[56] Collins, P.G., Avouris, Phaedon, Nanotubes for electronics, Scientific american, 283 (2000) 62-69.

[57] Makar, J., Beaudoin, J., Carbon nanotubes and their application in the construction industry, Special Publication-Royal Society of Chemistry, 292 (2004) 331-342.

[58] Chen, S., Collins, FG, Macleod, AJN, Pan, Zhu, Duan, WH, Wang, CM, Carbon nanotube–cement composites: A retrospect, The IES Journal Part A: Civil & Structural Engineering, 4 (2011) 254-265.

[59] Han, B., Sun, Shengwei, Ding, Siqi, Zhang, Liqing, Yu, Xun, Ou, Jinping, Review of nanocarbon-engineered multifunctional cementitious composites, Composites Part A: Applied Science and Manufacturing, 70 (2015) 69-81.

[60] Sobolkina, A., Mechtcherine, V., Khavrus, V., Maier, D., Mende, M., Ritschel, M.*, et al.*, Dispersion of carbon nanotubes and its influence on the mechanical properties of the cement matrix, Cement and Concrete Composites, 34 (2012) 1104-1113.

[61] Cota, F.D.P., Panzera, T.H., Schiavon, M.A., Christoforo, A.L., Borges, P.H.R., Bowen, C., *et al.*, Full factorial design analysis of carbon nanotube polymer-cement composites, Materials Research, 15 (2012) 573-580.

[62] Tamimi, A., Hassan, N.M., Fattah, K., Talachi, A., Performance of cementitious materials produced by incorporating surface treated multiwall carbon nanotubes and silica fume, Construction and Building Materials, 114 (2016) 934-945.

[63] Kang, S.T., Seo, J.Y., Park, S.H., The characteristics of CNT/cement composites with acid-treated MWCNTs, Advances in Materials Science and Engineering, 2015 (2015) 1-9.

[64] Chaipanich, A., Nochaiya, T., Wongkeo, W., Torkittikul, P., Compressive strength and microstructure of carbon nanotubes–fly ash cement composites, Materials Science and Engineering: A, 527 (2010) 1063-1067.

[65] Morsy, M.S., Alsayed, S.H., Aqel, M., Hybrid effect of carbon nanotube and nano-clay on physico-mechanical properties of cement mortar, Construction and Building Materials, 25 (2011) 145-149.

[66] Sun, G., Liang, R., Lu, Z., Zhang, J., Li, Z., Mechanism of cement/carbon nanotube composites with enhanced mechanical properties achieved by interfacial strengthening, Construction and Building Materials, 115 (2016) 87-92.

[67] Kim, S.W., Kim, T., Kim, Y.S., Choi, H.S., Lim, H.J., Yang, S.J., *et al.*, Surface modifications for the effective dispersion of carbon nanotubes in solvents and polymers, Carbon, 50 (2012) 3-33.

[68] Chen, S.J., Zou, B., Collins, F., Zhao, X.L., Majumber, M., Duan, W.H., Predicting the influence of ultrasonication energy on the reinforcing efficiency of carbon nanotubes, Carbon, 77 (2014) 1-10.

[69] Pierard, N., Fonseca, A., Konya, Z., Willems, I., Van Tendeloo, G., Nagy, J.B., Production of short carbon nanotubes with open tips by ball milling, Chemical physics letters, 335 (2001) 1-8.

[70] Bentz, D.P., Garboczi, E.J., Haecker, C.J., Jensen, O.M., Effects of cement particle size distribution on performance properties of portland cement-based materials, Cement and Concrete Research, 29 (1999) 1663-1671.

[71] Kumar Mehta, P., Durability-critical issues for the future, CANMET/ACI. Séminaire international, 2000.

[72] Makar, J.M., Margeson, J.C., Luh, J., Carbon nanotube/cement composites-early results and potential applications, 3rd International Conference on Construction Materials: Performance, Innovations and Structural Implications, Vancouver, B.C., Canada, 2005, pp. 1-10.

[73] Hunashyal, A., Sundeep, G.V., Quadri, S.S., Banapurmath, N.R., Experimental investigations to study the effect of carbon nanotubes reinforced in cement-based matrix composite beams, Proceedings of the Institution of Mechanical Engineers, Part N: Journal of Nanoengineering and Nanosystems, (2011) 17-22.

[74] Sun, S., Yu, X., Han, B., Ou, J., In situ growth of carbon nanotubes/carbon nanofibers on cement/mineral admixture particles: A review, Construction and Building Materials, 49 (2013) 835-840.

[75] Ludvig, P., Calixto, J.M., Ladeira, L.O., Gaspar, I.C.P., Using converter dust to produce low cost cementitious composites by in situ carbon nanotube and nanofiber synthesis, Materials, 4 (2011) 575-584.

[76] Cwirzen, A., Habermehl-Cwirzen, K., Nasibulina, L.I., Shandakov, S.D., Nasibulin, A.G., Kauppinen, E.I.*, et al.*, CHH cement composite, Nanotechnology in construction 3, Springer2009, pp. 181-185.

[77] Nasibulina, L., Anoshkin, I., Shandakov, S., Nasibulin, A., Cwirzen, A., Mudimela, P.*, et al.*, Direct synthesis of carbon nanofibers on cement particles, Transportation Research Record: Journal of the Transportation Research Board, (2010) 96-101.

[78] Nasibulin, A.G., Shandakov, S.D., Nasibulina, L.I., Cwirzen, A., Mudimela, P.R., Habermehl-Cwirzen, K.*, et al.*, A novel cement-based hybrid material, New Journal of Physics, 11 (2009) 1-10.

[79] Cwirzen, A., Habermehl-Cwirzen, K., Shandakov, D., Nasibulina, L.I., Nasibulin, A.G., Mudimela, P.R.*, et al.*, Properties of high yield synthesised carbon nano fibres/portland cement composite, Advances in Cement Research, 21 (2009) 141-146.

[80] Mudimela, P.R., Nasibulina, L.I., Nasibulin, A.G., Cwirzen, A., Valkeapää, M., Habermehl-Cwirzen, K.*, et al.*, Synthesis of carbon nanotubes and nanofibers on silica and cement matrix materials, Journal of Nanomaterials, 2009 (2009) 1-4.

[81] Nasibulin, A.G., Koltsova, T., Nasibulina, L.I., Anoshkin, I.V., Semencha, A., Tolochko, O.V.*, et al.*, A novel approach to composite preparation by direct synthesis of carbon nanomaterial on matrix or filler particles, Acta Materialia, 61 (2013) 1862-1871.

[82] Hlavacek, P., Smilauer, V., Fracture properties of cementitious composites reinforced with carbon nanofibers/nanotubes, Eng Mech, 211 (2012) 391-397.

[83] HLAVACEK, P., Smilauer, V., Padevet, P., Nasibulina, L.I., Nasibulin, A.G., Cement grains with surface-shyntetized carbon nanofibres: Mechanical properties and

nanostructure, 3rd International Conference NANOCON, Brno, Czech Republic, 2011, pp. 75-80.

[84] Ghaharpour, F., Bahari, A., Abbasi, M., Ashkaran, A.A., Parametric investigation of CNT deposition on cement by cvd process, Construction and Building Materials, 113 (2016) 523-535.

[85] Dunens, O.M., MacKenzie, K.J., Harris, A.T., Synthesis of multiwalled carbon nanotubes on fly ash derived catalysts, Environmental science & technology, 43 (2009) 7889-7894.

[86] Liu, Z., Wang, J., Kushvaha, V., Poyraz, S., Tippur, H., Park, S.H., *et al.*, Poptube approach for ultrafast carbon nanotube growth, Chemical Communications, 47 (2011) 9912-9914.

[87] Zhang, X., Liu, Z., Recent advances in microwave initiated synthesis of nanocarbon materials, Nanoscale, 4 (2012) 707-714.

[88] Strano, M.S., Moore, V.C., Miller, M.K., Allen, M.J., Haroz, E.H., Kittrell, C., *et al.*, The role of surfactant adsorption during ultrasonication in the dispersion of single-walled carbon nanotubes, Journal of Nanoscience and Nanotechnology, 3 (2003) 81-86.

[89] Hilding, J., Grulke, E.A., George Zhang, Z., Lockwood, F., Dispersion of carbon nanotubes in liquids, Journal of dispersion science and technology, 24 (2003) 1-41.

[90] Huang, Y.Y., Terentjev, E.M., Dispersion of carbon nanotubes: Mixing, sonication, stabilization, and composite properties, Polymers, 4 (2012) 275-295.

[91] Chuah, S., Pan, Zhu, Sanjayan, Jay G, Wang, Chien Ming, Duan, Wen Hui, Nano reinforced cement and concrete composites and new perspective from graphene oxide, Construction and Building Materials, 73 (2014) 113-124.

[92] Cwirzen, A., Habermehl-Cwirzen, K., Penttala, V., Surface decoration of carbon nanotubes and mechanical properties of cement/carbon nanotube composites, Advances in cement research, 20 (2008) 65-73.

[93] Parveen, S., Rana, S., Fangueiro, R., Paiva, M.C., Microstructure and mechanical properties of carbon nanotube reinforced cementitious composites developed using a novel dispersion technique, Cement and Concrete Research, 73 (2015) 215-227.

[94] Collins, F., Lambert, J., Duan, W.H., The influences of admixtures on the dispersion, workability, and strength of carbon nanotube–OPC paste mixtures, Cement and Concrete Composites, 34 (2012) 201-207.

[95] Makar, J., The effect of SWCNT and other nanomaterials on cement hydration and reinforcement, Nanotechnology in civil infrastructure, Springer2011, pp. 103-130.

[96] Makar, J.M., Chan, Gordon W, Growth of cement hydration products on single-walled carbon nanotubes, Journal of the American Ceramic Society, 92 (2009) 1303-1310.

[97] Fakhim, B., Hassani, A., Rashidi, A., Ghodousi, P., Preparation and microstructural properties study on cement composites reinforced with multi-walled carbon nanotubes, Journal of Composite Materials, 49 (2015) 85-98.

[98] Li, G.Y., Wang, P.M., Zhao, X., Mechanical behavior and microstructure of cement composites incorporating surface-treated multi-walled carbon nanotubes, Carbon, 43 (2005) 1239-1245.

[99] Hu, Y., Luo, D., Li, P., Li, Q., Sun, G., Fracture toughness enhancement of cement paste with multi-walled carbon nanotubes, Construction and Building Materials, 70 (2014) 332-338.

[100] Kowald, T., Trettin, R, Influence of surface-modified carbon nanotubes on ultrahigh performance concrete, Proceedings of International Symposium on Ultra High Performance Concrete, 2004, pp. 195-203.

[101] Rhee, I., Roh, Y.-S., Properties of normal-strength concrete and mortar with multi-walled carbon nanotubes, Magazine of Concrete Research, 65 (2013) 951-961.

[102] Kelly, A., Tyson, A.W., Tensile properties of fibre-reinforced metals: Copper/tungsten and copper/molybdenum, Journal of the Mechanics and Physics of Solids, 13 (1965) 329-350.

[103] Halpin, J., Kardos, J., The halpin-tsai equations: A review, Polymer Engineering & Science, 16 (1976) 344-352.

[104] Pukanszky, B., Influence of interface interaction on the ultimate tensile properties of polymer composites, Composites, 21 (1990) 255-262.

[105] Zare, Y., Effects of interphase on tensile strength of polymer/cnt nanocomposites by Kelly–Tyson theory, Mechanics of Materials, 85 (2015) 1-6.

[106] Chen, B., Kondoh, K., Imai, H., Umeda, J., Takahashi, M., Simultaneously enhancing strength and ductility of carbon nanotube/aluminum composites by improving bonding conditions, Scripta Materialia, 113 (2016) 158-162.

[107] Chen, B., Shen, J., Ye, X., Jia, L., Li, S., Umeda, J.*, et al.*, Length effect of carbon nanotubes on the strengthening mechanisms in metal matrix composites, Acta Materialia, 140 (2017) 317-325.

[108] Lachman, N., Wiesel, E., de Villoria, R.G., Wardle, B.L., Wagner, H.D., Interfacial load transfer in carbon nanotube/ceramic microfiber hybrid polymer composites, Composites Science and Technology, 72 (2012) 1416-1422.

[109] Liao, J.-z., Tan, M.-J., Sridhar, I., Spark plasma sintered multi-wall carbon nanotube reinforced aluminum matrix composites, Materials & Design, 31 (2010) S96-S100.

[110] Wang, B., Han, Y., Zhang, T., Reinforcement of surface-modified multi-walled carbon nanotubes on cement-based composites, Advances in Cement Research, 26 (2014) 77-84.

[111] Gdoutos, E.E., Konsta-Gdoutos, M.S., Danoglidis, P.A., Shah, S.P., Advanced cement based nanocomposites reinforced with MWCNTs and CNFs, Frontiers of Structural and Civil Engineering, 10 (2016) 142-149.

[112] Danoglidis, P.A., Falara, M.G., Katotriotou, M.K., Konsta-Gdoutos, M.S., Gdoutos, E.E., MWCNT and CNF cementitious nanocomposites for enhanced strength and toughness, Mechanics of Composite and Multi-functional Materials, 7 (2016) 241-246.

[113] Metaxa, Z.S., Seo, J.W.T., Konsta-Gdoutos, M.S., Hersam, M.C., Shah, S.P., Highly concentrated carbon nanotube admixture for nano-fiber reinforced cementitious materials, Cement and Concrete Composites, 34 (2012) 612-617.

[114] Wang, B., Han, Y., Liu, S., Effect of highly dispersed carbon nanotubes on the flexural toughness of cement-based composites, Construction and Building Materials, 46 (2013) 8-12.

[115] Nasibulina, L.I., Anoshkin, I.V., Nasibulin, A.G., Cwirzen, A., Penttala, V., Kauppinen, E.I., Effect of carbon nanotube aqueous dispersion quality on mechanical properties of cement composite, Journal of Nanomaterials, 2012 (2012) 1-6.

[116] Kumar, S., Kolay, P., Malla, S., Mishra, S., Effect of multiwalled carbon nanotubes on mechanical strength of cement paste, Journal of Materials in Civil Engineering, 24 (2012) 84-91.

[117] Musso, S., Tulliani, J.M., Ferro, G., Tagliaferro, A., Influence of carbon nanotubes structure on the mechanical behavior of cement composites, Composites Science and Technology, 69 (2009) 1985-1990.

[118] Manzur, T., Yazdani, N., Strength enhancement of cement mortar with carbon nanotubes: Early results and potential, Transportation Research Record: Journal of the Transportation Research Board, (2010) 102-108.

[119] Fawaz, J., Mittal, V., Polymer nanotube nanocomposites: A review of synthesis methods, properties and applications, Polymer nanotube nanocomposites: Synthesis, properties, and applications, John Wiley & Sons,2014, pp. 1-44.

[120] Park, S.H., Bandaru, P.R., Improved mechanical properties of carbon nanotube/polymer composites through the use of carboxyl-epoxide functional group linkages, Polymer, 51 (2010) 5071-5077.

[121] Tyson, B.M., Carbon nanotube and nanofiber reinforcement for improving the flexural strength and fracture toughness of portland cement paste, Texas A&M University, 2010.

[122] Bakshi, S.R., Agarwal, A., An analysis of the factors affecting strengthening in carbon nanotube reinforced aluminum composites, Carbon, 49 (2011) 533-544.

[123] Swamy, R., Mangat, P., A theory for the flexural strength of steel fiber reinforced concrete, Cement and Concrete Research, 4 (1974) 313-325.

[124] Tassew, S., Lubell, A., Mechanical properties of glass fiber reinforced ceramic concrete, Construction and Building Materials, 51 (2014) 215-224.

[125] Teng, T.-L., Chu, Y.-A., Chang, F.-A., Chin, H.-S., Calculating the elastic moduli of steel-fiber reinforced concrete using a dedicated empirical formula, Computational materials science, 31 (2004) 337-346.

[126] Fu, S.-Y., Feng, X.-Q., Lauke, B., Mai, Y.-W., Effects of particle size, particle/matrix interface adhesion and particle loading on mechanical properties of particulate–polymer composites, Composites Part B: Engineering, 39 (2008) 933-961.

[127] Kurita, H., Estili, M., Kwon, H., Miyazaki, T., Zhou, W., Silvain, J.-F*., et al.*, Load-bearing contribution of multi-walled carbon nanotubes on tensile response of aluminum, Composites Part A: Applied Science and Manufacturing, 68 (2015) 133-139.

[128] Tjong, S.C., Carbon nanotube reinforced composites: Metal and ceramic matrices, John Wiley & Sons2009.

[129] Shokrieh, M.M., Rafiee, R., Investigation of nanotube length effect on the reinforcement efficiency in carbon nanotube based composites, Composite Structures, 92 (2010) 2415-2420.

[130] Chowdhury, S., Haque, B.G., Okabe, T., Gillespie Jr, J., Modeling the effect of statistical variations in length and diameter of randomly oriented cnts on the properties of CNT reinforced nanocomposites, Composites Part B: Engineering, 43 (2012) 1756-1762.

[131] Agarwal, B.D., Broutman, L.J., Chandrashekhara, K., Analysis and performance of fiber composites, John Wiley & Sons2017.

[132] Thostenson, E.T., Chou, T.-W., On the elastic properties of carbon nanotube-based composites: Modelling and characterization, Journal of Physics D: Applied Physics, 36 (2003) 573.

[133] Krenchel, H., Fibre reinforcement; theoretical and practical investigations of the elasticity and strength of fibre-reinforced materials, Akademisk Forlag, (1964).

[134] Rosenthal, J., A model for determining fiber reinforcement efficiencies and fiber orientation in polymer composites, Polymer composites, 13 (1992) 462-466.

[135] Yeh, M.-K., Tai, N.-H., Liu, J.-H., Mechanical behavior of phenolic-based composites reinforced with multi-walled carbon nanotubes, Carbon, 44 (2006) 1-9.

[136] Montazeri, A., Javadpour, J., Khavandi, A., Tcharkhtchi, A., Mohajeri, A., Mechanical properties of multi-walled carbon nanotube/epoxy composites, Materials & Design, 31 (2010) 4202-4208.

[137] Tai, N.-H., Yeh, M.-K., Peng, T.-H., Experimental study and theoretical analysis on the mechanical properties of SWCNTs/phenolic composites, Composites Part B: Engineering, 39 (2008) 926-932.

[138] Hawreen, A., Bogas, J., Guedes, M., Pereira, M., Dispersion and reinforcement efficiency of carbon nanotubes in cementitious composites, Magazine of Concrete Research, (2018) 1-57.

[139] Nicolais, L., Narkis, M., Stress-strain behavior of styrene-acrylonitrile/glass bead composites in the glassy region, Polymer Engineering & Science, 11 (1971) 194-199.

[140] Zare, Y., Daraei, A., Vatani, M., Aghasafari, P., An analysis of interfacial adhesion in nanocomposites from recycled polymers, Computational Materials Science, 81 (2014) 612-616.

[141] Bilotti, E., Zhang, R., Deng, H., Quero, F., Fischer, H., Peijs, T., Sepiolite needle-like clay for pa6 nanocomposites: An alternative to layered silicates?, Composites Science and Technology, 69 (2009) 2587-2595.

[142] Ramezani, M., Kim, Y.H., Sun, Z., Modeling the mechanical properties of cementitious materials containing CNTs, Cement and Concrete Composites, 104 (2019) 1-21.

[143] Lazzeri, A., Phuong, V.T., Dependence of the pukánszky's interaction parameter b on the interface shear strength (IFSS) of nanofiller-and short fiber-reinforced polymer composites, Composites Science and Technology, 93 (2014) 106-113.

[144] Cox, H., The elasticity and strength of paper and other fibrous materials, British journal of applied physics, 3 (1952) 72.

[145] Mori, T., Tanaka, K., Average stress in matrix and average elastic energy of materials with misfitting inclusions, Acta metallurgica, 21 (1973) 571-574.

[146] Taya, M., Arsenault, R., A comparison between a shear lag type model and an Eshelby type model in predicting the mechanical properties of a short fiber composite, Scripta Metallurgica, 21 (1987) 349-354.

[147] Kim, H.G., Kwac, L.K., Evaluation of elastic modulus for unidirectionally aligned short fiber composites, Journal of Mechanical Science and Technology, 23 (2009) 54-63.

[148] Mouritz, A.P., Gibson, A.G., Fire properties of polymer composite materials, Springer Science & Business Media, (2007).

[149] De Villoria, R.G., Miravete, A., Mechanical model to evaluate the effect of the dispersion in nanocomposites, Acta Materialia, 55 (2007) 3025-3031.

[150] Hill, R., Theory of mechanical properties of fibre-strengthened materials—iii. Self-consistent model, Journal of the Mechanics and Physics of Solids, 13 (1965) 189-198.

[151] Chow, T., Hermans, J., The elastic constants of fiber reinforced materials, Journal of Composite materials, 3 (1969) 382-396.

[152] Nochaiya, T., Chaipanich, Arnon, Behavior of multi-walled carbon nanotubes on the porosity and microstructure of cement-based materials, Applied Surface Science, 257 (2011) 1941-1945.

[153] Yakovlev, G., Pervushin, G., Maeva, I., Keriene, J., Pudov, I., Shaybadullina, A.*, et al.*, Modification of construction materials with multi-walled carbon nanotubes, Procedia Engineering, 57 (2013) 407-413.

[154] Wang, X., Rhee, Inkyu, Wang, Yao, Xi, Yunping, Compressive strength, chloride permeability, and freeze-thaw resistance of mwnt concretes under different chemical treatments, The Scientific World Journal, 2014 (2014).

[155] Chen, P.-W., Chung, D., Effect of polymer addition on the thermal stability and thermal expansion of cement, Cement and concrete research, 25 (1995) 465-469.

[156] Xuli, F., Chung, D., Effect of methylcellulose admixture on the mechanical properties of cement, Cement and Concrete Research, 26 (1996) 535-538.

[157] Mahajan, A., Kingon, A., Kukovecz, Á., Konya, Z., Vilarinho, P.M., Studies on the thermal decomposition of multiwall carbon nanotubes under different atmospheres, Materials Letters, 90 (2013) 165-168.

[158] Amin, M.S., El-Gamal, S.M.A., Hashem, F.S., Fire resistance and mechanical properties of carbon nanotubes–clay bricks wastes (homra) composites cement, Construction and Building Materials, 98 (2015) 237-249.

[159] El-Didamony, H., El-Rahman, E.A., Osman, R.M., Fire resistance of fired clay bricks–fly ash composite cement pastes, Ceramics International, 38 (2012) 201-209.

[160] Mehta, K., Monteiro, P., Concrete: Microstructure, properties, and materials, McGraw-Hill, (2006).

[161] Shafaatian, S.M., Akhavan, Alireza, Maraghechi, Hamed, Rajabipour, Farshad, How does fly ash mitigate alkali–silica reaction (ASR) in accelerated mortar bar test (ASTM C1567)?, Cement and Concrete Composites, 37 (2013) 143-153.

[162] Chatterji, S., The role of $Ca(OH)^2$ in the breakdown of portland cement concrete due to alkali-silica reaction, Cement and concrete research, 9 (1979) 185-188.

[163] Hobbs, D.W., Alkali-silica reaction in concrete, Thomas Telford Publishing, (1988).

[164] Vaganov, V., Popov, M., Korjakins, A., Šahmenko, G., Effect of CNT on microstructure and minearological composition of lightweight concrete with granulated foam glass, Procedia Engineering, 172 (2017) 1204-1211.

[165] Aly, M., Hashmi, M., Olabi, A., Messeiry, M., Hussain, A., Effect of nano clay particles on mechanical, thermal and physical behaviours of waste-glass cement mortars, Materials Science and Engineering: A, 528 (2011) 7991-7998.

[166] Peyvandi, A., Holmes, Daniel, Soroushian, Parviz, Balachandra, Anagi M, Fundamental assessment of graphite nanoplatelet effects on progress of alkali-silica reactions, ACI Materials Journal, 112 (2015).

[167] Tazawa, E.-i., Autogenous shrinkage of concrete, CRC Press, (1999).

[168] Metaxa, Z., Konsta-Gdoutos, MS, Shah, SP, Crack free concrete made with nanofiber reinforcement, Developing a Research Agenda for Transportation Infrastructure Preservation and Renewal Conference, 2009.

[169] Blandine, F., Habermehi-Cwirzen, K., Cwirzen, A., Contribution of CNTs/CNFs morphology to reduction of autogenous shrinkage of portland cement paste, Frontiers of Structural and Civil Engineering, (2016) 1-12.

[170] Hawreen, A., Bogas, J., Dias, A., On the mechanical and shrinkage behavior of cement mortars reinforced with carbon nanotubes, Construction and Building Materials, 168 (2018) 459-470.

[171] Isfahani, F.T., Li, W., Redaelli, E., Dispersion of multi-walled carbon nanotubes and its effects on the properties of cement composites, Cement and Concrete Composites, 74 (2016) 154-163.

[172] Hawreen, A., Bogas, J., Creep, shrinkage and mechanical properties of concrete reinforced with different types of carbon nanotubes, Construction and Building Materials, 198 (2019) 70-81.

[173] Chen, X., Wu, S., Zhou, J., Influence of porosity on compressive and tensile strength of cement mortar, Construction and Building Materials, 40 (2013) 869-874.

[174] Hassan, N.M., Fattah, K.P., Tamimi, A.K., Modelling mechanical behavior of cementitious material incorporating CNTs using design of experiments, Construction and Building Materials, 154 (2017) 763-770.

[175] Siddique, R., Mehta, Ankur, Effect of carbon nanotubes on properties of cement mortars, Construction and Building Materials, 50 (2014) 116-129.

[176] Yu, J., Grossiord, N., Koning, C.E., Loos, J., Controlling the dispersion of multi-wall carbon nanotubes in aqueous surfactant solution, Carbon, 45 (2007) 618-623.

[177] Grossiord, N., Regev, O., Loos, J., Meuldijk, J., Koning, C.E., Time-dependent study of the exfoliation process of carbon nanotubes in aqueous dispersions by using uv-visible spectroscopy, Analytical chemistry, 77 (2005) 5135-5139.

[178] Lu, K., Lago, R., Chen, Y., Green, M., Harris, P., Tsang, S., Mechanical damage of carbon nanotubes by ultrasound, Carbon, 34 (1996) 814-816.

[179] Kerr, C., Huang, Y., Marshall, J., Terentjev, E., Effect of filament aspect ratio on the dielectric response of multiwalled carbon nanotube composites, Journal of Applied Physics, 109 (2011) 094109.

[180] Huang, Y.Y., Knowles, T.P., Terentjev, E.M., Strength of nanotubes, filaments, and nanowires from sonication-induced scission, Advanced Materials, 21 (2009) 3945-3948.

[181] Ayatollahi, M., Shadlou, S., Shokrieh, M., Chitsazzadeh, M., Effect of multi-walled carbon nanotube aspect ratio on mechanical and electrical properties of epoxy-based nanocomposites, Polymer Testing, 30 (2011) 548-556.

[182] Martone, A., Formicola, C., Giordano, M., Zarrelli, M., Reinforcement efficiency of multi-walled carbon nanotube/epoxy nano composites, Composites science and technology, 70 (2010) 1154-1160.

[183] Poh, L., Della, C., Ying, S., Goh, C., Li, Y., Micromechanics model for predicting effective elastic moduli of porous ceramic matrices with randomly oriented carbon nanotube reinforcements, AIP Advances, 5 (2015) 097153.

[184] Manzur, T., Yazdani, N., Emon, M.A.B., Effect of carbon nanotube size on compressive strengths of nanotube reinforced cementitious composites, Journal of Materials, 2014 (2014) 1-8.

[185] Jang, S.H., Kawashima, S., Yin, H., Influence of carbon nanotube clustering on mechanical and electrical properties of cement pastes, Materials, 9 (2016) 1-11.

[186] Kumar, K.S., Nair, C.P., Ninan, K.N., Effect of fiber length and composition on mechanical properties of carbon fiber-reinforced polybenzoxazine, Polymers for Advanced Technologies, 19 (2008) 895-904.

[187] Chen, Y.L., Liu, B., He, X.Q., Huang, Y., Hwang, K.C., Failure analysis and the optimal toughness design of carbon nanotube-reinforced composites, Composites Science and Technology, 70 (2010) 1360-1367.

[188] Wichmann, M.H.G., Schulte, K., Wagner, H.D., On nanocomposite toughness, Composites Science and Technology, 68 (2008) 329-331.

[189] Nochaiya, T., Tolkidtikul, P, Singjai, P., Chaipanich, A., Microstructure and characterizations of portland-carbon nanotubes pastes, Advanced Materials Research, Trans Tech Publ, 2008, pp. 549-552.

[190] Cwirzen, A., Habermehl-Cwirzen, K., The effect of carbon nano-and microfibers on strength and residual cumulative strain of mortars subjected to freeze-thaw cycles, Journal of Advanced Concrete Technology, 11 (2013) 80-88.

[191] Cheng, Q., Debnath, S., Gregan, E., Byrne, H.J., Ultrasound-assisted SWNTs dispersion: Effects of sonication parameters and solvent properties, The Journal of Physical Chemistry C, 114 (2010) 8821-8827.

[192] Chen, S.J., Zou, Bo, Collins, Frank, Zhao, Xiao Ling, Majumber, Mainak, Duan, Wen Hui, Predicting the influence of ultrasonication energy on the reinforcing efficiency of carbon nanotubes, Carbon, 77 (2014) 1-10.

[193] Yazdanbakhsh, A., Grasley, Z., Tyson, B., Al-Rub, R.A., Challenges and benefits of utilizing carbon nanofilaments in cementitious materials, Journal of Nanomaterials, 2012 (2012) 19.

[194] Yazdanbakhsh, A., Grasley, Zachary, Tyson, Bryan, Abu Al-Rub, Rashid, Distribution of carbon nanofibers and nanotubes in cementitious composites,

Transportation Research Record: Journal of the Transportation Research Board, (2010) 89-95.

[195] ASTM C150. Standard specification for portland cement, ASTM International, West Conshohocken, PA, USA, (2009).

[196] Taylor, H.F., Cement chemistry, Thomas Telford1997.

[197] ASTM C494. Standard specification for chemical admixtures for concrete, ASTM International, West Conshohocken, PA, USA, (2005).

[198] ASTM C1017. Standard specification for chemical admixtures for use in producing flowing concrete, ASTM International, West Conshohocken, PA, USA, (2003).

[199] ASTM C1260. Standard test method for potential alkali reactivity of aggregates (mortar-bar method), ASTM International, West Conshohocken, PA, USA, (2014).

[200] ASTM C778. Standard specification for standard sand, ASTM International, West Conshohocken, PA, USA, (2006).

[201] ASTM C33. Standard specification for concrete aggregates, ASTM International, West Conshohocken, PA, USA, (2013).

[202] ASTM C305. Standard practice for mechanical mixing of hydraulic cement pastes and mortars of plastic consistency, ASTM International, West Conshohocken, PA, USA, (2006).

[203] ASTM C1437. Standard test method for flow of hydraulic cement mortar, ASTM International, West Conshohocken, PA, USA, (2007).

[204] Tattersall, G.H., Banfill, P.F., The rheology of fresh concrete, 1983.

[205] Ferraris, C.F., Measurement of the rheological properties of high performance concrete: State of the art report, Journal of Research-National Institute of Standards and Technology, 104 (1999) 461-478.

[206] Yahia, A., Khayat, KH, Applicability of rheological models to high-performance grouts containing supplementary cementitious materials and viscosity enhancing admixture, Materials and Structures, 36 (2003) 402-412.

[207] ASTM C109. Standard test method for compressive strength of hydraulic cement mortars (using 2-in. or [50-mm] cube specimens, ASTM International, West Conshohocken, PA, USA, (2008).

[208] ASTM C348. Standard test method for flexural strength of hydraulic-cement mortars, ASTM International, West Conshohocken, PA, USA, (2008).

[209] ASTM C215. Standard test method for fundamental transverse, longitudinal, and torsional resonant frequencies of concrete specimens, ASTM International, West Conshohocken, PA, USA, (2002).

[210] Feys, D., Verhoeven, Ronny, De Schutter, Geert, Fresh self compacting concrete, a shear thickening material, Cement and Concrete Research, 38 (2008) 920-929.

[211] Cyr, M., Legrand, Claude, Mouret, Michel, Study of the shear thickening effect of superplasticizers on the rheological behaviour of cement pastes containing or not mineral additives, Cement and Concrete Research, 30 (2000) 1477-1483.

[212] Katz, A., Li, V.C., Kazmer, A., Bond properties of carbon fibers in cementitious matrix, Journal of materials in civil engineering, 7 (1995) 125-128.

[213] Ahmed, H., Bogas, J.A., Guedes, M., Mechanical behavior and transport properties of cementitious composites reinforced with carbon nanotubes, Journal of Materials in Civil Engineering, 30 (2018) 04018257.

[214] Sargolzahi, M., Kodjo, S.A., Rivard, P., Rhazi, J., Effectiveness of nondestructive testing for the evaluation of alkali–silica reaction in concrete, Construction and Building Materials, 24 (2010) 1398-1403.

[215] Chen, W., Brouwers, H., Alkali binding in hydrated portland cement paste, Cement and Concrete Research, 40 (2010) 716-722.

[216] Giaccio, G., Bossio, M., Torrijos, M., Zerbino, R., Contribution of fiber reinforcement in concrete affected by alkali–silica reaction, Cement and Concrete Research, 67 (2015) 310-317.

[217] Giaccio, G., Zerbino, R., Ponce, J., Batic, O.R., Mechanical behavior of concretes damaged by alkali-silica reaction, Cement and Concrete Research, 38 (2008) 993-1004.

[218] Park, S.-B., Lee, B.-C., Studies on expansion properties in mortar containing waste glass and fibers, Cement and concrete research, 34 (2004) 1145-1152.

[219] Gardoni, P., Kiureghian, A.D., Mosalam, K.M., Probabilistic capacity models and fragility estimates for reinforced concrete columns based on experimental observations, Journal of Engineering Mechanics, 128 (2002) 1024-1038.

[220] Cox, R.T., Probability, frequency and reasonable expectation, American journal of physics, 14 (1946) 1-13.

[221] Box, G.E., Tiao, G.C., Bayesian inference in statistical analysis, John Wiley & Sons2011.

[222] Gardoni, P., Trejo, D., Kim, Y.H., Time-variant strength capacity model for GFRP bars embedded in concrete, Journal of Engineering Mechanics, 139 (2013) 1435-1445.

[223] Lopez, R.H., Beck, A.T., Reliability-based design optimization strategies based on form: A review, Journal of the Brazilian Society of Mechanical Sciences and Engineering, 34 (2012) 506-514.

[224] Ditlevsen, O., Madsen, H.O., Structural reliability methods, Wiley New York1996.

[225] Hohenbichler, M., Rackwitz, R., Sensitivity and importance measures in structural reliability, Civil Engineering Systems, 3 (1986) 203-209.

[226] Choe, D.E., Gardoni, P., Rosowsky, D., Closed-form fragility estimates, parameter sensitivity, and bayesian updating for RC columns, Journal of engineering mechanics, 133 (2007) 833-843.

[227] Der Kiureghian, A., Ke, J., Finite-element based reliability analysis of frame structures, Proc. 4th Int. Conference on Structural Safety and Reliability, 1985, pp. 395-404.

[228] Gerstenberg, T., Tenenbaum, J.B., Intuitive theories, Oxford handbook of causal reasoning, (2017) 515-548.

[229] Al-Dahawi, A., Sarwary, M.H., Öztürk, O., Yıldırım, G., Akın, A., Şahmaran, M.*, et al.*, Electrical percolation threshold of cementitious composites possessing self-sensing functionality incorporating different carbon-based materials, Smart Materials and Structures, 25 (2016) 105005.

[230] Al-Dahawi, A., Yıldırım, G., Öztürk, O., Şahmaran, M., Assessment of self-sensing capability of engineered cementitious composites within the elastic and plastic ranges of cyclic flexural loading, Construction and Building Materials, 145 (2017) 1-10.

[231] Nishida, I., Precipitation of calcium carbonate by ultrasonic irradiation, Ultrasonics Sonochemistry, 11 (2004) 423-428.

[232] Mohod, A.V., Gogate, P.R., Ultrasonic degradation of polymers: Effect of operating parameters and intensification using additives for carboxymethyl cellulose (CMC) and polyvinyl alcohol (PVA), Ultrasonics Sonochemistry, 18 (2011) 727-734.

[233] ACI Committee 209-2R. Guide for modeling and calculating shrinkage and creep in hardened concrete, American Concrete Institute Farmington Hills, MI, 2008.

[234] Tabandeh, A., Gardoni, P., Probabilistic capacity models and fragility estimates for RC columns retrofitted with FRP composites, Engineering Structures, 74 (2014) 13-22.

[235] Kim, Y.H., Park, Y., Bai, J.-W., Probabilistic shear capacity models for concrete members with internal composite reinforcement, Journal of Composites for Construction, 21 (2016) 1-18.

[236] Burnham, K.P., Anderson, D.R., Multimodel inference: Understanding AIC and BIC in model selection, Sociological methods & research, 33 (2004) 261-304.

[237] Li, W.W., Ji, W.M., Wang, Y.C., Liu, Y., Shen, R.X., Xing, F., Investigation on the mechanical properties of a cement-based material containing carbon nanotube under drying and freeze-thaw conditions, Materials, 8 (2015) 8780-8792.

[238] Elkashef, M., Wang, K., Abou-Zeid, M.N., Acid-treated carbon nanotubes and their effects on mortar strength, Frontiers of Structural and Civil Engineering, (2015) 1-9.

[239] Nochaiya, T., Tolkidtikul, P., Singjai, P., Chaipanich, A., Microstructure and characterizations of portland-carbon nanotubes pastes, Advanced Materials Research, 55 (2008) 549-552.

[240] Luo, J., Duan, Z., Li, H., The influence of surfactants on the processing of multi-walled carbon nanotubes in reinforced cement matrix composites, physica status solidi (a), 206 (2009) 2783-2790.

[241] Al-Rub, R.K.A., Tyson, B.M., Yazdanbakhsh, A., Grasley, Z., Mechanical properties of nanocomposite cement incorporating surface-treated and untreated carbon nanotubes and carbon nanofibers, Journal of Nanomechanics and Micromechanics, (2012) 1-6.

[242] Lelusz, M., Carbon nanotubes influence on the compressive strength of cement composites, Czasopismo Techniczne, (2015) 5-11.

[243] Choi, H., Kang, D., Seo, G., Chung, W., Effect of some parameters on the compressive strength of MWCNT-cement composites, Advances in Materials Science and Engineering, 2015 (2015) 1-8.

[244] Petrunin, S., Vaganov, V., Sobolev, K., The effect of functionalized carbon nanotubes on the performance of cement composites, 5th International Conference NANOCON, Brno, Czech Republic, (2013), 1-5.

APPENDIX A. DATABASE

This section presents the database used in different parts of this research.

Table A-1. Database used to Identify Optimum Ranges of CNT Properties

Ref.	CNTs					*w/c* ratio	Dispersion method		Age (days)	Mechanical Properties Percent Change (%)							
	Type	$\bar{\kappa}$ (c-wt%)	$\bar{L}$ (μm)	$\bar{d}$ (nm)	$\overline{AR}$					CS	DC	FS	DF	E	DE	T	DT
[26]	MWCNTs	0.03	10	30	333.3	0.2	Nanosand mill + PVP + TP		7	4.6	G	5.1	G	-	-	-	-
		0.05							7	5.6	G	7.5	G	-	-	-	-
		0.1							7	2.9	B	3.3	B	-	-	-	-
		0.15							7	0.7	B	-0.7	B	-	-	-	-
		0.03							28	4.2	G	-	-	-	-	-	-
		0.05							28	4.6	G	-	-	-	-	-	-
		0.1							28	2.1	B	-	-	-	-	-	-
		0.15							28	-2	B	-	-	-	-	-	-
[20]	MWCNTs	0.15	10	26	384.6	0.25	Diy mix + SP +	w/o SF	14	2	G	-	-	-	-	-	-
		0.15						10% SF		32	G	-	-	-	-	-	-
		0.15						20% SF		15	G	-	-	-	-	-	-
		0.15						30% SF		16	G	-	-	-	-	-	-
		0.3						w/o SF		-7	B	-	-	-	-	-	-
		0.3						10% SF		12	B	-	-	-	-	-	-
		0.3						20% SF		15	B	-	-	-	-	-	-
		0.3						30% SF		-6	B	-	-	-	-	-	-
[62]	MWCNTs	0.15	20	30	666.7	0.3	Diy mix +	w/o SF	14	6.5	G	-	-	-	-	-	-
	C-MWCNTs							w/o SF		8.7	G	-	-	-	-	-	-
	O-MWCNTs							w/o SF		8.7	G	-	-	-	-	-	-
	H-MWCNTs							w/o SF		13	G	-	-	-	-	-	-
	MWCNTs							15% SF		3.6	G	-	-	-	-	-	-
	C-MWCNTs							15% SF		3.6	G	-	-	-	-	-	-
	O-MWCNTs							15% SF		7.1	G	-	-	-	-	-	-
	H-MWCNTs							15% SF		12.5	G	-	-	-	-	-	-
	MWCNTs							30% SF		-5.1	B	33.8	G	-	-	-	-
	C-MWCNTs							30% SF		20.3	G	50.6	G	-	-	-	-
	O-MWCNTs							30% SF		15.2	G	47.4	G	-	-	-	-
	H-MWCNTs							30% SF		-16.94	B	30.4	G	-	-	-	-
[110]	MWCNTs	0.02	10	30	333.3	0.3	US + GA		28	2.7	G	25.5	G	-	-	35.5	G
		0.05								6.8	G	29.4	G	-	-	80.6	G
		0.08								17.8	G	39.2	G	-	-	151.6	G
		0.1								23.3	G	33.3	B	-	-	29	B
		0.12								16.4	B	15.7	B	-	-	22.6	B
		0.15								13.7	B	7.8	B	-	-	19.3	B
[97]	MWCNTs	0.1	10	50	200	0.4	US + SP		28	-	-	50.4 *	G	-	-	-	-

Ref.	CNTs					*w/c* ratio	Dispersion method	Age (days)	Mechanical Properties Percent Change (%)							
	Type	$\bar{\kappa}$ (*c-wt*%)	$\bar{L}$ (μm)	$\bar{d}$ (nm)	$\overline{AR}$				CS	DC	FS	DF	E	DE	T	DT
		0.3							-	-	69.2 *	G	-	-	-	-
		0.5							-	-	7.4 *	B	-	-	-	-
		1							-	-	-15.5 *	B	-	-	-	-
		1.5							-	-	-36.3 *	B	-	-	-	-
		2							-	-	-47 *	B	-	-	-	-
[237]	C-MWCNTs	0.1	20	15	1333.3	0.45	Ball millimg + SP	28	18.7	G	18.2	G	-	-	-	-
		0.3							22.9	G	21.2	G	-	-	-	-
		0.5							12.5	B	12.1	B	-	-	-	-
[98]	A-MWCNTs	0.5	0.5-500	20	-	0.45	Dry mix	28	18.9	G	25.1	G	-	-	-	-
[111, 112]	MWCNTs	0.1	> 10	32.5	307.7	0.485	US + SP	3	-	-	73.2	G	68.6	G	70	G
								7	-	-	53.8	G	53.6	G	55.8	G
								28	-	-	86.7	G	92.4	G	86.1	G
[65]	MWCNTs	0.005	-	5.5	-	0.5	Dry mix + nanometakaolin	28	5.5	G	-	-	-	-	-	-
		0.02							11.1	G	-	-	-	-	-	-
		0.05							3.7	B	-	-	-	-	-	-
		0.1							-1.8	B	-	-	-	-	-	-
[238]	A-MWCNTs	0.2	-	35	-	0.5	US	28	32	G	-	-	-	-	-	-
[239]	MWCNTs	0.5	-	-	-	0.5	US	7	24.5	G	24	G	-	-	-	-
		1						7	34.1	G	10.8	B	-	-	-	-
		0.5						28	10.3	G	31	G	-	-	-	-
		1						28	16.5	G	21.7	B	-	-	-	-
[64]	MWCNTs	0.5	-	-	-	0.5	US + FA	7	9.5	G	-	-	-	-	-	-
		1						7	9.15	B	-	-	-	-	-	-
		0.5						28	8	G	-	-	-	-	-	-
		1						28	9.7	G	-	-	-	-	-	-
		0.5						60	8.2	G	-	-	-	-	-	-
		1						60	8.9	G	-	-	-	-	-	-
[25]	MWCNTs	0.025	10	60	166.7	0.33	US + TNWDIS	7	9.4	G	-	-	-	-	-	-
		0.05						7	18.3	G	-	-	-	-	-	-
		0.1						7	21.8	G	-	-	-	-	-	-
		0.025						28	6.2	G	7.5	G	-	-	-	-
		0.05						28	12.7	G	15	G	-	-	-	-
		0.1						28	14.6	G	30	G	-	-	-	-
		0.2						28	-	-	40	G	-	-	-	-
[24]	MWCNTs	0.05	10	30	333.3	0.35	US + GA	28	7	G	6	G	-	-	-	-
		0.08							7.3	G	43.4	G	-	-	-	-
		0.1							9.1	G	36.1	B	-	-	-	-
		0.12							4.3	B	19.5	B	-	-	-	-
		0.15							-5.7	B	-4.6	B	-	-	-	-
[158]	MWCNTs	0.02	7.5	25	300	0.3	US + SP	1	15.8	G	-	-	-	-	-	-
		0.05						1	27.6	G	-	-	-	-	-	-
		0.1						1	35.5	G	-	-	-	-	-	-

Ref.	CNTs					*w/c* ratio	Dispersion method	Age (days)	Mechanical Properties Percent Change (%)							
	Type	$\bar{\kappa}$ (*c-wt*%)	$\bar{L}$ (μm)	$\bar{d}$ (nm)	$\overline{AR}$				CS	DC	FS	DF	E	DE	T	DT
		0.2						1	7.9	B	-	-	-	-	-	-
		0.02						3	5.4	G	-	-	-	-	-	-
		0.05						3	12.7	G	-	-	-	-	-	-
		0.1						3	20	G	-	-	-	-	-	-
		0.2						3	14.5	B	-	-	-	-	-	-
		0.02						7	5.1	G	-	-	-	-	-	-
		0.05						7	10.3	G	-	-	-	-	-	-
		0.1						7	15.4	G	-	-	-	-	-	-
		0.2						7	8.1	B	-	-	-	-	-	-
		0.02						28	6.5	G	-	-	-	-	-	-
		0.05						28	10	G	-	-	-	-	-	-
		0.1						28	12.5	G	-	-	-	-	-	-
		0.2						28	2.5	B	-	-	-	-	-	-
		0.02						90	10	G	-	-	-	-	-	-
		0.05						90	23	G	-	-	-	-	-	-
		0.1						90	28.2	G	-	-	-	-	-	-
		0.2						90	15.9	B	-	-	-	-	-	-
[113]	MWCNTs	0.08	20	30	666.7	0.3	US + SP	3	-	-	43.7	G	38.8	G	-	-
								7	-	-	34.4	G	33.8	G	-	-
								28	-	-	37.6	G	32.7	G	-	-
[11]	MWCNTs	0.048	20	30	666.7	0.3	US + SP	3	-	-	22.5	G	-	-	-	-
		0.08	20		666.7			3	-	-	45	G	42.1	G	-	-
		0.1	20		666.7			3	-	-	31.2	B	-	-	-	-
		0.025	10-100		1833.3			3	-	-	28.7	G	31.4	G	-	-
		0.048	10-100		1833.3			3	-	-	33.7	G	33.1	G	-	-
		0.08	10-100		1833.3			3	-	-	15	B	-	-	-	-
		0.048	20		666.7			7	-	-	18.9	G	-	-	-	-
		0.08	20		666.7			7	-	-	34.4	G	37.1	G	-	-
		0.1	20		666.7			7	-	-	25	B	-	-	-	-
		0.025	10-100		1833.3			7	-	-	22.2	G	36.4	G	-	-
		0.048	10-100		1833.3			7	-	-	25.5	G	27.3	B	-	-
		0.08	10-100		1833.3			7	-	-	8.9	B	-	-	-	-
		0.048	20		666.7			28	-	-	17.2	G	-	-	-	-
		0.08	20		666.7			28	-	-	36.5	G	34.3	G	-	-
		0.1	20		666.7			28	-	-	23.6	B	-	-	-	-
		0.025	10-100		1833.3			28	-	-	22.6	G	34.3	G	-	-
		0.048	10-100		1833.3			28	-	-	23.6	G	23.3	B	-	-
		0.08	10-100		1833.3			28	-	-	9.7	B	-	-	-	-
[66]	A-MWCNTs	0.05	> 1	13	-	0.3	US	28	-	-	99.4	G	-	-	-	-
[114]	MWCNTs	0.05	10	30	333.3	0.35	US + GA	28	-	-	-	-	-	-	31	G
		0.08							-	-	-	-	-	-	57.5	G
		0.1							-	-	-	-	-	-	47.1	B

Ref.	CNTs					*w/c* ratio	Dispersion method	Age (days)	Mechanical Properties Percent Change (%)							
	Type	$\bar{\kappa}$ (*c-wt*%)	$\bar{L}$ (μm)	$\bar{d}$ (nm)	$\overline{AR}$				CS	DC	FS	DF	E	DE	T	DT
		0.12							-	-	-	-	-	-	31.6	B
		0.15							-	-	-	-	-	-	10.3	B
[240]	MWCNTs	0.2	10	30	333.3	0.4	US + SDBS	28	13.8	G	15	G	-	-	-	-
							US + NaDC		29.5	G	35	G	-	-	-	-
							US + GA		2.5	G	4.7	G	-	-	-	-
							US+SDBS+TX10		21	G	28.7	G	-	-	-	-
[73]	MWCNTs	0.25	1.5	20	75	0.4	US in cement & Ethanol	28	-	-	3.7	G	-	-	-	-
		0.5							-	-	25.9	G	-	-	-	-
		0.65							-	-	85.2	G	-	-	-	-
		0.75							-	-	-48.1	B	-	-	-	-
[63]	A-MWCNTs	0.15	13	20	650	0.4	Dry mix + SP + SF	14	57.8	G	25.6 ^	G	-	-	-	-
	MWCNTs						Dry mix + SP + SF		17.8	G	11.6 ^	G	-	-	-	-
	A-MWCNTs						Dry mix + SF		68.9	G	46.5 ^	G	-	-	-	-
[116]	MWCNTs	0.5	25.25	80	315.6	0.4	US	7	21.4	G	17.8^	G	-	-	-	-
		0.75						7	16.7	B	-1.9 ^	B	-	-	-	-
		1						7	-16.7	B	-41.2 ^	B	-	-	-	-
		0.5						28	14.7	G	36.3 ^	G	-	-	-	-
		0.75						28	-2.9	B	24.1 ^	B	-	-	-	-
		1						28	-29.4	B	5.4 ^	B	-	-	-	-
		0.5						60	7.9	G	9.8 ^	G	-	-	-	-
		0.75						60	-2.4	B	0 ^	B	-	-	-	-
		1						60	-27	B	-10 ^	B	-	-	-	-
		0.5						90	11.6	G	9.8 ^	G	-	-	-	-
		0.75						90	-2.1	B	-13 ^	B	-	-	-	-
		1						90	-28.6	B	-43.3 ^	B	-	-	-	-
		0.5						180	12.7	G	9.8 ^	G	-	-	-	-
		0.75						180	-1.6	B	0 ^	B	-	-	-	-
		1						180	-27	B	-20 ^	B	-	-	-	-
[241]	MWCNTs	0.1	1.5	9.5	157.9	0.4	US + SP	7	-	-	-29.2	B	-9.8	B	-28.6	B
	MWCNTs	0.2						7	-	-	-67.7	B	-39.2	B	21.4	G
	A-MWCNTs	0.1						7	-	-	63.1	G	-14.4	B	207.1	G
	A-MWCNTs	0.2						7	-	-	50.8	B	-15	B	142.8	B
	MWCNTs	0.1						14	-	-	-69.7	B	-16.7	B	-67.3	B
	MWCNTs	0.2						14	-	-	-53.9	B	-29.5	B	-38.5	B
	A-MWCNTs	0.1						14	-	-	-60.5	B	-14.4	B	-73.1	B
	A-MWCNTs	0.2						14	-	-	-59.2	B	-25.7	B	-69.2	B
	MWCNTs	0.1						28	-	-	-47.1	B	4	G	-24.4	B
	MWCNTs	0.2						28	-	-	37.9	G	23.5	G	64.4	G
	A-MWCNTs	0.1						28	-	-	-51.7	B	-20.1	B	-64.4	B
	A-MWCNTs	0.2						28	-	-	-73	B	-51	B	-68.9	B
[13]	MWCNTs	0.1	1.5	9.5	157.9	0.4	US + SP	7	-	-	-21.4	B	-10.3	B	-29.4	B
		0.2						7	-	-	-64.3	B	-37.9	B	5.9	G

Ref.	CNTs					*w/c* ratio	Dispersion method		Age (days)	Mechanical Properties Percent Change (%)							
	Type	$\bar{\kappa}$ (*c-wt*%)	$\bar{L}$ (μm)	$\bar{d}$ (nm)	$\overline{AR}$					CS	DC	FS	DF	E	DE	T	DT
		0.1							14	-	-	-73.3	B	-23.1	B	-77.8	B
		0.2							14	-	-	-60	B	-42.3	B	-37	B
		0.1							28	-	-	-52.9	B	6.4	G	-31.8	B
		0.2							28	-	-	41.2	G	16.1	G	72.7	G
[23]	MWCNTs	0.04	1.5	9.5	157.9	0.4	US + SP		7	-	-	76.7	G	-7.3	B	153.3	G
		0.1	1.5	9.5	157.9				7	-	-	20.9	B	14.7	G	60	B
		0.2	1.5	9.5	157.9				7	-	-	-34.9	B	4.4	B	46.7	B
		0.04	20	< 8	3000				7	-	-	27.9	G	-12.5	B	86.7	G
		0.1	20	< 8	3000				7	-	-	39.5	G	-43.4	B	20	B
		0.04	1.5	9.5	157.9				14	-	-	-22.2	B	15.2	G	-33.3	B
		0.1	1.5	9.5	157.9				14	-	-	-46.7	B	2.8	B	-20	B
		0.2	1.5	9.5	157.9				14	-	-	-28.9	B	-16.2	B	13.3	G
		0.04	20	< 8	3000				14	-	-	26.7	G	10.5	G	6.7	G
		0.1	20	< 8	3000				14	-	-	-33.3	B	-24.8	B	-78	B
		0.04	1.5	9.5	157.9				28	-	-	18.2	G	-14.5	B	66.7	G
		0.1	1.5	9.5	157.9				28	-	-	33.3	G	4.8	G	196.7	G
		0.2	1.5	9.5	157.9				28	-	-	260.6	G	17.2	G	516.7	G
		0.04	20	< 8	3000				28	-	-	51.5	G	5.5	G	41.7	G
		0.1	20	< 8	3000				28	-	-	60.6	G	-11.7	B	33.3	B
[60]	Mixed CNTs	0.05				0.4	US +	SDS		44.8	G	6.7 *	G	-	-	-	-
		0.25						SDS		20.7	B	6.7 *	B	-	-	-	-
		0.05	20	< 8	3000			Brij 35	28	15	G	-30 *	B	-	-	-	-
		0.25						Brij 35		-12.5	B	-15 *	B	-	-	-	-
[242]	MWCNTs	0.06				0.45	US + SP		7	-9.4	B	-	-	-	-	-	-
		0.12	> 2	11.5	-				7	-16.3	B	-	-	-	-	-	-
		0.06							28	29.7	G	-	-	-	-	-	-
		0.12							28	4.6	B	-	-	-	-	-	-
[115]	A-MWCNTs	0.02				0.4	US			83.3	G	-	-	-	-	-	-
		0.03					US			97.2	G	-	-	-	-	-	-
		0.05	-	7	-		US		28	80.5	B	-	-	-	-	-	-
		0.09					US			63.9	B	-	-	-	-	-	-
		-					US + SDS			-65	B	-	-	-	-	-	-
[117]	MWCNTs		400-1000	60	-	0.4	SP + VMA		28	10.6	G	34.7	G	-	-	-	-
	C-MWCNTs	0.5	5.1	15	336.7	0.4				-85.1	B	-61.3	B	-	-	-	-
	C-MWCNTs		5.1	15	336.7	0.56				-26.3	B	-3.2	B	-	-	-	-
[99]	MWCNTs	0.05		15	1333.3	0.2	US + surfactants		28	0.5	G	-	-	-	-	6.3	G
	MWCNTs	0.1		15	1333.3					-2.3	B	-	-	-	-	9.4	G
	C-MWCNTs	0.05	20	< 8	3000					5.3	G	-	-	-	-	6.9	G
	C-MWCNTs	0.1		< 8	3000					5	B	-	-	-	-	19.2	G
[243]	MWCNTs	1				0.4	US + surfactant		7	34.6	G	-	-	-	-	-	-
						0.4			14	50	G	-	-	-	-	-	-

Ref.	CNTs					*w/c* ratio	Dispersion method		Age (days)	Mechanical Properties Percent Change (%)							
	Type	$\bar{\kappa}$ (*c-wt*%)	$\bar{L}$ (μm)	$\bar{d}$ (nm)	$\overline{AR}$					CS	DC	FS	DF	E	DE	T	DT
						0.4			28	34	G	-	-	-	-	-	-
						0.6			7	-27.8	B	-	-	-	-	-	-
			15	5	3000	0.6			14	9.5	G	-	-	-	-	-	-
						0.6			28	4	G	-	-	-	-	-	-
						0.65			7	-35.3	B	-	-	-	-	-	-
						0.7			7	-43.7	B	-	-	-	-	-	-
						0.35			7	22.2	G	-	-	-	-	-	-
						0.45			7	12	G	-	-	-	-	-	-
[118]	MWCNTs	0.1	15	50	300	0.6	US +	-	7	6.2	G	-	-	-	-	-	-
		0.2	15	50	300	0.6		-	7	7.8	G	-	-	-	-	-	-
		0.3	15	50	300	0.485		-	7	-10.6	B	-	-	-	-	-	-
		0.3	15	50	300	0.6		-	7	6.2	B	-	-	-	-	-	-
		0.3	15	50	300	0.485		SP	7	3.6	G	-	-	-	-	-	-
		0.3	15	50	300	0.485		SP	7	5.3	G	-	-	-	-	-	-
		0.3	15	50	300	0.485		SP	7	2	G	-	-	-	-	-	-
		0.5	15	50	300	0.485		-	7	-18.7	B	-	-	-	-	-	-
		0.5	15	50	300	0.6		-	7	7	G	-	-	-	-	-	-
		0.5	15	50	300	0.485		SP	7	4.5	G	-	-	-	-	-	-
		0.5	15	50	300	0.485		SP	7	6.9	G	-	-	-	-	-	-
		0.5	15	50	300	0.485		SP	7	-17.9	B	-	-	-	-	-	-
		0.8	15	50	300	0.485		-	7	-29.3	B	-	-	-	-	-	-
		0.8	15	50	300	0.6		-	7	-4.1	B	-	-	-	-	-	-
		0.8	15	50	300	0.485		SP	7	-10.6	B	-	-	-	-	-	-
		0.8	15	50	300	0.485		SP	7	-3.6	B	-	-	-	-	-	-
		0.3	20	25	800	0.485		-	7	13	G	-	-	-	-	-	-
		0.3	20	25	800	0.6		-	7	28.5	G	-	-	-	-	-	-
		0.3	20	25	800	0.485		SP	7	17.9	G	-	-	-	-	-	-
		0.5	20	25	800	0.6		-	7	1.6	B	-	-	-	-	-	-
		0.8	20	25	800	0.6		-	7	0.4	B	-	-	-	-	-	-
		0.1	15	50	300	0.6		-	28	10.2	G	-	-	-	-	-	-
		0.2	15	50	300	0.6		-	28	10.8	G	-	-	-	-	-	-
		0.3	15	50	300	0.485		-	28	-0.5	B	-	-	-	-	-	-
		0.3	15	50	300	0.6		-	28	16.5	G	-	-	-	-	-	-
		0.3	15	50	300	0.485		SP	28	9.1	G	-	-	-	-	-	-
		0.3	15	50	300	0.485		SP	28	8	G	-	-	-	-	-	-
		0.3	15	50	300	0.485		SP	28	10.3	G	-	-	-	-	-	-
		0.5	15	50	300	0.485		-	28	-25.9	B	-	-	-	-	-	-
		0.5	15	50	300	0.6		-	28	8.4	B	-	-	-	-	-	-
		0.5	15	50	300	0.485		SP	28	-12.4	B	-	-	-	-	-	-
		0.5	15	50	300	0.485		SP	28	-16.5	B	-	-	-	-	-	-
		0.5	15	50	300	0.485		SP	28	-24.2	B	-	-	-	-	-	-
		0.8	15	50	300	0.485		-	28	-30.1	B	-	-	-	-	-	-

Ref.	CNTs					*w/c* ratio	Dispersion method		Age (days)	Mechanical Properties Percent Change (%)							
	Type	$\bar{\kappa}$ (*c-wt*%)	$\bar{L}$ (μm)	$\bar{d}$ (nm)	$\overline{AR}$					CS	DC	FS	DF	E	DE	T	DT
		0.8	15	50	300	0.6		-	28	-1.5	B	-	-	-	-	-	-
		0.8	15	50	300	0.485		SP	28	-16.5	B	-	-	-	-	-	-
		0.8	15	50	300	0.485		SP	28	-7.4	B	-	-	-	-	-	-
		0.3	20	25	800	0.485		-	28	3.83	G	-	-	-	-	-	-
		0.3	20	25	800	0.6		-	28	24.8	G	-	-	-	-	-	-
		0.3	20	25	800	0.485		SP	28	-0.6	B	-	-	-	-	-	-
		0.5	20	25	800	0.6		-	28	3.6	B	-	-	-	-	-	-
		0.8	20	25	800	0.6		-	28	-1.2	B	-	-	-	-	-	-
[185]	MWCNTs	0.05	12.5	20	625	0.5	US + SP		28	2.2	G	6.1 *	G	-	-	-	-
		0.1					US + SP			6.5	G	30.6 *	G	-	-	-	-
		0.25					US + SP			11.9	G	36.7 *	G	-	-	-	-
		0.5					US + SP			9.8	B	14.3 *	B	-	-	-	-
		0.05					US			-1.1	B	10.9 *	G	-	-	-	-
		0.1					US			-3.3	B	26.1 *	G	-	-	-	-
		0.25					US			-11	B	32.6 *	G	-	-	-	-
		0.5					US			-12.1	B	8.7 *	B	-	-	-	-
[16]	MWCNTs	0.048	20	30	666.7	0.5	US + SP		3	-	-	13.1	G	19	G	-	-
		0.08	20		666.7				3	-	-	34.2	G	37.9	G	-	-
		0.048	10-100		1833.3				3	-	-	26.3	G	48.3	G	-	-
		0.08	10-100		1833.3				3	-	-	15.8	B	8.6	B	-	-
		0.048	20		666.7				7	-	-	14.6	G	23.6	G	-	-
		0.08	20		666.7				7	-	-	22.9	G	50	G	-	-
		0.048	10-100		1833.3				7	-	-	20.8	G	43	G	-	-
		0.08	10-100		1833.3				7	-	-	18.8	B	11.1	B	-	-
		0.048	20		666.7				28	-	-	12.9	G	36.6	G	-	-
		0.08	20		666.7				28	-	-	20.4	G	51.2	G	-	-
		0.048	10-100		1833.3				28	-	-	25.9	G	47.6	G	-	-
		0.08	10-100		1833.3				28	-	-	22.2	B	14.6	B	-	-
[94]	MWCNTs	0.5	10	80	125	0.5	-		28	-7.8	B	-	-	-	-	-	-
				20	500		-			-6.5	B	-	-	-	-	-	-
				15	666.7		-			-11.2	B	-	-	-	-	-	-
				80	125		US			200.4	G	-	-	-	-	-	-
				80	125		Air entrainer			-10.1	B	-	-	-	-	-	-
				80	125		US + Air entrainer			-13.8	B	-	-	-	-	-	-
				80	125		Lignosulphonate			-28.5	B	-	-	-	-	-	-
				80	125		US+Lignosulphonate			-35.4	B	-	-	-	-	-	-
				80	125		SP			25.8	G	-	-	-	-	-	-
				80	125		US + SP			22.9	G	-	-	-	-	-	-
[75]	CNTs/CNFs	0.3	-	-	-	0.4	Direct synthesis + Lignosulphonate		7	-	-	24.2	G	-	-	-	-
									28	88.3	G	14.1	G	-	-	-	-

Ref.	CNTs					*w/c* ratio	Dispersion method	Age (days)	Mechanical Properties Percent Change (%)							
	Type	$\bar{\kappa}$ (*c-wt*%)	$\bar{L}$ (μm)	$\bar{d}$ (nm)	$\overline{AR}$				CS	DC	FS	DF	E	DE	T	DT
[93]	MWCNTs	0.1	20	< 8	3000	0.5	US (Bath) + Surfactants	28	-42.7	B	-27.1	B	-	-	-	-
	MWCNTs	0.1						28	-15.5	B	-	-	-	-	-	-
	MWCNTs	0.1						28	-8.9	B	-	-	-	-	5	G
	MWCNTs	0.08						28	-1.7	B	-	-	-	-	-	-
	C- MWCNTs	0.1						28	-10.1	B	-	-	-	-	-	-
	C- MWCNTs	0.1						28	-0.6	B	-	-	-	-	39	G
	MWCNTs	0.1						28	-	-	-11.2	B	-	-	-	-
	C- MWCNTs	0.1						28	-	-	-0.8	B	-	-	-	-
	MWCNTs	0.1						28	-	-	-16	B	-	-	-	-
	C- MWCNTs	0.1						28	-	-	-8	B	-	-	-	-
	MWCNTs	0.08						28	-	-	3.1	B	-	-	-	-
	C- MWCNTs	0.08						28	-	-	-6.1	B	-	-	-	-
	MWCNTs	0.15						28	-	-	-	-	-	-	24	G
	C- MWCNTs	0.15						28	-	-	-	-	-	-	96	G
	SWCNTs	0.1						28	-	-	6.2	G	-	-	-	-
	C-SWCNTs	0.1						28	-	-	-0.8	B	-	-	-	-
	SWCNTs	0.1						28	19.1	G	6.7	G	-	-	109	G
	SWCNTs	0.1						28	9.8	G	-	-	-	-	-	-
	C-SWCNTs	0.1						28	-8.9	B	-6.4	B	-	-	52	G
	SWCNTs	0.08						28	15.4	G	5.6	G	-	-	-	-
	SWCNTs	0.08						42	12.4	G	-18.9	B	-	-	-	-
	SWCNTs	0.08						56	12.36	G	13.3	G	-	-	-	-
	C-SWCNTs	0.08						28	-12.6	B	-10.2	B	-	-	-	-
	C-SWCNTs	0.08	17.5	1.5	11667			42	1.12	G	11.9	G	-	-	-	-
	C-SWCNTs	0.08						56	20.8	G	17.5	G	-	-	-	-
	C-SWCNTs	0.1						28	1.1	-	-	-	-	-	-	-
	SWCNTs	0.15						28	-	-	-	-	-	-	60	B
	C-SWCNTs	0.15						28	-	-	-	-	-	-	48	B
[12]	C-MWCNTs	0.038	1.5	9.5	157.9	0.4	US+SP	28	-	-	10.7	G	4.8	G	15.2	G
		0.038							-	-	25.3	G	14.1	G	33.9	G
		0.038							-	-	24.8	G	13.2	G	31	G
		0.038							-	-	19.5	G	12.4	G	24.2	G
		0.038							-	-	17	G	11.7	G	20.6	G
		0.075							-	-	7.8	G	4.6	G	15.1	G
		0.075							-	-	32.1	G	21.1	G	40.9	G
		0.075							-	-	49.9	G	31.5	G	62.5	G
		0.075							-	-	48.7	G	30.1	G	55.1	G
		0.075							-	-	38.2	G	27.4	G	48.9	G
[92]	MWCNTs	0.0007	<10	10	650	0.3	US + PAP		-14.6	B	-40.3	B	-	-	-	-
	MWCNTs	0.03	<10		650	0.3			-39	B	-22.8	B	-	-	-	-
	MWCNTs	0.042	<10		650	0.3			-6.7	B	17.5	G	-	-	-	-
	MWCNTs	0.03	<10		650	0.3	GA		5.3	B	2.2	B	-	-	-	-

Ref.	CNTs					*w/c* ratio	Dispersion method		Age (days)	Mechanical Properties Percent Change (%)							
	Type	$\bar{\kappa}$ (*c-wt*%)	$\bar{L}$ (μm)	$\bar{d}$ (nm)	$\overline{AR}$					CS	DC	FS	DF	E	DE	T	DT
	MWCNTs	0.0007	<10		650	0.3		GA		13.2	G	11.1	G	-	-	-	-
	MWCNTs	0.042	<10		650	0.3		GA	28	-21.1	B	-24.4	B	-	-	-	-
	C-MWCNTs	0.06	3		300	0.4		-		-0.5	B	13.3	G	-	-	-	-
	C-MWCNTs	0.05	3		300	0.4		PAP		6.06	G	6.7	G	-	-	-	-
	C-MWCNTs	0.15	3		300	0.3		PAP		1.92	G	15.9	G	-	-	-	-
	C-MWCNTs	0.045	3		300	0.3		PAP		63.16	G	-0.5	B	-	-	-	-
[244]	MWCNTs	0.01	-	45	-	0.3	US + SP		1	-0.5	B	-	-	-	-	-	-
	MWCNTs	0.02							1	6.8	G	-	-	-	-	-	-
	MWCNTs	0.05							1	22.7	G	-	-	-	-	-	-
	A-MWCNTs	0.05							1	29.5	G	-	-	-	-	-	-
	MWCNTs	0.13							1	36.4	G	-	-	-	-	-	-
	MWCNTs	0.25							1	-2.3	B	-	-	-	-	-	-
	MWCNTs	0.01							7	2.1	G	-	-	-	-	-	-
	MWCNTs	0.02							7	2.1	G	-	-	-	-	-	-
	MWCNTs	0.05							7	6.4	G	-	-	-	-	-	-
	A-MWCNTs	0.05							7	10.6	G	-	-	-	-	-	-
	MWCNTs	0.13							7	10.6	B	-	-	-	-	-	-
	MWCNTs	0.25							7	8.5	B	-	-	-	-	-	-
	MWCNTs	0.01							28	3.9	G	-	-	-	-	-	-
	MWCNTs	0.02							28	11.8	G	-	-	-	-	-	-
	MWCNTs	0.05							28	21.6	G	-	-	-	-	-	-
	A-MWCNTs	0.05							28	11.7	G	-	-	-	-	-	-
	MWCNTs	0.13							28	25.5	G	-	-	-	-	-	-
	MWCNTs	0.25							28	2	B	-	-	-	-	-	-
[29]	MWCNTs	0.125	21.25	30	708.33	0.485	US+SP +	-	7	-	-	5.1	G	6.5	G	-	-
	MWCNTs							SF	7	-	-	4.6	G	3.5	G	-	-
	S-MWCNTs							-	7	-	-	-1	B	15.9	G	-	-
	S-MWCNTs							-	7	-	-	2	G	11	G	-	-
	MWCNTs							-	28	-	-	4.4	G	14.7	G	-	-
	MWCNTs							SF	28	-	-	4.6	G	6.4	G	-	-
	S-MWCNTs							-	28	-	-	9.2	G	19.2	G	-	-
	S-MWCNTs							-	28	-	-	7.2	G	20.8	G	-	-

*: direct tension test, ^: splitting tensile strength

CS: compressive strength, FS; flexural strength, E: elastic modulus, T: toughness

DC: CNT dispersion quality for compressive strength, DF: CNT dispersion quality for flexural strength, DY: CNT dispersion quality for elastic modulus, DT: CNT dispersion quality for toughness

C-MWCNTs: COOH functionalized MWCNTs, O-MWCNTs: OH functionalized MWCNTs, A-MWCNTs: acid treated MWCNTs, H-MWCNTs: commercial pre-dispersed MWCNTs in water, S-MWCNTs: silica functionalized MWCNTs

US: ultrasonication, SP: superplasticizer, SF: silica fume, FA: fly ash, PVP: polyvinyl pyrrolidone, TP: tributyl phosphate, GA: gum Arabic, VMA: viscosity modifying agent, PAP: polyacrylic acid polymer, TNWDIS: CNT-based Water dispersant, SDS: sodium dodecyl sulfate, Brij 35: polyoxyethylene (23) lauryl ether, SDBS: sodium dodecyl benzene sulfonate, NaDC: sodium deoxycholate, TX10: Triton X-100, B: bad, G: good

Table A-2. Estimated and Measured Critical Relations for f_{FS} and E_F

Ref.	Experimental parameters								Flexural strength (f_{FS})										Static elastic modulus (E_F)								
	w/c ratio	*s/c* ratio	*AR*	κ (c-wt%)	v_f	*UEI*	*SP/CNTs* ratio	*t* (days)	σ_m (*MPa*)	$\sigma_c^{exp.}$ (*MPa*)	$\sigma_c^{prd.}$ (*MPa*)	$\eta_D^{x_F^E}$	$\eta_D^{x_F^m}$	$\eta_H^{y_F^E}$	$\eta_H^{y_F^m}$	$\eta_M^{z_F^E}$	$\eta_M^{z_F^m}$	E_m (*GPa*)	$E_c^{exp.}$ (*GPa*)	$E_c^{prd.}$ (*GPa*)	$\eta_D^{x_E^E}$	$\eta_D^{x_E^m}$	$\eta_H^{y_E^E}$	$\eta_H^{y_E^m}$	$\eta_M^{z_E^E}$	$\eta_M^{z_E^m}$
[111]	0.485	2.75	300	0.100	0.00097	28.2	4.0	3	-	-	-	-	-	-	-	-	-	9.2	16.0	13.6	0.98	1.16	0.97	1.14	1.56	1.83
	0.485	2.75	300	0.100	0.00097	28.2	4.0	7	-	-	-	-	-	-	-	-	-	10.8	18.1	16.4	0.98	1.09	0.98	1.09	1.56	1.72
	0.485	2.75	300	0.100	0.00097	28.2	4.0	28	5.9	11.1	8.9	0.99	1.23	1.00	1.25	1.51	1.89	13.5	27.1	20.8	0.98	1.29	1.00	1.31	1.56	2.04
[12]	0.4	0	150	0.038	0.00049	0.9	22.4	28	4.1	4.6	4.9	0.98	0.92	1.00	0.94	1.20	1.13	16.4	17.1	19.5	0.98	0.86	1.00	0.88	1.22	1.07
	0.4	0	150	0.038	0.00049	2.7	22.4	28	4.1	5.2	4.9	0.99	1.04	1.00	1.05	1.20	1.26	16.4	18.7	19.8	0.99	0.94	1.00	0.94	1.22	1.15
	0.4	0	150	0.038	0.00049	5.4	22.4	28	4.1	5.1	4.9	1.00	1.04	1.00	1.04	1.20	1.25	16.4	18.5	19.9	1.00	0.93	1.00	0.93	1.22	1.14
	0.4	0	150	0.038	0.00049	8.9	22.4	28	4.1	4.9	4.9	1.00	0.99	1.00	0.99	1.20	1.20	16.4	18.4	19.9	1.00	0.92	1.00	0.92	1.22	1.13
	0.4	0	150	0.038	0.00049	14.3	22.4	28	4.1	4.8	4.9	1.00	0.97	1.00	0.97	1.20	1.17	16.4	18.3	19.9	1.00	0.92	1.00	0.92	1.22	1.12
	0.4	0	150	0.075	0.00097	0.9	15.3	28	4.1	4.4	4.7	0.95	0.90	1.00	0.94	1.20	1.14	16.4	17.1	18.7	0.93	0.86	1.00	0.92	1.22	1.12
	0.4	0	150	0.075	0.00097	2.7	15.3	28	4.1	5.4	4.9	0.98	1.10	1.00	1.12	1.20	1.34	16.4	19.8	19.5	0.98	0.99	1.00	1.02	1.22	1.24
	0.4	0	150	0.075	0.00097	5.4	15.3	28	4.1	6.2	4.9	0.99	1.25	1.00	1.26	1.20	1.51	16.4	21.5	19.7	0.99	1.08	1.00	1.09	1.22	1.33
	0.4	0	150	0.075	0.00097	8.9	15.3	28	4.1	6.1	4.9	0.99	1.23	1.00	1.24	1.20	1.49	16.4	21.3	19.8	0.99	1.07	1.00	1.07	1.22	1.31
	0.4	0	150	0.075	0.00097	14.3	15.3	28	4.1	5.7	4.9	1.00	1.15	1.00	1.15	1.20	1.39	16.4	20.8	19.9	1.00	1.04	1.00	1.05	1.22	1.28
[11]	0.3	0	700	0.048	0.00076	18.7	4.0	3	8.2	9.8	9.8	0.97	0.96	0.98	0.97	1.28	1.27	-	-	-	-	-	-	-	-	-
	0.3	0	700	0.048	0.00076	18.7	4.0	7	9.1	10.6	11.1	0.97	0.92	0.99	0.95	1.28	1.22	-	-	-	-	-	-	-	-	-
	0.3	0	700	0.048	0.00076	18.7	4.0	28	9.3	10.9	11.5	0.97	0.91	1.00	0.95	1.28	1.21	-	-	-	-	-	-	-	-	-
	0.3	0	700	0.080	0.00127	18.7	4.0	3	8.2	11.5	9.5	0.94	1.15	0.96	1.17	1.28	1.55	12.1	16.8	14.2	0.93	1.10	0.97	1.15	1.30	1.54
	0.3	0	700	0.080	0.00127	18.7	4.0	7	9.1	12.1	10.8	0.94	1.06	0.98	1.11	1.28	1.43	14.5	19.4	17.3	0.93	1.04	0.99	1.11	1.30	1.46
	0.3	0	700	0.080	0.00127	18.7	4.0	28	9.3	12.6	11.2	0.94	1.06	1.00	1.13	1.28	1.44	16.5	21.9	19.9	0.93	1.02	1.00	1.10	1.30	1.43
	0.3	0	700	0.100	0.00158	18.7	4.0	3	8.2	10.4	9.2	0.93	1.05	0.96	1.08	1.28	1.44	-	-	-	-	-	-	-	-	-
	0.3	0	700	0.100	0.00158	18.7	4.0	7	9.1	11.2	10.6	0.93	0.99	0.98	1.04	1.28	1.35	-	-	-	-	-	-	-	-	-
	0.3	0	700	0.100	0.00158	18.7	4.0	28	9.3	11.5	11.0	0.93	0.97	1.00	1.04	1.28	1.33	-	-	-	-	-	-	-	-	-
	0.3	0	1600	0.025	0.00040	18.7	4.0	3	8.2	10.2	9.9	0.96	0.99	0.99	1.02	1.28	1.31	12.1	15.9	14.8	0.95	1.02	0.99	1.07	1.30	1.40
	0.3	0	1600	0.025	0.00040	18.7	4.0	7	9.1	11.0	11.1	0.96	0.95	0.99	0.99	1.28	1.27	14.5	19.5	17.8	0.95	1.04	1.00	1.09	1.30	1.42
	0.3	0	1600	0.025	0.00040	18.7	4.0	28	9.3	11.4	11.4	0.96	0.96	1.00	1.00	1.28	1.28	16.5	21.9	20.3	0.95	1.02	1.00	1.08	1.30	1.40
	0.3	0	1600	0.048	0.00076	18.7	4.0	3	8.2	10.6	9.4	0.92	1.04	0.98	1.11	1.28	1.44	12.1	16.1	13.9	0.90	1.04	0.98	1.14	1.30	1.50
	0.3	0	1600	0.048	0.00076	18.7	4.0	7	9.1	11.2	10.6	0.92	0.97	0.99	1.05	1.28	1.35	14.5	18.2	16.9	0.90	0.97	0.99	1.07	1.30	1.40
	0.3	0	1600	0.048	0.00076	18.7	4.0	28	9.3	11.5	10.9	0.92	0.97	1.00	1.05	1.28	1.34	16.5	20.1	19.3	0.90	0.94	1.00	1.04	1.30	1.35
	0.3	0	1600	0.080	0.00127	18.7	4.0	3	8.2	9.1	8.8	0.87	0.91	0.96	1.00	1.28	1.33	-	-	-	-	-	-	-	-	-
	0.3	0	1600	0.080	0.00127	18.7	4.0	7	9.1	9.8	10.0	0.87	0.85	0.98	0.96	1.28	1.25	-	-	-	-	-	-	-	-	-
	0.3	0	1600	0.080	0.00127	18.7	4.0	28	9.3	10.2	10.4	0.87	0.86	1.00	0.98	1.28	1.25	-	-	-	-	-	-	-	-	-
[28]	0.5	3	307	0.100	0.00094	28.2	4.0	3	4.2	6.0	6.0	0.99	0.99	0.96	0.96	1.52	1.53	10.0	16.3	14.9	0.98	1.07	0.97	1.05	1.57	1.71
	0.5	3	307	0.100	0.00094	28.2	4.0	7	5.2	6.9	7.7	0.99	0.89	0.98	0.88	1.52	1.37	12.0	18.1	18.3	0.98	0.97	0.98	0.98	1.57	1.56
	0.5	3	307	0.100	0.00094	28.2	4.0	28	5.9	10.5	8.9	0.99	1.17	1.00	1.18	1.52	1.80	14.3	26.8	22.1	0.98	1.19	1.00	1.21	1.57	1.90
	0.5	3	200	0.100	0.00098	28.2	4.0	3	4.2	5.7	6.0	0.99	0.94	0.96	0.91	1.52	1.45	10.0	15.5	15.0	0.99	1.02	0.97	1.00	1.57	1.62
	0.5	3	200	0.100	0.00098	28.2	4.0	7	5.2	6.5	7.7	0.99	0.84	0.98	0.83	1.52	1.29	12.0	17.3	18.4	0.99	0.93	0.98	0.93	1.57	1.48
	0.5	3	200	0.100	0.00098	28.2	4.0	28	5.9	10.2	8.9	0.99	1.14	1.00	1.15	1.52	1.74	14.3	26.3	22.2	0.99	1.17	1.00	1.18	1.57	1.86
	0.5	3	333	0.100	0.00095	28.2	4.0	3	4.2	8.8	6.0	0.99	1.46	0.96	1.41	1.52	2.25	10.0	17.8	14.9	0.98	1.17	0.97	1.15	1.57	1.87
	0.5	3	333	0.100	0.00095	28.2	4.0	7	5.2	10.1	7.6	0.99	1.30	0.98	1.29	1.52	2.01	12.0	24.0	18.2	0.98	1.29	0.98	1.30	1.57	2.07
	0.5	3	333	0.100	0.00095	28.2	4.0	28	5.9	12.9	8.9	0.99	1.44	1.00	1.46	1.52	2.22	14.3	32.0	22.1	0.98	1.42	1.00	1.45	1.57	2.28
	0.5	3	333	0.100	0.00095	28.2	4.0	3	4.2	6.2	6.0	0.99	1.03	0.96	0.99	1.52	1.59	-	-	-	-	-	-	-	-	-
	0.5	3	333	0.100	0.00095	28.2	4.0	7	5.2	7.5	7.6	0.99	0.97	0.98	0.96	1.52	1.49	-	-	-	-	-	-	-	-	-
	0.5	3	333	0.100	0.00095	28.2	4.0	28	5.9	10.6	8.9	0.99	1.18	1.00	1.20	1.52	1.82	14.3	26.6	22.1	0.98	1.18	1.00	1.21	1.57	1.89
[16]	0.5	0	700	0.048	0.00046	18.7	4.0	3	3.8	4.3	4.2	0.98	0.99	0.98	0.99	1.15	1.17	5.8	6.9	6.5	0.97	1.04	0.98	1.05	1.16	1.24
	0.5	0	700	0.048	0.00046	18.7	4.0	7	4.8	5.4	5.4	0.98	0.98	0.99	0.99	1.15	1.15	7.2	8.9	8.1	0.97	1.07	0.99	1.09	1.16	1.28
	0.5	0	700	0.048	0.00046	18.7	4.0	28	5.3	6.1	5.9	0.98	1.01	1.00	1.03	1.15	1.19	8.2	11.2	9.3	0.97	1.17	1.00	1.21	1.16	1.40
	0.5	0	700	0.080	0.00076	18.7	4.0	3	3.8	5.0	4.1	0.97	1.19	0.96	1.18	1.15	1.41	5.8	8.0	6.3	0.96	1.22	0.97	1.24	1.16	1.48
	0.5	0	700	0.080	0.00076	18.7	4.0	7	4.8	5.9	5.2	0.97	1.08	0.98	1.10	1.15	1.28	7.2	10.8	7.9	0.96	1.31	0.99	1.35	1.16	1.59
	0.5	0	700	0.080	0.00076	18.7	4.0	28	5.3	6.7	5.8	0.97	1.11	1.00	1.15	1.15	1.32	8.2	12.4	9.1	0.96	1.30	1.00	1.36	1.16	1.58
	0.5	0	1600	0.048	0.00046	18.7	4.0	3	3.8	4.7	4.1	0.95	1.10	0.98	1.13	1.15	1.33	5.8	8.6	6.2	0.94	1.30	0.98	1.36	1.16	1.60
	0.5	0	1600	0.048	0.00046	18.7	4.0	7	4.8	5.7	5.2	0.95	1.03	0.99	1.07	1.15	1.25	7.2	10.3	7.8	0.94	1.24	0.99	1.31	1.16	1.53
	0.5	0	1600	0.048	0.00046	18.7	4.0	28	5.3	6.7	5.8	0.95	1.11	1.00	1.16	1.15	1.34	8.2	12.1	9.0	0.94	1.27	1.00	1.35	1.16	1.57
	0.5	0	1600	0.080	0.00076	18.7	4.0	3	3.8	4.4	3.9	0.92	1.04	0.96	1.09	1.15	1.30	5.8	6.3	5.9	0.90	0.96	0.97	1.04	1.16	1.24

Ref.	Experimental parameters								Flexural strength (f_{FS})									Static elastic modulus (E_E)								
	w/c ratio	*s/c* ratio	*AR*	κ (c-wt%)	v_f	*UEI*	*SP/CNTs* ratio	*t* (days)	σ_m (MPa)	$\sigma_c^{exp.}$ (MPa)	$\sigma_c^{prd.}$ (MPa)	$\eta_D^{X_E^g}$	$\eta_D^{X_F^m}$	$\eta_H^{Y_E^g}$	$\eta_H^{Y_F^m}$	$\eta_M^{Z_F^g}$	$\eta_M^{Z_E^m}$	E_m (GPa)	$E_c^{exp.}$ (GPa)	$E_c^{prd.}$ (GPa)	$\eta_D^{X_E^g}$	$\eta_D^{X_E^m}$	$\eta_H^{Y_E^g}$	$\eta_H^{Y_E^m}$	$\eta_M^{Z_E^g}$	$\eta_M^{Z_E^m}$
[31]	0.5	0	1600	0.080	0.00076	18.7	4.0	7	4.8	5.6	5.0	0.92	1.03	0.98	1.10	1.15	1.29	7.2	8.0	7.5	0.90	0.97	0.99	1.06	1.16	1.25
	0.5	0	1600	0.080	0.00076	18.7	4.0	28	5.3	6.7	5.6	0.92	1.11	1.00	1.20	1.15	1.38	8.2	9.4	8.6	0.90	0.99	1.00	1.09	1.16	1.27
	0.485	2.75	307	0.080	0.00078	28.2	4.0	3	4.2	6.3	6.0	0.99	1.04	0.96	1.01	1.51	1.59	9.2	13.9	13.8	0.99	1.00	0.97	0.98	1.56	1.57
	0.485	2.75	307	0.080	0.00078	28.2	4.0	7	5.2	6.5	7.7	0.99	0.84	0.98	0.84	1.51	1.28	10.8	16.0	16.4	0.99	0.96	0.99	0.96	1.56	1.52
	0.485	2.75	307	0.080	0.00078	28.2	4.0	28	5.9	10.2	8.8	0.99	1.14	1.00	1.16	1.51	1.75	14.1	24.3	21.7	0.99	1.10	1.00	1.12	1.56	1.75
	0.485	2.75	307	0.100	0.00097	28.2	4.0	3	4.2	6.7	5.9	0.99	1.12	0.96	1.08	1.51	1.71	9.2	16.0	13.6	0.98	1.15	0.97	1.13	1.56	1.83
	0.485	2.75	307	0.100	0.00097	28.2	4.0	7	5.2	7.2	7.6	0.99	0.93	0.98	0.93	1.51	1.43	10.8	18.1	16.3	0.98	1.09	0.98	1.09	1.56	1.73
	0.485	2.75	307	0.100	0.00097	28.2	4.0	28	5.9	11.1	8.8	0.99	1.24	1.00	1.26	1.51	1.91	14.1	27.4	21.6	0.98	1.25	1.00	1.27	1.56	1.98
	0.485	2.75	307	0.300	0.00291	28.2	4.0	3	4.2	4.5	5.3	0.96	0.82	0.87	0.75	1.51	1.29	9.2	11.0	12.3	0.95	0.85	0.90	0.81	1.56	1.39
	0.485	2.75	307	0.300	0.00291	28.2	4.0	7	5.2	6.5	7.1	0.96	0.88	0.94	0.86	1.51	1.38	10.8	14.5	15.3	0.95	0.90	0.96	0.91	1.56	1.48
	0.485	2.75	307	0.300	0.00291	28.2	4.0	28	5.9	9.1	8.6	0.96	1.02	1.00	1.06	1.51	1.60	14.1	21.5	20.9	0.95	0.98	1.00	1.03	1.56	1.60
	0.485	2.75	307	0.500	0.00487	28.2	4.0	3	4.2	4.2	4.7	0.94	0.84	0.79	0.71	1.51	1.36	9.2	9.9	11.1	0.92	0.82	0.84	0.75	1.56	1.39
	0.485	2.75	307	0.500	0.00487	28.2	4.0	7	5.2	6.2	6.6	0.94	0.87	0.90	0.84	1.51	1.41	10.8	12.2	14.4	0.92	0.78	0.93	0.79	1.56	1.33
	0.485	2.75	307	0.500	0.00487	28.2	4.0	28	5.9	8.6	8.4	0.94	0.96	1.00	1.03	1.51	1.55	14.1	20.1	20.2	0.92	0.91	1.00	0.99	1.56	1.55
[30]	0.485	2.75	307	0.100	0.00194	28.2	4.0	28	-	-	-	-	-	-	-	-	-	13.5	27.1	20.4	0.97	1.29	1.00	1.33	1.56	2.08
	0.485	2.75	307	0.200	0.00194	28.2	4.0	28	-	-	-	-	-	-	-	-	-	13.5	23.0	20.4	0.97	1.09	1.00	1.13	1.56	1.76
[112]	0.485	2.75	500	0.100	0.00097	28.2	4.0	3	4.2	6.7	5.9	0.98	1.12	0.96	1.09	1.51	1.73	9.2	16.0	13.5	0.97	1.16	0.97	1.15	1.56	1.85
	0.485	2.75	500	0.100	0.00097	28.2	4.0	7	5.2	7.9	7.5	0.98	1.03	0.98	1.03	1.51	1.58	10.8	18.1	16.2	0.97	1.09	0.98	1.10	1.56	1.74
	0.485	2.75	500	0.100	0.00097	28.2	4.0	28	5.9	11.1	8.8	0.98	1.23	1.00	1.26	1.51	1.91	13.5	27.1	20.5	0.97	1.29	1.00	1.32	1.56	2.06
This study	0.45	2.25	800	0.025	0.00027	8.7	4.0	7	4.7	5.3	6.8	0.97	0.76	0.99	0.77	1.49	1.16	19.8	20.8	29.2	0.96	0.68	1.00	0.71	1.54	1.09
	0.45	2.25	800	0.025	0.00027	15.1	4.0	7	4.7	5.8	6.9	0.98	0.82	0.99	0.83	1.49	1.25	19.8	22.7	29.7	0.98	0.75	1.00	0.76	1.54	1.17
	0.45	2.25	800	0.025	0.00027	8.7	12.0	7	4.7	5.8	7.0	0.99	0.83	0.99	0.83	1.49	1.25	19.8	23.6	30.0	0.99	0.78	1.00	0.79	1.54	1.21
	0.35	2	800	0.050	0.00070	25.0	6.0	28	6.2	7.0	9.3	0.98	0.73	1.00	0.74	1.54	1.15	27.8	31.0	43.3	0.98	0.70	1.00	0.72	1.59	1.14
	0.35	2	2500	0.050	0.00070	25.0	6.0	28	6.2	7.9	9.0	0.94	0.83	1.00	0.88	1.54	1.35	27.8	35.7	41.2	0.93	0.80	1.00	0.87	1.59	1.38
	0.45	2.25	800	0.100	0.00109	15.0	3.0	7	4.7	5.5	6.3	0.91	0.79	0.98	0.85	1.49	1.30	19.8	23.3	26.5	0.88	0.78	0.98	0.87	1.54	1.35
	0.45	2.25	800	0.100	0.00109	8.7	3.0	7	4.7	5.2	5.9	0.85	0.75	0.98	0.87	1.49	1.33	19.8	21.1	24.2	0.81	0.70	0.98	0.86	1.54	1.34
	0.45	2.25	800	0.100	0.00109	7.6	3.0	7	4.7	5.6	5.7	0.83	0.81	0.98	0.97	1.49	1.47	19.8	21.8	23.4	0.78	0.72	0.98	0.91	1.54	1.43
	0.45	2.25	800	0.100	0.00109	10.2	3.0	7	4.7	5.9	6.0	0.87	0.86	0.98	0.97	1.49	1.47	19.8	23.7	25.0	0.83	0.79	0.98	0.93	1.54	1.46
	0.45	2.25	800	0.100	0.00109	25.2	3.0	7	4.7	5.6	6.5	0.94	0.80	0.98	0.83	1.49	1.27	19.8	22.6	27.9	0.93	0.75	0.98	0.80	1.54	1.24
	0.45	2.25	800	0.100	0.00109	12.3	3.0	7	4.7	5.4	6.2	0.89	0.78	0.98	0.85	1.49	1.30	19.8	21.7	25.8	0.86	0.72	0.98	0.83	1.54	1.29
	0.45	2.25	800	0.100	0.00109	15.1	3.0	7	4.7	5.9	6.3	0.91	0.84	0.98	0.91	1.49	1.39	19.8	22.8	26.5	0.88	0.76	0.98	0.84	1.54	1.32
	0.45	3	800	0.100	0.00109	15.8	6.0	28	5.0	5.7	7.4	0.96	0.74	1.00	0.77	1.56	1.20	22.6	26.2	34.3	0.94	0.72	1.00	0.77	1.61	1.23
	0.45	3	800	0.100	0.00109	20.0	12.0	28	5.0	6.5	7.6	0.98	0.84	1.00	0.85	1.56	1.32	22.6	35.0	35.5	0.98	0.96	1.00	0.99	1.61	1.59
	0.6	2	800	0.100	0.00081	25.0	6.0	28	5.0	6.0	6.7	0.98	0.87	1.00	0.89	1.38	1.23	16.9	19.8	23.3	0.97	0.83	1.00	0.85	1.42	1.21
	0.45	0	800	0.100	0.00109	25.0	6.0	28	3.2	4.0	3.7	0.97	1.04	1.00	1.07	1.18	1.26	14.6	17.7	16.7	0.96	1.02	1.00	1.06	1.19	1.26
	0.35	2	800	0.100	0.00140	25.0	6.0	28	6.2	9.1	9.2	0.96	0.95	1.00	0.99	1.54	1.53	27.8	40.0	42.3	0.95	0.90	1.00	0.95	1.59	1.51
	0.35	2	800	0.100	0.00140	25.0	6.0	3	5.2	7.6	7.3	0.96	1.00	0.96	0.99	1.54	1.61	14.3	21.0	21.1	0.95	0.95	0.97	0.97	1.59	1.59
	0.45	3	800	0.100	0.00109	25.0	6.0	28	5.0	6.8	7.6	0.97	0.87	1.00	0.90	1.56	1.40	22.6	33.1	35.0	0.96	0.91	1.00	0.95	1.61	1.52
	0.35	2	2500	0.100	0.00141	25.0	6.0	28	6.2	7.6	8.5	0.89	0.80	1.00	0.90	1.54	1.38	27.8	33.8	38.2	0.86	0.76	1.00	0.89	1.59	1.41
	0.35	2	800	0.300	0.00420	25.0	6.0	3	5.2	5.7	6.2	0.89	0.82	0.87	0.80	1.54	1.42	14.3	15.2	17.9	0.87	0.74	0.90	0.77	1.59	1.36
	0.35	2	800	0.300	0.00420	25.0	6.0	28	6.2	7.6	8.5	0.89	0.80	1.00	0.90	1.54	1.38	27.8	32.0	38.5	0.87	0.72	1.00	0.83	1.59	1.33
	0.35	2	2500	0.300	0.00424	25.0	6.0	28	6.2	7.0	6.6	0.70	0.73	1.00	1.05	1.54	1.62	27.8	31.2	27.9	0.63	0.70	1.00	1.12	1.59	1.78

σ_m: flexural strength of control specimen (without CNTs), $\sigma_c^{exp.}$: experimental flexural strength of CNT-cement nanocomposite, $\sigma_c^{prd.}$: predicted flexural strength of CNT-cement nanocomposite, E_m: flexural modulus of elasticity of control specimen, $E_c^{exp.}$: experimental flexural modulus of elasticity of CNT-cement nanocomposite, $E_c^{prd.}$: predicted flexural modulus of elasticity of CNT-cement nanocomposite, $\eta_D^{X_E^g}$: estimated dispersion relation for flexural strength, $\eta_D^{X_E^m}$: measured dispersion relation for flexural strength, $\eta_D^{X_E^g}$: estimated dispersion relation for flexural modulus of elasticity, $\eta_D^{X_E^m}$: measured dispersion relation for flexural modulus of elasticity, $\eta_H^{Y_E^g}$: estimated hydration age relation for flexural strength, $\eta_H^{Y_E^m}$: measured hydration age relation for flexural strength, $\eta_H^{Y_E^g}$: estimated hydration age relation for flexural modulus of elasticity, $\eta_H^{Y_E^m}$: measured hydration age relation for flexural modulus of elasticity, $\eta_M^{Z_F^g}$: estimated matrix relation for flexural strength, $\eta_M^{Z_F^m}$: measured matrix relation for flexural strength, $\eta_M^{Z_E^g}$: estimated matrix relation for flexural modulus of elasticity, $\eta_M^{Z_E^m}$: measured matrix relation for flexural modulus of elasticity.

APPENDIX B. EXPERIMENTAL TEST RESULTS

This section presents the summary of the experimental test results for flow (Section B.1), mechanical (Section B.2), and durability (Section B.3) properties.

B.1. Fresh Properties

Table B-1. Mini-Cone Slump Test Results for Cement Mortars (*M* series)

Test ID	*w/c* ratio	*s/c* ratio	CNTs (*c-wt*%)	Flow diameter (*mm*)				
				Batch #1	Batch #2	Batch #3	Batch #4	Average
*M*1	0.35	2.6	0.05	153.00	152.75	-	-	152.88
*M*2			0.1	153.75	155.25	-	-	154.50
*M*3			0.15	152.10	151.10	-	-	151.60
*M*4*			0.00	170.50	-	-	-	170.50
*M*5	0.45	3.0	0.05	180.50	177.75	183.75	176.75	179.69
*M*6			0.1	176.51	176.75	175.58	-	176.28
*M*7			0.15	169.25	172.50	173.00	-	171.58
*M*8*			0.00	196.99	192.49	-	-	194.74
*M*9	0.6	3.6	0.05	196.00	193.75	194.00	-	194.58
*M*10			0.1	184.50	188.25	188.75	-	187.17
*M*11			0.15	182.25	183.17	181.30	185.97	183.17
*M*12*			0.00	208.25	-	-	-	208.25

B.2. Mechanical Properties

Table B-2. 7-day Mechanical Properties of Cement Pastes (*C* series)

Test ID	Compressive strength (*MPa*)				Flexural strength (*MPa*)					Elastic modulus (*GPa*)				
	Cube #1	Cube #2	Cube #3	Average	Beam #1	Beam #2	Beam #3	Beam #4	Average	Beam #1	Beam #2	Beam #3	Beam #4	Average
*C*1	85.49	81.90	82.45	83.28	5.37	5.55	5.70	3.54^	5.54	15.58	15.35	9.22^	16.89	15.94
*C*2	83.60	82.90	82.65	83.05	6.21	6.82	6.16	5.46^	6.40	3.63^	17.88	15.45	15.40	16.24
*C*3	83.05	80.56	82.05	81.90	6.33	7.30	3.95^	6.92	6.85	14.88	14.91	15.44	17.06	15.57
*C*4	78.12	73.56	75.01	75.56	6.95	7.13	5.42^	-	7.04	17.1	15.23	17.34	-	16.56
*C*5*	88.32	87.84	-	88.08	8.18	6.95	6.85	8.17	7.54	17.04	16.23	15.36	16.34	16.24
*C*6	59.23	58.59	58.05	58.62	5.07	5.73^	4.32^	4.98	5.03	10.88	10.21	10.29	10.85	10.56
*C*7	54.49	55.62	53.74	54.62	5.23	5.41	4.68	-	5.11	12.45	10.12	4.81^	-	11.29
*C*8	49.68	50.19	50.81	50.23	4.80	5.76^	5.49	4.76	5.02	11.44	9.92	10.61	10.86	10.71
*C*9	54.83	53.33	55.50	54.55	5.01	5.59	5.57	6.76^	5.39	12.02	7.70^	10.14	11.03	11.06
*C*10*	53.78	52.26	55.16	53.73	6.04	5.80	6.72	-	6.19	11.44	11.42	10.75	-	11.20
*C*11	39.26	34.90	34.57	36.24	-	-	-	-	-	-	-	-	-	-
*C*12	36.58	34.05	38.94	36.52	-	-	-	-	-	-	-	-	-	-
*C*13	36.96	38.00	36.58	37.18	-	-	-	-	-	-	-	-	-	-
*C*14	36.62	36.96	32.90	35.49	-	-	-	-	-	-	-	-	-	-
*C*15*	35.66	33.51	35.6	34.92	-	-	-	-	-	-	-	-	-	-

Note: *indicates the control mix (without CNTs), ^ indicates test result was discarded.

Table B-3. 28-day Mechanical Properties of Cement Mortars (*M* series)

Test ID	Flexural strength (*MPa*)				Elastic modulus (*GPa*)			
	Beam #1	Beam #2	Beam #3	Average	Beam #1	Beam #2	Beam #3	Average
*M*1	7.68	7.66	6.78	7.37	16.43	18.98	18.54	17.98
*M*2	-	-	-	-	-	-	-	-
*M*3	-	-	-	-	-	-	-	-
*M*4*	7.9	7.69	7.78	7.79	19.72	17.48	20.90	19.37
*M*5	5.42	4.42	4.52	4.79	14.26	14.52	13.78	14.19
*M*6	4.91	4.38	4.71	4.67	15.11	13.96	9.06^	14.54
*M*7	4.25	3.52	3.96	3.91	12.37	13.18	10.68^	12.78
*M*8*	4.83	5.08	5.44	5.12	16.03	15.67	15.66	15.79
*M*9	4.65	4.45	4.23	4.44	14.52	13.93	6.78^	14.23
*M*10	3.85	4.15	4.06	4.02	12.13	13.35	12.86	12.78
*M*11	4.28	4.12	4.34	4.25	14.13	11.80	12.68	12.87
*M*12*	4.79	4.75	4.69	4.74	8.60^	13.56	14.51	14.04

Note: *indicates the control mix (without CNTs), ^indicates test result was discarded.

Table B-4. Mechanical Properties Test Results: f_{CS}, f_{FS}, and E_F (*I*~*V* series)

Interaction	Tests ID	Compressive strength (*MPa*)				Flexural strength (*MPa*)						Elastic modulus (*GPa*)					
		Cube #1	Cube #2	Cube #3	Average	Beam #1	Beam #2	Beam #3	Beam #4	Beam #5	Average	Beam #1	Beam #2	Beam #3	Beam #4	Beam #5	Average
I	*I*-800/0.05	72.21	73.29	70.27	71.92	6.79	6.60	7.00	7.42	-	6.95	33.58	30.87	28.91	30.58	-	30.99
	I-800/0.1‡	80.48	81.67	81.13	81.09	8.45	9.67	9.28	8.85	-	9.06	38.61	38.43	11.31^	42.89	-	39.98
	I-800/0.3+	73.38	75.51	74.84	74.58	7.39	7.30	7.99	7.84	-	7.63	31.96	33.34	18.53^	30.67	-	31.99
	I-2500/0.05	79.55	82.22	78.88	80.22	8.16	7.47	7.99	5.80^	-	7.87	37.14	35.79	34.01	18.60^	-	35.65
	I-2500/0.1	76.36	79.34	73.38	76.36	7.36	7.82	7.17	7.98	-	7.58	33.96	31.02	21.34^	36.37	-	33.78
	I-2500/0.3	67.88	69.72	64.07	67.22	7.32	6.80	7.38	6.44	-	6.99	29.76	38.56^	30.15	33.82	-	31.24
II	*II*-500/50	50.47	51.18	53.35	51.67	5.15	5.27	5.25	-	-	5.22	20.74	21.41	15.41^	-	-	21.08
	II-1000/50	51.93	54.38	-	53.16	5.24	5.37	5.51	-	-	5.37	22.48	20.90	21.61	-	-	21.66
	II-1500/50	56.59	60.95	57.52	58.35	6.08	5.76	5.71	-	-	5.85	22.78	23.79	23.39	-	-	23.32
	II-200/75	48.67	55.31	57.92	53.97	5.94	5.35	5.64	-	-	5.64	21.85	21.79	21.63	-	-	21.76
	II-300/75	49.13	57.78	54.61	53.84	6.08	5.75	5.95	-	-	5.93	24.04	23.28	23.83	-	-	23.71
	II-500/75	54.38	54.87	55.14	54.80	5.64	N/A	5.34	-	-	5.49	23.46	N/A	22.06	-	-	22.76
	II-1000/75	47.29	50.35	53.35	50.33	5.58	5.52	4.57^	-	-	5.55	8.93^	23.48	21.71	-	-	22.60
III	*III*-500/4	51.56	49.18	50.69	50.48	5.64	5.39	4.91	-	-	5.31	21.96	20.47	19.89	-	-	20.77
	III-500/12	58.62	59.52	60.90	59.68	6.28	5.50	5.70	-	-	5.83	24.91	23.69	22.31	-	-	23.64
	III-1500/4	63.16	55.04	56.50	58.23	5.88	6.08	5.37	-	-	5.78	22.96	23.45	21.63	-	-	22.68
	III-1216/6	49.68	51.23	49.71	50.21	6.06	5.69	5.46	4.50^	-	5.74	27.01	27.90	13.79^	23.81	-	26.24
	III-1850/12	49.85	54.44	50.10	51.46	6.45	6.31	6.20	7.02	-	6.50	N/A	34.72	35.23	35.18	-	35.04
	III-2733/6*	54.97	55.80	56.54	55.77	6.73	6.47	4.92^	7.19	-	6.80	33.15	35.20	22.49^	30.94	-	33.10
IV	*IV*-0.35/2‡	80.48	81.67	81.13	81.09	8.45	9.67	9.28	8.85	-	9.06	38.61	38.43	11.31^	42.89	-	39.98
	IV-0.45/0	77.34	74.22	79.15	76.90	4.06	3.84	3.42	4.46	-	3.95	18.03	16.90	16.80	19.14	-	17.72
	IV-0.45/3*	54.97	55.80	56.54	55.77	6.73	6.47	4.92^	7.19	-	6.80	33.15	35.20	22.49^	30.94	-	33.10
	IV-0.6/2	55.62	60.29	60.73	58.88	6.04	6.09	5.75	-	-	5.96	20.52	18.97	20.02	-	-	19.84
V	*V*-*0.1/3*‡	68.03	68.79	70.65	69.16	7.41	7.72	7.89	7.50	-	7.63	21.53	21.15	20.45	9.81^	-	21.04
	V-0.3/3+	52.90	53.27	54.59	53.59	5.38	5.39	6.14	5.97	-	5.72	14.64	15.41	15.54	15.25	-	15.21
	V-0.1/28‡	80.48	81.67	81.13	81.09	8.45	9.67	9.28	8.85	-	9.06	38.61	38.43	11.31^	42.89	-	39.98
	V-0.3/28+	73.38	75.51	74.84	74.58	7.39	7.30	7.99	7.84	-	7.63	31.96	33.34	18.53^	30.67	-	31.99
Control (without CNTs)	*R*1 (b1)	65.31	67.02	68.9	66.85	5.85	5.97	6.05	6.59	6.33	6.16	27.08	28.56	27.12	29.80	26.47	27.81
	*R*1 (b2)	63.91	69.1	-		-	-	-	-	-		-	-	-	-	-	
	*R*2	45.95	48.57	45.78	46.77	4.77	4.54	4.91	-	-	4.74	20.73	18.92	12.03^	-	-	19.83
	*R*3	48.25	49.73	49.92	49.30	4.52^	4.99	5.28	5.21	-	5.00	23.13	21.08	24.94	21.16	-	22.58
	*R*4 (b1)	73.34	70.57	-	71.21	2.81^	2.61^	3.07	-	-	3.22	14.09	14.28	15.73	-	-	14.55
	*R*4 (b2)	69.33	-	-		3.29	3.29	-	-	-		14.24	14.41	-	-	-	
	*R*5	47.73	49.28	48.52	48.51	5.33^	4.94	4.97	-	-	4.96	16.01	19.17	15.46	-	-	16.88
	*R*6 (b1)	50.68	52.50	52.00	51.43	5.07	5.01	5.25	5.29	-	5.16	14.31	7.05^	14.45	13.37	-	14.33
	*R*6 (b2)	50.92	51.07	-		5.33	5.16	5.00	5.19	-		27.01^	14.21	15.31	17.55^	-	

Note: *, ‡, and + indicate the same mix proportions; b1 and b2 represent batch numbers 1 and 2, respectively; ^ indicates test result was discarded, f_{CS}: compressive strength, f_{FS}: flexural strength, E_F: elastic modulus

Table B-5. Mechanical Properties Test Results: E_d (*I*~*V* series)

Interaction	Tests ID	Age (days)																			
		1			2			3			7			14			21			28		
		Beam #1	Beam #2	avg.	Beam #1	Beam #2	avg.	Beam #1	Beam #2	avg.	Beam #1	Beam #2	avg.	Beam #1	Beam #2	avg.	Beam #1	Beam #2	avg.	Beam #1	Beam #2	avg.
I	*I*-800/0.05	34.02	35.12	34.57	39.36	40.58	39.97	40.78	42.34	41.56	43.14	43.87	43.51	45.63	46.02	45.83	45.91	46.30	46.11	46.30	47.30	46.80
	I-800/0.1‡	36.90	36.41	36.66	48.99	46.67	47.83	51.70	48.08	49.89	53.12	50.55	51.84	54.52	51.83	53.18	56.04	52.87	54.46	55.91	53.31	54.61
	I-800/0.3+	30.56	32.30	31.43	42.66	42.26	42.46	43.91	44.40	44.16	46.17	46.77	46.47	47.95	48.18	48.07	48.45	50.06	49.26	48.95	50.21	49.58
	I-2500/0.05	34.82	36.15	35.49	40.56	44.10	42.33	42.39	44.90	43.65	43.46	45.68	44.57	46.27	48.24	47.26	46.51	48.29	47.40	48.60	49.73	49.17
	I-2500/0.1	37.08	37.45	37.27	42.43	42.41	42.42	44.32	43.30	43.81	47.18	46.63	46.91	48.45	47.48	47.97	48.43	47.66	48.05	49.39	48.76	49.08
	I-2500/0.3	30.89	33.34	32.12	42.38	41.51	41.95	43.32	43.47	43.40	47.15	45.89	46.52	47.08	46.97	47.03	47.77	47.94	47.86	48.93	48.17	48.55
III	*III*-1216/6	28.80	29.78	29.29	34.72	35.70	35.21	36.56	36.47	36.52	37.98	40.55	39.27	38.65	41.71	40.18	39.18	41.47	40.33	40.01	43.00	41.51
	III-1850/12	34.01	31.50	32.76	42.99	38.97	40.98	46.44	44.04	45.24	46.71	43.05	44.88	48.53	45.63	47.08	49.12	46.82	47.97	49.62	46.74	48.18
	III-2733/6*	34.01	34.83	34.42	40.11	39.03	39.57	41.42	40.12	40.77	43.51	42.37	42.94	45.63	43.33	44.49	46.06	43.48	44.77	46.29	44.17	45.23
IV	*IV*-0.35/2‡	36.90	36.41	36.66	48.99	46.67	47.83	51.70	48.08	49.89	53.12	50.55	51.84	54.52	51.83	53.18	56.04	52.87	54.46	55.91	53.31	54.61
	IV-0.45/0	11.59	13.43	12.51	16.67	16.49	16.58	17.26	18.03	17.65	20.70	19.01	19.86	21.16	22.64	21.90	22.91	22.60	22.76	23.57	23.21	23.39
	IV-0.45/3*	34.01	34.83	34.42	40.11	39.03	39.57	41.42	40.12	40.77	43.51	42.37	42.94	45.63	43.33	44.49	46.06	43.48	44.77	46.29	44.17	45.23
	IV-0.6/2	22.60	28.40	25.50	29.89	35.12	32.51	31.29	37.84	34.57	34.10	41.16	37.63	35.97	43.33	39.65	37.77	44.07	40.92	37.68	44.76	41.22
V	*V*-0.1/28‡	36.90	36.41	36.66	48.99	46.67	47.83	51.70	48.08	49.89	53.12	50.55	51.84	54.52	51.83	53.18	56.04	52.87	54.46	55.91	53.31	54.61
	V-0.3/28+	30.56	32.30	31.43	42.66	42.26	42.46	43.91	44.40	44.16	46.17	46.77	46.47	47.95	48.18	48.07	48.45	50.06	49.26	48.95	50.21	49.58
Control (without CNTs)	*R*1	33.50	31.76	32.63	38.31	38.75	38.53	39.79	39.46	39.63	40.99	41.09	41.04	42.71	42.90	42.81	44.14	43.70	43.92	44.14	44.92	44.53
	*R*3	28.11	28.37	28.24	32.77	31.71	32.24	32.95	32.80	32.88	35.09	36.26	35.68	36.76	37.46	37.11	38.81	38.06	38.44	39.16	38.96	39.06
	*R*4	11.08	11.23	11.16	14.16	15.94	15.05	15.65	17.11	16.38	17.37	19.16	18.27	20.73	21.67	21.20	21.41	22.39	21.90	22.18	21.63	21.91
	*R*5	17.97	18.20	18.09	25.23	25.17	25.20	27.90	26.31	27.11	29.48	30.07	29.78	31.89	31.38	31.64	32.69	33.16	32.93	34.84	34.21	34.53

Note: *, ‡, and + indicate the same mix proportions, E_d: dynamic elastic modulus

B.2.1. Effect of Sand Gradation and Mixing Procedure

In this section, the influence of sand gradation (Section B.2.1.1) and mixing procedure (Section B.2.1.2) on the mechanical properties of CNT-cement mortars is investigated. The details are discussed as follows

To study the influence of sand gradation and mixing procedure, Test ID *P*1 was selected as the base specimen, which was identical to Test ID *III*-500/12 (see Table 5-7). The control mix (without CNTs) for these test IDs is *R*2 (see Table 5-8). The test IDs and mix proportions are listed in Table B-6.

Table B-6. Test Identifications and Mix Proportions for Sand Gradation and Mixing Procedure

Test ID	*w/c* ratio	*s/c* ratio	*AR*	κ (*c-wt*%)	UE_T (*J/ml*)	*UA* (%)	*SP/CNTs ratio*	Mixing procedure
*P*1	0.45	2.25 (*R*)	800	0.025	500	50	12	*B*
*P*2		2.25 (*S*)						
*P*3		2.25 (*S*)						*A*

Note: *R*: river sand, *S*: silica sand

To study the influence of sand gradation, test ID *P*1 (which used river sand; *R*) was compared with test ID *P*2 (which used silica sand; *S*). Both test IDs had the same mix proportion and mixing procedure.

To study the influence of mixing procedure, test ID *P*1 (which used mixing procedure *B*; see Section 5.3.2.2) was compared with test ID *P*3 (which used mixing procedure *A*; see Section 5.3.2.2). Both test IDs had the same mix proportion and sand gradation.

B.2.1.1. Effect of Sand Gradation

Figure B-1 shows the influence of sand gradation (river sand vs. silica sand) on C_R (Figure B-1 (a)), F_R (Figure B-1 (b)), and E_R (Figure B-1 (c)), respectively.

When using river sand (test ID $P1$), the values of C_R, F_R, and E_R were 1.28, 1.23, and 1.19, respectively. When using silica sand (test ID $P2$), the values of C_R, F_R, and E_R were 1.28, 1.17, and 1.15, respectively. This suggests that the two different sand gradation used in this study does not exhibit a clear change in the mechanical properties (p-value > 0.05; see Figure B-1).

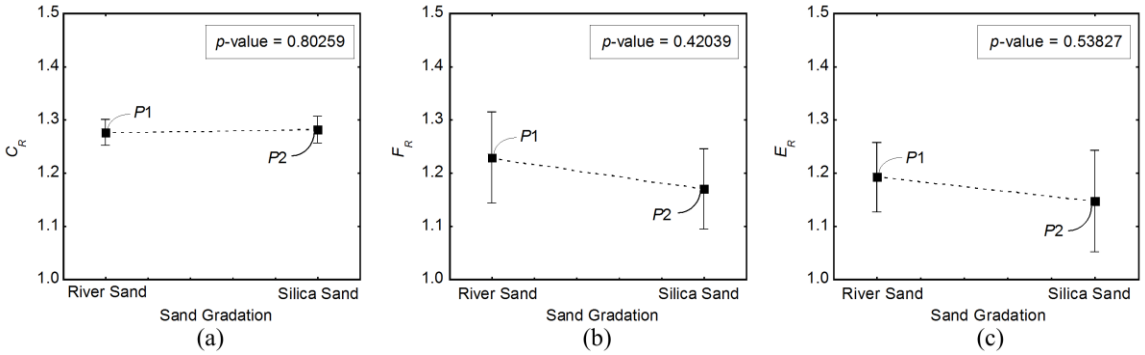

Figure B-1. Effect of sand gradation: (a) C_R (b) F_R (c) E_R

B.2.1.2. Effect of Mixing Procedure

Figure B-2 shows the influence of mixing procedure (A vs. B) on C_R (Figure B-2 (a)), F_R (Figure B-2 (b)), and E_R (Figure B-2 (c)), respectively.

It can be seen that utilizing mixing procedure of either A or B does not affect the mechanical by showing the p-values > 0.05 for C_R (p-value = 0.57), F_R (p-value = 0.81), and E_R (p-value = 0.67).

It seems that neither sand gradation nor mixing procedure affects the mechanical properties of CNT-cement nanocomposites. Therefore, they are not considered as important variables in the modeling process (see Chapter 8). Note that this conclusion is based on the limited range of sand gradation and mixing procedure used in this research program and might not be generalized.

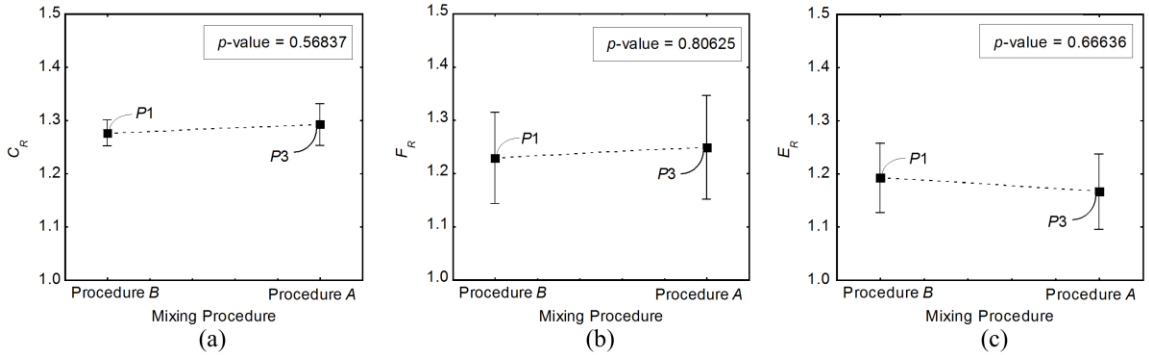

Figure B-2. Effect of mixing procedure: (a) C_R (b) F_R (c) E_R

B.2.2. General Trend of E_d over Time

This section discusses the influence of interactions between multiple variables on E_d of CNT-cement nanocomposites over time.

B.2.2.1. Interactions between κ and *AR* (Interaction *I*)

Figure B-3 shows the influence of different concentrations of CNTs with *AR* of 800 (Figure B-3 (a)) and 2500 (Figure B-3 (b)) on E_d over time. In general, E_d increased rapidly at early ages (up to t = 3 days), beyond which the rate of increase in E_d decreased and it eventually stabilized beyond t = 7 days.

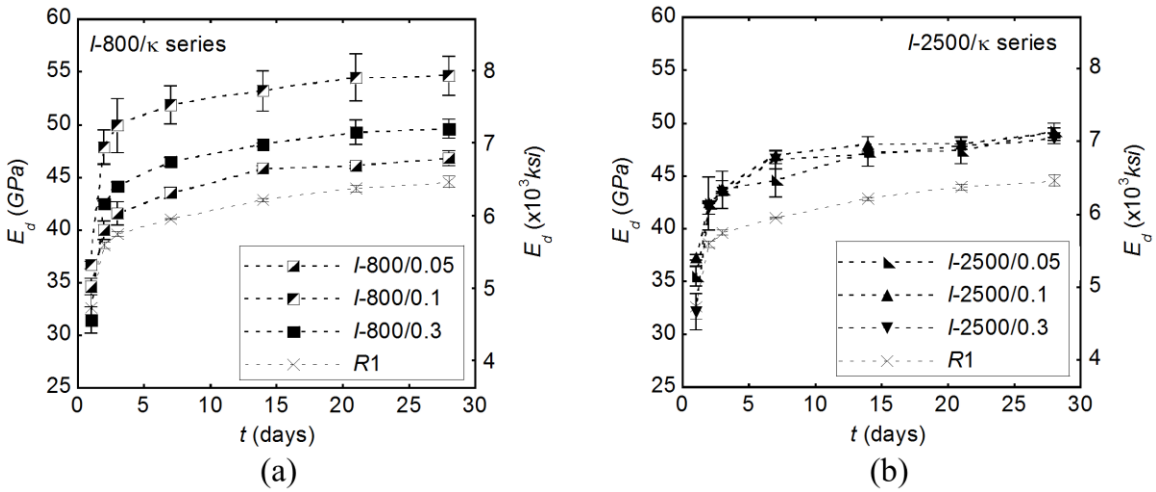

Figure B-3. Influence of κ on E_d over time: (a) *AR* = 800 (b) *AR* = 2500

Figure B-3 (a) shows that addition of CNTs was effective in increasing E_d, regardless of κ. However, the effectiveness of CNTs reduced beyond κ = 0.1 *c-wt*%, most probably due to the dispersion issues which increased the porosity. The highest improvement in 28-day E_d was achieved using test ID *I*-800/0.1 which exhibited 22.6% increase compared with the control specimen (test ID *R*1).

Figure B-3 (b) shows that, in case of *AR* = 2500, different concentrations of CNTs resulted in similar level of improvements in E_d. Therefore, κ = 0.05 *c-wt*% can be considered as the optimum dosage for *AR* = 2500 to increase E_d. This shows good agreement with the findings in f_{CS}, f_{FS}, and E_F (see Section 6.3.1). The 28-day E_d of *I*-2500/0.05 was 49.17 *GPa* (7132 *ksi*) which showed 10.4% increase compared with *R*1 ($E_d = 44.53$ *GPa* [6459 *ksi*]).

B.2.2.2. Interactions between UE_T and *SP/CNTs* Ratio (Interaction *III*)

Figure B-4 shows the contributions of UE_T and *SP/CNTs* ratio to E_d over time for CNT-cement mortars (*w/c* and *s/c* ratios of 0.45 and 0.3, respectively) with and without inclusion of 0.1 *c-wt*% of Type II CNTs (*AR* = 800). The control mix is *R*3. In case of *III*-1216/6, 28-day E_d exhibited a modest increased of 6.30% compared with *R*3 (*p*-value = 0.24431 > 0.05). However, Test IDs of either *III*-2733/6 or *III*-1850/12 resulted in a significant increase in 28-day E_d by 15.8% (*p*-value = 0.02851 < 0.05) and 23.4% (*p*-value = 0.02415 < 0.05), respectively, compared with *R*3.

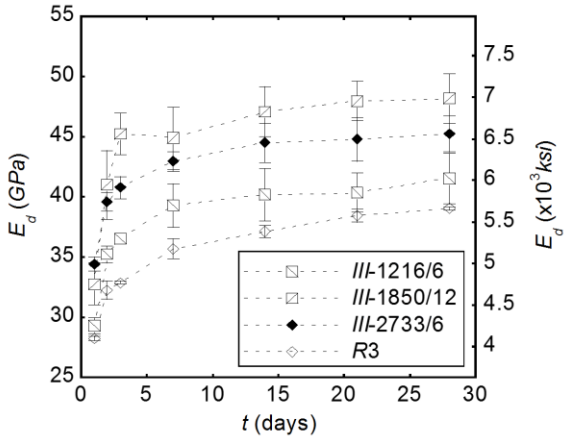

Figure B-4. Effect of UE_T and *SP/CNTs* ratio on E_d over time

B.2.2.3. Interactions between *w/c* and *s/c* ratios (Interaction *IV*)

Figure B-5 shows the influence of cement matrix composition (various *w/c* and *s/c* ratios) on E_d over time. Figure B-5 (a) and (b) compares the influence of *w/c* ratio (*w/c* = 0.35 and 0.6) at a fixed *s/c* = 2. Figure B-5 (c) and (d) compares the influence of *s/c* ratio (*s/c* = 0 and 3) at a fixed *w/c* = 0.45.

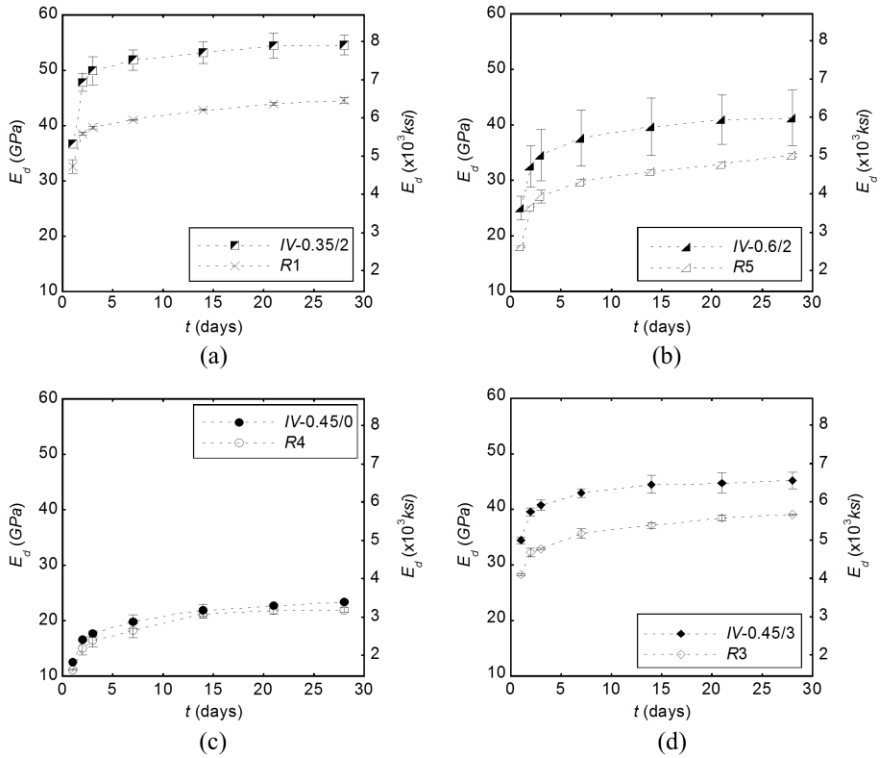

Figure B-5. Effect of matrix composition on E_d over time

The results indicate that utilizing the same type and concentration of CNTs exhibited higher contribution to increase E_d in denser cement matrix (i.e., lower *w/c* ratio or higher *s/c* ratio). For example, the 28-day E_d increased by 22.6% and 19.4% in case of *IV*-0.35/2 (see Figure B-5 (a)) and *IV*-0.6/2 (see Figure B-5 (b)), respectively, compared with their control specimens. In addition, *IV*-0.35/2 showed lower variability in E_d at different ages than *IV*-0.6/2. Also, as *s/c* ratio increased from 0 to 3, *IV*-0.45/0 resulted in the lowest increase in 28-day E_d by 6.8%, while *IV*-0.45/3 exhibited 15.8% increase, compared with the respective control specimen.

B.3. Durability: Alkali-Silica Reaction

B.3.1. Effect of CNT Concentration and Aspect Ratio

Figure B-6 (a) and (b) present the influence of different concentrations (0.1 and 0.3 *c-wt*%) of Type II CNTs (*AR* = 800) on the progress in the average expansion and E_d over time, respectively, for mortar bars with *w/c* ratio of 0.35 subjected to ASTM C1260 severe ASR conditions. The standard deviation of different mixtures is also included.

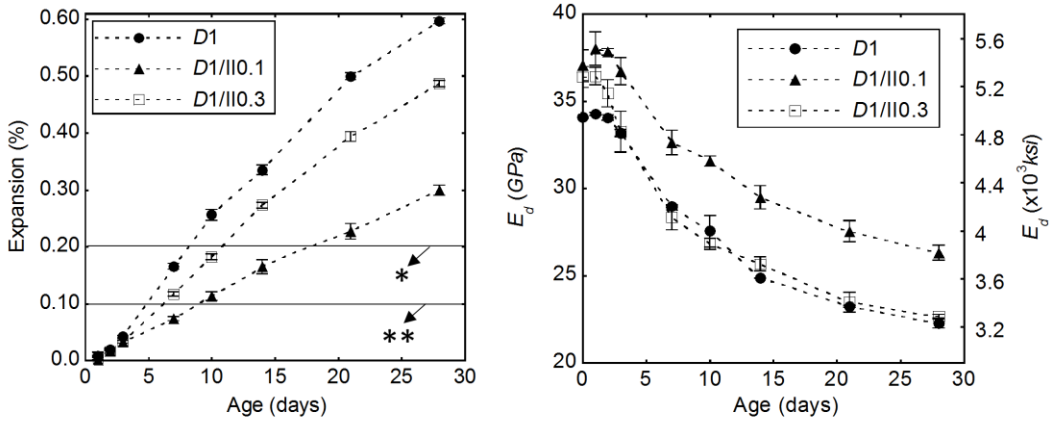

Figure B-6. Influence of Type II CNTs: (a) expansion (b) E_d (*w/c* = 0.35)
Note: * ASTM C1260 ASR reactive limit at 14 days, ** ASTM C1260 ASR non-reactive limit at 14 days

Figure B-6 (a) shows that utilizing 0.1 *c-wt*% Type II CNTs (*D*1/II0.1) resulted in a significant decrease in the average expansion at various ages compared with the control specimen (*D*1). However, in case of *D*1/II0.3, the benefits of adding CNTs significantly decreased.

Figure B-6 (b) shows the contributions of *D*1/II0.1 and *D*1/II0.3 to controlling ASR cracks by showing E_d as a function of age of mortar bars. Note that age of 0 is used for E_d of mortar bars after 1 day submersion in water at 80±2℃ (zero reading) followed by E_d of mortar bars at 1, 2, 3, 7, 10, 14, and 28 days submersion in 1N NaOH solution at 80±2℃. The average E_d exhibited a slight increase after 1 day submersion in 1N NaOH solution compared with the zero reading for all the test IDs. Beyond this point, E_d degraded over time. The zero day E_d for *D*1 was 34.1 *GPa* (4946 *ksi*). As ASR progressed, the 14- and 28-day E_d of *D*1 reduced to 24.9 *GPa* (3611 *ksi*) and 22.3 *GPa* (3234 *ksi*), respectively. In case of *D*1/II0.1, E_d exhibited higher values than *D*1. For example, *D*1/II0.1exhibited almost 20% higher values of E_d at 14 and 28 days compared with *D*1. Even though *D*1/II0.3 outperformed compared with *D*1 in the expansion test results (see Figure B-6 (a)), the average E_d exhibited marginal difference by showing *p*-values > 0.05 beyond age of 2 days.

The benefits of utilizing *D*1/II0.1 and *D*1/II0.3 in suppressing ASR cracks can be statistically confirmed using ANOVA test results. Table C-16 shows the *p*-values between 0-day E_d and various ages up to 28-day, for different test IDs. In case of *D*1, the degradation in E_d compared with zero-reading started at age of 3 days by showing *p*-values smaller than 0.05 afterwards. Conversely, *D*1/II0.1 and *D*1/II0.3 did not exhibit the *p*-values smaller than 0.05 until age of 7 days. This indicates that incorporating CNTs might

restrain the propagation of internal cracks due to ASR.

Figure B-7 shows the average expansion of three mortar bars over time for *w/c* ratio of 0.35 with and without inclusion of different concentrations (0.1 and 0.3 *c-wt*%) of Type I MWCNTs. Similar to Type II MWCNTs (see Figure B-6 (a)), utilizing 0.1 *c-wt*% of Type I MWCNTs (test ID *D*1/I0.1) outperformed compared with concentration of 0.3 *c-wt*% (test ID *D*1/I0.3) at different ages. In Case of *D*1/I0.1, the average expansion was 0.172 and 0.308 at 14 and 28 days, respectively, which exhibited around 49% reduction compared with *D*1. Conversely, *D*1/I0.3 exhibited marginal difference compared with *D*1 by exhibiting *p*-values > 0.05 at different ages except for 28-day expansion (*p*-value = 0.04049 < 0.05). The average expansion of *D*1/I0.3 exhibited 1.2% increase and 6.4% decrease at 14 and 28 days, respectively, compared with *D*1.

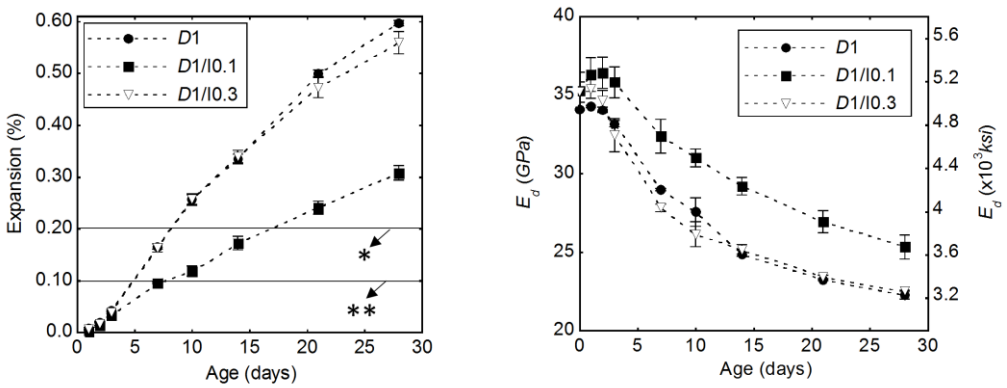

Figure B-7. Influence of Type I CNTs: (a) expansion (b) E_d (*w/c* = 0.35)
Note: * ASTM C1260 ASR reactive limit at 14 days, ** ASTM C1260 ASR non-reactive limit at 14 days

Figure B-7 (b) shows the influence of different concentrations (0.1 and 0.3 *c-wt*%) of Type I MWCNTs on the average E_d of mortar bars with *w/c* ratio of 0.35. The average E_d of *D*1 and *D*1/I0.3 started to decrease after 1 day exposure to ASTM C1260 extreme laboratory ASR conditions. However, in case of *D*1/I0.1, the average E_d continued to increase up to 2 days, beyond which it started to degrade. This can also be statistically

confirmed through ANOVA test results (see Table C-16). The 3-day E_d of $D1$ showed significant decrease compared with 0-day (p-value = 0.02591 < 0.05), while it did not exhibit significant decrease (p-value > 0.05) until age of 7 days and 10 days for $D1$/I0.3 and $D1$/I0.1, respectively (see Table C-16). In case of $D1$/I0.1, the E_d exhibited higher values than $D1$ for all the investigated ages up to 17.5% at age of 14 days. Conversely, in case of $D1$/I0.3, the average E_d exhibited marginal increase compared with $D1$ by showing the p-values > 0.05 at different ages (except for age of 7 days; p-value = 0.02156 < 0.05).

B.3.2. Effect of Cement Matrix Composition

Figure B-8 (a) and (b) show the average expansion and E_d of cement mortars with *w/c* and *s/c* of 0.45 and 3, respectively, with and without inclusion of 0.1 *c-wt*% Type II CNTs, respectively, when the ultrasonication procedure *A* was used (same ultrasonication procedure as $D1$/I and $D1$/II series).

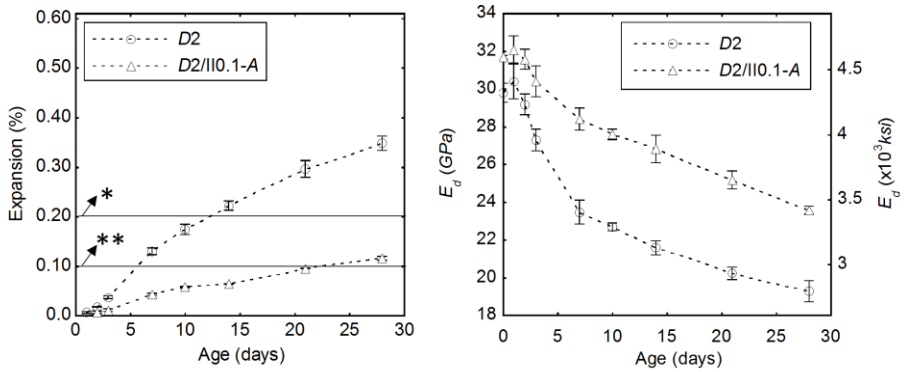

Figure B-8. Influence of CNTs: (a) expansion (b) E_d (*w/c* = 0.45)
Note: * ASTM C1260 ASR reactive limit at 14 days, ** ASTM C1260 ASR non-reactive limit at 14 days

Figure B-8 (a) shows that the control cement mortar (test ID $D2$) expanded beyond the acceptable limit of ASTM C1260 (0.22% and 0.35% at age of 14 and 28 days, respectively). Conversely, $D2$/II0.1-*A* significantly reduced the expansion by 72.7% (expansion of 0.06%) and 65.7% (expansion of 0.12%) at 14 and 28 days, respectively,

compared with *D*2. This expansion level is below the expansion limit of 0.1% of ASTM C1260 test method at 14 days. This suggests that adding CNTs (up to threshold concentration of 0.1 *c-wt*% in this study) might prevent the ASR expansion under field conditions.

Figure B-8 (b) shows the contribution of *D*2/II0.1-*A* on E_d. The 1-day E_d of *D*2 was 30.4 *GPa* (4409 *ksi*). The average E_d significantly decreased by 36.5% to 19.3 *GPa* (2799 *ksi*), after 28 days exposure to ASR conditions. Conversely, *D*2/II0.1-*A* resulted in 26.5% decrease in E_d from 1 to 28 days (from 32.1 to 23.6 *GPa* [4656 to 3423 *ksi*]). Although the average E_d exhibited a marginal difference between *D*2 and *D*2/*II*0.1-*A* at age of 1 day (5.4%), the 28-day E_d exhibited 20.1% difference. This might be attributed to a good degree of CNT dispersion. The well-dispersed CNTs might reduce the permeability as well as delaying the propagation of cracks by bridging between them. Therefore, E_d of *D*2/II0.1-*A* reduced in a lower rate than *D*2.

B.3.3. Effect of Ultrasonication Procedure

Figure B-9 (a) and (b) show the influence of *D*2/II0.1-*B* on time-dependent expansion and E_d, respectively. The control mix is *D*2. Figure B-9 (a) shows that despite the exceptional performance of *D*2/II0.1-*A* in reducing ASR expansion (see Figure B-8 (a)), *D*2/II0.1-*B* exhibited the 14- and 28-day average expansion of 0.24 (6.8% higher than *D*2) and 0.37 (7.4% higher than *D*2), respectively. Nevertheless, the *p*-values > 0.05 suggest that there is no significant difference between *D*2 and *D*2/II0.1-*B*. Also, in terms of E_d (see Figure B-9 (b)), *D*2/II0.1-*B* exhibited marginal difference compared with *D*2 (*p*-value > 0.05). These results indicate that to exploit CNT advantages to control ASR progress, their proper dispersion is vital.

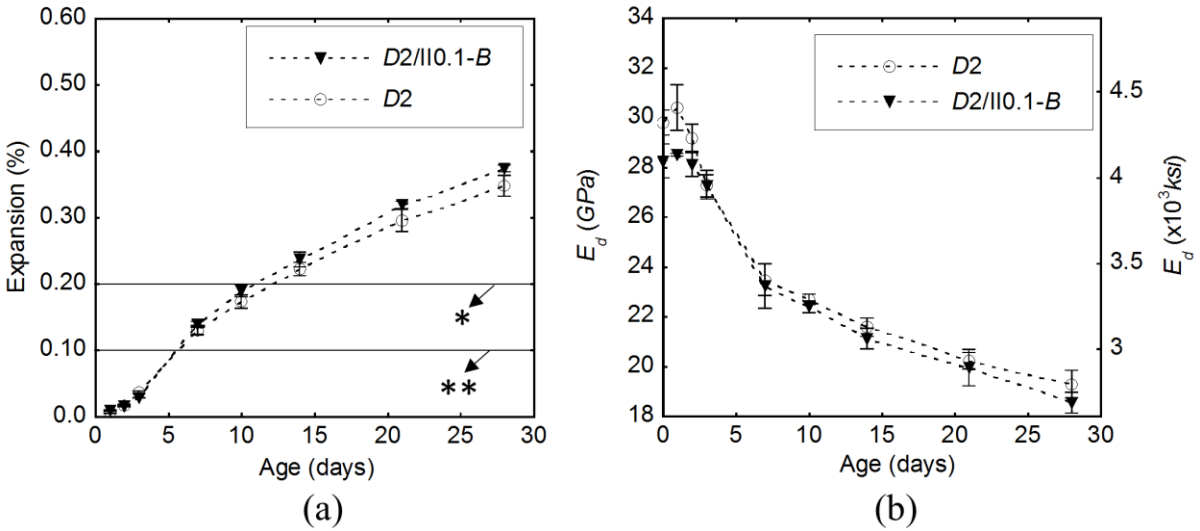

Figure B-9. Influence of ultrasonication procedure *B*: (a) expansion (b) E_d (w/c = 0.45)
Note: * ASTM C1260 ASR reactive limit at 14 days, ** ASTM C1260 ASR non-reactive limit at 14 days

Table B-7. 28-Day Mechanical Properties Test Results (*D* series)

Tests *ID*	Compressive strength (*MPa*)				Flexural strength (*MPa*)						Elastic modulus (*GPa*)					
	Cube #1	Cube #2	Cube #3	Average	Beam #1	Beam #2	Beam #3	Beam #4	Beam #5	Average	Beam #1	Beam #2	Beam #3	Beam #4	Beam #5	Average
D1/I0.1	63.24	64.22	-	63.73	5.76	5.03	5.35	4.61^	5.66	5.45	13.67	10.63	11.93	13.37	11.54	12.23
D1/II0.1	68.96	66.88	-	67.92	6.36	6.62	6.20	4.94^	6.02	6.30	13.20	13.22	14.25	12.46	13.15	13.26
D1/I0.3	57.74	60.07	-	58.91	4.35	4.42	4.21	4.76	4.27	4.40	12.46	10.31	10.13	11.00	11.40	11.06
D1/II0.3	63.41	63.81	-	63.61	4.75	4.45	4.97	4.03	4.10	4.46	11.51	12.88	14.01	11.67	11.13	12.24
D2/II0.1-A	50.75	54.37	-	52.56	4.87	4.94	5.39	4.63	4.56	4.88	12.25	12.71	11.72	13.85	14.00	12.91
D2/II0.1-B	40.78	41.73	39.49	40.67	3.26	3.20	2.89	-	-	3.12	7.63	6.80	6.55	-	-	6.99
D1	57.17	61.66	-	59.42	4.63	4.54	4.04	3.94	4.09	4.25	9.05	11.37^	8.71	8.84	9.74	9.09
D2	42.47	43.73	-	43.10	3.92	3.38	3.41	3.51	3.70	3.58	6.87	6.76	10.07	9.78	3.92^	8.37

APPENDIX C. STATISTICAL ANALYSIS: ANOVA

This section presents the summary of the statistical analysis (p-values) to analyze the influences of main variables and their interactions for evaluating different properties of CNT-cement nanocomposites.

Table C-1. ANOVA Results: p-Values of Different CNT Concentrations for Mini-Cone Slump Test (M series)

CNT concentration (c-wt%)	w/c = 0.35				w/c = 0.45				w/c = 0.6			
	CNT concentration (c-wt%)											
	0.00	0.05	0.10	0.15	0.00	0.05	0.10	0.15	0.00	0.05	0.10	0.15
0.00	-	0.0078	0.05169	0.02888	-	0.00526	0.00179	0.00199	-	0.01067	0.0158	0.00155
0.05		-	0.1669	0.12995		-	0.12957	0.01191		-	0.00812	0.00036
0.10			-	0.08446			-	0.01874			-	0.05853
0.15				-				-				-

Table C-2. ANOVA Results: p-Values between Different Test IDs within Interaction I for f_{CS}, f_{FS}, and E_F

Interaction	Test ID	I-800/0.05			I-800/0.1‡			I-800/0.3⁺			I-2500/0.05			I-2500/0.1			I-2500/0.3		
		f_{CS}	f_{FS}	E_F	f_{CS}	f_{FS}	E_F	f_{CS}	f_{FS}	E_F	f_{CS}	f_{FS}	E_F	f_{CS}	f_{FS}	E_F	f_{CS}	f_{FS}	E_F
I	I-800/0.05	-	-	-	0.00064	0.00056	0.00300	0.07069	0.03191	0.47866	0.00356	0.01932	0.01932	N/A	N/A	N/A	N/A	N/A	N/A
	I-800/0.1‡				-	-	-	0.00081	0.00379	0.00838	N/A	N/A	N/A	0.05422	0.00390	0.04351	N/A	N/A	N/A
	I-800/0.3⁺							-	-	-	N/A	N/A	N/A	N/A	N/A	N/A	0.01444	0.06069	0.64595
	I-2500/0.05										-	-	-	0.12609	0.35316	0.35737	0.00264	0.03765	0.04940
	I-2500/0.1													-	-	-	0.01882	0.08794	0.27626
	I-2500/0.3																-	-	-

Note: f_{CS}: compressive strength; f_{FS}: flexural strength; E_F: elastic modulus; "_" indicates the evaluation is not valid.

Table C-3. ANOVA Results: *p*-Values between Different Test IDs within Interaction *II* for f_{CS}, f_{FS}, and E_F

Interaction	Test ID	*II*-500/50			*II*-1000/50			*II*-1500/50			*II*-200/75			*II*-300/75			*II*-500/75			*II*-1000/75		
		f_{CS}	f_{FS}	E_F	f_{CS}	f_{FS}	E_F	f_{CS}	f_{FS}	E_F	f_{CS}	f_{FS}	E_F	f_{CS}	f_{FS}	E_F	f_{CS}	f_{FS}	E_F	f_{CS}	f_{FS}	E_F
II	*II*-500/50	-	-	-	0.4123	0.1574	0.4261	0.0135	0.0068	0.0159	N/A	N/A	N/A	N/A	N/A	N/A	0.0249	0.1160	0.1621	N/A	N/A	N/A
	II-1000/50				-	-	-	0.2670	0.0270	0.0380	N/A	N/A	N/A	N/A	N/A	0.2209	N/A	N/A	N/A	0.4503	0.1851	0.3697
	II-1500/50							-	-	-	N/A	N/A	N/A	N/A	N/A	0.2209	N/A	N/A	N/A	N/A	N/A	N/A
	II-200/75										-	-	-	0.9746	0.2209	0.0011	0.7788	0.5783	0.1539	0.3274	0.7013	0.2966
	II-300/75													-	-	-	0.7252	0.0792	0.2088	0.3171	0.0581	0.2188
	II-500/75																-	-	-	0.0645	0.7327	0.8972
	II-1000/75																			-	-	-

Note: f_{CS}: compressive strength; f_{FS}: flexural strength; E_F: elastic modulus; "_" indicates the evaluation is not valid.

Table C-4. ANOVA Results: *p*-Values between Different Test IDs within Interaction *III* for f_{CS}, f_{FS}, and E_F

Interaction	Test ID	*III*-500/4			*III*-500/12			*III*-1500/4			*III*-1216/6			*III*-1850/12			*III*-2733/6*		
		f_{CS}	f_{FS}	E_F	f_{CS}	f_{FS}	E_F	f_{CS}	f_{FS}	E_F	f_{CS}	f_{FS}	E_F	f_{CS}	f_{FS}	E_F	f_{CS}	f_{FS}	E_F
III	*III*-500/4	-	-	-	0.00066	0.18086	0.04210	0.04033	0.19847	0.08118	N/A	N/A	N/A	N/A	N/A	N/A	N/A	N/A	N/A
	III-500/12				-	-	-	0.60566	0.88167	0.36047	N/A	N/A	N/A	N/A	N/A	N/A	N/A	N/A	N/A
	III-1500/4							-	-	-	N/A	N/A	N/A	N/A	N/A	N/A	N/A	N/A	N/A
	III-1216/6										-	-	-	0.46976	0.03341	0.00216	0.00124	0.01793	0.01721
	III-1850/12													-	-	-	0.05059	0.32816	0.19173
	III-2733/6*																-	-	-

Note: f_{CS}: compressive strength; f_{FS}: flexural strength; E_F: elastic modulus; "_" indicates the evaluation is not valid.

Table C-5. ANOVA Results: *p*-Values between Different Test IDs within Interaction *IV* for C_R, F_R, and E_R

Interaction	Test ID	*IV*-0.35/2‡			*IV*-0.45/0			*IV*-0.45/3*			*IV*-0.6/2		
		C_R	F_R	E_R	C_R	F_R	E_R	C_R	F_R	E_R	C_R	F_R	E_R
IV	*IV*-0.35/2‡	-	-	-	N/A	N/A	N/A	0.00148	0.12985	0.72751	0.98446	0.00021	0.00019
	IV-0.45/0				-	-	-	0.08214	0.00026	< 0.0001	N/A	N/A	N/A
	IV-0.45/3*							-	-	-	N/A	N/A	N/A
	IV-0.6/2										-	-	-

Note: C_R: relative compressive strength; F_R: relative flexural strength; E_R: relative elastic modulus; "_" indicates the evaluation is not valid.

Table C-6. ANOVA Results: *p*-Values between Different Test IDs within Interaction *V* for C_R, F_R, and E_R

Interaction	Test ID	*V-0.1/3*‡			*V*-0.3/3+			*V*-0.1/28‡			*V*-0.3/28+		
		C_R	F_R	E_R	C_R	F_R	E_R	C_R	F_R	E_R	C_R	F_R	E_R
V	*V-0.1/3*‡	*	-	-	<0.0001	0.00014	< 0.0001	0.00119	0.89928	0.61711	N/A	N/A	N/A
	V-0.3/3+				*	-	-	N/A	N/A	N/A	0.0058	0.03132	0.02587
	V-0.1/28‡							*	-	-	0.00081	0.00379	0.00838
	V-0.3/28+										*	-	-

Note: C_R: relative compressive strength; F_R: relative flexural strength; E_R: relative elastic modulus; "_" indicates the evaluation is not valid.

Table C-7. ANOVA Results: *p*-Values between Different Test IDs within Interaction *I* for 28-day E_d

Interaction	Test ID	*I*-800/0.05	*I*-800/0.1‡	*I*-800/0.3+	*I*-2500/0.05	*I*-2500/0.1	*I*-2500/0.3
I	*I*-800/0.05	-	0.03036	0.07447	0.08847	N/A	N/A
	I-800/0.1‡		-	0.0735	N/A	0.05374	N/A
	I-800/0.3+			-	N/A	N/A	0.29648
	I-2500/0.05				-	0.90209	0.46174
	I-2500/0.1					-	0.39892
	I-2500/0.3						-

Table C-8. ANOVA Results: *p*-Values between Different Test IDs within Interaction *III* for 28-day E_d

Interaction	Test ID	*III*-1216/6	*III*-1850/12	*III*-2733/6*
III	*III*-1216/6	-	0.08461	0.17914
	III-1850/12		-	0.24076
	III-2733/6*			-

Table C-9. ANOVA Results: *p*-Values between Different Test IDs within Interaction *IV* for 28-day Relative E_d

Interaction	Test ID	*IV*-0.35/2‡	*IV*-0.45/0	*IV*-0.45/3*	*IV*-0.6/2
IV	*IV*-0.35/2‡	-		0.22828	0.78961
	IV-0.45/0		-	0.08628	
	IV-0.45/3*			-	
	IV-0.6/2				-

Table C-10. ANOVA Results: *p*-Values between Different Test IDs within Interaction *V* for Relative E_d

Interaction	Test ID	*V*-0.05/1	*V*-0.1/1‡	*V*-0.3/1+	*V*-0.05/28	*V*-0.1/28‡	*V*-0.3/28+
V	*V*-0.05/1	-	0.07423	0.09274	0.71619		
	V-0.1/1‡		-	0.02864		0.076	
	V-0.3/1+			-			0.0381
	V-0.05/28				-	0.03036	0.07447
	V-0.1/28‡					-	0.0735
	V-0.3/28+						-

Table C-11. ANOVA Results: *p*-Values between Different Test IDs for 14- and 28-day E_d (*D* series)

Test ID	*D1* (14-day)	*D1/II0.1* (14-day)	*D1/II0.3* (14-day)	*D1/I0.1* (14-day)	*D1/I0.3* (14-day)	*D1* (28-day)	*D1/II0.1* (28-day)	*D1/II0.3* (28-day)	*D1/I0.1* (28-day)	*D1/I0.3* (28-day)
D1 (14-day)	-	0.01015	0.10358	0.00795	0.42292	0.00481	-	-	-	-
D1/II0.1 (14-day)		-	0.02048	0.69162	0.01494	-	0.02976	-	-	-
D1/II0.3 (14-day)			-	0.01853	0.28696	-	-	0.00964	-	-
D1/I0.1 (14-day)				-	0.01306	-	-	-	0.02811	-
D1/I0.3 (14-day)					-	-	-	-	-	0.01056
D1 (28-day)						-	0.00758	0.16239	0.03208	0.25736
D1/II0.1 (28-day)							-	0.0073	0.25591	0.00656
D1/II0.3 (28-day)								-	0.03868	0.20292
D1/I0.1 (28-day)									-	0.03493
D1/I0.3 (28-day)										-

Table C-12. ANOVA Results: *p*-Values between Different Test IDs for 14- and 28-day ASR Expansion (*D* series)

Test ID	*D1* (14-day)	*D1/II0.1* (14-day)	*D1/II0.3* (14-day)	*D1* (28-day)	*D1/II0.1* (28-day)	*D1/II0.3* (28-day)
D1 (14-day)	-	<0.0001	0.00041	<0.0001	-	-
D1/II0.1 (14-day)		-	0.00014	-	0.0001	-
D1/II0.3 (14-day)			-	-	-	<0.0001
D1 (28-day)				-	<0.0001	<0.0001
D1/II0.1 (28-day)					-	<0.0001
D1/II0.3 (28-day)						-

Table C-13. ANOVA Results: *p*-Values between Different Test IDs for 28-day f_{ES} (*D* series)

Test ID	*D1*	*D1/I0.1*	*D1/II0.1*	*D1/I0.3*	*D1/II0.3*	*D2*	*D2/II0.1-A*	*D2/II0.1-B*
D1	-	0.00354	0.00055	0.39215	0.38256	-	-	-
D1/I0.1		-	0.07078	0.00529	0.01835	-	-	-
D1/II0.1			-	0.0007	0.00178	-	-	-
D1/I0.3				-	0.78489	-	-	-
D1/II0.3					-	-	-	-
D2						-	<0.0001	0.02566
D2/II0.1-A							-	0.00017
D2/II0.1-B								-

Table C-14. ANOVA Results: *p*-Values between Different Test IDs for 28-day E_F (*D* series)

Test ID	*D1*	*D1/I0.1*	*D1/II0.1*	*D1/I0.3*	*D1/II0.3*	*D2*	*D2/II0.1-A*	*D2/II0.1-B*
D1	-	0.00727	0.00018	0.04637	0.00575	-	-	-
D1/I0.1		-	0.14569	0.13728	0.98808	-	-	-
D1/II0.1			-	0.00251	0.13044	-	-	-
D1/I0.3				-	0.11902	-	-	-
D1/II0.3					-	-	-	-
D2						-	0.00209	0.26587
D2/II0.1-A							-	<0.0001
D2/II0.1-B								-

Table C-15. ANOVA Results: *p*-Values between Different Test IDs for 28-day f_{CS} (*D* series)

Test ID	*D1*	*D1/I0.1*	*D1/II0.1*	*D1/I0.3*	*D1/II0.3*	*D2*	*D2/II0.1-A*	*D2/II0.1-B*
D1	-	0.20119	0.07521	0.85885	0.20377	-	-	-
D1/I0.1		-	0.06773	0.06227	0.84169	-	-	-
D1/II0.1			-	0.02872	0.05541	-	-	-
D1/I0.3				-	0.05771	-	-	-
D1/II0.3					-	-	-	-
D2						-	0.03868	0.08519
D2/II0.1-A							-	0.00493
D2/II0.1-B								-

Table C-16. ANOVA Results: *p*-Values between Different Ages for E_d (*D* series)

Test ID	Groups (between different ages (day))							
	0 & 1	0 & 2	0 & 3	0 & 7	0 & 10	0 & 14	0 & 21	0 & 28
*D*1	0.084	0.913	0.025	0.0002	0.010	<0.0001	<0.0001	0.0002
*D*1/II0.1	0.413	0.359	0.726	0.032	0.014	0.011	0.006	0.004
*D*1/II0.3	0.930	0.319	0.079	0.006	0.003	0.002	0.002	0.001
*D*1/I0.1	0.458	0.404	0.670	0.120	0.042	0.021	0.013	0.010
*D*1/I0.3	0.772	0.490	0.089	0.004	0.006	0.003	0.002	0.001

APPENDIX D. NOMENCLATURE

σ_c: flexural strength of CNT-cement nanocomposite

σ_m: flexural strength of the matrix

σ_f: tensile strength of the fiber

v_f: CNT volume fraction

χ_o: orientation factor

χ_L: length factor

d: CNT diameter

L: CNT length

L_c: CNT critical length

τ_i: interfacial shear stress between CNTs and matrix

Φ_n: orientation angle

a_n: fraction of fibers with same orientation angle Φ_n

AR: CNT aspect ratio

B: Pukanszky adhesion parameter

$\bar{\sigma}_{ij}$: average stress

$\bar{\varepsilon}_{ij}$: average strain

n: elastic modulus for longitudinal uniaxial straining

l: associated cross modulus

k: plain strain bulk modulus for lateral dilatation without longitudinal extension

m: transverse shear modulus

μ: longitudinal shear modulus

S: radial stress

u_f: radial displacement of fiber

u_m: radial displacement of matrix

r: radius of fiber

E_c: elastic modulus of CNT-cement nanocomposite

E_m: elastic modulus of the matrix

E_f: elastic modulus of the fiber

ξ: measure of fiber geometry ($\xi = 2\,{}^{L}/_{d}$; for cylindrical fibers)

$E_{f'}$: equivalent elastic modulus of CNT

w/c: water-to-cement ratio

s/c: sand-to-cement ratio

t: hydration age of specimen

SP/CNTs: superplasticizer-to-CNTs ratio

UA: ultrasonication amplitude

UE_T: total ultrasonication energy

UE_m: ultrasonication energy per minute of sonication

t_S: duration of ultrasonication process

UEI: ultrasonication energy indicator

κ: CNT concentration

η_D: dispersion relation

η_H: hydration age relation

η_M: matrix relation

f_{CS}: compressive strength

f_{FS}: flexural strength

$\bar{L}$: CNT average length

$\bar{d}$: CNT average diameter

$\overline{AR}$: CNT average aspect ratio

Δf_{CS}: percent change in compressive strength compared with control

Δf_{FS}: percent change in flexural strength compared with control

$\Delta\bar{\kappa}$: change in CNT concentration ($\kappa_2 - \kappa_1;\ \kappa_2 > \kappa_1$)

ΔS: change in the strength in two levels of CNT concentration ($\Delta S = S_{\kappa_2} - S_{\kappa_1}$)

$\Delta S_{CS} = f_{CS(\kappa_2)} - f_{CS(\kappa_1)}$

$\Delta S_{FS} = f_{FS(\kappa_2)} - f_{FS(\kappa_1)}$

$\Delta S/\Delta\bar{\kappa}$: dispersion quality indicator

Δf_E: percent change in elastic modulus compared with control

Δf_T: percent change in toughness compared with control

τ_0: yield stress

μ_P: plastic viscosity

$\dot{\gamma}$: shear rate

K: consistency

$\dot{n}$: flow index

P_{CS}: maximum compression load applied

P_{FS}: maximum flexural load applied

A: cross sectional area

E_F: static elastic modulus from flexural strength test

I: second moment of inertia

$\frac{\bar{P}}{\bar{\Delta}}$: slope of a flexural load-deflection curve ranging from 15 to 40% of P_f

E_d: dynamic elastic modulus

M: mass of the specimen

n': longitudinal resonant frequency

P_c: mechanical properties of CNT-cement nanocomposite

P_m: mechanical properties of matrix

P_R: relative mechanical properties of CNT-cement nanocomposite

C_R: relative compressive strength of CNT-cement nanocomposite

F_R: relative flexural strength of CNT-cement nanocomposite

E_R: relative elastic modulus of CNT-cement nanocomposite

X, Y, Z: unknown model parameters used to fit the data for regression model

$C(\boldsymbol{x}, \boldsymbol{\Theta})$: probabilistic capacity model of interest (herein, σ_c and E_c)

$\boldsymbol{x}$: set of measurable variables

$C(\boldsymbol{x})$: deterministic model

$\boldsymbol{\Theta}$: vector of unknown model parameters; $\boldsymbol{\Theta} = (\theta, \partial)$

θ_i: set of unknown model parameters used to fit the data for probabilistic models

$\gamma(x, \theta)$: correction term (herein, η_D, η_H, and η_M)

∂: standard deviation of the error term

ε: random variable with zero mean and unit variance

$\partial\varepsilon$: error term of the model

$p(\boldsymbol{\Theta})$: prior distribution of $\boldsymbol{\Theta}$

$L(\boldsymbol{\Theta})$: likelihood function

λ: normalizing factor; $\lambda = [\int L(\boldsymbol{\Theta})p(\boldsymbol{\Theta})\, d(\boldsymbol{\Theta})]^{-1}$

$f(\boldsymbol{\Theta})$: posterior distribution of $\boldsymbol{\Theta}$

$M_{\boldsymbol{\Theta}}$: posterior mean vector

$\Sigma_{\boldsymbol{\Theta\Theta}}$: covariance matrix

P_f: probability of failure

C: capacity

D: demand

$f_D(D)$: probability distribution of demand

$f_C(C)$: probability distribution of capacity

$f_{CD}(C, D)$: joint probability density function

$g(\cdot)$: limit state function

f_{FS-c}: flexural strength of CNT-cement nanocomposite (herein, σ_c)

f_{FS-m}: flexural strength of the matrix (herein, σ_m)

E_{F-m}: elastic modulus of the matrix (herein, E_m)

E_{F-c}: elastic modulus of CNT-cement nanocomposite (herein, E_c)

ψ: minimum design requirement

$\boldsymbol{\delta}$: vector of sensitivity measure

$\boldsymbol{\sigma_s}$: diagonal matrix with diagonal elements given by standard deviation of random variables

β: reliability index

$\boldsymbol{\nabla_{\Theta_f}}\beta$: gradient vector of β with respect to $\boldsymbol{\Theta}_f$ computed at the mean point

$\boldsymbol{\gamma}$: vector of importance measure

$\boldsymbol{\alpha}$: row vector of negative normalized gradient of limit state function at design point in standard normal space

$\boldsymbol{z}$: vector of random variables

$\boldsymbol{J_{u^*z^*}}$: Jacobian of probability transformation from original space to standard normal space

$\boldsymbol{SD'}$: standard deviation diagonal matrix of equivalent normal variables at the design point

$log\ L(\boldsymbol{\Theta})$: measure of model fit

N_p: number of unknown model parameters included in $\boldsymbol{\Theta}$

N_s: number of samples (data)

AIC: Akaike Information Criterion

BIC: Bayesian Information Criterion

CURRICULUM VITA

Name: Mahyar Ramezani

Address: Department of Civil and Environmental Engineering, University of Louisville, 40208

Email Address: mahyar.ramezani@louisville.edu

Education: Ph.D., Civil Engineering, University of Louisville, 2019

M.Sc., Civil Engineering, National University of Malaysia, 2013

B.Sc., Civil Engineering, Azad University, 2010

Related Publications:

Ramezani, M., Kim, Y.H., Hasanzadeh, B., and Sun, Z. "*Influence of Carbon Nanotubes on SCC Flowability*." 8th Int. RILEM Symp. Self-Compacting Concr., Washington DC, USA 15-18 May 2016: 397-406

Ramezani, M., Kim, Y.H., and Sun, Z. "*Mechanical Properties of Carbon Nanotube Reinforced Cementitious Materials: Database and Statistical Analysis*." Magazine of Concrete Research (2019): 1-24

Ramezani, M., Kim, Y.H., and Sun, Z. "*Modeling the Mechanical Properties of Cementitious Materials containing CNTs*." Cement and Concrete Composites 104 (2019): 1-21

Ramezani, M., Kim, Y.H., and Sun, Z. "*Probabilistic Model for Elastic Modulus of Cementitious Materials containing Carbon Nanotubes.*" International Conference on Cement-Based Materials Tailored for a Sustainable Future (CBMT 2020), Istanbul, Turkey 7-8 May 2020

Presentation: **Ramezani, M**., Kim, Y.H., and Sun, Z. "*Probabilistic Model for Flexural Strength of Carbon Nanotube Reinforced Cement-based Materials*: EMI 2018, Engineering Mechanics Institute Conference, Massachusetts Institute of Technology, May 29-June 1, 2018